FLAMMABILITY CHARACTERISTICS AT HEAT FLUX LEVELS UP TO 200 kW/m^2

AND

THE EFFECT OF OXYGEN ON FLAME HEAT FLUX

by

Patricia A. Beaulieu

A Dissertation

Submitted to the Faculty

of

Worcester Polytechnic Institute

in partial fulfillment for the requirements for the

Degree of Doctor of Philosophy

in Fire Protection Engineering

October 2005

APPROVED:

_____

Professor Nicholas A. Dembsey, Major Advisor

_____

Dr. Robert G. Bill, Jr., Co-Advisor, FM Global

_____

Professor John P. Woycheese, Co-Advisor

_____

Professor Kathy A. Notarianni, Head of Department

ABSTRACT

This dissertation documents two interrelated studies that were conducted to more fundamentally understand the scalability of flame heat flux. The first study used an applied heat flux in the bench scale horizontal orientation which simulates a large scale flame heat flux. The second study used enhanced ambient oxygen to actually increase the bench scale flame heat flux itself. Understanding the scalability of flame heat flux more fully will allow better ignition and combustion models to be developed as well as improved test methods.

The key aspect of the first study was the use of real scale applied heat flux up to 200 kW/m^2. An unexpected non-linear trend is observed in the typical plotting methods currently used in fire protection engineering for ignition and mass loss flux data for several materials tested. This non-linearity is a true material response. This study shows that viewing ignition as an inert material process is inaccurate at predicting the surface temperature at higher heat fluxes and suggests that decomposition kinetics at the surface and possibly even in-depth may need to be included in an analysis of the process of ignition. This study also shows that viewing burning strictly as a surface process where the decomposition kinetics is lumped into the heat of gasification may be inaccurate and the energy balance is too simplified to represent the physics occurring.

The key aspect of the second study was direct experimental measurements of flame heat flux back to the burning surface for 20.9 to 40 % ambient oxygen concentrations. The total flame heat flux in enhanced ambient oxygen does not simulate large scale flame heat flux in the horizontal orientation. The vertical orientation shows that enhanced ambient oxygen increases the flame heat flux more significantly and also increases the measured flame spread velocity.

ACKNOWLEDGEMENTS

TABLE OF CONTENTS

LIST OF FIGURES

xi

LIST OF TABLES

INTRODUCTION

BACKGROUND

Mechanical and chemical properties are usually used to choose a suitable material system for a given application. However, the fire performance of this system is also needed by designers and engineers to help design active protection systems that would control the fire and minimize damage if the system ignites. Alternatively, if no active protection system is to be used, selection of another appropriate material system for the application would be prudent based on ignitability and flame spread parameters.

There are two basic approaches to determine the fire performance of materials in realistic scenarios. The first is to conduct a large scale evaluation and obtain the results directly. The second is to conduct bench scale experiments to obtain material flammability parameters for ignition and combustion. Use of material flammability parameters obtained from these small scale experiments can then be used in conjunction with "first principle" mathematical models or calculation procedures to estimate full scale performance. Of the two basic approaches, the second is more desirable from a practical viewpoint, since it is more versatile and time and cost efficient. However, for a flammability parameter obtained from small scale experiments to be considered a true material "property" independent of apparatus or scale, the same value must be obtained in various scale tests.

This dissertation documents two interrelated studies that were conducted to more fundamentally understand the scalability of flame heat flux since it has been reported that flame heat flux back to

the burning surface in bench scale experiments is not the same as for large scale fires. The first study used an applied heat flux in the bench scale horizontal orientation which, combined with the flame heat flux, would simulate a large scale flame heat flux. The second study used enhanced ambient oxygen via the Flame Radiation Scaling Technique to actually increase the bench scale flame heat flux itself. Understanding the scalability of flame heat flux more fully will allow better ignition and combustion models to be developed as well as improved test methods, although these are beyond the scope of this dissertation.

THE APPARATUS

The bench scale experiments were conducted using an instrument called the Advanced Flammability Measurements (AFM) Apparatus. It was created as part of an on going apparatus evaluation, improvement and development program. The AFM is closely related to the bench scale Fire Propagation Apparatus (FPA) (ASTM E 2058), and similar to the bench scale Cone Calorimeter (ASTM E 1354). However, the AFM is of intermediate scale in terms of its design with greater capability of applied heat flux range, maximum sample size, and incorporation of additional measurement techniques needed to assess flame and material heat transfer directly. These characteristics of the AFM will improve measurement of key material flammability parameters needed for computer simulation of end use fire scenarios. The AFM is currently used in "research mode," but has potential to become a commercial production apparatus.

The AFM consists primarily of (i) eight radiant heaters to supply an applied heat flux to a sample up to 220 kW/m^2, (ii) a spark igniter, (iii) a load cell system to determine the mass loss rate of the sample as it is burning, (iv) gas analyzers to measure the level of CO, CO_2, O_2 and total gaseous

hydrocarbons in the combustion products, (v) a smoke obscuration system to determine the soot yield and (vi) a data acquisition system to record all the measurements for analysis. Characterization of the AFM shows that the total applied heat flux uncertainty, including apparatus heat up, spatial variation, day to day variations and DAS resolution, is $\pm\,2$ kW/m^2.

APPLIED HEAT FLUX STUDY

Ignition and steady state burning behavior in the horizontal orientation for a "standard" 20.9 % oxygen atmosphere were investigated in this study. The key aspect was the use of real scale applied heat flux up to 200 kW/m^2 which is well beyond that typically considered in contemporary testing. An unexpected non-linear trend is observed in the typical plotting methods currently used in fire protection engineering for ignition and mass loss flux data for several materials tested. There also exist literature results showing the same non-linear trend as the current study, although not as clearly due to the limited heat flux range used. Conditions required for plotting the data in this fashion, including 1D conduction and thermally thick behavior, have been confirmed. The non-linearity is not related to operation of the AFM but is considered a true material response.

The current study takes a simple approach to investigating the non-linear results of the ignition and mass loss flux data. This approach is to investigate the measured temperature profile by comparing it to a predicted profile during heat up to ignition and through steady burning. Using this approach to investigate decomposing material behavior shows that viewing ignition as an inert material process is inaccurate at predicting the surface temperature at higher heat fluxes. (This viewpoint is the basis for the "typical technique" currently used in fire protection

3

engineering for ignition.) This investigation of thermal effects suggests that decomposition kinetics at the surface and possibly even in-depth may need to be included in an analysis of the process of ignition.

The steady burning temperature profiles appear to be invariant with applied heat flux. This shows that viewing burning strictly as a surface process where the decomposition kinetics is lumped into the heat of gasification may be inaccurate. (This viewpoint is the basis for the "typical technique" currently used in fire protection engineering for burning.) This possible inaccuracy was investigated by obtaining the heat of gasification via the "typical technique" using the mass loss flux data and comparing it to the commonly considered "fundamental" value obtained from DSC measurements. This comparison suggests that the "typical technique" energy balance is too simplified to represent the physics occurring for any range of applied heat flux. Hence, a new energy balance needs to be developed.

ENHANCED AMBIENT OXYGEN STUDY

The use of enhanced ambient oxygen to obtain large scale flame heat flux values from small scale tests comes from the Flame Radiation Scaling Technique which was developed by Tewarson. Ignition and steady state burning behavior in enhanced ambient oxygen atmospheres were investigated in this study. Enhanced ambient oxygen had no effect on the time to ignition as a function of applied heat flux for the horizontal orientation. Additionally, the non-linear trend seen in the "standard" 20.9 % oxygen atmosphere in the first study is also seen for enhanced ambient oxygen. Experimental measurements for free burn, black PMMA show that the total flame heat flux in enhanced ambient oxygen does not simulate large scale flame heat flux.

The increase of the total flame heat flux to the levels seen in large scale was thought to be why vertical flame spread tests in small scale, enhanced ambient oxygen concentration would show "large scale results" for flame spread. Since the horizontal orientation results show that the total flame heat flux is not being brought up to large scale levels, additional investigation in the vertical orientation was needed to understand the vertical flame spread situation.

Experimental measurements in the vertical orientation show that enhanced ambient oxygen increases the flame heat flux more significantly than for the horizontal orientation. Enhanced ambient oxygen also increases the measured flame spread velocity. From consistent results between the measured value and those calculated using a "thermal" model, it is reasonable to suggest that the increase in the flame spread velocity that occurs with enhanced ambient oxygen is due predominately to the increase in the flame heat flux (thermally driven).

ORGANIZATION

The dissertation consists of three chapters and eight appendices. Chapter 1 documents the first study which used an applied heat flux in the bench scale horizontal orientation to simulate a large scale flame heat flux. Chapter 2 documents the second study using enhanced ambient oxygen, via the Flame Radiation Scaling Technique, in the horizontal orientation and Chapter 3 contains the vertical orientation enhanced ambient oxygen.

Appendix A is a literature review to determine the effect of ambient oxygen concentration on flame soot, height, temperature and heat flux. Surface temperature, time to ignition, mass loss rate, flame spread and understanding of general mechanisms were also included.

Appendix B describes the Advanced Flammability Measurements Apparatus (AFM) which was used for a major portion of the experiments. It is of intermediate scale and is closely related to the bench scale Fire Propagation Apparatus and is similar to the Cone Calorimeter. The AFM was developed to provide an apparatus with greater capability in terms of applied heat flux, maximum sample size and incorporation of additional measurement techniques needed to assess flame and material heat transfer directly.

Appendix C describes various preliminary checks that were conducted to confirm proper operation of the Advanced Flammability Measurements apparatus (AFM). Checks were also conducted to confirm that the proper experimental procedure for ignition and combustion tests were being performed such that the data acquired was extremely well characterized.

Appendix D describes various secondary checks that were conducted. The effect of sample shape, sample thickness, sample surface preparation, inlet airflow velocity, heater type, igniter type, heater orientation and a limited variation of material brand on time to ignition and mass loss rate was investigated for black PMMA. These results were also compared to several "in-house" apparatus and literature results. Test results obtained in the AFM are repeatable and consistent with in-house and literature results.

Appendix E explains five techniques used to obtain the flame heat flux of black PMMA including the commonly used engineering technique of inferring the flame heat flux from the mass loss rate intercept as well as from the individual mass loss rate at each applied heat flux. Also included are using embedded thin film gages and embedded Medtherm Gardon gages to measure (early) the

conduction in the solid as well as (later) the flame heat flux directly. Embedded thermocouples are also used to obtain the solid conduction.

Appendix F contains details of oxygen consumption calorimetry used to calculate the heat release rate of materials. The most commonly used equations are those developed by Parker which are given in simplified form in the Cone Calorimeter ASTM E-1354 Standard, however, the simplifications are not the same as those used by carbon dioxide generation calorimetry. The present study shows improvements and refinements to obtain more accurate equations of heat release rate using oxygen consumption calorimetry.

Appendix G contains measurements of soot yield for the materials tested in this study while Appendix H investigates current techniques commonly utilized for the analysis of ignition.

CHAPTER 1: FLAMMABILITY CHARACTERISTICS AT APPLIED HEAT FLUX LEVELS UP TO 200 kW/m^2

ABSTRACT

This Chapter documents the first of two interrelated studies that were conducted to more fundamentally understand the scalability of flame heat flux since it has been reported that flame heat flux back to the burning surface in small scale experiments is not the same as for large scale fires. The key aspect was the use of real scale applied heat flux up to 200 kW/m^2 which is well beyond that typically considered in contemporary testing. The main conclusions are that decomposition kinetics needs to be included in the study of ignition and the energy balance for burning is too simplified to represent the physics occurring.

An unexpected non-linear trend is observed in the typical plotting methods currently used in fire protection engineering for ignition and mass loss flux data for several materials tested and this non-linearity is a true material response. Using measured temperature profiles in the condensed phase shows that viewing ignition as an inert material process is inaccurate at predicting the surface temperature at higher heat fluxes. The steady burning temperature profiles appear to be invariant with applied heat flux. This possible inaccuracy was investigated by obtaining the heat of gasification via the "typical technique" using the mass loss flux data and comparing it to the commonly considered "fundamental" value obtained from differential scanning calorimetry measurements. This comparison suggests that the "typical technique" energy balance is too simplified to represent the physics occurring for any range of applied heat flux. Observed bubbling and melting phenomena provides a possible direction of study.

INTRODUCTION

This Chapter documents the first of two interrelated studies that were conducted to more fundamentally understand the scalability of flame heat flux since it has been reported that flame heat flux back to the burning surface in small scale experiments is not the same as for large scale.

The Advanced Flammability Measurements Apparatus[1] (AFM) was used to conduct small scale experiments at ambient oxygen concentrations of 20.9 % oxygen for various materials. The key aspect was the use of real scale applied heat flux up to 200 kW/m^2 which is well beyond that typically considered in contemporary testing. Ignition and steady state burning behavior in the horizontal orientation were investigated using the typical approaches common to fire protection engineering. Additionally, the temperature profile in the condensed phase was measured and compared it to a predicted profile during heat up to ignition and through steady burning. The apparent heat of gasification using the mass loss flux data was also calculated and compared to that obtained from commonly used Differential Scanning Calorimetry (DSC) techniques.

BACKGROUND

Mechanical and chemical properties are usually used to choose a suitable material system for a given application. However, the fire performance of this system is also needed by designers and engineers to help design active protection systems that would control the fire and minimize damage if the system ignites. Alternatively, if no active protection system is to be used, selection of another appropriate material system for the application would be prudent based on ignitability and flame spread parameters.

There are two basic approaches to determine the fire performance of materials in realistic scenarios. The first is to conduct a large scale evaluation and obtain the results directly. The second is to conduct small scale experiments to obtain material flammability parameters for ignition and combustion. Use of material flammability parameters obtained from these small scale experiments can then be used in conjunction with "first principle" mathematical models[2] or calculation procedures to estimate full scale performance. Of the two basic approaches, the second is more desirable from a practical viewpoint, since it is more versatile and time and cost efficient.[3] However, for a flammability parameter obtained from small scale experiments to be considered a true material "property" independent of apparatus or scale, the same value must be obtained in various scale tests.

The small scale experiments were conducted using an apparatus called the Advanced Flammability Measurements (AFM) Apparatus.[1] It was created as part of an on going apparatus evaluation, improvement and development program. The AFM is closely related to the small scale Fire Propagation Apparatus[4] (FPA), and similar to the small scale Cone[5] Calorimeter. However, the AFM is of intermediate scale in terms of its design with greater capability of applied heat flux range, maximum sample size, and incorporation of additional measurement techniques needed to assess flame and material heat transfer directly. These characteristics will improve measurement of key material flammability parameters needed for computer simulation of end use fire scenarios. Apparatus details are given in Appendix B.

IGNITION RESULTS

Various checks were conducted to confirm that the proper experimental procedure for ignition

tests was being performed such that the data acquired was extremely well characterized. These experimental checks, described in Appendix C and D, confirmed the definition of visual ignition with other techniques, confirmed the assumption of one dimensional (1D) conduction behavior in the sample and the assumption of thermally thick behavior. Also there was no effect of sample shape, manufacturers brand, production type and inlet air velocity. The radiation source wavelength was found to have an effect on the time to ignition. In depth radiative absorption was found to occur with the IR lamp source of the AFM but not for a radiant coil source used with the cone calorimeter. The in depth absorption could be eliminated by applying a carbon black coating to the sample exposed to an IR lamp source.

Black PMMA

Figure 1.1 shows ignition results obtained in the AFM, FPA and Cone Calorimeter as well as some literature results from Tewarson,[6] Hopkins and Quintiere[7] for 25 mm thick black PMMA. The typical plotting method currently used in fire protection engineering for ignition data is used to plot the inverse of the square root of time to ignition vs. applied heat flux. This method is based on an inert material assumption.

For the present study, the sample material has a physical thickness of 25 mm and a round cross sectional area of 0.0073 m^2. To have the same experimental conditions for comparison to the Cone, Tewarson, Hopkins and Quintiere (i.e., all applied heat flux absorption occurring at sample surface) the AFM and FPA samples, had a fine coating of carbon black. The comparability between the AFM, Cone, FPA and literature results show that the AFM is operating properly and giving results as expected for applied heat flux ranges reachable by the Cone and FPA. The

11

agreement provides support for the accuracy of higher heat fluxes achievable by the AFM, given that the same calibration procedures were used for the entire applied heat flux range. Understanding of the material behavior at higher applied heat flux than commonly tested is important because there are practical applications in the real world where the heat flux from fires can reach 200 kW/m^2 or beyond. Note the unexpected non-linear trend starting at around 60 kW/m^2.
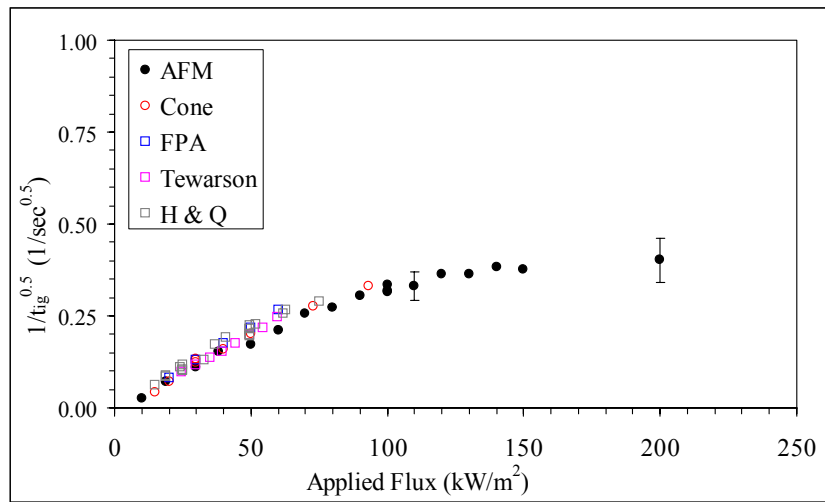
Figure 1.1   Inverse of the square root of time to ignition vs. applied heat flux for thermally thick behaving black PMMA. Experimental time uncertainty = ± 2 sec.

The possibility that the applied heat flux was blocked by the pyrolysis products from reaching the surface was investigated as a probable cause. The applied heat flux was measured using a Schmidt-Boelter heat flux gage embedded in the sample surface for black PMMA and Gray PVC but the result should be applicable to other materials. See from Figure 1.2 that there is a minor fluctuation of the applied heat flux once pyrolysis begins but there is no reduction in the mean

heat flux. This minor variation is within the uncertainty of the applied heat flux and as such is considered insignificant. Hence, all of the applied heat flux reaches the sample surface.
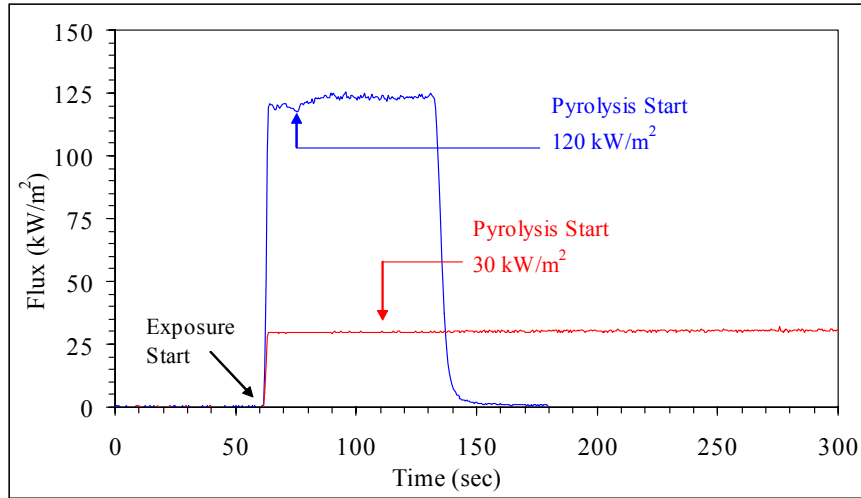
Figure 1.2   Applied heat flux measured at sample surface during pyrolysis of black PMMA.

In order to obtain higher applied heat fluxes, the IR lamp source must increase in temperature. This shifts the temperature higher and the peak emission wavelength shorter. From 10 to 200 kW/m^2, the IR lamp peak emission temperature increases from 1000 to 2500 K. The possibility that the sample absorbs these wavelengths differently was investigated by Hallman[8] who showed that the absorptivity of black PMMA does not change when exposed to a source temperature from 1000 to 3500 K. As such, all of the applied heat flux that is reaching the surface is likely being absorbed by the sample identically for the whole applied heat flux range.

It is concluded that the unexpected non-linear trend in the ignition plot is not due to specifics of the AFM apparatus including blockage of the applied heat flux by the pyrolysis products or

13

surface absorptivity changes with wavelength. Conditions required for plotting the data in typical

engineering fashion, including 1D conduction and thermally thick behavior, have been confirmed.

The non-linearity appears to be a true material response and an investigation of the temperature

profile was conducted.

Other Materials

Other materials were tested in the current study including Delrin, Gray PVC, pine and plywood

which are shown in Figures 1.3 through 1.6. Note that the time uncertainty of $\pm$ 2 sec is also

applicable for these materials. Figures 1.7 and 1.8 show literature data for plywood[9] and asphalt[10]

shingle where the applied heat flux was not sufficient to clearly show the non-linear trend but the

beginnings of it can be seen.
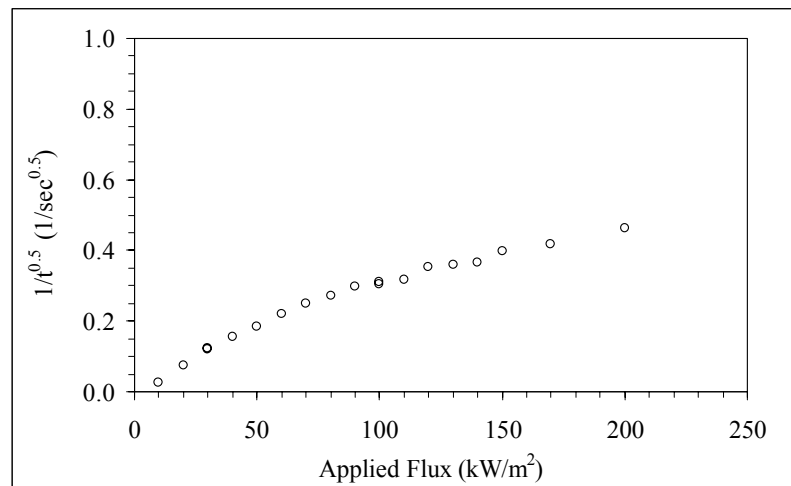
Figure 1.3   Inverse of the square root of time to ignition vs. applied heat flux for thermally

thick behaving Delrin.
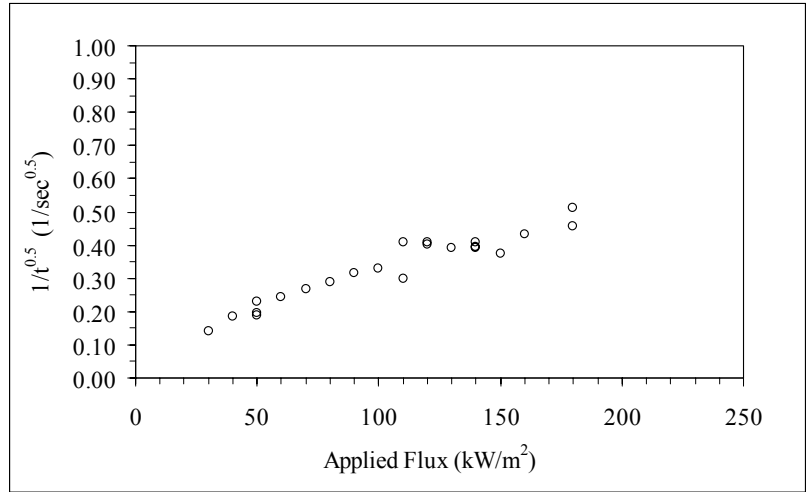
Figure 1.4   Inverse of the square root of time to ignition vs. applied heat flux for thermally
thick behaving gray PVC.
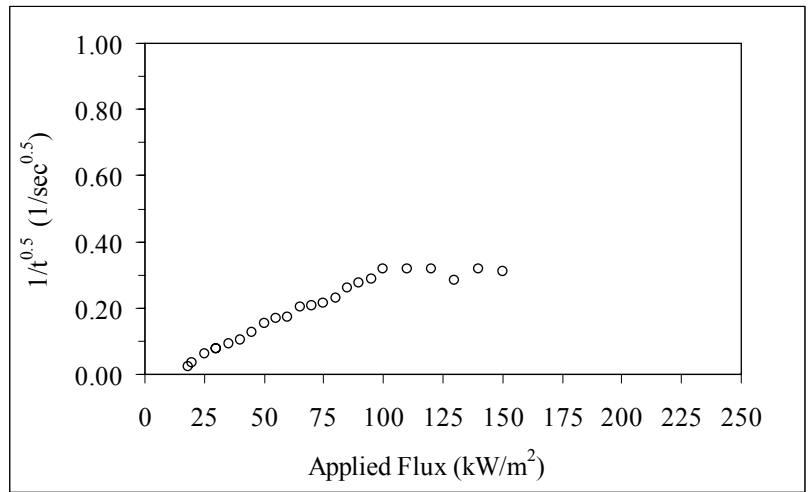
Figure 1.5   Inverse of the square root of time to ignition vs. applied heat flux for thermally
thick behaving pine.

15
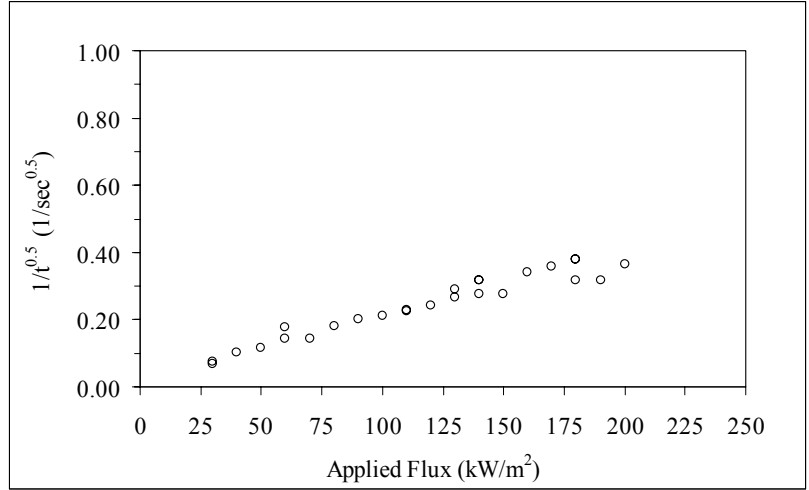
Figure 1.6   Inverse of the square root of time to ignition vs. applied heat flux for thermally

thick behaving plywood.
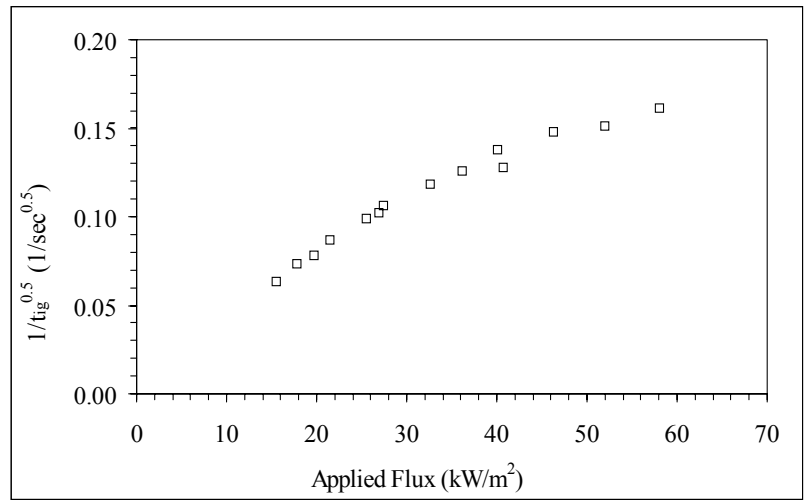
Figure 1.7   Inverse of the square root of time to ignition vs. applied heat flux for thermally

thick behaving asphalt shingle.[10]
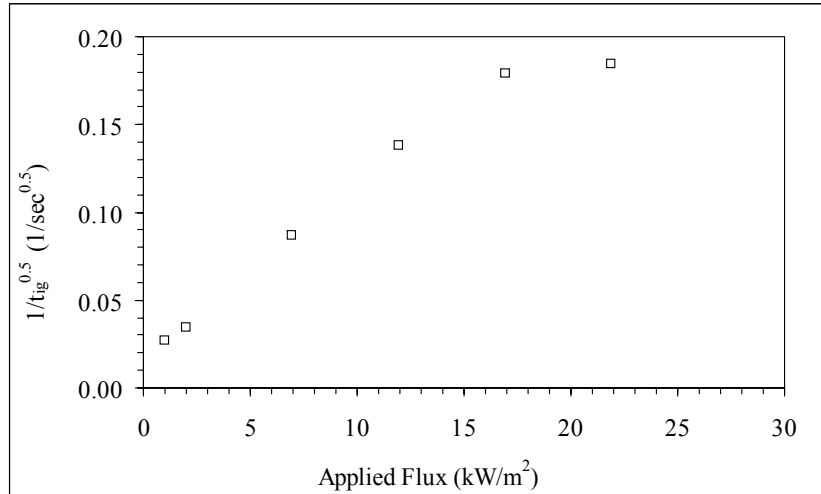
Figure 1.8   Inverse of the square root of time to ignition vs. applied heat flux for thermally thick behaving plywood.[9]

IGNITION TEMPERATURE PROFILE

A first approach to investigating the unexpected non-linear results of the ignition data is to examine the measured temperature profile of a confirmed 1D conduction, thermally thick behaving solid exposed to a constant applied heat flux and comparing it to a predicted profile. The equation used to obtain the predicted profile is the analytical solid, 1D conduction solution for an inert material with semi-infinite behavior, constant applied heat flux, constant heat transfer coefficient, all absorption taking place at the surface and constant thermal properties.[11] This equation has been used extensively in the study of ignition by others[12,13,14,15] and details of these are given in Appendix H.

The equation is given as

17

$$T = T_0 + \frac{\dot{q}''_{applied}}{H}\left[\text{erfc}\left(\frac{x}{2\sqrt{\alpha t}} \right) - \exp\left(\frac{Hx}{k} + \frac{\alpha H^2 t}{k^2} \right)\text{erfc}\left(\frac{x}{2\sqrt{\alpha t}} + \sqrt{\frac{\alpha H^2 t}{k^2}} \right) \right] \qquad (1\text{-}1)$$

where T is temperature, T_0 is initial temperature, t is time, k is thermal conductivity, ρ is density, c is specific heat capacity, $\dot{q}''$ is heat flux, x is depth, α is thermal diffusivity and H is the effective heat transfer coefficient for convection and radiation. Although Mowrer[16] states that the predictions from this analytical solution "are not accurate," he presents no experimental data to compare against his numerical results. The current study has experimentally measured temperature profiles for various applied heat fluxes.

The first issue of concern is that the effective heat transfer coefficient, H, is a constant in the equation but in the experiment, it varies as the sample heats up. This is an inherent error in using the analytical solution to predict the temperature profile, however, the significance of this error needs to be explored before concluding that this easy to use analytical approach is inaccurate such that a numerical approach to solving the governing equation is required. The effect of using a constant effective heat transfer coefficient was investigated by doing a sensitivity analysis of the predicted temperature profile for a range of H values. These values were bounded by using the following equation to solve for the effective heat transfer coefficient

$$H = h_c + \frac{\varepsilon\sigma\left(T^4 - T_0^4\right)}{\left(T - T_0\right)} \qquad (1\text{-}2)$$

where h_c is the convective heat transfer coefficient, ε is the emissivity and σ is the Stephan-Boltzman constant. The measured range for the surface temperature is 20 °C ambient to

approximately 350 °C ignition for the test materials. The natural convection test conditions indicate that h_c should[17,18] be approximately 15 W/m^{2}K hence the range of h_c from 10 to 20 W/m^{2}K was investigated. This variation in surface temperature and convective heat transfer coefficient gives a range of effective heat transfer coefficient, H, from 15 to 45 W/m^{2}K. Neither of these H values is correct because the material is always changing temperature during heating, being somewhere between room and ignition temperature. An average value of 30 W/m^{2}K for H was used.

Alumina Silicate Temperature Profile

Alumina silicate was chosen since it is a truly inert material for the full range of applied heat flux and the thermal properties for ceramics[19] are stated to be constant from 20 to 800 °C. This will allow one to determine if using an average effective heat transfer coefficient value in the analytical model is reasonable to simulate experimental results.

The sample is assembled by layering four 6 mm thick pieces. A very thin layer of silicone grease was used to insure good thermal contact between the layers and the thermocouples inserted between the layers. According to the manufacturer's specification sheet, the thermal conductivity of the silicone grease is 2.58 W/mK which is significantly larger than the value for alumina, and as such, the silicone will not be a barrier to heat flow through the sample. The recommended usage temperature range of the grease is -55 to 205 °C and experimental observations show no degradation of the grease after testing the alumina silicate sample. Temperature profiles were experimentally measured and compared to those predicted by the inert material analytical solution using the average H. Typical profiles are shown in Figure 1.9.
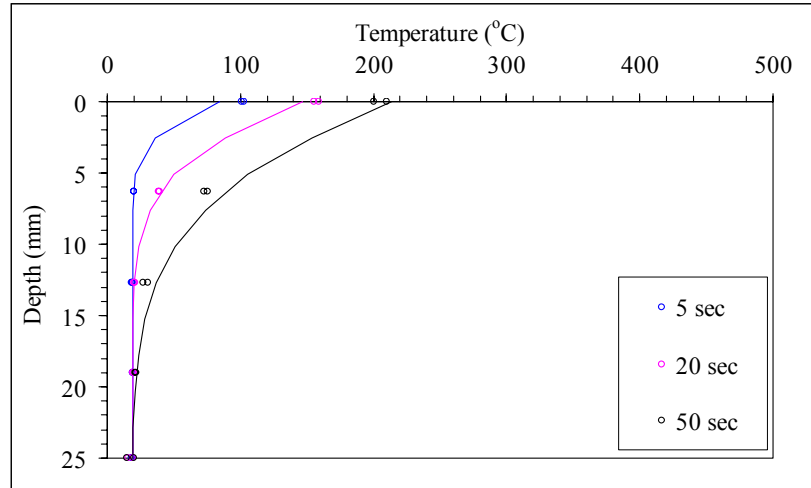
Figure 1.9   Temperature profile for thermally thick behaving alumina silicate, 50 kW/m^2 applied heat flux. This result is typical for other heat fluxes. Symbols: data, lines: analytical solution.

The figure shows that the profile from the inert solution predicts the inert material behavior even at the surface. The maximum difference between the experimental values and the prediction is 20 °C, which will be considered the uncertainty of the analytical solution for this study. Hence, using an average H in the solution is reasonable

Black PMMA Temperature Profile

The typical fire engineering assumption is that ignition is a "surface" event, which means that decomposition and ignition occur simultaneously when the surface reaches the ignition temperature. This is because heating the solid from ambient to pyrolysis temperature is the longest characteristic time in the development of the ignition phenomena and many studies have considered the heating process as the primary mechanism controlling material flammability. This

philosophy says that the ignition of non-inert materials can be viewed as an inert material process. The analytical equation used for the inert material analysis above can be applied to non-inert materials to see if this holds true.

The non-inert material chosen was black PMMA. An investigation was completed of the variation of k,[20] ρ[21] and c[22] with temperature for the range of 300 to 650 K, which is the range that the material experiences from room temperature to ignition. Note that once decomposition begins, the thermal properties are no longer that of an inert material but have decomposition effects mixed-in and the properties are now considered "effective." Decomposition is determined to begin at 475 K via experimental observation of pyrolysis products and use of Arrhenius theory.[23]

The analytical solution was used to predict the temperature profile which was compared to the experimental profile while the black PMMA was behaving as inert with no decomposition occurring. This will determine if using average thermal properties in the analytical model is reasonable to simulate experimental results for this material with temperature dependent properties. The average thermal properties will be taken from a temperature range of 300 to 475 K, before decomposition starts, where the material is inert. Figure 1.10 shows that the profile obtained from the analytical solution with constant H and constant, average properties does indeed match the actual profile within the experimental uncertainties for a non-decomposing real world material. The spatial experimental uncertainty of the thermocouple position is ± 0.5 mm and the uncertainty for the analytical solution is ± 10 °C from the above alumina silicate results. (The thermocouple uncertainty is ± 2 °C). Hence, this analytical approach, although not strictly correct for the physical phenomena, can be used to investigate the details of material behavior.
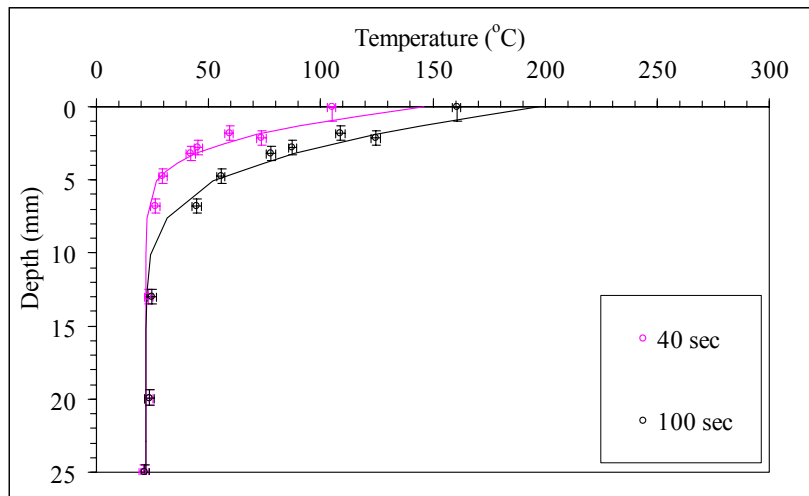
Figure 1.10   Temperature profile for thermally thick behaving black PMMA with constant properties: 15 kW/m^2 applied heat flux, No decomposition. Symbols: data, lines: analytical solution.

Using the Temperature Profile to Understand Ignition Behavior

The inert analytical solution will be used to investigate the non-linearity of the ignition plot by looking at the temperature profiles for an applied heat flux within the "linear" region (28 kW/m^2), near the "transition" region (60 kW/m^2) and well within the "non-linear" region (90 kW/m^2). These are shown in Figures 1.11 through 1.13. Note that the times shown are the time after start of applied heat flux exposure. The symbols represent the experimental data and the lines represent the analytical solution. The uncertainty of the experimental data is shown on the figures. For clarity, the ± 10 °C uncertainty of the analytical solution is not represented by the line thickness.
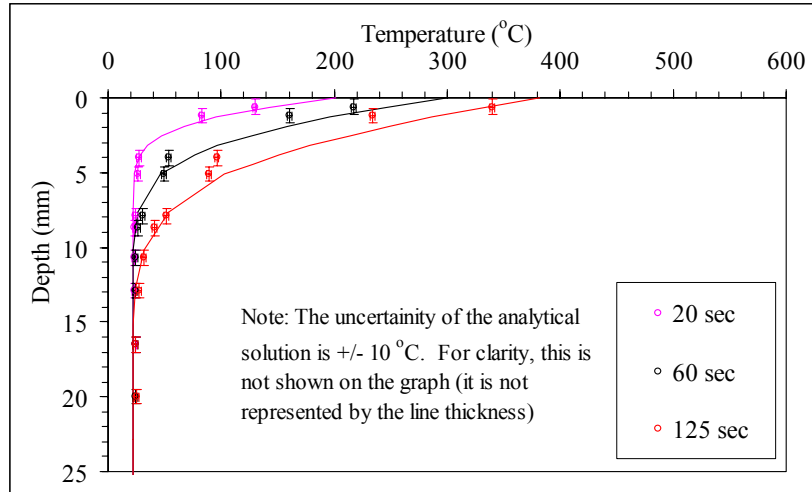
Figure 1.11   Temperature profile for thermally thick behaving black PMMA with constant

properties: 28 kW/m^2 applied heat flux, "linear" region, time to ignition = 125 sec.

Observe from Figure 1.11 that the predicted temperature profile is a match to the experimental

profile, within the uncertainty, for the 28 kW/m^2 applied heat flux "linear" region case. The

surface temperature of 380 ± 10 °C predicted by the analytical solution is within the surface

temperature of 350 ± 50 °C measured from experiments. It is interesting to note that while using

average thermal properties from a range of 20 to 200 °C that the predicted and experimental

temperatures match even up to 350 °C. This is most likely due to the 1 mm uncertainty of the

thermocouple location combined with the steep gradient of the profile near the surface.

See from Figures 1.12 and 1.13 for the "transition" and "non-linear" regions that the predicted

temperature profile is a match to the experimental profile, within the spatial uncertainty of the

thermocouples, except within 3 mm of the surface, where the surface temperatures at ignition are

predicted as 480 and 600 ± 10 °C, well above the 350 ± 50 °C observed experimentally.

23
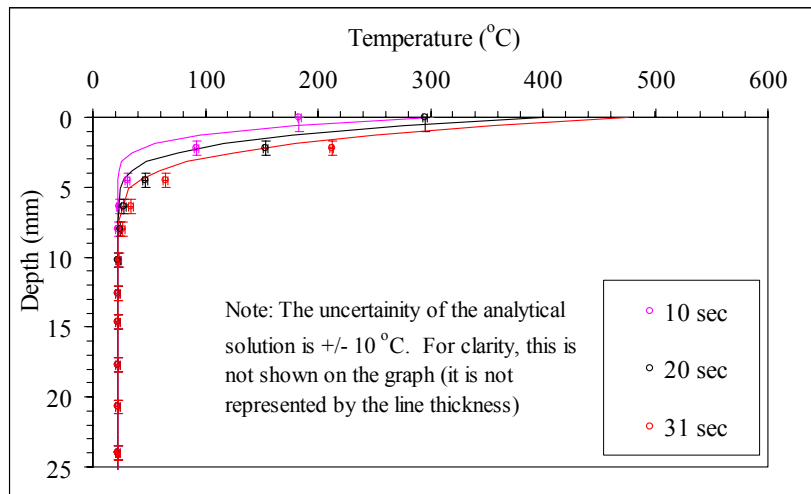
Figure 1.12   Temperature profile for thermally thick behaving black PMMA, with constant properties: 60 kW/m^2 applied heat flux, "transition" region, time to ignition = 31 sec.
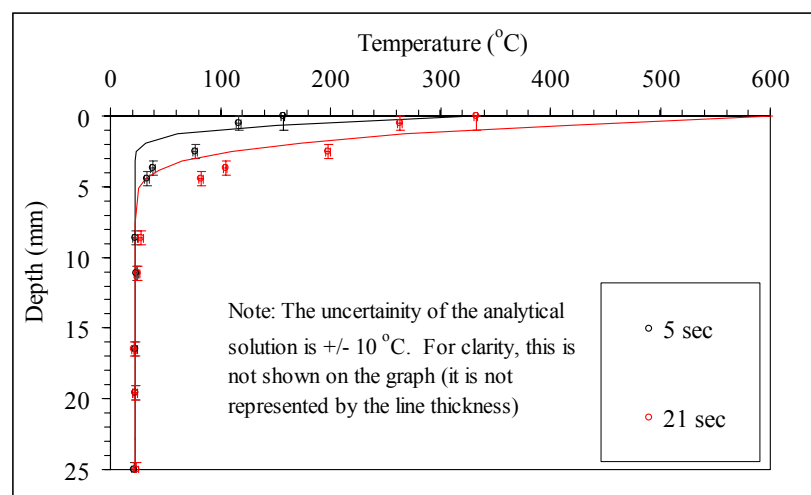
Figure 1.13   Temperature profile for thermally thick behaving black PMMA with constant properties. 90 kW/m^2 applied heat flux, "non-linear" region, time to ignition = 21 sec.

24

To address the argument that using the thermal properties at the ignition temperature would give

a closer match to the experimental values near the surface than shown in the figures, the thermal

properties at 350 °C can be used to predict the surface temperature at the experimentally observed

time to ignition. This results in predicted surface temperatures from the analytical solution shown

in Table 1.1. Recall from Figure 1.13 that the surface temperatures are high using average properties.

Table 1.1   Predicted surface temperature from the analytical solution using the experimental

obtained ignition time for that heat flux level and thermal properties at 350 °C.

Applied Flux (kW/m^2)	Predicted Surface Temperature (°C)
10	273
18.7	324
30	348
60	415
80	449
100	489
150	554
200	662

Note that up to 60 kW/m^2, the predicted surface temperature is within the uncertainty of the

experimental value of 350 ± 50 °C. Above that, the actual surface temperature starts to become

significantly different from the value predicted by the analytical solution. This explains why the

ignition data goes non-linear (has longer times to ignition) in the typical plotting method which is

25

based on an inert material solution. The ignition process at heat fluxes above 60 kW/m^2 has energy lost to something not accounted for by the inert assumption, resulting in a lower actual temperature and delayed times to ignition. Figure 1.13 is also suggestive of this: the actual temperature profiles have a lesser gradient than does the inert material predicted profiles.

Using the approach taken in this study to investigate decomposing material behavior shows that viewing ignition as an inert material process is inaccurate at predicting the surface temperature at higher heat fluxes. The investigation of thermal effects suggests that decomposition kinetics at the surface and possibly even in-depth may need to be included in an analysis of the process of ignition, especially at higher heat fluxes.

MASS LOSS FLUX RESULTS

Various checks, including the confirmation of thermally thick behavior, were conducted to confirm that the proper experimental procedure for burning tests was being performed such that the data acquired was extremely well characterized. These experimental checks are described in Appendix C and D. Mass loss data is collected during testing and a standard five point differentiation technique[5] is used to obtain mass loss flux. The mass loss flux is determined to be steady when the mass loss flux trace, as well as the CO_2 and O_2 traces, is "flat" for a significant time compared to the ignition time. For the tests in this study, this means "flat" for 200-400 seconds.

Black PMMA

Figure 1.14 shows the steady state mass loss flux vs. applied heat flux for tests done in the AFM[1] and Cone Calorimeter[5] as well as some results from Tewarson,[6] Hopkins and Quintiere.[7] The

26

typical plotting method currently used in fire protection engineering for mass loss data is used to plot the mass loss flux vs. applied heat flux. The comparability between the AFM, Cone and literature results show that the AFM is operating properly and giving results as expected for applied heat flux ranges reachable by the Cone and FPA. This provides support for the accuracy of higher heat fluxes in the AFM given that the same calibration procedures were used for the entire applied heat flux range.
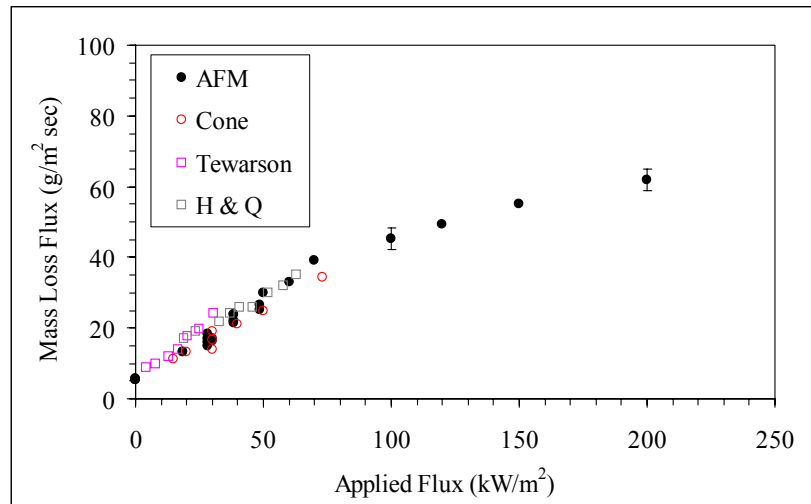
Figure 1.14   Steady mass loss flux vs. applied heat flux for thermally thick behaving black PMMA. Experimental mass loss flux uncertainty $= \pm 3$ g/m^2 sec.

Note the unexpected non-linear trend starting at around 60 kW/m^2. Characteristics, including inlet airflow, blockage of the radiant source and surface conditions, of the AFM were investigated to insure that the non-linearity was not an artifact of the apparatus.

The AFM provides inlet combustion air since the sample environment is contained within a quartz tube. The inlet flow rate ranging from 100 to 1000 lpm was found to not have an effect on

27

the mass loss flux for a specified heat flux. The stoichiometry of the combustion process was checked to insure that the combustion was not being oxygen starved, i.e., the fire was well ventilated, at the large mass loss fluxes obtained at high heat fluxes.

The possibility that the applied heat flux was blocked by the flame from reaching the surface was also investigated. A burning sample could not be used since the separation of flame heat flux and applied heat flux can not be made with certainty. Propylene gas was used (so it would have a significant amount of soot) with a 10.2 cm diameter burner in which a Schmidt-Bolter gage was embedded. The gas flow was controlled to a constant flow rate via a mass flow meter and needle valve such that any blockage of the applied heat flux by the flame could be measured. Figure 1.15 shows gage measurements from the propylene flame without and with added heat flux.
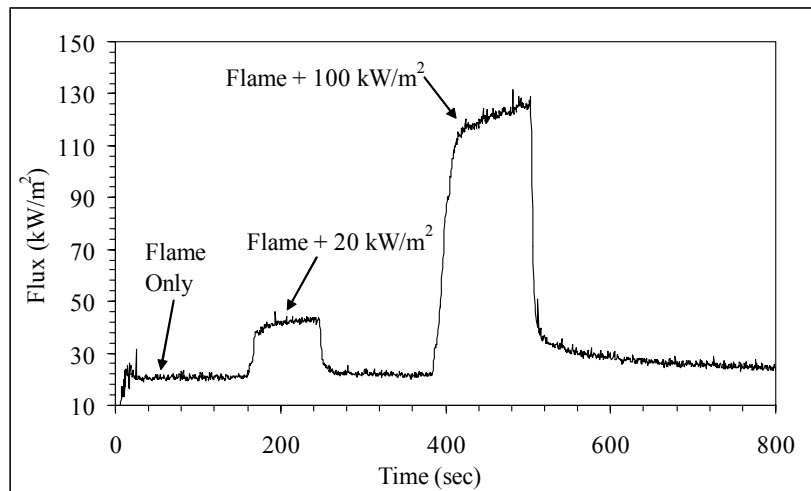
Figure 1.15   Gage measurements from propylene flame without and with applied heat flux added.

The measurements for the flame only are 20 kW/m^2, the flame plus 20 kW/m^2 applied flux is 42 kW/m^2 and the flame plus 100 kW/m^2 applied flux starts at 120 kW/m^2. Note the slight rise of the

28

"flame plus flux" signal with time for the 100 kW/m^2 case. The rise is about 6 kW/m^2 which is slightly greater than the uncertainty of the applied heat flux of ± 2 kW/m^2. It is believed that this is due to the heating up of the glass beads of the burner which increases the conductive heat transfer to the gage. This can be ignored since the initial application of the heat flux is the important item of interest and it shows no blockage of the applied heat flux by the flame. Rhodes and Quinterie[24] suggest the flame to be transparent to the radiant coil source of the Cone Calorimeter.

The possibility of a changing absorption for the different peak emission wavelengths present at various applied heat fluxes was considered during burning. The surface of a burning sample is experimentally observed to be covered with soot and as such, the absorptivity should be unity. As was seen for ignition, the applied heat flux should be absorbed for all ranges identically during combustion.

It is concluded that the unexpected non-linear trend in the mass loss flux plot is not due to specifics of the AFM apparatus including blockage of the combustion products or surface absorptivity changes with wavelength. Conditions required for plotting the data in typical engineering fashion, including 1D conduction and thermally thick behavior, have been confirmed. The non-linearity appears to be a true material response.

Other Materials

Other materials tested in the current study including Delrin, Gray PVC, pine and plywood. Delrin was "well behaved" similar to black PMMA in that it did not intumesce or char. Gray PVC

intumesced and pine and plywood charred which is behavior not addressed in the current study. As such, only Delrin mass loss flux is presented.
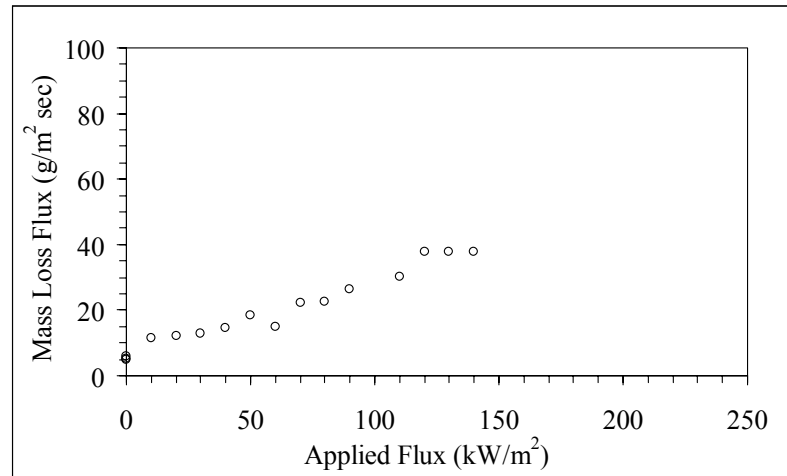
Figure 1.16   Steady mass loss flux vs. applied heat flux for thermally thick behaving Delrin. Experimental mass loss flux uncertainty $= \pm 3$ g/m^2 sec.

Figure 1.16 shows that Delrin mass loss flux data goes non-linear at approximately 110 kW/m2 applied heat flux. This is consistent with the ignition data value of 100 kW/m^2. This value is much greater than for black PMMA.

BURNING TEMPERATURE PROFILE

Before investigating the non-linearity of the mass loss flux data using the typical plotting technique, some thought needs to be given as to the basis for this technique. This technique evolved from the classic ablation problem[25] which views burning strictly as a surface process where the only energy related to the decomposition process is the heat of vaporization plus the

heat up to temperature. The assumed temperature profile in the solid comes from applying a constant temperature boundary condition at the surface. As such, the actual temperature profile in the solid during burning as well as information about any decomposition occurring in-depth would be helpful in investigating the mass loss flux results.

Figure 1.17 shows the temperature profile normalized to the regressing surface for applied heat fluxes of 28, 60 and 90 kW/m^2 as well as a 0 kW/m^2 free burn run. Note that the profiles are different from the predicted profiles and can be considered invariant with applied heat flux due to the positional uncertainty of the thermocouples of 1 mm. This comparison suggests that the ablation viewpoint of applying a constant temperature boundary condition to the solid to obtain an assumed temperature profile is inaccurate.
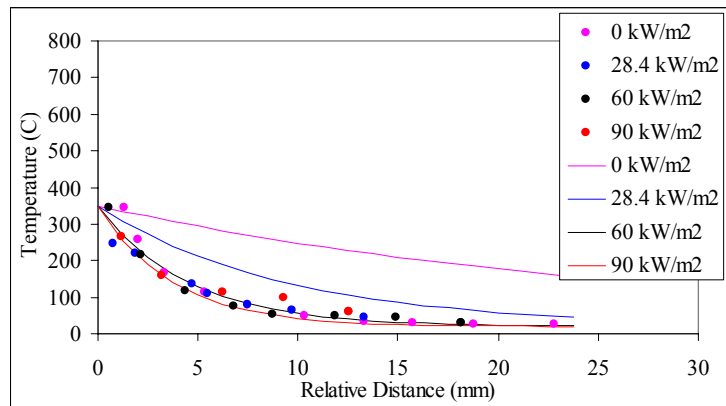
Figure 1.17   Temperature profile normalized to regressing surface for various applied heat flux for thermally thick behaving PMMA. Symbols: data, Lines: predicted.

Experimental observations, also seen by others,[26,27,28,29,30] during burning show surface "bubbling" occurring as well as some flame "jetting" which is presumably related to the bursting "bubbles". The sample was inspected after burning to obtain the depth that bubbles were formed. The size of

the bubbles and the depth of the "bubbling layer" during burning change with applied heat flux. At lower fluxes the bubbles are "large" and the depth of the bubble layer "thick." These observations indicate that in-depth decomposition is occurring, especially at the lower applied heat fluxes. As the applied heat flux increases, the bubbles get smaller (i.e., decrease in diameter) and the bubble layer gets thinner until at the highest applied heat flux in this study, the bubble size and layer depth appear to be of the same magnitude.

It can be seen from Figure 1.17 that the ablation problem temperature profile more accurately predicts the measured profile at the higher applied heat fluxes. This makes sense since the bubbling layer depth is getting very thin at the higher applied heat flux levels so that it is reasonable to consider the decomposition a surface event. However, this has interesting implications for the mass loss flux plot given in Figure 1.16. It was assumed that the linear curve fit of the data at the lower applied heat fluxes indicated that the ablation viewpoint was representing the physics accurately and that the higher heat flux results were a divergence. The temperature profiles and experimental observations of bubbling layers indicate the opposite in that the simplified ablation solution should work better at the higher applied heat fluxes and not the lower. Since the lower applied heat flux results of the mass loss flux plot are used to obtain the apparent heat of gasification, a closer look was taken at this parameter.

HEAT OF GASIFICATION

The apparent heat of gasification can be obtained from the typical plotting technique currently used in the fire protection engineering field. This plot is a representation of the energy balance

$$\dot{q}''_{flame} = \dot{q}''_{radloss} - a\dot{q}''_{applied} + \dot{m}''h_g \qquad (1\text{-}3)$$

32

where $\dot{q}''$ is heat flux, a is the surface absorptivity, usually assumed to be unity, $\dot{m}''$ is the mass loss flux and h_g is the apparent heat of gasification. The implied simplification is that the apparent heat of gasification includes only the change in the sensible and latent heat of the material. The mass loss flux data[31] as a function of applied heat flux is plotted (representing the equation) and a linear curve fit is made to the data. The inverse of the slope is interpreted as the apparent heat of gasification, h_g. This calculation of apparent heat of gasification assumes that the mass loss flux data plotted as a function of applied heat flux follows a linear curve fit for all levels of applied heat flux.

Black PMMA

As was seen in Figure 1.14, the mass loss flux data for black PMMA does not follow the expected linear trend at the higher applied heat fluxes. This presents a complication in fitting a linear curve to the data in order to find the heat of gasification. Forcing a line that fits all the data is not reasonable since the non linearity represents a true material response. Fitting a linear curve through only either the lower or higher applied heat flux levels would imply that either (i) the heat of gasification is changing with applied heat flux (rate of heating) which would only be possible if the products of decomposition change with heating rate or (ii) the ablation "surface only decomposition" viewpoint energy balance does not accurately represent the physics occurring for the entire applied heat flux range.

For the lower range of applied heat flux, the current study obtains an apparent heat of gasification value of 2.4 ± 0.2 kJ/g for black PMMA for 20.9 % ambient oxygen concentration as seen in Figure 1.18. The uncertainty comes from the variation of the linear curve fit through the experimental data. (The slope can fit differently through the data and is bounded. The uncertainty comes from this

variation and not from a regression analysis.) This current value is also found by other literature[7,24,32,33] sources, however, Tewarson's historical data, using a FPA, gives an apparent heat of gasification of 1.6 ± 0.2 kJ/g for 20.9 % ambient oxygen concentration.
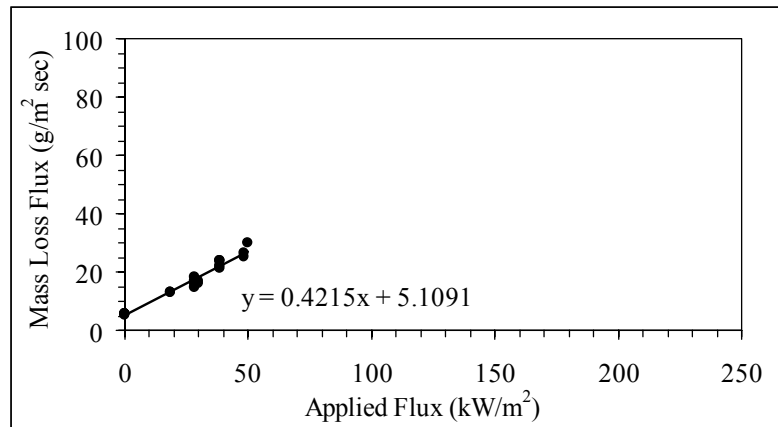
Figure 1.18   Linear region steady mass loss flux vs. applied heat flux for thermally thick behaving PMMA in a 20.9 % oxygen atmosphere. Experimental mass loss flux uncertainty = ± 3 g/m^2 sec.

Agrawal and Atreya[34] use a Cone Calorimeter and give a value of 1.6 kJ/g for the apparent heat of gasification but close inspection of their data traces shows that they are using the peak mass loss flux and not the steady state value which is indicative of thermally thick behavior. Using their steady state values for the mass loss flux gives an apparent heat of gasification of 2.2 kJ/g. Magee and Reitz[35] conduct steady burning experiments at applied heat flux levels up to 15 kW/m^2 and obtain an apparent heat of gasification of 1.7 kJ/g.

The typical plotting method currently used in fire protection engineering implicitly assumes that

the sample surface absorptivity is equal to 1 by virtue of its abscissa being the applied heat flux and not the absorbed heat flux. For luminous flames where soot is observed to be on the sample surface, this assumption is valid, however, tests were also conducted with a coating of carbon black as a check. The apparent heat of gasification values were unchanged.

The typical plotting method also assumes that the flame heat flux is constant, otherwise the axis would be the applied heat flux plus the flame heat flux. This assumption is found to be true from measurements in the current study, however, an additional look should be taken at the data in a nitrogen atmosphere, where there will be no flame nor oxygen. The results are shown below.
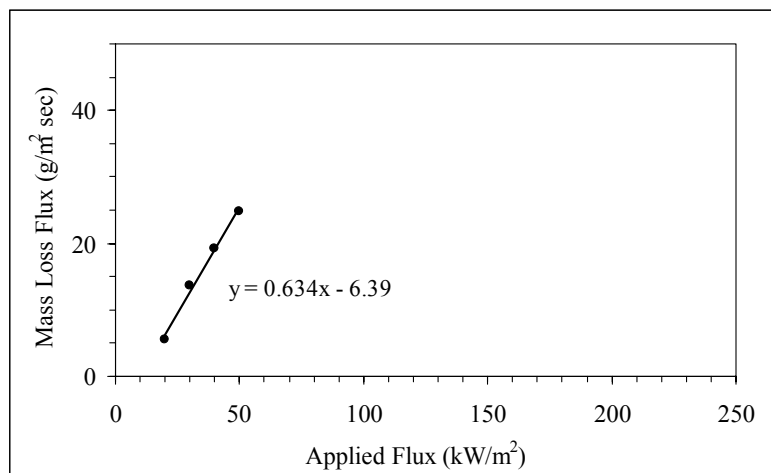
Figure 1.19   Linear region steady mass loss flux vs. applied heat flux for thermally thick behaving PMMA in a nitrogen atmosphere. Experimental mass loss flux uncertainty $= \pm 3$ g/m^2 sec.

It is seen from this plot, that the apparent heat of gasification from pyrolysis data conducted in a nitrogen atmosphere, 1.6 kJ/g, is different than the 2.4 kJ/g obtained for steady burning in an

atmosphere containing 20.9 % oxygen shown in Figure 1.18. Interestingly the nitrogen pyrolysis value matches DSC measurements conducted by a third party. They obtain a heat of vaporization value of 0.9 kJ/g for a heating rate of 100 °C/min which leads to a heat of gasification of 1.6 kJ/g (No uncertainty is given by the provider). This heating rate is the average of what is obtained in AFM, FPA and Cone steady burning tests for applied heat flux levels up to 60 kW/m^2. Note that DSC tests are normally conducted in a nitrogen atmosphere but this study also had DSC tests run with a 20.9 % oxygen atmosphere giving 0.9 kJ/g for the heat of vaporization at a 100 °C/min heating rate, which leads to a heat of gasification of 1.6 kJ/g. Vovelle, Akrich and Delfau[36] did pyrolysis experiments with 10 cm samples in both nitrogen and air environments for applied heat fluxes up to 30 kW/m^2. They obtained an apparent heat of gasification of 1.6 kJ/g in both cases.

As seen above, the heat of gasification obtained from steady burning experiments is different than that obtained from pyrolysis experiments. It is likely the presence of the flame and not simply the oxygen that makes the difference. However, the work of Magee and Reitz[35] contradict this. It is debatable if the oxygen presence by itself or the flame is the underlying cause of the difference.

From a more practical angle, the question arises as to which heat of gasification is the proper one to use in models. First, one must decide if (i) there is only one heat of gasification that does not change with heating rate, or (ii) it changes with heating rate. A change in the heat of gasification with heating rate implies that the products of decomposition are changing with heating rate and this would need to be incorporated into the energy balance.

If one adopts the viewpoint that there is to be only one heat of gasification that does not change with heating rate, then a decision needs to be made to use either the value obtained from pyrolysis tests or burning tests. If the value obtained from the DSC, which is usually considered the

"correct" and "fundamental" value, is used then the ablation solution energy balance is too simplified to represent the physics occurring for steady burning for any applied heat flux since it does not obtain this value. If one uses the steady burning value, then the energy balance is reasonable to apply at the lower fluxes but would need to be modified to be able to predict the higher applied heat flux results. Related work presented in Chapter 2 Figure 2.14 shows that the apparent heat of gasification obtained from steady burning tests can be a practically useful parameter when used to obtain large scale results of flame heat flux whereas the DSC value could not.

Delrin

The mass loss flux data was used to calculate the heat of gasification using the same technique presented for black PMMA. The heat of gasification from the linear portion of the data is 4.8 ± 0.5 kJ/g as seen in Figure 1.20. Hirsch, Beeson and Friedman[37] obtain a value of 4.0 kJ/g in a 22.0 % oxygen atmosphere. Tewarson's historical data gives a value of 2.4 ± 0.5 kJ/g.
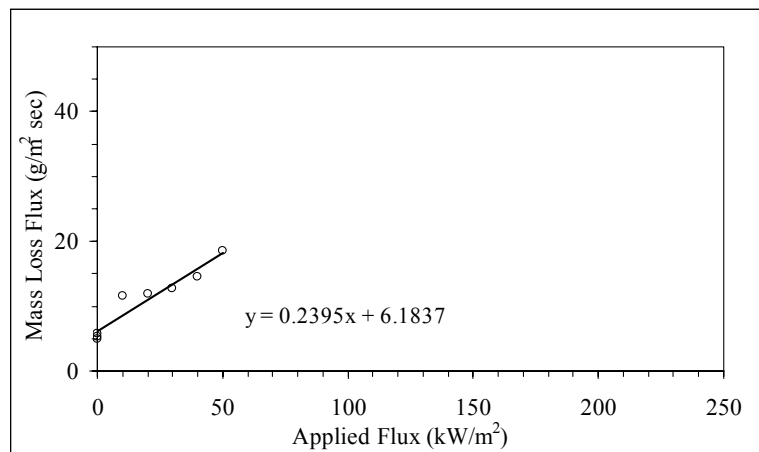
Figure 1.20   Linear region steady mass loss flux vs. applied heat flux for thermally thick behaving Delrin in a 20.9 % oxygen atmosphere. Experimental mass loss flux uncertainty = ± 3 g/m^2 sec.

For the non luminous flame produced by Delrin, which essentially has no soot, the assumption of surface absorptivity equal to 1 is not strictly valid. The solid sample absorptivity is most likely not the right choice either since the surface is actually a "bubbling layer" consisting of translucent bubbles and liquid "melt." As such, the actual absorptivity is not known. A solution to this is to put a coating of carbon black on the surface to force its absorptivity to 1. Interestingly, no difference was seen in the mass loss flux data for Delrin using a carbon black coating, hence the apparent heat of gasification is unchanged. Nitrogen atmosphere tests were also conducted for Delrin and the results are shown in Figure 1.21.
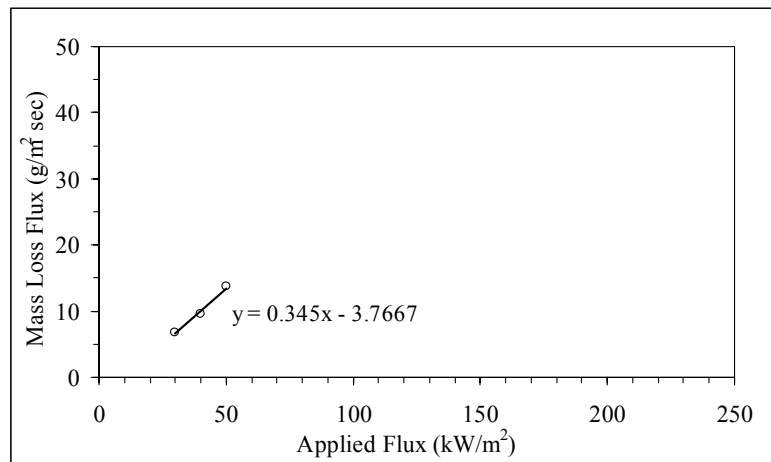
Figure 1.21   Linear region steady mass loss flux vs. applied heat flux for thermally thick behaving Delrin in a nitrogen atmosphere. Experimental mass loss flux uncertainty $= \pm 3$ g/m^2 sec.

It is seen from this plot, that the apparent heat of gasification from pyrolysis data conducted in a nitrogen atmosphere, 2.4 kJ/g, is different than the 4.8 kJ/g obtained for steady burning in an atmosphere containing 20.9 % oxygen shown in Figure 1.20. Similarly as raised for black PMMA, it is debatable if the presence of the oxygen by itself or the flame is the underlying cause.

MOVING FORWARD

It has been shown that the testing conditions are not the cause for the non linearity of the ignition data. Viewing ignition as an inert material process is inaccurate at predicting the condensed phase temperature profiles at higher applied heat fluxes. The investigation of thermal effects suggests that decomposition kinetics at the surface and possibly even in-depth may need to be included in an analysis of the process of ignition, especially at higher heat fluxes.

It appears that the "typical technique" energy balance, which evolved from the classic ablation problem, is too simplified to represent the physics occurring for all range of applied heat flux. Hence, a new energy balance needs to be developed and two items provide insight into a possible direction, (i) the measured temperature profile and (ii) the observations of the surface and in-depth bubbling behavior. As such, the control volume given by Figure 1.22 is presented that includes an energy term for this process.
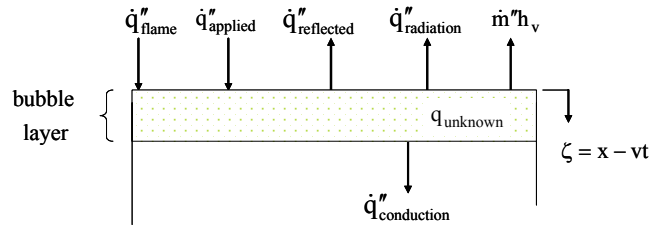
$$\dot{q}''_{flame} = \dot{q}''_{radloss} - a\dot{q}''_{applied} + \dot{m}''h_g + \dot{q}''_{unknown}$$

Figure 1.22   Bubble zone control volume and energy balance.

Further work is needed to determine what the $\dot{q}''_{unknown}$ term should be. This term, for polymers,

could be related to (1) transport limitations of the in-depth bubbles or (2) effect of bubbling/melting layer on aborptivity and conduction, (3) an effect of oxygen reacting with the solid sample, (4), a difference in decomposition products due to heating rate (5) presence of flames or (6) some combination of these.

Launtergerber and Fernandez-Pello[38] have developed a closed form solution for the mass loss flux of a thermally thick material irradiated by an external applied heat flux. They use a critical mass loss flux as the ignition criteria to attempt to recreate the non-linear trend of the ignition data presented in this paper. Their resultant formula is the same as the classical thermal ignition theory with an important difference of a non constant surface temperature at ignition. Since they are unable to simulate the data, they state that the analysis presented is missing some physics of the problem. They put forward several possible explanations that include those suggested in the current paper. Others are also looking at these possibilities as described below.

Kashiwagi[29] states that transport of the subsurface degradation products (i.e., bubbles) might be the controlling factor in mass loss of a sample especially at high heating rates. He claims it is clear that subsurface degradation is important for gasification of a sample but it is not clear what the main transport process is. The role of bubbles and of oxygen in the gasification process must be clearly understood. If the gasification is affected by the bubbles, then the transport of the bubbles through the polymer to the sample surface must also be understood.

Olsen and Tien[28] say that it is important to understand the behavior of the near surface layer since it plays a significant role in the vaporization process. Also that the in depth formation and diffusion are the rate controlling item in the vaporization process. They did tests at low heating

rates for PMMA and focused on the solid phase and show that a two phase layer at the burning surface has been found repeatedly consisting of a solid, molten layer and then a two phase bubble layer.

Shlenskii[39] did a study to determine the rate of thermal destruction (i.e., mass loss flux) of a material under intense heating rates and concluded that the processes of nucleation, secondary pore formation (i.e., bubbles) and the reasons for their occurrence affect the rate of thermal destruction. Shlenskii[40] also found that "the deviation of the thermal decomposition rate of a material from the Arrhenius dependence at high intensity heating of the material surface is caused by structural variations near the phase state boundary." This means that the structure of the solid near the surface (i.e., a bubbling/melting layer) is an important contributor to the mass loss flux.

Hertzberg and Zlochower[41] studied PMMA exposed to a laser beam at incident flux levels of 15 – 500 W/cm^2. They have photographic data that reveal the bubble structure within the PMMA which is consistent with the current study. "The observed bubble shapes and bubble locations also suggest the increasing significance of mass transport limitations at low driving fluxes and the absence of such limitations at high fluxes." Their data supports the argument that the applied heat flux is the driving force for decomposition and not the surface temperature. At low fluxes, the temperature gradients are not very steep so more of the pyrolysis process occurs further removed from the surface and mass transport limitations become significant.

Vovelle et al.[42] looked at PMMA both experimentally and numerically and found that "a contribution of the subsurface region of the sample to the rate of gasification must be taken into account in a thermal degradation model."

Wichman[26] studied the gasification of thermoplastics including PMMA and PE in response to an

applied heat flux and found that the external flux liquefies a region near the surface of the sample, allowing the nucleation of bubbles that grow and transport volatile gases to the surface by moving through this molten layer.

Chen et al.[30] suggest that emphasis be placed on the formation, transportation and combustion mechanism of the bubble layer and oxygen diffusion into it to fully understand the combustion process of noncharring materials.

Cullis[43] presents experimental evidence from several different types of measurements for the involvement of oxygen in solid phase polymer degradation. Zhou and Fernandez-Pello[44] develop a numerical model for pyrolysis and ignition delay of composite materials exposed to an external heat flux which takes into account surface oxidative pyrolysis.

Dakka, Jackson and Torero[45] studied degradation of PMMA in both nitrogen and oxygenated atmospheres and conclude that mass transport limitations, which are indicated by evolved gas profiles, and that oxygen transport into the material must be included in a proper analysis of piloted ignition.

Zeng, Li and Chow[27] found that the decomposition of PMMA in air was different from those in nitrogen. Gao et al.[46] investigated the degradation process of PMMA and claim that the initiation of degradation may be sensitive to heating rate.

SUMMARY AND CONCLUSIONS

An unexpected non-linear trend is observed in the typical plotting method currently used in fire

protection engineering for ignition and mass loss flux data for several materials tested in the AFM. There also exist literature results showing the same non-linear trend as the current study. The non-linearity is not related to the AFM apparatus.

The temperature profile predicted by the analytical solid, 1D conduction solution for an inert material with semi-infinite behavior and constant applied heat flux and constant thermal properties gives a good match, within the uncertainty, to the experimental profile for alumina silicate, which is truly inert, and black PMMA with inert behavior. Hence, an analytical approach, although not strictly correct for the physical phenomena, can be used to investigate the details of the solid material behavior during the ignition and burning process. Using this approach to investigate decomposing material behavior shows that viewing ignition as an inert material process is inaccurate at predicting the surface temperature at higher heat fluxes. This analysis of thermal effects suggests that decomposition kinetics at the surface and possibly even in-depth may need to be included in an analysis of the temperature profile and the process of ignition. This is further evidenced by the results of investigating burning behavior using the temperature profile obtained during burning.

The black PMMA apparent heat of gasification value of 2.4 ± 0.2 kJ/g calculated from small scale mass loss flux data does not match the value of 1.6 ± 0.2 kJ/g obtained from DSC measurements, which is commonly considered "correct" and "fundamental." The Delrin apparent heat of gasification value of 4.8 ± 0.5 kJ/g calculated from mass loss flux data does not match the value of 2.4 ± 0.5 kJ/g obtained from Tewarson and DSC measurements. Small scale pyrolysis tests conducted in a nitrogen atmosphere obtain approximately 1.6 kJ/g and 2.4 kJ/g for black PMMA and Delrin respectively which match DSC measurements from both nitrogen and air atmospheres.

It appears that the "typical technique" energy balance is too simplified to represent the physics occurring for all range of applied heat flux since the non-linearity is not captured nor is the commonly considered "correct" apparent heat of gasification. Hence, a new energy balance needs to be developed and a possible direction would focus on the in-depth bubbling behavior.

REFERENCES

1   Beaulieu, P., Dembsey, N., and Alpert, R., "A New Material Flammability Apparatus and Measurement Techniques," Composites 2003, Anaheim, CA, 2003.

2   Croce, P., "The Forum for International Cooperation on Fire Research," Fire Safety Journal, 36, p. 715-717, 2001.

3   <u>Handbook of Fire Protection Engineering</u>, 2nd edition, "Chapter 3-4, Generation of Heat and Chemical Compounds in Fires," Society of Fire Protection Engineers, Boston, MA, 1995.

4   Standard Test Methods for Measurement of Synthetic Polymer Material Flammability Using a Fire Propagation Apparatus, ASTM E 2058, American Society of Testing Materials, Philadelphia, PA, 2001.

5   ASTM Standard Method for Heat and Visible Smoke Release Rates for Materials and Products Using an Oxygen Consumption Calorimeter, ASTM E 1354, American Society of Testing Materials, Philadelphia, PA, 1999.

6   Tewarson, A., and Ogden, S., "Fire Behavior of PMMA," Combustion and Flame, 89, p. 237-259, 1992.

7   Hopkins, D., and Quintiere, J., "Material Fire Properties and Predictions for Thermoplastics," Fire Safety Journal, 26, p. 241-268, 1996.

8   Hallman, J., "Ignition Characteristics of Plastics and Rubber," PhD Dissertation, University of Oklahoma, Norman, OK, 1971.

9   Piloted Ignition of Solid Materials Under Radiant Exposure, An Engineering Guide, p.30, Society of Fire Protection Engineers, Boston, MA, 2002.

10   Principles of Fire Behavior, p. 75, Quintiere, J., Delmar Publishers, Albany, NY, 1998.

11   Conduction in Solids, 2nd edition, Carslaw, H.S., and Jaeger, J.C, "Chapter 2-8 Semi-Infinite Solid," Oxford University Press, Oxford, 1959.

12   Lawson, D. and Simms, D., "The Ignition of Wood by Radiation," British Journal of Applied Physics, 3, p. 288-292, 1952.

13   Tewarson, A., Factory Mutual Research Technical Report # JI 1A6R1.RC, FM Global Research, Norwood, MA, 1979.

14   Mikkola, E., and Wichman, I., "On the Thermal Ignition of Combustible Materials," Fire and Materials, 14, p. 87-96, 1989.

15   Janssens, M., "Improved Method of Analysis for The Lift Apparatus, Part 1:Ignition," Proceedings of the 2nd Fire and Materials Conference, p. 37-46, 1993.

16   Mowrer, F., "An Analysis of Effective Thermal Properties of Thermally Thick Materials," Fire Safety Journal, 40, 5, p. 395 – 410, July 2005.

17   Quintiere, J. and Harkleroad, M., "New Concepts for Measuring Flame Spread Properties," Fire Safety: Science and Engineering, ASTM STP 882, American Society for Testing and Materials, Philadelphia, p. 239 – 267, 1985.

18   Janssens, M., "Fundamental Thermophysical Characteristics of Wood and Their Role in Enclosure Fire Growth," PhD dissertation, University of Gent, Belgium, 1991.

19   <u>Manufacturers Catalog</u>, Cotronics Corporation, Brooklyn, NY, 2001.

20   Putnam, S., Cahill, D., Ash, B and Schadler, L., "High Precision Thermal Conductivity Measurements as a Probe of Polymer/Nanoparticle Interfaces," 2003.

21   <u>Polymers: A Property Database (Online CD)</u>, CRC Press, 2000.

22   <u>Handbook of Fire Protection Engineering</u>, 2nd edition, "Chapter 3-4, Generation of Heat and Chemical Compounds in Fires," Society of Fire Protection Engineers, Boston, MA, 1995.

23   Cordova, J., Fernandez-Pello, A., "Convection Effects on the Endothermic Gasification of a Radiatively Heated Combustible Solid," Combustion Science and Technology, 156, p. 271-289, 2000.

24   Rhodes, B., and Quintiere, J., "Burning Rate and Flame Heat Flux for PMMA in a Cone Calorimeter," Fire Safety Journal, 26, p. 221 – 240, 1996.

25   <u>Heat Transfer</u>, Holman, J., McGraw Hill Book Company, New York, NY, p. 622-624, 1986.

26   Wichman, I., "A Model Describing the Steady State Gasification of Bubble Forming Thermoplastics in Response to an Incident Heat Flux," Combustion and Flame, 63, p. 217 – 229, 1986.

27   Zeng, W., Li, S. and Chow, W., "Review on Chemical Reactions of Burning PMMA," Journal of Fire Sciences, 20, p. 401 – 433, 2002.

28   Olsen, S. and Tien, J., "Near Surface Vapour Bubble Layers in Buoyant Low Stretch Burning of PMMA," Fire and Materials, 23, p. 227 – 237, 1999.

29   Kashiwagi, T., "Polymer Combustion and Flammability – Role of the Condensed Phase," 25th Symposium (International) on Combustion, p. 1423 – 1437, 1994.

30   Chen, C, Yao, B., Weicheng, F and Liao, G., "A Comparative Experimental Study on Heat Release Rates of Charring and Noncharring Solid Combustible Materials," Journal of Fire Sciences, 21, p. 369-380, 2003.

31   <u>Handbook of Fire Protection Engineering</u>, 3rd edition, "Chapter 3-2, Calorimetry," Society of Fire Protection Engineers, Boston, MA, 2002.

32   de Wilde, J., "The Heat of Gasification of Polyethylene and Polymethylmethacrylate," Prins Maurits Laboratory Report PML 1988-C42, Delft University of Technology, Netherlands, 1988.

33   Rhodes, B., "Burning Rate and Flame Heat Flux for PMMA in the Cone Calorimeter," M.S. Thesis, University of Maryland, 1994.

34   Agrawal, S. and Atreya, A., "Wind Aided Flame Spread Over an Unsteady Vaporizing Solid," 24th International Symposium on Combustion, p. 1685 – 1693, 1992.

35   Magee, R. and Reitz, R., "Extinguishment of Radiation Augmented Fires by Water Sprays," Proceedings of the Combustion Institute, 15, p. 237 – 247, 1974.

36   Vovelle, C., Akrich, R. and Delfau, J., "Mass Loss Rate Measurements on Solid Materials Under Radiative Heating," Combutsion Science and Technology, 36, p. 1-18, 1984.

37   Hirsch, D., Beeson, H, and Friedman, R., "Microgravity Effects on Combustion of Polymers," NASA Report 209900-2000, Houston, TX, 2000.

38   Launterberger, C. and Fernandez-Pello, C, "Approximate Analytical Solutions for the Transient Mass Loss Rate and Piloted Ignition Time of a Radiatively Heated Solid in the

High Heat Flux Limit," Fire Safety Science – Proceedings of the Eighth International Symposium, p. 445, 2005.

39   Shlenskii, O., "An Effect of Nucleation Processes on the Thermal Destruction Rate of Materials Under Intense Thermal Actions," Doklady Physics, v. 46, 5, p. 317 – 320, 2001.

40   Shlenskii, O., "An Effect of Structural Variations on the Decomposition of Materials Under High Intensity Thermal Actions," Doklady Physics, v. 46, 10, p. 701 – 704, 2001.

41   Hertzberg, M. and Zlochower, I., "Devolatilization Wave Structures and Temperatures for the Pyrolyis of PMMA, Ammonium Perchlorate and Coal at Combustion Level Heat Fluxes," Combustion and Flame, v. 84, p. 15 – 37, 1991.

42   Vovelle, C., Delfau, J., Reuillion, M, Bransier, J. and Laraqui, N., "Experimental and Numerical Study of the Thermal Degradation of PMMA," Combustion Science and Technology, 53, p. 187 – 201, 1987.

43   Cullis, C., "The Involvement of Oxygen in the Primary Decomposition Stage of Polymer Combustion," Fire Safety Science – Proceedings of the First International Symposium, p. 371.

44   Zhou, Y. and Fernandez-Pello, C., "Numerical Modeling of Endothermic Pyrolysis and Ignition Delay of Composite Materials Exposed to An External Radiant Heat Flux," Proceedings of the Combustion Institute, 28, p. 2769, 2000.

45   Dakka, SD., Jackson, G. and Torero, J, "Mechanisms Controlling the Degradation of PMMA Prior to Piloted Ignition," Proceedings of the Combustion Institute, 29, p. 281, 2002.

46   Gao, Z., Kaneko, T., Hou, D. and Nakada, M., "Kinetics of Thermal Degradation of PMMA Studied with the Assistance of the Fractional Conversion at the Maximum Reaction Rate," Polymer Degradation and Stability, 84, p. 399 – 403, 2004.

CHAPTER 2: EFFECT OF OXYGEN ON FLAME HEAT FLUX IN THE HORIZONTAL ORIENTATION

ABSTRACT

This Chapter documents the horizontal orientation of the second of two interrelated studies that were conducted to more fundamentally understand the scalability of flame heat flux while Chapter 3 documents the vertical orientation. The key aspect of this study was direct experimental measurements of flame heat flux back to the burning surface for 20.9 to 40 % ambient oxygen concentrations. The main conclusion is that the total flame heat flux in enhanced ambient oxygen does not simulate large scale flame heat flux in the horizontal orientation.

The Advanced Flammability Measurements Apparatus was used to conduct small scale horizontal orientation experiments for black PMMA, propylene and Delrin. The key aspect of this study was direct experimental measurements of flame heat flux back to the burning surface for 20.9 to 40 % ambient oxygen concentrations. The total flame heat flux, as well as the radiative and convective components, was experimentally measured with various gages. To gain more insight into the effects of oxygen, the flame emissivity, flame height and flame temperature were obtained and used to calculate the radiative and convective components of the flame heat flux. These were also used to calculate the radiative and convective components of the flame heat flux. Horizontal gas burner experiments were conducted to decouple the solid and gas phase effects of the ambient oxygen. Large scale tests of black PMMA were conducted and used for comparison to the small scale, enhanced oxygen results.

INTRODUCTION

It is commonly[1] thought that enhanced oxygen increases the flame heat flux which in turn controls the heat release rate and flame spread. The complete details and quantification of the effect remain unanswered since various researchers have studied the effect of ambient oxygen concentration on a small range of materials with assorted and sometimes opposite results as seen in a literature review given in Appendix A. There have not been systematic experimental measurements to directly quantify the increase in the flame heat flux at small scale. Hence, a systematic empirical and analytical study of the effect of ambient oxygen concentration was conducted to directly quantify the effect of increased ambient oxygen concentration on flame heat flux at small scale.

The Advanced Flammability Measurements Apparatus[2] (AFM) was used to conduct small scale experiments at ambient oxygen concentrations of 20.9 to 40 % oxygen for various materials. Black polymethylmethacrylate (PMMA) and polyoxymethylene (Delrin) were chosen since they are "well behaved" materials that do not intumesce. The total flame heat flux, as well as the radiative and convective components, was experimentally measured with various gages. As an internal consistency check, the mass loss flux and surface temperature were measured and used to calculate the flame heat flux via a commonly used technique. To gain more insight into the effects of ambient oxygen, the flame emissivity, flame height and flame temperature were obtained.

Horizontal gas burner experiments were conducted to decouple the solid and gas phase effects of the ambient oxygen. The total flame heat flux, as well as the radiative and convective

51

components, was experimentally measured with various gages. The flame emissivity, flame height and flame temperature were obtained and used to calculate the radiative and convective components of the flame heat flux in the same manner as was done for PMMA.

Large scale tests of black PMMA were conducted to obtain flame heat flux measurements which were used for comparison to the small scale, enhanced oxygen results to determine the level of scalability that enhanced oxygen provides, i.e., the relationship of enhanced oxygen small scale experiments to fires occurring at larger scale.

BACKGROUND

Mechanical and chemical properties are usually used to choose a suitable material system for a given application. However, the fire performance of this system is also needed by designers and engineers to help design active protection systems that would control the fire and minimize damage if the system ignites. Alternatively, if no active protection system is to be used, selection of another appropriate material system for the application would be prudent based on ignitability and flame spread parameters.

There are two basic approaches to determine the fire performance of materials in realistic scenarios. The first is to conduct a large scale evaluation and obtain the results directly. The second is to conduct small scale experiments to obtain material flammability parameters for ignition and combustion. Use of material flammability parameters obtained from these small scale experiments can then be used in conjunction with "first principle" mathematical models[3] or calculation procedures to estimate full scale performance. Of the two basic approaches, the

52

second is more desirable from a practical viewpoint, since it is more versatile and time and cost efficient.[4] However, for a flammability parameter obtained from small scale experiments to be considered a true material "property" independent of apparatus or scale, the same value must be obtained in various scale tests.

Review of Tewarson

The Flame Radiation Scaling Technique[5] was developed by Tewarson to obtain large scale flame heat flux values from small scale tests. The technique basically consists of conducting a small scale experiment with an enhanced oxygen atmosphere, measuring the mass loss flux and calculating the total flame heat flux using a surface energy balance. Tewarson found that as the ambient oxygen concentration of the small scale test was increased above 20.9 %, the calculated flame heat flux would reach an asymptotic limit comparable to the limit found in large scale fires. Hence, "variation of oxygen concentration values in small scale fires to simulate flame heat flux values, expected in large scale fires, is defined as the Flame Radiation Scaling Technique.[5]

An initial step of this investigation was to duplicate the historical data of Tewarson[6] on the effect of enhanced ambient oxygen concentration on flame heat flux since it is well accepted by the fire science community. This was attempted for black PMMA, however the results were not reproducible and no literature data was found that duplicated Tewarson's results. The present study had very repeatable results so the historical Tewarson data was investigated further. Investigation of the original Tewarson documentation[7] shows a drawing of the sample holder used which is reproduced in Figure 2.1. Note that this holder design allows the sample to have exposed sides, which will burn in addition to the sample top when subject to a radiant flux.
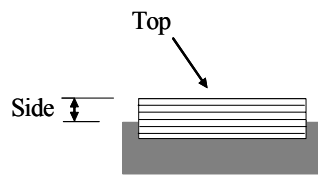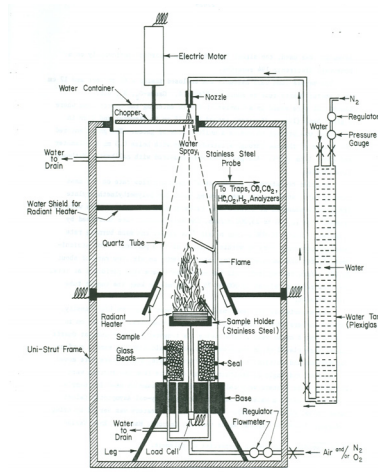
Figure 2.1   Sample holder for Tewarson historical data.

This burning pattern was confirmed by running tests in the current study with a Replicated Sample Holder (RSH) where the exposed sides as well as the sample top did indeed burn. This is shown in Figure 2.2.
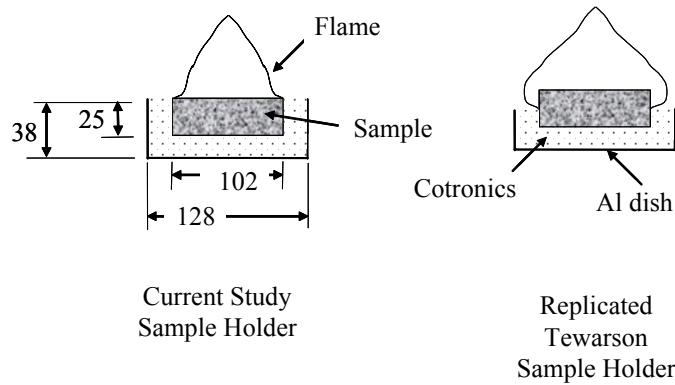
Figure 2.2   Burning area pattern for sample holder type. Measurements in mm.

The experimentally measured mass loss rate needs to be converted to a mass loss flux using the actual area of the sample that is burning. For a sample in the RSH, this "actual burning" area would be the top plus the exposed sides as shown in Figure 2.2. The area value used by Tewarson was not given so it was questioned if he used the top area only instead of the "actual burning" area.
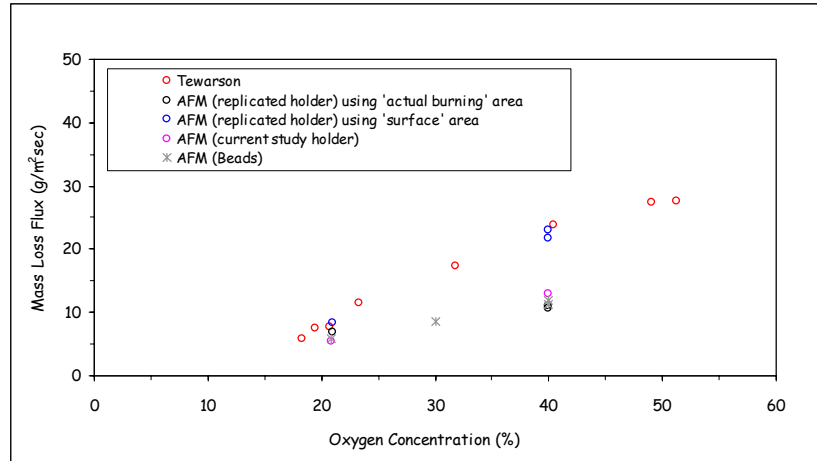
Figure 2.3   Mass loss flux for free burn black PMMA as a function of oxygen concentration

Figure 2.3 shows the historical Tewarson results of a change in mass loss flux from 7.7 to 23.8 g/m^2sec as the oxygen concentration is increased from 20.9 to 40 %. These were for free burn conditions (no applied heat flux) of thermally thick behaving samples with a physical thickness of 2.5 cm. Also shown is the mass loss flux that is calculated using the top area only instead of the "actual burning" area of the RSH tests of the current study. These values change from 8 ± 1 g/m^2sec to 24 ± 1 g/m^2sec as the ambient oxygen concentration is increased from 20.9 to 40 %. The mass loss flux that is calculated using the "actual burning" area of the RSH tests is 5.5 ± 1 g/m^2sec to 11 ± 1 g/m^2sec. The current study holder tests show the mass loss flux changing from 5.8 ± 1 g/m^2sec to 12 ± 1 g/m^2sec as the ambient oxygen concentration is increased from 20.9 to

40 %. These results support the assumption that Tewarson used just the top area and not the "actual burning" area of the sample to get the mass loss flux from the experimentally measured mass loss rate. Tewarson's "interpretation" of the historical data gives the appearance that oxygen has a much larger effect on the horizontal burning behavior than actually occurs for black PMMA.

EXPERIMENTAL RESULTS FOR BLACK PMMA

Measurements obtained for horizontal orientation steady state burning of 25 mm thick, thermally thick behaving, black PMMA include visual observations of flame structure and brightness, total flame heat flux, radiative flame heat flux, convective flame heat flux, mass loss flux, surface temperature, flame height, flame emissivity and flame temperature.

Visual Observations

Visual observations show turbulent flame characteristics which is evidenced by multiple flame sheets, eddies and wrinkles. The addition of oxygen resulted in an increase in the brightness of the flame indicating increased soot and/or temperature (which would result in an increased emissive output). A more pronounced smoke mantel is observed as well as a slightly shorter flame height for the 40 % concentration. Copious amounts of soot were observed going up the exhaust stack for the 40 % ambient oxygen concentration. The 20.9 % ambient oxygen concentration showed very little soot by comparison. In both cases, soot is seen on the sample surface post test indicating it is there during burning.

Bubbling of the sample surface is observed visually for both the 20.9 and 40 % oxygen

concentration. The bubble size and "bubble zone" depth decrease as the heating rate (i.e., the applied heat flux) increases. The "bubble zone" is determined by measuring the depth of bubble formation after the test when the sample has cooled.

Total Flame Heat Flux

Commercially available Schmidt-Boelter heat flux gages[8] of different sizes from 6 mm to 25 mm diameter were used to measure the "total" flame heat flux back to the burning surface during heat up, ignition and burning. "Total" is defined as the sum of the radiative and convective components of the flame heat flux. (This is not the "net" flame heat flux which is defined as the difference between the total flame heat flux and the radiative heat flux loss from the sample surface.) As per Figure 2.4, the gage face was placed flush with the sample surface. A 3 mm thick thermal ceramic insulation[9] was used between the gage and the sample to hold the gage in place.
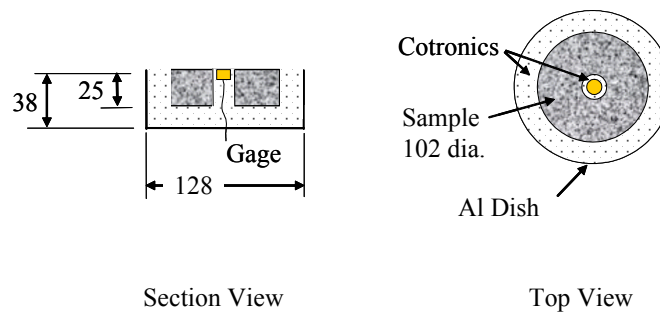
Figure 2.4   Experimental setup for heat flux gage. Measurements in mm.

The gage was cooled with 65 °C water during the test to prevent condensation from forming on the gage face and to prevent distortion of the sample. (Distortion of the sample occurred when "cold" water was used for cooling the gage.) Any convection change due to the high temperature

57

of the ceramic insulation is neglected since the area is a very small fraction of the total surface area. Also neglected is any conduction to the gage from the ceramic paper and angular effects of the incoming radiation. Since this is a "cold" gage, the flame heat flux value is simply the reading of the gage.

Thin film heat flux gages, sometimes called Micro-foil heat flux sensors[10] were also used to measure the total flame heat flux. They function as a self-generating thermopile transducer with low thermal impedance that measures heat flux by differentiating temperature between opposite sides of a certain material. The gages used are polyimide film bonded using a Teflon lamination process and are 0.18 mm thick. The gages are placed in a sample as shown in Figure 2.5. The output wires are slightly thicker than the gage itself and are placed outside the sample edge. These embedded thin film heat flux gages measure conduction into the solid until the regressing surface reaches the level of each gage. The gage then becomes exposed and very quickly is coated with soot. The gage moves with the regressing surface, giving a "hot gage" flame heat flux reading. As such, the flame heat flux value is the reading from the thin film gage plus the radiative loss from the gage.
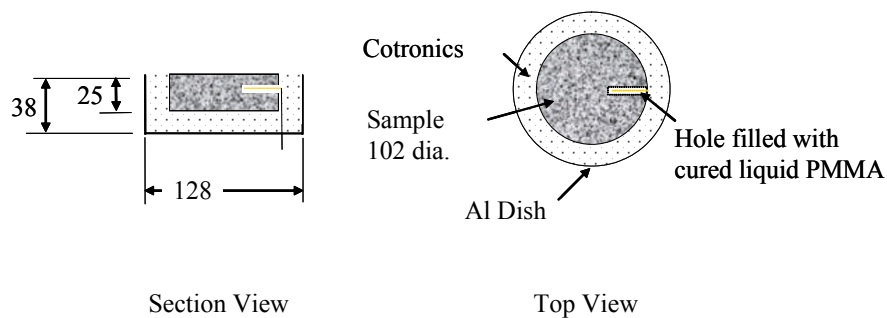
Figure 2.5   Experimental setup for thin film heat flux gage. Measurements in mm.

For applied heat flux, the total flame heat flux measured by any gage is determined by subtracting the known applied heat flux from the gage value. For free burn conditions with no applied heat flux, the gage value is the flame heat flux directly. The steady state measured total flame heat flux is 20 ± 3 kW/m^2 for 20.9 % ambient oxygen and 30 kW/m$^2 \pm 3$ kW/m^2 for 40 % ambient oxygen concentration for the 10.2 cm diameter black PMMA sample. These values are found to be approximately constant across the sample surface. The values obtained were the same for both free burn conditions and for applied heat flux levels up to 200 kW/m^2. Note that the uncertainty of the gage value contains the "test to test" statistical variation and gage diameter variation as well as the manufacturers stated value.

Convective and Radiative Heat Flux

Two methods were used to measure the radiative and convective components of the total flame heat flux. The first was to use a commercially available Schmidt-Boelter[8] heat flux gage that had individual sensors for total and radiative measurements where the convective component is the difference between them. The gage was placed in the sample with the face level with the sample surface as shown previously in Figure 2.4.

The second method consisted of two steps. A heat flux gage was placed at the sample surface to measure the total flame heat flux. This gage was then recessed 0.64 cm below the surface at the same location to obtain the radiative component, with the convective component being the difference between the "flush" measurement and the "recessed" measurement. The recessed gage should be exposed to the radiative component only since it is assumed that the hot gases can not reach the gage face.

Both methods obtained the same results. For black PMMA, the radiative component of the flame heat flux was 12 ± 3 kW/m^2 and the convective component was 8 ± 3 kW/m^2 for 20.9 % ambient oxygen concentration. For 40 % ambient oxygen concentration, the radiative and convective component was 20 ± 3 kW/m^2 and 10 ± 3 kW/m^2, respectively. This strongly suggests that the flame heat flux increase which occurs with enriching the ambient oxygen concentration is due primarily to an increase in the radiative component.

Mass Loss Flux

Mass loss data is collected during heat up, ignition and burning of the sample. A standard five point differentiation technique[11] is used to obtain mass loss rate and the mass loss flux is simply the mass loss rate per unit burning area. Burning is determined to be steady state when the mass loss flux trace, as well as the carbon dioxide and oxygen traces from the exhaust gases, is "flat" for a significant time compared to the ignition time. For the tests in this study, this means "flat" for 200-400 seconds. Figure 2.6 shows mass loss flux results obtained for black PMMA in the typical plotting method currently used in fire protection engineering for mass loss data. Observe from the figure that an increase from 5.8 ± 1 g/m^{2}sec to 12 ± 1 g/m^{2}sec in the mass loss flux occurs as the ambient oxygen concentration is increased from 20.9% to 40 % for free burn conditions. For applied heat flux conditions, the average increase is approximately 6 g/m^{2}sec regardless of the applied heat flux level.

Since high applied heat flux levels combined with enhanced ambient oxygen concentration could cause some aluminum components of the AFM to deform, for safety reasons tests were not run with enhanced oxygen above 70 kW/m^2 applied heat flux.
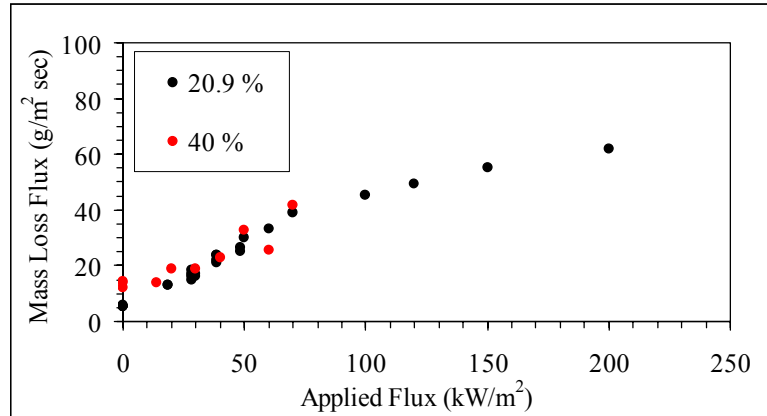
Figure 2.6   Mass loss flux vs. applied heat flux for thermally thick behaving black PMMA.

Note, however, the non-linear trend starting at around 50 kW/m^2, of the 20.9 % ambient oxygen concentration results. This non-linearity has been found to be a true material response and not related to the AFM apparatus. The non linearity represents a deviation of the material behavior from that presumed to occur by the existing theory. This phenomenon has been discussed in detail and is presented in Chapter 1. The uncertainty of the mass loss flux represents the full statistical variation of the average steady state value from repeated tests.

Surface Temperature

The temperature of the sample surface was measured by embedding a bare bead thermocouple on the surface. The temperature during heat up, ignition and burning was measured. Any radiation effect of the flame or applied heat flux to the thermocouple was eliminated by covering the bead with a very thin layer of PMMA such that the measurement was of the sample surface. The average surface temperature during burning in 20.9 % ambient oxygen concentration was found

to be 623 ± 50 K over all applied heat flux levels, as shown in Figure 2.7. Others have found the surface temperature to vary by 40 °C with varying applied heat flux for black PMMA but the current study could not resolve this difference due to the uncertainty of the measurement.
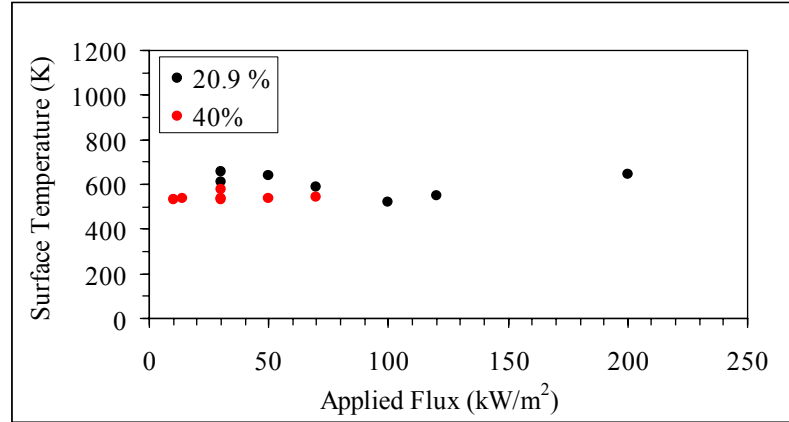
Figure 2.7   Surface temperature measurements for thermally thick behaving black PMMA.

The average surface temperature during burning in 40 % ambient oxygen concentration is 543 ± 50 K. The difference between the surface temperature for the two ambient oxygen concentrations needs to be resolved more accurately by obtaining temperature measurements with a smaller uncertainty.

Flame Height

The "visually averaged" flame height was measured during steady state burning by observation of the flame tip against a scale as shown in Figure 2.8. The height was found to be 17.8 ± 0.64 cm for 20.9 % and 12.7 ± 0.64 cm for 40 % ambient oxygen concentration for free burn conditions.

The flame height changed for each applied heat flux level but the difference between the heights for 20.9 % and 40 % ambient oxygen concentration, at a specific applied heat flux, was always approximately 5.1 cm. The ± 0.64 cm represents the measurement uncertainty of the "visual average" height.

Person   Sample   Scale
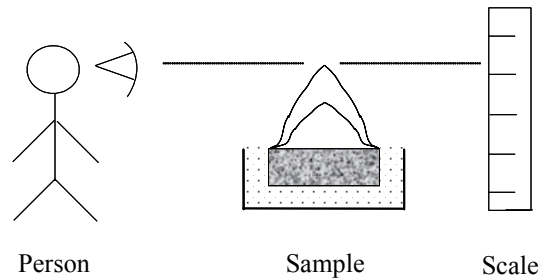
Figure 2.8   Flame height measurements technique.

Flame Emissivity

Extinction measurements were taken through the flame for a black PMMA sample during steady state burning at a single wavelength of 0.623 μm and at a location 25 mm above the sample surface as shown in Figure 2.9.

Laser   Receiver

Sample   Quartz
                          Tube
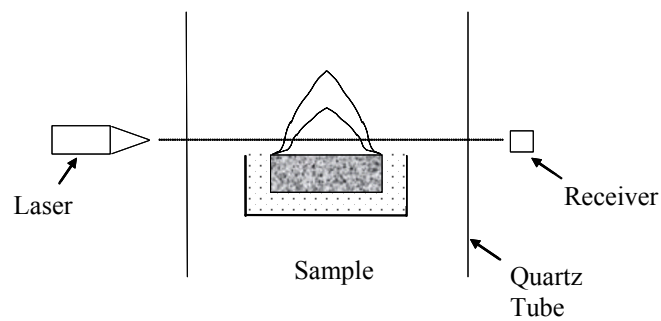
Figure 2.9   Extinction measurement set-up.

According to Siegel and Howell[12] for typical flame temperatures and soot particle size, scattering is negligible compared to absorption. Hence, the "extinction" coefficient is actually the "absorption" coefficient for a luminous flame when the carrier gas is non-radiating. The absorption coefficient is for the soot only since the 0.623 μm wavelength light absorption is not affected by carbon dioxide or water vapor. The spectral absorption coefficient, κ_λ, is determined from

$$\kappa_\lambda = -\frac{1}{L}\ln\left(\frac{I_0}{I}\right)$$ (2-1)

where L is the pathlength and I_0/I is the intensity ratio of the incident and transmitted light. Assuming the soot is diffuse, the spectral emissivity, ε_λ is

$$\varepsilon_\lambda = 1 - \exp(-\kappa_\lambda L)$$ (2-2).

The measured spectral emissivity average for all applied heat flux levels as well as free burn conditions, is 0.31 ± 0.05 for 20.9% ambient oxygen concentration and 0.57 ± 0.05 for 40 % ambient oxygen concentration, where the full statistical variation is represented by the uncertainty. Note this spectral emissivity is for the 0.623 μm wavelength.

The spectral emissivity can be converted to a soot volume fraction following the technique of Pagni and Bard[13] using

$$f_v \approx \frac{-\lambda\ln\left(\dfrac{I}{I_0}\right)}{36\pi L F_a(\lambda)}$$ (2-3)

where λ is the laser wavelength and $F_a(\lambda)$ contains the optical constants. The determination of the path length L is not as simple as it seems at first glance. On first guess, one would think that the "overall" flame width is a reasonable selection. Experimental observations show that this may not be a proper choice for small scale flames. For the 10.2 cm diameter samples tested in the current study, visual observation shows that the bottom of the flame consists of a "flame sheet" on the edge of the sample with no flame in the center, as opposed to a continuous flame across the sample surface, as shown in Figure 2.10.
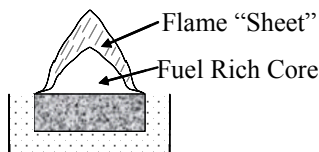
Figure 2.10   Flame geometry.

This geometry is also suggested by Corlett.[14] As such, the path length will be considered two times the flame sheet thickness since the laser beam encounters the flame sheet twice as it travels across the sample diameter. Shaddix and Smyth[15] determined that flame sheet thickness is approximately 2 mm for laminar flames so the path length used in this study is 4 mm. Using this path length, the spectral emissivities measured above calculate to soot volume fractions of 11.3 ± 0.6 x 10^{-6} and 27.3 ± 0.6 x 10^{-6} for the 20.9 and 40 % ambient oxygen concentrations, respectively. The enrichment of ambient oxygen results in an increase in the soot volume fraction at the measuring location which is consistent with the decreased flame height that occurs.

Pagni and Bard[13] report soot volume fraction results of 0.31 x 10^{-6} for horizontal samples of PMMA while Tien, Lee and Sttretton[16] report 0.22 x 10^{-6} for 20.9 % ambient oxygen

concentration. Note that although these are small scale tests of approximately the same size as the current study, the path length used by those researchers was the "overall" flame width, i.e., the sample width. No comment is made by those sources as to the flame structure and whether there appeared to be a "no flame" center as seen in the current study. For comparison, the current study obtains a soot volume fraction of 0.45×10^{-6} when the "overall" flame width is used as the path length to convert the 20.9 % ambient oxygen concentration spectral emissivity to soot volume fraction. This soot volume fraction is comparable to those obtained by Tien, Lee and Sttretton,[16] Pagni and Bard.[13] This shows that the current study extinction measurements are reasonable and that the observation of the flame structure and hence the choice of path length is critical to the soot volume fraction calculation.

If the optical constants are assumed to be a weak function of wavelength, then the total emissivity, ε, given by

$$\varepsilon = 1 - \exp(-\kappa L) \qquad (2\text{-}4)$$

can be calculated using[12]

$$\kappa = \frac{3.6kf_v T}{C_2} \qquad (2\text{-}5)$$

where κ is the total absorption coefficient, T is the flame temperature, C_2 is Plank's second constant and k is a constant depending on the type of soot. The k used in this study is 4.7 which is the value found by Pagni and Bard[13] as well as Yuen and Tien.[19] The total emissivities are 0.06

for 20.9 % ambient oxygen and 0.16 for 40 % ambient oxygen. The 20.9 % ambient concentration value is comparable to that reported for propane fires for the same product of concentration and path length.

Flame Temperature

The spectral emissivity calculated above can be used with narrow band infrared pyrometer measurements to obtain the flame temperatures. The experimental setup is shown in Figure 2.11.
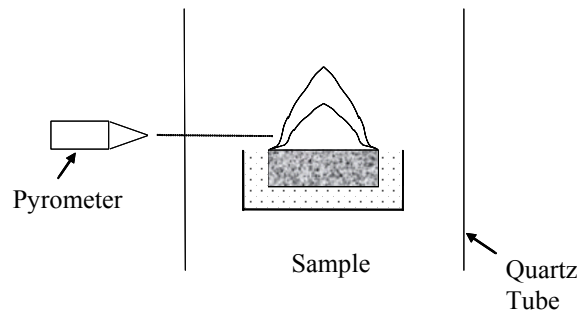
Figure 2.11   Infrared pyrometer set-up.

The infrared pyrometer obtained temperature readings assuming a spectral emissivity of 1. These can be corrected[17] using

$$T = T_r \sqrt[n]{\frac{1}{\varepsilon_\lambda}} \qquad \text{where} \qquad n = \frac{C_2}{\lambda_e T_{act}} \qquad (2\text{-}6)$$

where T is the temperature corrected for emissivity, T_r is the temperature reading, C_2 is Plank's second constant, λ_e is the wavelength response of the infrared pyrometer and ε_λ is the spectral

emissivity of the flame at the infrared pyrometer wavelength. The infrared pyrometer wavelength range is 1 – 1.6 μm which is different than the 0.623 μm wavelength of the laser used to obtain the spectral emissivity. As such, the spectral emissivity measured for 0.623 μm can not be used directly to correct the temperature readings. However, the soot volume fraction determined from the spectral emissivity at 0.623 μm can be used to calculate the spectral emissivity at other wavelengths according to Equation 2.2 where the spectral absorption coefficient can be calculated from the soot volume fraction and the optical properties of the soot using[12]

$$\kappa_\lambda = -\frac{36\pi f_v}{\lambda}\frac{nk}{\left(n^2 - k^2 + 2\right) + 4n^2 k^2} \tag{2-7}$$

where the optical constants n and k are functions of wavelength.

The average flame temperature is measured as 1184 ± 100 K at 20.9 % ambient oxygen concentration and 1300 ± 100 K with the enrichment of oxygen to 40 % concentration for the 10.2 cm diameter black PMMA sample. Accounting for the measurement uncertainty, the flame temperatures in the current study do not increase, however, this may be due to the precision of the temperature measurement. Stepniczka[18] has found that the flame temperature increases a maximum of approximately 100 K with increasing oxygen concentration up to 100 % oxygen for various non flame-retarded polymers including polystyrene, ABS and polyester. Temperature measurements with a smaller uncertainty should be obtained in the future to better resolve any difference between the 20.9 % and the 40 % ambient oxygen concentration conditions.

The flame temperature for 20.9 % oxygen of 1184 ± 100 K is lower than the 1538 K presented in literature by Tien, Lee and Sttretton.[16] They refer to the work of Yuen and Tien[19] for this value,

who in turn cite an earlier paper by Buckius and Tien[20] who completed the actual temperature measurements. They used thermocouples of approximately 40 AWG, coated with an yttrium oxide - beryllium oxide compound to minimize catalytic effects and applied a standard radiation correction by balancing the convective and radiative losses of the bead. They[20] found that "the experimental measurements showed oscillation of the order of 100 K due to the unsteady nature of the flames. Therefore, the curves drawn through the data are only meant to be approximate representations for the temperature distribution." This statement, along with scrutiny of their data presented in graphical form show that the average flame temperature should be stated as 1538 ± 100 K to properly reflect the measurement uncertainty as stated and shown by the authors. The current study flame temperature of 1184 ± 100 K is slightly lower than their value. However, Orloff, Modak and Alpert[21] report a value of 1367 K as the effective flame radiation temperature (called the "Schmidt temperature") for PMMA pool fires although no uncertainty (or details) is provided. Santo and Tamanini[22] present a Schmidt temperature for PMMA of 1300 to 1400 K at a height of 1 to 5 cm above the pool surface.

ANALYSIS OF BLACK PMMA EXPERIMENTAL DATA

Analysis conducted with the experimental data of black PMMA include the calculation of the radiative and convective flame heat flux using the flame emissivity, temperature and height. The flame emissivity, height and temperature can be used to gain insight into the effect of oxygen. They can also be used to calculate the convective and radiative heat fluxes for both the 20.9 % and 40% ambient oxygen concentrations. Assuming that the thickness of the flame, shown in Figure 2.10, allows it to be viewed as a surface emitter and not a volume emitter, the radiative heat flux is calculated by the following equation

$$\dot{q}''_{rad} = \varepsilon\varphi\sigma T^4 \tag{2-8}$$

where φ is the view factor and σ is the Stefan Boltzmann constant. Considering the visual observation showing a "flame sheet" on the edge of the sample with no flame in the center, as opposed to a continuous flame across the sample surface, which was shown previously in Figure 2.10, the view factor is determined from
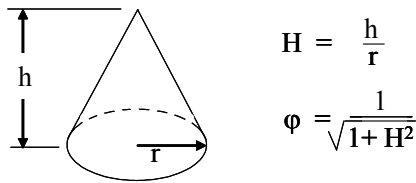
Figure 2.12   View factor for flame shape.

The convective heat flux is determined by the following equation

$$\dot{q}''_{conv} = h(T_g - T_s) \tag{2-9}$$

where T_g is the temperature of the gas cloud, T_s is the surface temperature and h is the convective heat transfer coefficient, assumed to be 15 ± 5 W/m^{2}K. This is same value used by others.[23,24,25] The gas temperature[15] is considered to be 200 °C below the flame sheet temperature.

The radiative and convective heat flux is calculated as 7 ± 8 kW/m^2 and 8 ± 2 kW/m^2 respectively for the 20.9 % ambient oxygen concentration which is consistent with the experimentally measured values of 12 ± 3 kW/m^2 (radiative) and 8 ± 3 kW/m^2 (convective). The uncertainties for the calculated values come from a propagation of the uncertainties of the parameters in each

function via the technique of Taylor.[26] For the 40 % ambient oxygen concentration, the radiative and convective heat flux is calculated as 24 ± 8 kW/m^2 and 10 ± 2 kW/m^2 respectively, which is again consistent with measurements of 20 ± 3 kW/m^2 (radiative) and 10 ± 3 kW/m^2 (convective). A volume emitter analysis provided by de Ris obtains similar results.[27]

The radiative and convective heat flux calculations obtained from the flame emissivity, height and temperature suggest that the flame heat flux increase that occurs with enriching the ambient oxygen concentration is due primarily to an increase in the radiative component, i.e., the effect of oxygen on soot production. This is consistent with suggestions from the measurements. The increase in the convective component suggests an increase in the flame temperature of about 100 K. Note that this can not be resolved by the flame temperature measurements with an uncertainty of ± 100 K, so an increase of this level could be present.

EXPERIMENTAL RESULTS FOR GAS BURNER

The flame heat flux, emissivity, soot volume fraction and temperature all increase with the enrichment of ambient oxygen. However, for the black PMMA sample they are coupled with the increase of the mass loss flux. To decouple these and to separate the solid and gas phase effects, a 10.2 cm diameter gas burner was used where the mass flow rate could be held constant. The ambient oxygen concentration could then be increased without the mass loss flux changing and the effect of the oxygen on the gas phase itself could be seen. Propylene was chosen as the fuel so there would be a sufficient amount of soot. Various heat release rate fires were run. Experimental measurements obtained include visual observations of flame structure and brightness, total flame heat flux, radiative and convective heat flux, flame height, flame emissivity and flame

71

temperature. There is no mass loss flux or surface temperature measurements for the gas burner experiments. The flame temperature and emissivity are used to calculate the radiative and convective heat fluxes for both the 20.9 % and enhanced ambient oxygen concentrations to be used as an internal consistency check for the measured flame heat flux values as well as providing insight into the effects of oxygen.

Visual Observations

Visual observations show turbulent flame characteristics which is evidenced by multiple flame sheets, eddies and wrinkles but the lower part of the flame had the same "no fuel" inner core structure as black PMMA flames. The addition of oxygen resulted in an increase in the brightness of the flame indicating increased soot and/or temperature (which would result in an increased emissive output). A more pronounced smoke mantel is observed as well as a slightly shorter flame height for the 40 % concentration. Copious amounts of soot were observed going up the exhaust stack for the 40 % ambient oxygen concentration. The 20.9 % ambient oxygen concentration showed very little soot by comparison.

Total Flame Heat Flux

Flame heat flux measurements were obtained with various heat flux gages[8] in the same fashion as was done for black PMMA. The total flame heat flux results were 15 ± 3 kW/m^2 at 20.9 % oxygen and 27 ± 3 kW/m^2 at 40 % oxygen regardless of the fire size. Since the propylene flow rate is controlled and there is no increase in the mass loss flux, these results show that oxygen is having an effect on the gas phase.

Convective and Radiative Heat Flux

The same methods that were used for black PMMA were also used for propylene to obtain measurements of the radiative and convective components of the total flame heat flux. These are 11 ± 3 kW/m^2 and 4 ± 3 kW/m^2 for the radiative and convective components, respectively for 20.9 % ambient oxygen concentration. For 40 % ambient oxygen concentration, they are 21 ± 3 kW/m^2 for the radiative and 6 ± 3 kW/m^2 for the convective heat flux. These results show that oxygen is indeed having an effect primarily on the radiative component of the flame heat flux as was seen for the black PMMA.

Flame Height

The flame height was measured during testing by visual observation of the flame tip against a scale as was done for black PMMA. The height was different for various fire heat release rates but the difference between 20.9 and 40 % ambient oxygen concentrations was always approximately 5 cm.

Flame Emissivity

Extinction measurements were taken through the flame at a single wavelength of 0.623 μm and at a location 25 mm above the sample surface. The same analysis technique as per black PMMA was used to obtain a total emissivity for free burn conditions of 0.08 ± 0.05 for 20.9% ambient oxygen concentration and 0.12 ± 0.05 for 40 % ambient oxygen concentration. The addition of oxygen results in an increase in the flame emissivity and accordingly, the soot volume fraction at

the measuring location. Using the same structure (2 flame sheets, path length of 4 mm) shown in Figure 2.10 for black PMMA, the soot volume fraction changes from 13.2 ± 0.6 x 10^{-6} to 22.6 ± 0.6 x 10^{-6} for 20.9 % and 40 % ambient oxygen concentration.

Flame Temperature

The spectral emissivity is used with narrow band infrared pyrometer measurements to obtain the flame temperatures as per the technique described previously for PMMA. The average flame temperature is measured as 1220 ± 100 K at 20.9 % ambient oxygen concentration and 1280 ± 100 K at 40 % ambient oxygen concentration. As was seen for PMMA, the flame temperatures in the current study do not increase, most likely due to the precision of the temperature calculation. The flame temperature for 20.9 % oxygen concentration of 1220 ± 100 K is essentially consistent with the 1490 ± 100 K literature value by Tien, Lee and Sttretton.[16]

ANALYSIS OF GAS BURNER EXPERIMENTAL DATA

Analysis conducted with the experimental data of propylene include the calculation of flame heat flux using the flame emissivity, temperature and height.

The flame temperature and emissivity can be used to calculate the convective and radiative heat fluxes for both the ambient and enhanced oxygen atmospheres to be used as an internal consistency check for the measured flame heat flux as was done per black PMMA.

The radiative and convective heat flux is calculated as 10 ± 8 kW/m^2 and 9 ± 2 kW/m^2 respectively for the 20.9 % oxygen condition which is consistent with the experimentally

measured values. For the 40 % oxygen condition, the radiative and convective heat flux is calculated as 18 ± 8 kW/m^2 and 10 ± 2 kW/m^2 respectively, which is again consistent with measurements. Since these show consistency, the flame heat flux measurements can be considered accurate, including the suggestion that the flame heat flux increase which occurs with enhancing the ambient oxygen concentration is due primarily to an increase in the radiative component.

EXPERIMENTAL RESULTS FOR DELRIN

Ambient oxygen concentration seems to be primarily affecting the soot production in the gas phase for black PMMA and propylene fires. However, the increase in the convective component suggests an additional effect on the fuel vapors in the flame. As such, it is prudent to test a material that does not produce soot. Delrin was chosen since it is non luminous at 20.9 % ambient oxygen concentration and is well behaved similar to black PMMA. Measurements obtained for horizontal orientation burning of 25 mm thick, thermally thick behaving, black Delrin include visual observations of flame structure and brightness, total flame heat flux, radiative and convective flame heat flux, mass loss flux, surface temperature and flame temperature.

<u>Visual Observations</u>

Visual observations show that the flame is bluish and barely visible unless the room is darkened at 20.9 % oxygen. The flame becomes slightly luminous at 40 % ambient oxygen concentration but no height difference was observable. No soot was observed going up the exhaust stack nor is seen on the sample surface post test. The same flame structure of a flame sheet, albeit blue color, with a "no flame" inner core at the lower height is seen for Delrin similar to black PMMA and propylene.

75

Bubbling of the sample surface is observed visually for both the 20.9 and 40 % oxygen concentration. The bubble size and "bubble zone" depth (determined in the same manner as for PMMA) decrease as the heating rate (i.e., the applied heat flux) increases.

Total Flame Heat Flux

Flame heat flux measurements were obtained in the same fashion as was done for black PMMA and propylene. The total flame heat flux results were 11 ± 3 kW/m^2 at 20.9 % oxygen and 33 ± 3 kW/m^2 at 40 % oxygen concentration.

Convective and Radiative Heat Flux

A Schmidt-Boelter heat flux gage[8] that had individual sensors for total and radiative measurements was used to obtain the flame heat flux measurements where the convective component is the difference between them. The gage was placed in the sample with the face level with the sample surface as shown previously in Figure 2.4. The radiative component of the flame heat flux was approximately 0 kW/m^2 and the convective component was 11 ± 3 kW/m^2 for 20.9 % ambient oxygen concentration. For 40 % oxygen concentration, the radiative and convective component was 3 ± 3 kW/m^2 and 30 ± 3 kW/m^2, respectively. Interestingly, this suggests that the flame heat flux increase which occurs with enriching the ambient oxygen concentration is due primarily to an increase in the convective component for Delrin.

Mass Loss Flux

Figure 2.13 shows mass loss flux results obtained for Delrin under 20.9 % and 40 % ambient oxygen concentration in the typical plotting method currently used in fire protection engineering

76

for mass loss data. Observe from the figure that an increase from 5.6 ± 1 g/m^{2}sec to 13 ± 1 g/m^{2}sec in the mass loss flux occurs as the ambient oxygen concentration is increased from 20.9% to 40 % for free burn conditions. For applied heat flux conditions, the average increase is approximately 6 g/m^{2}sec regardless of the applied heat flux level.
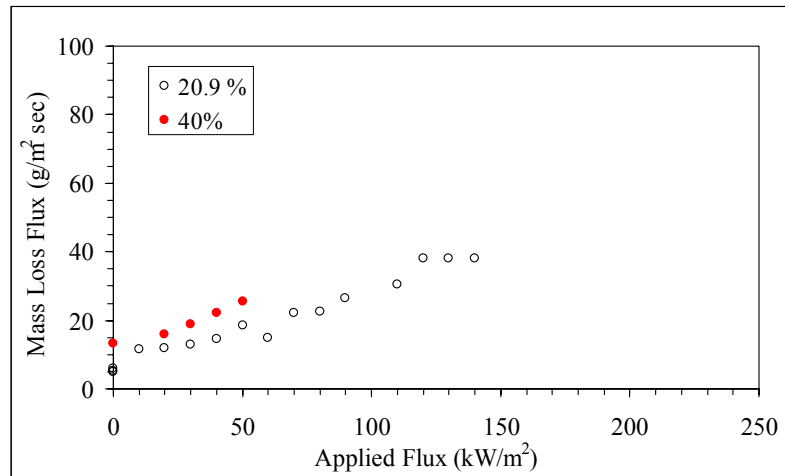
Figure 2.13   Mass loss flux vs. applied heat flux for thermally thick behaving Delrin in 20.9 % or 40 % ambient oxygen concentration.

Surface Temperature

The temperature of the sample surface was measured by embedding a bare bead thermocouple on the surface. The temperature during heat up, ignition and burning was measured. Any radiation effect of the flame or applied heat flux to the thermocouple was eliminated by covering the bead with a very thin layer of Delrin such that the measurement was of the sample surface. The average surface temperature during burning in 20.9 % ambient oxygen concentration was found to be 240 ± 50 ºC for free burn conditions. For 40 % ambient oxygen concentration, the surface temperature was 200 ± 50 ºC.

77

<u>Flame Temperature</u>

The flame temperature was measured, and radiation corrected, with a bare bead thermocouple as 1023 ± 50 K for 20.9 % ambient oxygen concentration and 1499 ± 50 K at 40 % ambient oxygen concentration. Since the flame was bluish, the thermocouple tip was placed in the general flame location and moved around until it glowed red indicting the "hottest" part of the flame. The heat transfer coefficient for the thermocouple was considered as 10 W/m^2 K and its emissivity was assumed to be equal to 1.

ANALYSIS OF DELRIN EXPERIMENTAL DATA

Analysis conducted with the experimental data of Delrin include the calculation of flame heat flux, using the flame temperature, which can be used as a consistency check against the measurements.

For the 20.9 % ambient oxygen concentration where the flame is non luminous, the total flame heat flux can be considered to be convective only with no radiative component. As such, the total flame heat flux is calculated from the flame temperature as 7 ± 2 kW/m^2 and the radiative heat flux should be 0 kW/m^2 for the 20.9 % ambient oxygen concentration. This is comparable to the measured values of 11 ± 3 kW/m^2 and 0 ± 3 kW/m^2 for the convective and radiative components, respectively. For the 40 % ambient oxygen concentration, the total flame heat flux can still be considered to be mainly convective with little radiative component. As such, the total flame heat flux is calculated from the flame temperature as 15 ± 2 kW/m^2 and the radiative heat flux should be 0 kW/m^2. This is "essentially" comparable to the measured values of 30 ± 3 kW/m^2 and 3 ± 3 kW/m^2 for the convective and radiative components, respectively.

A calculation of the increase in the adiabatic flame temperature for Delrin when the ambient oxygen concentration changes from 20.9 % to 40 % is 1100 °C. This does not account for radiation loss from the gas nor disassociation. Since the experimental increase is approximately 500 °C, it is reasonable to suggest that oxygen is increasing the gas phase temperature by the simple displacement of nitrogen for the non luminous flame of Delrin.

THE EFFECT OF OXYGEN EXPLAINED

Results from the solid and gas fuel experiments, as well as similar literature results given in Appendix A, lead to the following explanation of what enhanced ambient oxygen concentration is doing. The addition of oxygen displaces nitrogen in the gas phase which raises the temperature of the fuel gases. This causes the chemical reactions of the fuel vapors leaving the sample surface to occur faster than at lower concentrations due to the increased temperature and increased oxygen available such that more fuel per "height" is burned and the flame gets shorter resulting in the concentration of soot in the flame near the surface being greater. The increased soot concentration results in an increased flame emissivity. This increased soot leads to more radiative energy loss than at lower concentrations. This loss of energy lowers the flame temperature. The competing processes of the added oxygen raising the temperature and the increased emissivity lowering the temperature reach a balanced state of flame emissivity and temperature, the values of which depend on the fuel. This explanation is consistent with the theoretical analysis of Tewarson. From a practical viewpoint, the higher flame heat flux, which is mostly the radiative component for typical fuels, results in an increased mass loss flux and heat release rate.

Others have found that oxygen also affects a solid fuel by oxidative pyrolysis. The above

explanation of the effect of oxygen does not preclude this from happening, however, the major effect is in the gas phase for steady state burning in the horizontal orientation.

COMPARISON TO LARGE SCALE

Recall that the reason for using oxygen in the small scale experiments is to simulate the flame heat flux for large scale tests typical of industrial fire scenarios. The Flame Radiation Scaling Technique[5] states that the flame heat flux at large scale has been achieved in enhanced ambient oxygen small scale tests. As such, the small scale results must be compared to various scale results to see if the addition of oxygen raises the flame heat flux to the large scale value.

A 17.8 cm diameter sample, which is the largest sample that could be handled in the AFM, was chosen to see if the flame heat flux increase was significant. Additionally, 122 cm and 61 cm diameter samples were chosen as the large scale scenario since they were the largest sizes that could be handled in the study. The measurements, taken in a way identical to the 10.2 cm sample, obtained include visual observations, total flame heat flux and mass loss flux, which is used to calculate the flame heat flux.

AFM Largest Sample Size

For safety reasons no applied heat flux was used with the 17.8 cm diameter sample and it was only allowed to free burn. Ignition was by propane torch. Visual observations show turbulent flame characteristics which is evidenced by multiple flame sheets, eddies and wrinkles. The lower part of the flame had multiple flame sheets in contrast to the 10.2 cm diameter sample. The

addition of oxygen resulted in an increase in the brightness of the flame and a more pronounced smoke mantel is observed as well as a slightly shorter flame height for the 40 % ambient oxygen concentration.

Experimentally measured total flame heat flux values showed a variation (about 8 kW/m^2) across the diameter of the sample with larger values near the center and lower values near the edge. As such, the "simple" average was 30 ± 4 kW/m^2 at 20.9 % ambient oxygen concentration and 41 ± 4 kW/m^2 at 40 % ambient oxygen concentration. These measured values are greater than 20 ± 3 kW/m^2 and 30 ± 3 kW/m^2 obtained at 20.9 and 40 % ambient oxygen respectively for the smaller sample. The large value in 20.9 % ambient oxygen concentration seen for the larger sample is probably due to the multiple flame sheets observed at the lower section of the flame (compared to the single "sheet" seen for the small sample diameter) which results in an increased view factor to the sample surface. Interestingly, the increase in flame heat flux due to the addition of oxygen is about the same for both sample diameters.

Study Largest Sample Size

Black PMMA samples of 122 cm and 61 cm diameter were used. Ignition was achieved by using PMMA beads and heptane on the surface. Visual observations show turbulent flame characteristics which is evidenced by multiple flame sheets, eddies and wrinkles. The lower part of the flame appeared to have "continuous" flame sheets near the surface. Upon extinguishment, a variation in the mass loss across the diameter was evidenced by an observable difference in the sample thickness with diameter. This variation was also observed by Croce and Modak.[28]

The total flame heat flux was found to vary considerably across the sample diameter for the 122

cm sample, as such it was measured at several locations. The center of the sample was the highest at 80 kW/m^2, with the value dropping to 33 kW/m^2 as one moved toward the outer edge. For the 61 cm sample, the value went from 55 to 46 kW/m^2 from center to outer edge. The "area" average value of total flame heat flux measured was 60 ± 10 kW/m^2 for the 122 cm sample and 51 ± 10 kW/m^2 for the 61 cm sample.

When this large scale flame heat flux is duplicated in the 10.2 cm small scale tests with applied heat flux, (i.e., an applied heat flux of about 35 kW/m^2 combined with the small scale flame heat flux of 20 kW/m^2) the mass loss results are within the linear region of the mass loss flux vs. applied heat flux plot. Hence, the small scale apparent heat of gasification obtained from the linear region can be successfully used with the 61 cm and 122 cm mass loss flux to calculate the flame heat flux as described in Chapter 1.

Note that the "Typical Technique" assumes that there is a constant flame heat flux across the surface resulting in a uniform mass loss flux across the surface. The large scale samples do not have this condition, so strictly speaking, the technique can not be applied. However, a single mass loss measurement should average out the variation in mass loss flux so it is reasonable to use the technique to get a rough estimate of the average flame heat flux.

A mass loss flux of 20 ± 6 g/m^2 sec was recorded for the 122 cm sample and 17 ± 6 g/m^2 sec for the 61 cm sample. Using these values plus the apparent heat of gasification from the small scale results gives a calculated flame heat flux of 48 ± 20 kW/m^2 and 41 ± 20 kW/m^2 for the 122 cm and 61 cm samples, respectively.

Figure 2.14 shows the measured total flame heat flux values for all sample sizes tested in the

current study, including the 10.2 cm diameter. Also shown is the total flame heat flux calculated from the mass loss flux and the apparent heat of gasification.
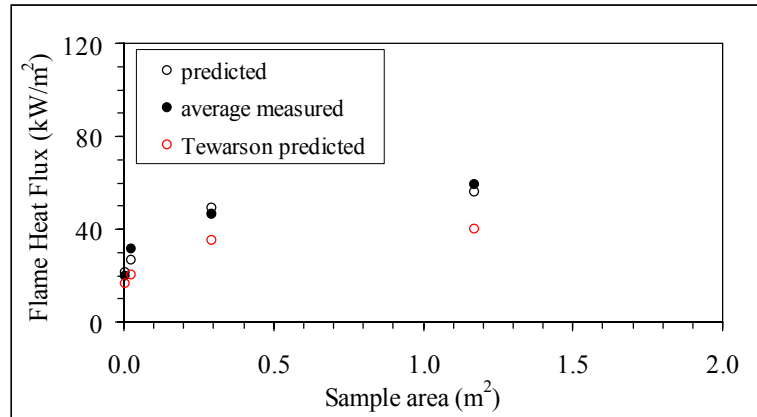
Figure 2.14   Flame heat flux measurements and calculations for thermally thick behaving black PMMA.

Observe from the figure that the total flame heat flux calculated from the mass loss flux data using Tewarson's DSC heat of gasification value of 1.6 kJ/g does not match the measured value. Use of the apparent heat of gasification value of 2.4 kJ/g obtained from Chapter 1 gives a calculated total flame heat flux value that reasonably matches the measured value. This is thought to be due to the "applicability" of the small scale apparent heat of gasification to the large scale test due to the correspondence of the large scale flame heat flux with the initial linear region of the mass loss flux vs. applied heat flux plot. In other words, the "heat of gasification" was obtained for material response to a flame heat flux less than 50 kW/m^2 and the average large scale flame heat flux is about this value. Apparently, whatever physics or chemical processes that are buried in the apparent heat of gasification term is the same for both small scale, 10.2 cm, and large scale, 122 cm, sample sizes.

Scalability

For black PMMA, the horizontal small scale, 10.2 cm diameter, free burn, 40% ambient oxygen concentration results for flame heat flux of 30 ± 3 kW/m^2 do not simulate the average large scale, 122 cm diameter results of 60 ± 10 kW/m^2 for flame heat flux. However, use of applied heat flux can get the "overall" heat flux in small scale up to the levels seen by the sample in large scale. The "overall" heat flux (applied heat flux plus flame heat flux) obtained via applied heat flux with enhanced ambient oxygen concentration could also be attained by simply increasing the applied heat flux for a 20.9 % ambient oxygen concentration.

This conclusion is made only for black PMMA. It is believed to be applicable to other materials also, but this can not be made definitive until other materials are tested in small scale with enhanced ambient oxygen and compared to large scale.

The increase of the total flame heat flux to the levels seen in large scale was thought to be why vertical flame spread tests in small scale, enhanced ambient oxygen concentration would show "large scale results" for flame spread. Since the horizontal orientation results show that the total flame heat flux is not being brought up to large scale levels, another study is needed to understand what is going on from a practical viewpoint in the vertical flame spread situation.

This related study entitled "The Effect of Oxygen on Flame Heat Flux in the Vertical Orientation," is presented in Chapter 3. The Advanced Flammability Measurements Apparatus (AFM) was used to conduct small scale experiments at ambient oxygen concentrations of 20.9 to 40 % oxygen for various materials in the vertical orientation. Black polymethylmethacrylate

(PMMA) and polyoxymethylene (Delrin) were chosen since they are "well behaved" materials that do not intumesce. The total flame heat flux was experimentally measured with heat flux gages. To gain more insight into the effects of ambient oxygen, the flame emissivity and flame temperature were used to calculate the radiative and convective components of the flame heat flux. Flame spread tests were conducted for PMMA and Delrin to quantify the effect of oxygen on flame spread velocity. Calculated flame spread velocities from a simple thermal model are compared to experimentally measured values. Literature data of flame heat flux for large scale vertical experiments of black PMMA were used for comparison to the small scale, enhanced oxygen flame heat flux results to determine the level of scalability that enhanced oxygen provides in the vertical orientation.

SUMMARY AND CONCLUSIONS

The Advanced Flammability Measurements Apparatus (AFM) was used to conduct small scale horizontal orientation experiments at ambient oxygen concentrations of 20.9 to 40 % ambient oxygen concentration for black PMMA, propylene and Delrin. The total flame heat flux, as well as the radiative and convective components, was experimentally measured with various gages. To gain more insight into the effects of oxygen, the flame emissivity, flame height and flame temperature were obtained. These were also used to calculate the radiative and convective components of the flame heat flux. Horizontal gas burner experiments were conducted to decouple the solid and gas phase effects of the ambient oxygen. Large scale tests of black PMMA were conducted to obtain flame heat flux measurements which were used for comparison to the small scale, enhanced oxygen results.

The steady state measured total flame heat flux is 20 ± 3 kW/m^2 for 20.9 % ambient oxygen and

30 kW/m^2 ± 3 kW/m^2 for 40 % oxygen concentration for the small scale 10.2 cm diameter black PMMA sample. The radiative component of the flame heat flux was 12 ± 3 kW/m^2 and the convective component was 8 ± 3 kW/m^2 for 20.9 % ambient oxygen concentration. For 40 % oxygen concentration, the radiative and convective component was 20 ± 3 kW/m^2 and 10 ± 3 kW/m^2, respectively.

The steady state measured total flame heat flux is 15 ± 3 kW/m^2 for 20.9 % ambient oxygen and 27 kW/m^2 ± 3 kW/m^2 for 40 % oxygen concentration for the small scale propylene. The radiative component of the flame heat flux was 11 ± 3 kW/m^2 and the convective component was 4 ± 3 kW/m^2 for 20.9 % ambient oxygen concentration. For 40 % oxygen concentration, the radiative and convective component was 21 ± 3 kW/m^2 and 6 ± 3 kW/m^2, respectively.

For the black Delrin sample, the steady state measured radiative component of the flame heat flux was 0 ± 3 kW/m^2 and the convective component was 11 ± 3 kW/m^2 for 20.9 % ambient oxygen concentration. For 40 % oxygen concentration, the radiative and convective component was 3 ± 3 kW/m^2 and 30 ± 3 kW/m^2, respectively.

Results from the solid and gas fuel experiments lead to the following explanation of what enhanced ambient oxygen concentration is doing. The addition of oxygen displaces nitrogen in the gas phase which raises the temperature of the fuel gases. This causes the chemical reactions of the fuel vapors leaving the sample surface occur faster than at lower concentrations due to the increased temperature and increased oxygen available such that more fuel per "height" is burned and the flame gets shorter resulting in the concentration of soot in the flame near the surface being greater. The increased soot concentration results in an increased flame emissivity. This

increased soot leads to more radiative energy loss than at lower concentrations. This loss of energy lowers the flame temperature. The competing processes of the added oxygen raising the temperature and the increased emissivity lowering the temperature reach a balanced state of flame emissivity and temperature, the values of which depend on the fuel. This explanation is consistent with the theoretical analysis of Tewarson. From a practical viewpoint, the higher flame heat flux, which is mostly the radiative component for typical fuels, results in an increased mass loss flux and heat release rate.

For black PMMA, the horizontal small scale, 10.2 cm diameter, free burn, 40% ambient oxygen concentration results of 30 ± 3 kW/m^2 do not simulate large scale, 122 cm diameter results of 60 ± 10 kW/m^2 for total flame heat flux. The use of applied heat flux can get the "overall" heat flux in small scale to the levels seen by the sample in large scale. The "overall" heat flux (applied heat flux plus flame heat flux) obtained via applied heat flux with enhanced ambient oxygen concentration could also be attained by simply increasing the applied heat flux for a 20.9 % ambient oxygen concentration. This conclusion is made only for black PMMA. It is believed to be applicable to other materials also, but this can not be made definitive until other materials are tested in both small scale with enhanced oxygen and compared to large scale.

The increase of the total flame heat flux to the levels seen in large scale was thought to be why vertical flame spread tests in small scale, enhanced ambient oxygen concentration would show "large scale results" for flame spread. Since the horizontal orientation results show that the total flame heat flux is not being brought up to large scale levels (122 cm diameter), another study is needed to understand what is going on from a practical viewpoint in the vertical flame spread situation. This is presented in Chapter 3.

Measurements and Calculation Results Summarized in Table Form

Table 2.1   Black PMMA horizontal small scale flame heat flux results summary.

	Measured Flame Heat Flux kW/m^2		Calculated Flame Heat Flux kW/m^2	
	20.9 %	40 %	20.9 %	40 %
Radiative	12 ± 3	20 ± 3	7 ± 8	24 ± 8
Convective	8 ± 3	10 ± 3	8 ± 2	10 ± 2
Total	20 ± 3	30 ± 3	15 ± 10	34 ± 10

Table 2.2   Black PMMA horizontal small scale results summary.

Oxygen %	$\dot{m}''$ g/m^{2}s	T_s K	T_f K	ε -	h_f cm	f_v -
	± 1	± 50	± 100	± 0.08	± 0.64	± 0.6 x 10^{-6}
20.9	5.8	623	1184	0.06	17.8	11.3 x 10^{-6}
40	12	543	1300	0.16	12.7	27.3 x 10^{-6}

Table 2.3   Propylene horizontal small scale flame heat flux results summary.

	Measured Flame Heat Flux kW/m^2		Calculated Flame Heat Flux kW/m^2	
	20.9 %	40 %	20.9 %	40 %
Radiative	11 ± 3	21 ± 3	10 ± 8	18 ± 8
Convective	4 ± 3	6 ± 3	9 ± 2	10 ± 2
Total	15 ± 3	27 ± 3	19 ± 10	28 ± 10

Table 2.4   Propylene horizontal small scale results summary.

Oxygen %	$\dot{m}''$ g/m^{2}s	T_s K	T_f K	ε -	h_f cm	f_v -
	± 1	± 50	± 100	± 0.05	± 0.64	± 0.6 x 10^{-6}
20.9	-	-	1220	0.08	x	12.3 x 10^{-6}
40	-	-	1280	0.12	x + 5	22.6 x 10^{-6}

Table 2.5   Delrin horizontal small scale flame heat flux results summary.

	Measured Flame Heat Flux kW/m^2		Calculated Flame Heat Flux kW/m^2	
	20.9 %	40 %	20.9 %	40 %
Radiative	0 ± 3	3 ± 3	0	0
Convective	11 ± 3	30 ± 3	7 ± 2	15 ± 2
Total	11 ± 3	33 ± 3	7 ± 2	15 ± 2

Table 2.6   Delrin horizontal small scale results summary.

Oxygen %	$\dot{m}''$ g/m^{2}s	T_s K	T_f K	ε -	h_f cm	f_v -
	± 1	± 50	± 100	± 0.08	± 0.64	-
20.9	5.6	513	1023	-	-	-
40	13.0	473	1499	-	-	-

Table 2.7   Black PMMA horizontal various scale results.

   *Average values given for these diameter samples.

   **Calculated from measured $\dot{m}''$ using $h_g = 2.4 \pm 0.2$ kJ/g obtained from Chapter 1.

Sample Diameter (cm)	Measured Total Flame Heat Flux kW/m^2		$\dot{m}''$ g/m^{2}s	$\dot{q}_f''$ ** kW/m^2
	20.9 %	40 %	20.9 %	20.9 %
10.2	20 ± 3	30 ± 3	5.8 ± 1	13.9 ± 3
17.8	30 ± 3	41 ± 3	-	-
61*	51 ± 3	-	17.6 ± 6	41 ± 20
122*	60 ± 10	-	20 ± 6	48 ± 20

REFERENCES

1   An Introduction to Fire Dynamics, 2nd edition, Drysdale, D., p. 247, John Wiley and Sons, New York, NY, USA, 1999.

2   Beaulieu, P., Dembsey, N., and Alpert, R., "A New Material Flammability Apparatus and Measurement Techniques," Composites 2003, Anaheim, CA, 2003.

3   Croce, P., 'The Forum for International Cooperation on Fire Research," Fire Safety Journal, 36, p. 715-717, 2001.

4   Handbook of Fire Protection Engineering, 2nd edition, "Chapter 3-4, Generation of Heat and Chemical Compounds in Fires," Society of Fire Protection Engineers, Boston, MA, 1995.

5   Tewarson, A., "Flammability Parameters of Materials: Ignition, Combustion and Fire Propagation," Journal of Fire Sciences, 12, p. 329-356, 1994.

6   Tewarson, A., Lee, J.L., and Pion, R.F., "The Influence of Oxygen Concentration on Fuel Parameters for Fire Modeling," Eighteenth Symposium (International) on Combustion, p. 563-570, 1981.

7   Tewarson, A., "Flammability of Polymers and Organic Liquids: Part I – Burning Intensity," FM Global Report # FMRC 22429, 1975.

8   Manufacturers Catalog, Medtherm Corporation, Huntsville, AL, 2004.

9   Manufacturers Catalog, Cotronics Corporation, Brooklyn, NY, 2000.

10   RdF Corporation Temperature Measurement Catalog, 2000.

11   ASTM Standard Method for Heat and Visible Smoke Release Rates for Materials and Products Using an Oxygen Consumption Calorimeter, ASTM E 1354, American Society of Testing Materials, Philadelphia, PA, 1999.

12   Thermal Radiation Heat Transfer, 2nd edition, Chapter 17-9: Flames, Luminous Flames and Particle Radiation, Hemisphere Publishing Corporation, New York, NY, 1981.

13   Pagni, P., and Bard, S., "Particulate Volume Fractions in Diffusion Flames," 17th Symposium on Combustion, p. 1017-1028, year.

14   Corlett, R. "Heat Transfer Data Summary Pool Burning Study," Harvard Technical Report # 19, NSF Grant G-9445, Harvard University, Boston, MA, USA, 1965.

15 Shaddix, C. and Smyth, K., "Laser Induced Incandescence Measurements of Soot Production in Steady and Flickering Methane, Propane and Ethylene Diffusion Flames," Combustion and Flame, 107, p. 418 – 452, 1996.

16 Handbook of Fire Protection Engineering, 2nd edition, Chapter 1-4, Radiation Heat Transfer, Society of Fire Protection Engineers, Boston, MA, 1995.

17 User Guide for Infrared Thermometer, Mikron Corporation, Oakland, NJ.

18 Stepniczka, H., "The Influence of Oxygen-Enriched Atmospheres on the Combustion Behavior of Polymers," Journal of Fire and Flammability, 5, p.16, 1974.

19 Yuen, W. and Tien, C., "A Simple Calculation Scheme for the Luminous Flame Emissivity," 16th International Symposium on Combustion, p. 1481 – 1487.

20 Buckius, R. and Tien, C., "Infrared Flame Radiation," International Journal of Heat and Mass Transfer, v. 20, p. 93 – 106, 1977.

21 Orloff, L., Modak, A. and Alpert, R., "Burning of Large Scale Vertical Surfaces," 16th International Symposium on Combustion, Combustion Institute, p. 1354 – 1354, 1976.

22 Santo, G., and Tamanini, F., "Influence of Oxygen Depletion on the Radiative Properties of PMMA Flames," 18th International Symposium on Combustion, 1981.

23 Mowrer, F., "An Analysis of Effective Thermal Properties of Thermally Thick Materials" Fire Safety Journal, 40, 5, p. 395 – 410, July 2005.

24 Quintiere, J. and Harkleroad, M., "New Concepts for Measuring Flame Spread Properties," Fire Safety: Science and Engineering, ASTM STP 882, American Society for Testing and Materials, Philadelphia, p. 239 – 267, 1985.

25 Janssens, M., "Fundamental Thermophysical Characteristics of Wood and Their Role in Enclosure Fire Growth," PhD dissertation, University of Gent, Belgium, 1991.

26   An Introduction to Error Analysis, John Taylor, University Science Books, Sausalito, CA, 1982.

27   De Ris, J., FM Global Memo entitled Radiant Heat Transfer from a Conical Flame, dated 7 September 2005, FM Global, Norwood, MA.

28   Modak, A. and Croce, P., "Plastic Pool Fires, Combustion and Flame," 30, p. 251-265, 1977.

CHAPTER 3: EFFECT OF OXYGEN ON FLAME HEAT FLUX IN THE VERTICAL ORIENTATION

ABSTRACT

The Advanced Flammability Measurements Apparatus (AFM) was used to conduct small scale vertical orientation experiments for black PMMA, propylene and Delrin. The key aspect of this study was direct experimental measurements of flame heat flux back to the burning surface for 20.9 to 40 % ambient oxygen concentrations. The total flame heat flux, as well as the radiative and convective components, was experimentally measured with various gages. To gain more insight into the effects of ambient oxygen, the flame emissivity and flame temperature were used to calculate the radiative and convective components of the flame heat flux. Vertical gas burner experiments were conducted to decouple the solid and gas phase effects of the ambient oxygen. Literature data was used for comparison to the small scale, enhanced oxygen results. Vertical flame spread experiments were also conducted. The main conclusion is that the total flame heat flux in enhanced ambient oxygen simulates a more severe large scale geometry flame heat flux in the vertical orientation and is useful for vertical flame spread. A related study has shown that the total flame heat flux in enhanced ambient oxygen does not simulate large scale flame heat flux in the horizontal orientation.

INTRODUCTION

In Chapter 2, a systematic empirical and analytical study of the effect of ambient oxygen concentration was conducted to directly quantify the effect of enhanced ambient oxygen

concentration on flame heat flux at small scale. However, this was in the horizontal orientation and the results may not be fully applicable to the vertical orientation. Hence, a systematic empirical and analytical study of the effect of ambient oxygen concentration on flame heat flux was conducted for steady state burning in the vertical orientation. The effect on flame spread in the vertical orientation was also studied.

The Advanced Flammability Measurements Apparatus[1] (AFM) was used to conduct small scale experiments at ambient oxygen concentrations of 20.9 to 40 % oxygen for various materials. Black polymethylmethacrylate (PMMA) and polyoxymethylene (Delrin) were chosen since they are "well behaved" materials that do not intumesce. The total flame heat flux was experimentally measured with heat flux gages. To gain more insight into the effects of ambient oxygen, the flame emissivity and temperature were used to calculate the radiative and convective components of the heat flux. These are also used as an internal consistency check of the measured flame heat flux.

Vertical gas burner experiments were conducted to decouple the solid and gas phase effects of the ambient oxygen. The total flame heat flux was experimentally measured with various gages. The flame emissivity and flame temperature were used to calculate the radiative and convective components of the flame heat flux in the same manner as was done for PMMA.

Flame spread tests were conducted for PMMA and Delrin to quantify the effect of oxygen on flame spread velocity. Calculated flame spread velocities from a simple thermal model are compared to experimentally measured values.

Literature data of flame heat flux for large scale vertical experiments of black PMMA were used

for comparison to the small scale, enhanced ambient oxygen flame heat flux results of the present study to determine the level of scalability that enhanced oxygen provides.

BACKGROUND

The Flame Radiation Scaling Technique[2] was developed by Tewarson to obtain large scale flame heat flux values from small scale tests. The technique consists of conducting a small scale experiment with an enhanced oxygen atmosphere, measuring the mass loss flux and calculating the total flame heat flux using a surface energy balance. Tewarson found that as the oxygen concentration of the small scale test was increased above 20.9 %, the flame heat flux would reach an asymptotic limit comparable to the limit found in large scale fires. Hence, increasing the oxygen concentration in small scale tests to obtain flame heat flux values comparable to large scale tests is defined as the Radiation Scaling Technique.

The concept that an enhanced ambient oxygen concentration can be used to simulate large scale results for flame heat flux has been extended to include ignitibility, flame spread and heat release rate by the FM Clean Room Flammability Test Protocol 4910,[3] which contains test requirements and procedures for the evaluation of materials used in the semiconductor industry. (This is also codified as NFPA 287, Standard Test Methods for Measurement of Flammability of Materials in Cleanrooms Using a Fire Propagation Apparatus[4]) This protocol was developed since the small scale results obtained for fire retarded materials used in semiconductor industry "clean-rooms" do not correspond to results for realistic large scale fire conditions. Fire resistant materials may not spread or even ignite at small scale while burning vigorously at large scale.[5] The use of enhanced ambient oxygen in small scale tests has been observed to cause these materials to have large scale

behavior for flame spread and heat release rate.[6,7]

The 4910 Test Protocol[3] is conducted in the Fire Propagation Apparatus[8]. A vertical orientation is used for a sample 100 mm wide, 300 mm long and up to 25 mm thick. For flame spread, a 40 % oxygen concentration – nitrogen mixture is co-flowed past the sample at a velocity of 0.15 m/sec. The bottom 10 cm of the sample, defined as the ignition zone, is exposed to an applied heat flux of 50 kW/m^2 in the presence of a pilot flame. Since the applied heat flux is minimal beyond the ignition zone, the driving force for spread beyond the ignition zone is the flame heat flux (self propagation).

The small scale experiments were conducted using an apparatus called the Advanced Flammability Measurements (AFM) Apparatus.[1] It was created as part of an on going apparatus evaluation, improvement and development program. The AFM is closely related to the small scale Fire Propagation[8] Apparatus (FPA) (ASTM E 2058), and similar to the small scale Cone[9] Calorimeter (ASTM E 1354). However, the AFM is of intermediate scale in terms of its design with greater capability of applied heat flux range, maximum sample size, and incorporation of additional measurement techniques needed to assess flame and material heat transfer directly. These characteristics of the AFM will improve measurement of key material flammability parameters needed for computer simulation of end use fire scenarios. Details of the apparatus are in Appendix B, C and D.

EXPERIMENTAL RESULTS FOR BLACK PMMA

Measurements obtained for vertical orientation burning of 25 mm thick, thermally thick behaving black PMMA, in oxygen atmospheres of 20.9 % to 40 % oxygen concentration include "total"

flame heat flux in the pyrolysis and forward heating zones, flame temperature and visual observations of flame structure and brightness. "Total" is defined as the sum of the radiative and convective components of the flame heat flux. (This is not the "net" flame heat flux which is defined as the difference between the total flame heat flux and the radiative loss from the sample surface.) Figures 3.1 shows the experimental set up.
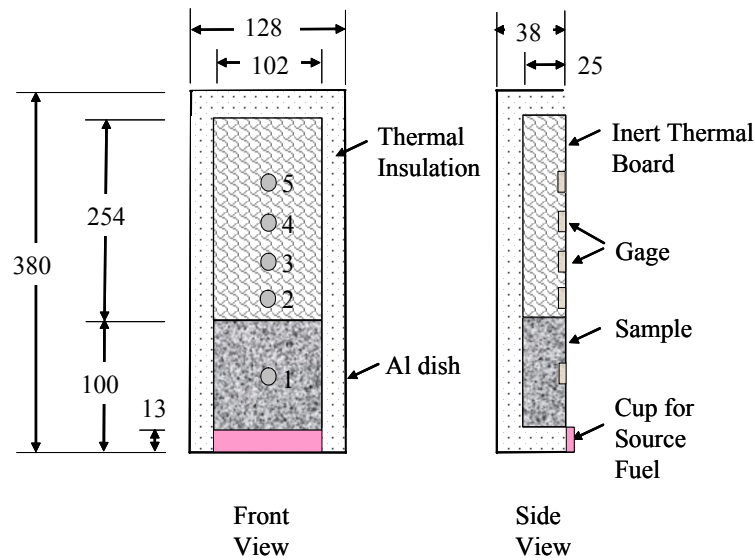
Figure 3.1   Experimental set up for vertical orientation tests for black PMMA, gas burner and Delrin. Measurements in mm.

Ignition was accomplished by using a small source flame of alcohol (2 mL) that would burn for a short time (about 2 minutes) igniting the sample at its base. The source flame would extinguish and the sample would continue to burn uniformly across the sample width at its base and slowly spread up its total length until the whole sample was burning in steady state mode. Only free burn tests, with no applied heat flux, were conducted since difficulty was encountered with using applied heat flux for the vertical sample in the AFM apparatus.

Visual observations made perpendicular to the sample show turbulent flame characteristics over the entire flame length which is evidenced by multiple flame sheets, eddies and wrinkles. This is consistent with flow conditions in the chamber and is not surprising given the fact that a clean leading edge is purposely not present due to the design of the source fuel holder. When viewed from the side, as shown in Figure 3.2, the flame appears to have a thickness similar to that seen in the horizontal orientation shown in Figure 2.10.
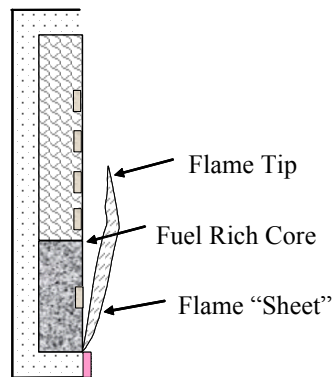
Figure 3.2   Side view of experimental setup vertical orientation tests.

The addition of oxygen resulted in an increase in the "brightness" of the flame is observed indicating increased soot and/or temperature. Copious amounts of soot were observed in the flame and forward heating zone as well as going up the exhaust stack for the 40 % ambient oxygen concentration. The 20.9 % ambient oxygen concentration showed very little soot by comparison.

Bubbling of the sample surface is observed visually through the flame and no material "melted"

(i.e., ran down the sample due to gravity) for either 20.9 or 40 % oxygen concentration. The sample was considered to be pyrolzing where there was bubbling present. Using this definition, a well-defined, uniform pyrolysis front was observed to travel from the bottom of the sample to the top as it reached steady state. Visual observations of this pyrolysis front show an increase in the "overall" flame spread rate with the enhancement of oxygen. This is also suggested by the timing of when the heat release rate curve reaches its steady state value. The 40 % oxygen concentration reaches the steady state value sooner than the 20.9 % oxygen concentration indicating that the entire sample is burning earlier at 40 % than at 20.9 % oxygen. This suggests that the "overall" flame spread rate has increased with the addition of oxygen, however, flame spread experiments were conducted on a longer sample to clarify this. This is presented later in the section called "PMMA Flame Spread."

Measured Total Flame Heat Flux

Commercially available Schmidt-Boelter heat flux gages[10] of different sizes and models were used to measure the total flame heat flux to the burning surface during heat up, ignition and burning. As per Figures 3.1 and 3.2, the gage face was placed flush with the sample surface. A 3 mm thick thermal ceramic insulation[11] was used between the gage and the sample to hold the gage in place. The gage was cooled with 65 °C water during the test to prevent condensation from forming on the gage face and to prevent local distortion on the sample burning behavior. Any convection increase due to the high temperature of the ceramic insulation is neglected since the area is a very small fraction of the total surface area. Also neglected is any conduction to the gage from the ceramic paper. Since this is a "cold" gage, the flame heat flux value is simply the gage reading.

Table 3.1   Measured total flame heat flux for black PMMA.   *In pyrolysis zone.   **The

steady state mean flame height was approximately 20 cm from the sample bottom.

Gage #	Height from bottom of sample cm	Total Heat Flux kW/m^2 ± 3	
		20.9 % O$_2$	40 % O$_2$
1	5.8*	33	58
2	13.9	33	55
3	19.7**	30	50
4	24.7	24	38
5	29.8	17	32

The measured total flame heat flux at 5.8 cm from the bottom of the sample, which is in the

pyrolysis zone, was 33 ± 3 kW/m^2 at 20.9 % oxygen and 58 ± 3 kW/m^2 at 40 % ambient oxygen

concentration. In the forward heating zone, the measured total flame heat flux at 20.9 % ambient

oxygen concentration was 33, 30, 24 and 17 ± 3 kW/m^2 for heights, measured from the bottom of

the sample, 13.9, 19.7, 24.7 and 29.8 cm respectively, as shown in Table 1. For 40 % ambient

oxygen concentration, the measurements were 55, 50, 38 and 32 ± 3 kW/m^2 for heights 13.9,

19.7, 24.7 and 29.8 cm, respectively.

Note that the uncertainty includes "test to test" variation as well as gage diameter effects. For the

40 % concentration, there was "a lot" of soot which tended to collect on the gage face and the

measured value would drop with time. As such, the values stated are taken from the "early" time of the steady state burning.

Flame Temperature

Extinction measurements similar to those obtained in horizontal orientation presented in Chapter 2 were not successfully obtained in the vertical orientation due to restrictions encountered by the apparatus layout. The extinction coefficient has been measured for the horizontal orientation and the spectral and total emissivities determined for a total flame width of 4 mm. (Details are given in Chapter 2.) The vertical flame thickness appears to be on this order. This rough correspondence allows the emissivities obtained from the horizontal work to be used for the vertical. Hence, the spectral emissivity obtained in the horizontal study will be used here to correct the infrared pyrometer measurements to obtain the flame temperature. The infrared pyrometer obtained temperature readings assuming a spectral emissivity of 1. These can be corrected using the actual emissivity by the following equation

$$ T = T_r \sqrt[n]{\frac{1}{\varepsilon_\lambda}} \qquad \text{where} \qquad n = \frac{C_2}{\lambda_e T} \qquad (3\text{-}1) $$

where T is the actual temperature, T_r is the temperature reading , ε_λ is the spectral emissivity of the flame at the infrared pyrometer wavelength C_2 is Plank's second constant, λ_e is the wavelength response of the infrared pyrometer and ε_λ is the spectral emissivity of the flame at the infrared pyrometer wavelength. Details of this can be found in Chapter 2, subsection "Flame Emissivity" page 63. The average flame temperature is measured as 1121 ± 100 K at 20.9 % ambient oxygen concentration and 1208 ± 100 K with the enrichment of oxygen to 40 % ambient

oxygen concentration for the black PMMA sample. Accounting for the measurement uncertainty, the flame temperature in the current study does not increase, however, this may be due to the resolution of the temperature calculation. As recommended in the related horizontal study, temperature measurements with a smaller uncertainty need to be obtained to better resolve any difference between the 20.9 % and 40 % ambient oxygen conditions.

ANALYSIS OF BLACK PMMA EXPERIMENTAL DATA

The flame emissivity and temperature are used to calculate the convective and radiative heat fluxes for the 20.9 % and 40 % ambient oxygen concentrations in the same way as was conducted for the horizontal orientation presented in Chapter 2. The radiative heat flux[12] is calculated by

$$\dot{q}'' = \varepsilon \varphi \sigma T^4 \tag{3-2}$$

where φ is the view factor and σ is the Stefan Boltzmann constant. The convective heat flux[13] is

$$\dot{q}'' = h\left(T - T_s\right) \tag{3-3}$$

where T is the temperature of the flame, T_s is the surface temperature and h is the convective heat transfer coefficient, assumed to be 15 ± 5 W/m^{2}K. This is same value used by others.[14,15,16] The sum of these heat fluxes can be used as a consistency check of the measured total flame heat flux value. Note that the view factor for the vertical wall[17] is equal to 1 instead of the 0.23 obtained for the horizontal study.

The radiative and convective heat flux is calculated as 28 ± 8 kW/m^2 and 5 ± 2 kW/m^2 respectively for the 20.9 % ambient oxygen concentration which is consistent with the

experimentally measured total value of 33 ± 3 kW/m^2. The uncertainty given for the flame heat flux is calculated from propagating the uncertainty for each of the equation parameters via the technique of Taylor.[18] For the 40 % ambient oxygen concentration, the radiative and convective heat flux is calculated as 69 ± 8 kW/m^2 and 6 ± 2 kW/m^2 respectively, which is "essentially" consistent with the measured value of 58 ± 3 kW/m^2. This suggests the same as the horizontal study, where the flame heat flux increase which occurs with enriching the ambient oxygen concentration is due primarily to an increase in the radiative component. The purpose of calculating the flame heat flux was to provide an internal consistency check for the flame heat flux measurements. Since the calculated values show consistency, the flame heat flux measurements can be considered accurate.

EXPERIMENTAL RESULTS FOR GAS BURNER

As was done for the related horizontal study presented in Chapter 2, a gas burner is used to decouple the condensed and gas phase effects. The ambient oxygen concentration could be increased without the mass loss flux changing and the effect of the oxygen on the gas phase itself could be seen. Propylene was chosen as the fuel so a significant amount of soot would be present. Experimental measurements obtained include total flame heat flux, flame temperature and visual observations of flame structure and brightness. The experimental setup is shown in Figures 3.1 and 3.2 except that the sample is replaced with a glass bead burner.

Visual Observations

Visual observations made perpendicular to the sample show turbulent flame characteristics over the entire flame length which is evidenced by multiple flame sheets, eddies and wrinkles. This is

again consistent with flow conditions in the chamber. When viewed from the side, the flame appears to have a thickness similar to that seen in the horizontal orientation. Note that there is a uniform mass flux over the burner surface which is different from the condensed sample (PMMA) which presumably varies with height.

The addition of oxygen resulted in an increase in the brightness of the flame is observed indicating increased soot and/or temperature. Large amounts of soot were observed in the flame and forward heating zone as well as going up the exhaust stack for the 40 % oxygen concentration. The 20.9 % oxygen concentration showed very little soot by comparison.

Measured Total Flame Heat Flux

Flame heat flux measurements in the pyrolysis zone were obtained with a heat flux gage in the same fashion as was done for black PMMA and shown in Figure 3.1. No measurements were made in the forward heating zone. The total flame heat flux results were 32 ± 3 kW/m^2 at 20.9 % oxygen and 55 ± 3 kW/m^2 at 40 % oxygen regardless of the fire heat release rate. Since the propylene flow rate is controlled and there is no increase in the mass loss flux with the enhanced oxygen, these results show, similar to the horizontal orientation that oxygen is having an effect on the gas phase in the vertical orientation.

Flame Temperature

The spectral emissivity is used with narrow band infrared pyrometer measurements to obtain the flame temperatures as per the technique described previously for PMMA. The extinction coefficient has been measured for the horizontal orientation and the spectral emissivity

determined for a total flame width of 4 mm. The vertical flame thickness appears to be on this order. This rough correspondence allows the emissivities obtained from the horizontal work to be used for the vertical. Hence, the previously measured total emissivity values of 0.08 ± 0.05 for 20.9% ambient oxygen concentration and 0.12 ± 0.05 for 40 % ambient oxygen concentration will be used for propylene. The average flame temperature is measured as 1013 ± 100 K at 20.9 % ambient oxygen concentration and 1083 ± 100 K at 40 % ambient oxygen concentration. Again this shows that the precision of the temperature measurements needs to be refined in future measurements.

ANALYSIS OF GAS BURNER EXPERIMENTAL DATA

The flame emissivity and temperature are used to calculate the convective and radiative heat fluxes for the 20.9 % and 40 % ambient oxygen concentrations as per the technique described previously for PMMA. The radiative and convective heat flux is calculated as 28 ± 8 kW/m^2 and 6 ± 2 kW/m^2 respectively for the 20.9 % ambient oxygen concentration which is consistent with the experimentally measured total value of 32 ± 3 kW/m^2. For the 40 % ambient oxygen concentration, the radiative and convective heat flux is calculated as 41 ± 8 kW/m^2 and 9 ± 2 kW/m^2 respectively, which is consistent with the measured value of 55 ± 3 kW/m^2. The flame heat flux increase which occurs with enhancing the ambient oxygen concentration is again due primarily to an increase in the radiative component.

EXPERIMENTAL RESULTS FOR DELRIN

As was found for the related horizontal study presented in Chapter 2, ambient oxygen

concentration seems to be primarily affecting the soot production in the gas phase for black PMMA and propylene samples in the vertical orientation. However, the increase in the convective component suggests an additional effect on the fuel vapors in the flame. As such, it is prudent to test a material that does not produce soot. Delrin was chosen since it is non luminous at 20.9 % ambient oxygen concentration and is "well behaved" similar to black PMMA. Measurements obtained for vertical orientation burning of 25 mm thick, thermally thick behaving, black Delrin include total flame heat flux in the pyrolysis zone, flame temperature and visual observations of flame structure and brightness.

Visual Observations

Visual observations show turbulent flame characteristics over the entire sample length from bottom to top which is evidenced by eddies and wrinkles of the flame shape. The turbulent flame structure is again consistent with flow conditions in the chamber. Difficulty was encountered in trying to obtain a side view of the flame.

The flame is bluish and barely visible unless the room is darkened at 20.9 % oxygen. The flame becomes slightly luminous at 40 % ambient oxygen concentration. No soot was observed to accumulate in the forward heating zone or going up the exhaust stack.

Bubbling of the sample surface is observed and some material "melted" (i.e., ran down the sample due to gravity). The 20.9 % oxygen concentration showed minimal "melting" while considerable "melting" for 40 % ambient oxygen concentration was observed. Similar to PMMA, the sample was considered to be pyrolzing where there was bubbling present. A well-defined,

uniform pyrolysis front was observed to travel from the bottom of the sample to the top as it reached steady state. Visual observations of this pyrolysis front show an increase in the "overall" flame spread rate with oxygen, however, flame spread tests were conducted on a longer sample to clarify this. This is presented later in the section called "Delrin Flame Spread."

Measured Total Flame Heat Flux

Flame heat flux measurements were obtained with a Schmidt-Bolter[10] heat flux gage in the same fashion as was done for black PMMA and propylene. Figures 3.1 and 3.2 show the experimental setup except that no measurements were made in the forward heating zone. The pyrolysis zone total flame heat flux results were 36 ± 3 kW/m^2 at 20.9 % oxygen and 49 ± 3 kW/m^2 at 40 % oxygen concentration.

Flame Temperature

The flame temperature was measured, and radiation corrected, with a thermocouple as 592 ± 50 °C for 20.9 % ambient oxygen concentration and 1336 ± 50 °C at 40 % ambient oxygen concentration. Since the flame was bluish, the thermocouple tip was placed in the general flame location and moved around until it glowed red indicting the "hottest" part of the flame.

ANALYSIS OF DERIN EXPERIMENTAL DATA

Similar to the horizontal orientation presented in Chapter 2, for the 20.9 % ambient oxygen concentration where the flame is non luminous, the total flame heat flux can be considered to be

convective only with no radiative component. As such, the total flame heat flux is calculated from the flame temperature as 30 ± 2 kW/m^2, which is consistent with the experimentally measured total value of 36 ± 3 kW/m^2. For the 40 % ambient oxygen concentration, the total flame heat flux can still be considered to be mainly convective with little radiative component. As such, the total flame heat flux is calculated from the flame temperature as 42 ± 2 kW/m^2 which is 'essentially" consistent with the measured value of 49 ± 3 kW/m^2. Interestingly, this suggests that the flame heat flux increase which occurs with enriching the ambient oxygen is due primarily to an increase in the convective component for Delrin.

THE EFFECT OF OXYGEN EXPLAINED

Results from the solid and gas fuel experiments, as well as similar literature results given in Appendix A, lead to the following explanation of what enhanced ambient oxygen concentration is doing similar to what was determined from the horizontal study. The addition of oxygen displaces nitrogen in the gas phase which raises the temperature of the flames. This causes the combustion reactions of the fuel vapors to occur faster than at lower concentrations due to the increased temperature and increased oxygen available such that more fuel per "height" is burned resulting in the concentration of soot in the flame being greater. The increased soot concentration results in an increased flame emissivity. This increased soot leads to more radiative energy loss than at lower oxygen concentrations. This loss of energy lowers the flame temperature. The competing processes of the added oxygen raising the temperature and the increased emissivity lowering the flame temperature reaches a balanced state of flame emissivity and temperature, the values of which depend on the fuel. This explanation is consistent with the theoretical analysis of Tewarson. From a practical viewpoint, the higher flame heat flux, which is mostly the radiative

110

component for typical fuels, results in an increased mass loss flux and heat release rate.

Others have found that oxygen affects a condensed fuel by oxidative pyrolysis.[19,20,21] The above explanation of the effect of oxygen does not preclude this from happening, however, the major effect is in the gas phase for steady state burning in the vertical orientation.

BLACK PMMA FLAME SPREAD

The increased flame heat flux with the enhancement of oxygen found in the current study for the vertical orientation indicates that the "thermally thick behavior" flame propagation should increase if flame spread is predominately controlled by the flame heat flux (i.e., the heat transfer from the flame to the sample). Visual observations in this study show an increased "overall" flame propagation rate with enhanced oxygen for PMMA, however, vertical flame spread tests were conducted on a longer sample to clarify this by obtaining measurements of an "average" flame spread rate.
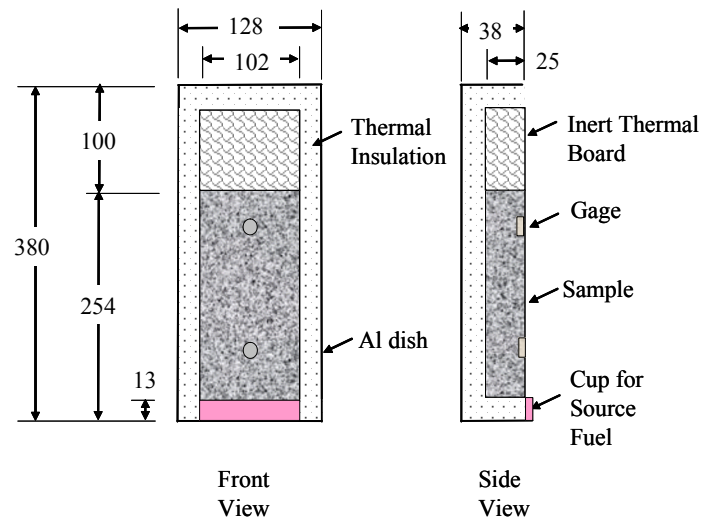
Figure 3.3   Experimental set-up for vertical flame spread velocity. Measurements in mm.

The experimental set up for flame propagation tests is shown in Figure 3.3. The sample was 10.2 cm wide by 25.4 cm long and ignition was by means of 2 mL ethyl alcohol. The sample would ignite uniformly across the width at the bottom 1 cm as the source fuel was on the verge of extinguishing. The sample would then start to spread about 1 minute later, hence, the fuel source did not affect the flame spread. Individual tests were run with 20.9 % or 40 % oxygen concentration and the pyrolysis front was determined by visual observation of surface bubbling. (Where bubbling was present, the sample was considered to be pyrolyzing.)

The "average" spread rate was determined by dividing the entire sample length by the time it took the pyrolysis front to spread from the bottom of the sample to the top. The result of added oxygen was to increase the measured overall "average" flame propagation rate from 1.3 ± 0.2 to 3.0 ± 0.2 mm/sec.

Model for Spread

Quintiere and Harkleroad[15] present a simple "thermal" flame propagation model developed by Sibulkin and Kim[22] given as

$$V = \frac{(\dot{q}'')^2 \delta_f}{k\rho c(T_{ig} - T_s)^2} \qquad (3\text{-}4)$$

where V is the pyrolysis front velocity, $\dot{q}''$ is the average flame heat flux over the surface downstream of the pyrolysis zone, δ_f is the flame length over this same zone (i.e., the forward heating zone), $k\rho c$ is the thermal inertia, T_{ig} is the ignition temperature and T_s is the surface temperature "before flame effects."

112

Using this equation, the calculated flame propagation for 20.9 % ambient oxygen concentration should be 1.3 ± 0.8 mm/sec. The independently measured values for the density,[23] thermal conductivity[24], and specific heat[25] of PMMA of 1180 kg/m^2, 0.19 W/mK and 1280 J/kg K were used. The heat flux measured in the pyrolysis zone by gage 1 at a height of 5.8 cm was given earlier as 33 ± 3 kW/m^2, the ignition temperature was measured as 623 K and the "before flame effects" surface temperature was considered as 293 K.
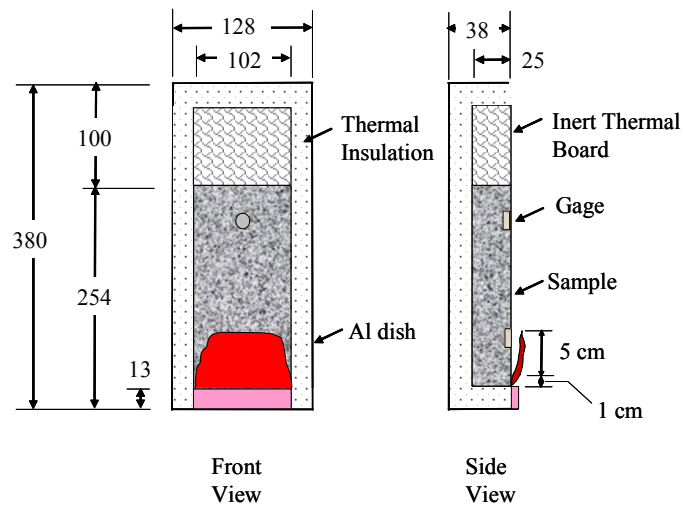
Figure 3.4   Forward heating zone length used in calculations. Measurements in mm.

The experimentally measured forward heating zone length changes as the pyrolysis front propagates but for simplicity a single length was used. This length, 5 cm as shown in Figure 3.4, when the source fuel extinguished and the beginning of flame spread started was used.

For the 40 % oxygen concentration, the properties are considered to be the same as the 20.9 % oxygen concentration. The forward heating zone length and ignition temperature were observed

to be the same as the 20.9 % oxygen concentration while the pyrolysis zone (gage 1) measured flame heat flux, given earlier, changed to 58 ± 2 kW/m^2. This gives a calculated flame propagation velocity of 4.1 ± 0.8 mm/sec.

A comparison can be made between the experimental values and those predicted by the model of Sibulkin and Kim.[22] For the 20.9 % oxygen concentration, the measured flame spread velocity is 1.3 ± 0.2 mm/sec while the calculated is 1.3 ± 0.8 mm/sec. Considering for the uncertainty, these are consistent. For the 40 % oxygen concentration, the measured velocity is 3.0 ± 0.2 mm/sec while the calculated is 4.1 ± 0.8 mm/sec which are consistent with each other. From the consistent results between the measured velocity and those calculated using a "thermal" model, it is reasonable to suggest that the increase in the flame spread velocity is due predominately to the increase in the flame heat flux for PMMA. However, the velocity calculations are very dependent on the forward heating zone length so more detailed measurements need to be made in future work.

Research[19] in the literature' shows that gas phase oxygen reacts with the forward heating zone material and enhances decomposition by oxidative pyrolysis resulting in a faster flame spread. Others[20,21] have also reported that gas phase oxygen effects the solid phase decomposition of organic polymers. According to the present results, this appears to be a minor contribution compared to the flame heat transfer effect but this area needs to be more thoroughly investigated.

Measured Total Flame Heat Flux During Flame Spread

As was seen in Figure 3.3, heat flux gages were used to measure the flame heat flux in the sample during flame spread. The value as the flame passed the gage and then stayed for the subsequent

steady burning was 37 ± 2 kW/m^2 for the 5.1 cm height and 36 ± 2 kW/m^2 for the 20.3 cm height

for 20.9 % oxygen concentration. (No heat flux measurements were made for 40 % oxygen

concentration.) This indicates that the flame heat flux back to the burning surface is

approximately constant over the flame height (pyrolysis zone and forward heating zone where

there is a flame) for these small scale samples. These values are essentially consistent, albeit

somewhat higher, with the values obtained during steady burning of the 10.2 cm high sample.

Note that the values from the steady burning experiments are used in the spread calculations since

no measurements were made during flame spread at 40 % oxygen concentration.

DELRIN FLAME SPREAD

For reasons similar to PMMA, vertical flame spread tests were conducted on a longer sample to

obtain measurements of an "average" flame spread rate for Delrin. The experimental set up was

the same as for PMMA, given in Figure 32, except the sample length was 30.5 cm. Individual

tests were run with 20.9 % or 40 % oxygen concentration and the pyrolysis front was determined

by visual observation of surface bubbling. The result of added oxygen was to increase the overall

"average" flame spread rate from 0.5 ± 0.2 mm/sec to 2.8 ± 0.2 mm/sec.

Model for Spread

Using the same model equation by Silbulkin and Kim[22] as described for PMMA, the calculated

flame spread for 20.9 % ambient oxygen concentration should be 1.5 ± 0.8 mm/sec. The

independently[26] measured values for the density, thermal conductivity and specific heat of Delrin

of 1420 kg/m^2, 0.37 W/mK and 1470 J/kg K were used. The experimentally measured forward

heating zone length, obtained in the same way as for PMMA, was 3.8 ± 1 cm, the pyrolysis zone

heat flux was 36 ± 2 kW/m^2, the ignition temperature was measured as 503 K and the "before flame effects" surface temperature was 293 K. For the 40 % oxygen concentration, the properties, forward heating zone length and ignition temperature are considered to be the same as the 20.9 % oxygen situation while the pyrolysis zone flame heat flux changed to 49 ± 2 kW/m^2. This gives a calculated flame spread velocity of 2.6 ± 0.8 mm/sec.

A comparison can be made between the experimental values and those predicted by the model of Sibulkin and Kim.[22] For the 20.9 % oxygen concentration, the measured flame spread velocity is 0.5 ± 0.2 mm/sec while the calculated is 1.5 ± 0.8 mm/sec. Considering for the uncertainty, these are consistent. For the 40 % oxygen concentration, the measured velocity is 2.8 ± 0.2 mm/sec while the calculated is 2.6 ± 0.8 mm/sec which are again consistent with each other. From the consistent results between the measured velocity and those calculated using a "thermal" model, it is reasonable to suggest that the increase in the flame spread velocity is due predominately to the increase in the flame heat flux for Delrin although the oxidative pyrolysis issue needs to be more thoroughly investigated.

Measured Total Flame Heat Flux

As was seen in Figure 3.3, heat flux gages were used to measure the flame heat flux in the sample during flame spread. The value as the flame passed the gage and then stayed for the subsequent steady burning at was 41 ± 3 kW/m^2 at the 5.1 cm height and 37 ± 3 kW/m^2 at the 25.4 cm height for 20.9 % oxygen concentration. For 40 % oxygen concentration, the values were 51 ± 3 kW/m^2 at the 5.1 cm height and 53 ± 3 kW/m^2 at the 25.4 cm height. These indicate that the flame heat flux back to the burning surface is approximately constant over the flame height for these small

scale samples. Note that the values from the steady burning experiments are used in the spread calculations to be consistent with what was done for PMMA.

COMPARISON TO LARGE SCALE

Literature data of flame heat flux for large scale vertical tests of black PMMA can be used for comparison to the small scale, enhanced oxygen flame heat flux results of the present study to determine the level of scalability that enhanced oxygen provides. (No large scale data for Delrin was found in the literature.) The question "does the flame heat flux obtained in small scale with added oxygen match that in ambient oxygen large scale ?" is to be answered. As such, large scale data is needed. Large scale vertical tests could not be run in the present study so literature data for outward and inward flame heat flux measurements were used as well as flame spread model results.

Literature Measurements - Outward

Orloff, Modak and Alpert[27,28] measure the "outward" radiation (out to the ambient and not back to the burning surface) for a 3.56 m high, 0.9 m wide, 6.4 cm thick vertical PMMA sample using a ray radiometer at various heights. All radiance measurements were made at 60° to the surface normal where it is shown that "π times the flame radiance at 60° to the surface yields the flame radiative heat flux in both the thick and thin limits." These readings are from the flame as well as the burning surface so the flame radiance is corrected for surface radiative losses and the flame transmittance, assuming that radiation scattering is negligible. Details of how the surface radiative loss is determined can be found in the paper. The convective heat flux is assumed to be constant with height at a value of 5.5 kW/m^2. The radiative and convective heat flux are added per height

to obtain the total flame heat flux back to the burning surface that increases almost linearly from

20.2 kW/m^2 at 0.51 m high to 42 kW/m^2 at 3.56 m high as shown in Figure 3.5.
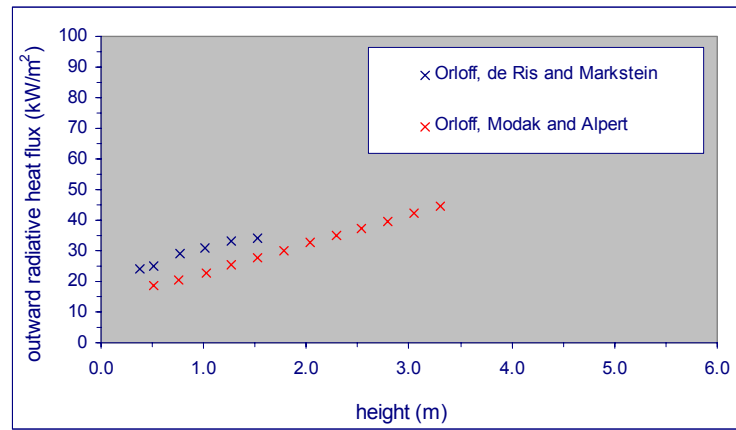
(a)
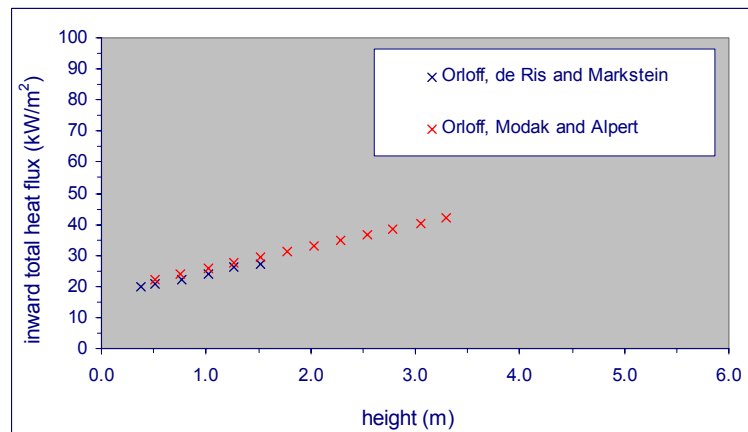
(b)

Figure 3.5   Literature data of Orloff, Modak and Alpert[27,28] and Orloff, de Ris and Markstein[29]

(a) outward radiative and (b) inward total heat flux.

Orloff, de Ris and Markstein[29] used a 1.57 m high, 0.4 m wide, 4.5 cm thick vertical PMMA

sample. Outward radiance measurements, which are from the flame and the burning surface, were made normal to the surface using a ray radiometer. The radiance due to the flame only was determined by subtracting the surface radiance loss from the measurements. Additionally, a correction is made for the presence of water cooled "sidewalls" in the experimental setup. Details of the surface radiative loss and the sidewall correction can be found in their paper. The inward flame radiative heat flux is determined from the outward flame radiance by assuming an optically thin flame and 7 % blockage. The flame convective heat flux is inferred from a surface energy balance and found to slightly decrease with height. It is added to the flame radiative flux per height to obtain the total flame heat flux back to the burning surface that increases almost linearly from 21 kW/m^2 at 0.38 m high to 27 kW/m^2 at 1.5 m high.

Both these papers used essentially the same experimental setup however, they obtain different outward measurements. This is reasonable since different laboratory conditions could have existed. Interestingly, they calculate the same inward total flame heat flux results from these different measurements. The extrapolated flame heat flux from this data at a height of 0.15 m and 0.25 m (which are the present study heights) is approximately 15 to 18 kW/m^2. These are lower than that measured directly in the current study. Additionally, Orloff, de Ris and Markstein[29] incorporate a correction for the presence of water cooled sidewalls, which the current study does not fully agree with. Due to these reasons, the literature data will be re-visited in the current study to gain more understanding.

To re-visit the data, the flame only outward radiance measurements provided by the papers are converted to outward radiative heat flux assuming optically thin flames. A 7% blockage (as used by the authors) is applied to obtain the inward radiative heat flux. The convective heat flux is

calculated from q = h*(T_f-T_s) where h* is the corrected heat transfer coefficient, considering for mass coming off, or "blowing" from the sample surface. T_f is the flame temperature and T_s is the surface temperature. The corrected heat transfer coefficient[30] is determined from

$$h* = \frac{\dot{m}''c_p}{e^{\left(\frac{\dot{m}''c_p}{h^0}\right)} - 1}$$ (3-5)

where $\dot{m}''$ is the mass flux blowing from the sample, c_p is the specific heat of the gas, assumed to be air, and h^0 is the convective heat transfer coefficient with no blowing, given earlier as 15 ± 5 kW/m^{2}s. The re-visited results for total flame heat flux are shown in Figure 3.6.

Observe from Figure 3.6b that the re-visited values are only slightly different from the literature values. This difference is due to the convection being handled differently. In contrast, Figure 3.6a shows quite a difference in the literature and re-visited values. This is probably due to the "sidewall" correction made in the literature results that is not made in the current study.

(a)
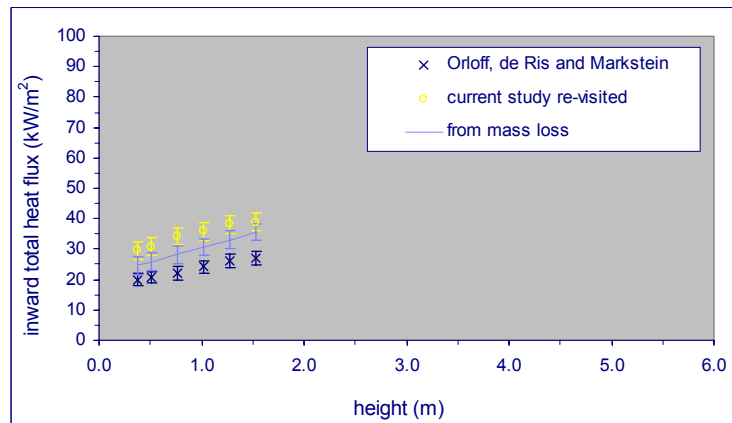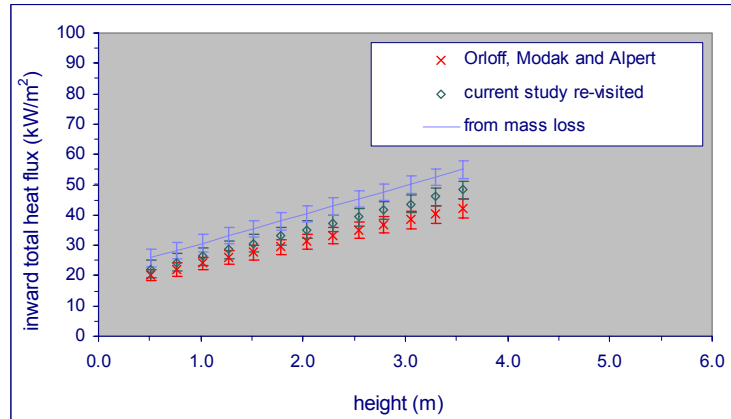
Figure 3.6   Literature data and current study re-visited data for PMMA inward total heat flux from (a) Orloff, de Ris and Markstein[29] and (b) Orloff, Modak and Alpert[27,28]

To determine if the re-visited results are reasonable, the flame heat flux is calculated from the literature[27,28,29] mass loss flux using $\dot{q}'' = \dot{m}''h_g$ where the h_g value used is 2.4 kJ/g determined in Chapter 1. This value obtained from horizontal tests can be used in the vertical since the same physical phenomena is occurring in both orientations. Observe from the figure that these calculated values overlap the re-visited data when considering for the uncertainty. This provides evidence that the current study re-visited values are reasonable and also that the sidewall correction is questionable.

The uncertainty levels shown are calculated from propagating the uncertainty of each parameter as given by the authors using Taylor's[18] equation. A look at additional literature data of inward measurements would be prudent at this point. All of the following literature data is presented as the total flame heat flux as defined in the current study and is shown in Figure 3.7.

Hasemi[31] used Gardon type heat flux gages to measure the inward total flame heat flux for methane line burners against isothermal and thermally thin walls. He classifies the wall into three distinct regions of solid flame, transition and plume. For the solid flame region (which includes the pyrolysis zone) the inward total flame heat flux is approximately constant with height (approximately 28 kW/m^2) for all tests except for the smallest size burner. Since these results may be different than for a vertical condensed fuel, a comparison was made to previous data of Ahmad and Faeth[32] made with 5-30 cm high vertical wicks, who state "the region of relatively constant wall heat flux ends as the average position of the end of the visible portion of the flame is approached."

Quintiere, Harkleroad and Hasemi[33] measured inward total flame heat flux for various materials including Douglas fir particleboard, flexible foam, carpet, rigid foam, PMMA and epoxy fiberite. Measurements were made in the forward heat zone using a Gardon type heat flux gage. A constant total flame heat flux of 20 - 30 kW/m^2 is found in the flame zone. Quintiere and Cleary[34] use these experimental results to state "results show that the heat flux to the wall surfaces starts at low values at the origin, rapidly rises to 20 to 30 kW/m^2, is nearly constant in that range up to half the flame height then drops off sharply."

Tewarson and Ogden[35] agree with Quintiere, Harkleroad and Hasemi[33] that the flame heat flux in the solid flame region varies from 20 – 30 kW/m^2 for vertical samples 0.1 m wide, 0.3 and 0.61 m high black PMMA, 0.025 m thick.

Brehob and Kulkarni[36] measured inward total flame heat flux, using a Gardon heat flux gage, for samples 120 cm high, 30 cm wide for various thickness materials including PMMA, Douglas Fir,

fire-retarded plywood, Poplar, cardboard and cotton textile. The data shows that the inward total flame heat flux is almost constant with height in the flame zone. They state "for all the heat flux data shown, each of the gages reached a fairly constant level of heat flux as the flame passed and remained at this level until the flame began to recede." For black PMMA, they report the flame heat flux value of Kim[37] as 35 kW/m². An estimation of their uncertainty is made from traces of their other materials.

Ohlemiller and Cleary[38] measured the inward total flame heat flux for a 1.22 m high, 0.38 m wide, 0.95 cm thick composite panel (vinyl ester/E-glass) that was heated with an electrical radiant panel located quite close to the sample. They show a variation of flame heat flux at the higher applied heat fluxes but do not indicate if there is a trend with height. Due to this and observing that the set-up can be considered a parallel panel orientation, no conclusion can be made as to a change in the flame heat flux with height for a single vertical wall. However, they present data from a related study for a free burn vertical wall of polyester. This data shows that the inward total flame heat flux does not change with height in the pyrolysis zone.

Wu and Tewarson[39] conducted experiments on a 5 m high, 0.6 m wide, 2.54 cm thick PMMA vertical sample. They measured inward total flame heat flux with gages at various heights. Evaluation of this data shows that, up to 3.4 m height, as the flame reached the gage the value rises sharply to an almost steady value that slightly increases with time. The values presented on Figure 7 are an average of that gage reading from rise to the test end at 1400 sec and the uncertainty represents the variation. For heights greater than 3.4 m, the heat flux trace never reaches a steady value but rises rapidly when the flame reaches the top of the sample (which is the same time that the flame reaches that gage). Calculations done in the current study, using the

123

mass loss flux with height provided in the literature, indicate that the bottom 0.5 m of the sample may be regressed by 0.7 cm. Additional calculations, using the flame heat flux measured in the current study, show that the bottom of the sample is no longer thermally thick behaving. These small changes in the leading edge could cause a difference in the boundary layer upstream. Since no explanation for the "non steady" behavior is provided by the authors for heights above 3.4 m, the data above 3.4 m height is not used in the current study of thermally thick behavior.

Figure 3.7 shows the inward total heat flux measurements of the current study and literature. Also shown is the re-visited inward total heat flux calculated from the outward radiative measurements of Orloff, de Ris and Markstein[29] and Orloff, Modak and Alpert.[27,28] When the data is viewed in aggregate, the variation of total heat flux with height as measured to date is not as clearly defined. Hence, the extent of the flame heat flux variation with height is inconclusive, although it is understood that it should increase with height, and needs to be explored further in a future study.
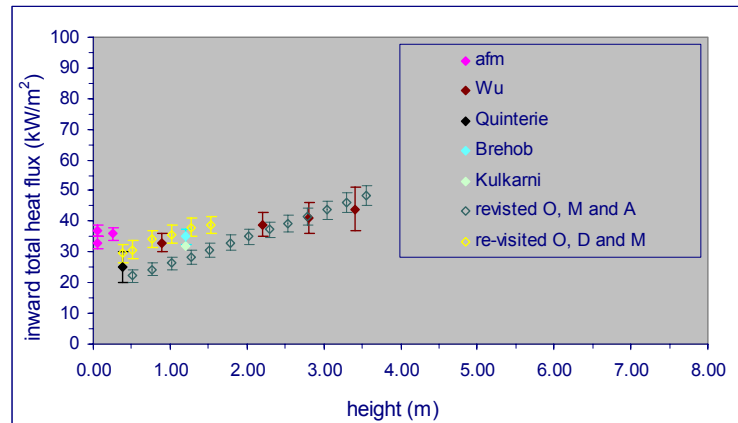
Figure 3.7   Inward total heat flux measurements including current study and literature data for Wu,[39] Quinterie,[33] Brehob[36] and Kulkarni. Also shown is (a) the re-visited data (calculated) of Orloff, Modak and Alpert[27,28] and Orloff, de Ris and Markstein.[29]

It is noted that the flame physical thickness increases with height causing a change in the optical thickness of the flame. The flame emissivity will increase such that the radiation component of the total flame heat flux goes up. Basic theory says that the convective heat transfer coefficient[40] must go down as the boundary layer thickness increases, which also happens as the vertical scale gets larger. Since this convective decrease should level off while the radiative keeps increasing, the total should increase with height. Some useful information may be gleaned by a look at flame spread models.

Literature – Flame Spread Models

Delichatsios[41] uses the flame spread data of Tewarson and Ogden[35] for a PMMA vertical wall to compare to his flame spread theory results. In order to get his results to match the experimental data, a constant value of 25 to 35 kW/m^2 is used for the inward flame heat flux in the wall orientation. For vertical cylinders, a value of 35 kW/m^2 is needed at 20.9 % oxygen while 42 and 60 kW/m^2 is needed for 28 % and 45 % oxygen respectively.

Delichatsios, Mathews and Delichatsios[42] use the flame spread data of Orloff, de Ris and Markstein[29] for a PMMA wall to compare to his flame spread model results. A constant value for the entire 1.5 m height of 32 kW/m^2 used as the inward total flame heat flux in the model gives satisfactory agreement with the experimental data but a value of 25 kW/m^2 gives better agreement.

Saito, Quintiere and Williams[43] present an upward flame spread theory for thermally thick behaving materials. A constant value of 25 kW/m^2 is used over the flame length where they

match their flame spread experimental results for a 1.3 cm thick, 30 cm wide sample of PMMA.

Kulkarni, Brehob, Manohar and Nair[44] quote Delichatsios' constant value of 25 kW/m^2 for the inward flame heat flux as a good starting place for the inward flame heat flux to be used in their flame spread model. However, they found the experimental value of 32 kW/m^2 from the work of Kim allowed a more accurate comparison of theory results to experimental data.

The flame heat flux values used by these flame spread models to obtain a match to experimentally measured flame spread results ranges from 25 to 35 kW/m^2 for PMMA. This is comparable to the experimentally measured inward flame heat flux range as shown in Figure 3.7. Hence, no additional information is gleaned to evaluate the extent of the flame heat flux variation with height. Carefully instrumented experiments need to be conducted in future studies.

SCALABILITY AND GEOMETRY

Interestingly, Figure 3.7 shows that the current study small scale flame heat flux for 20.9 % oxygen concentration is approximately the same as for the geometrically similar large scale up to 3.4 m for thermally thick behaving PMMA when the uncertainty is considered. The flame heat flux for 0.1 m high vertical PMMA, is 36 ± 3 kW/m^2 while for 3.4 m high it is 44 ± 7 kW/m^2. Recall that the small scale tests conducted in the current study had turbulent flame characteristics over its entire height.

The heat flux the sample is exposed to in the small scale test, being only that contributed by the flame itself, can be increased by enriching the ambient oxygen concentration of the sample

environment as was shown in the current study. However, since the flame heat flux is already about the large scale level, the increase is greater than that obtained in the same single wall geometry. The small scale flame heat flux for PMMA obtained for 40 % ambient oxygen concentration is 58 ± 2 kW/m^2 which is the value obtained, up to 0.6 m high, from parallel panel tests of PMMA.[45] For the parallel panel, the total heat flux is from the flame (25 kW/m^2) and the source fire (40 kW/m^2) which is 65 kW/m^2 at 0.6 m height.[46] As such, the flame spread results of small scale, enhanced ambient oxygen concentration should correlate well with parallel panel results. This has been observed by Wu and Bill.[46]

The test protocol[3] used by Wu and Bill[46] for propagation is NFPA 287, Standard Test Methods for Measurement of Flammability of Materials in Cleanrooms Using a Fire Propagation Apparatus,[4] which contains test requirements and procedures for the evaluation of materials used in the semiconductor industry. It prescribes the method for both the small scale test using a Fire Propagation Apparatus and the intermediate scale test using the Parallel Panel Apparatus, which is shown in Figure 3.8.
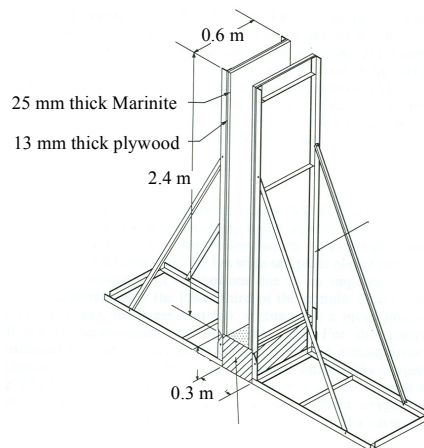
Figure 3.8   Parallel Panel Apparatus used by Wu and Bill. [46]

Materials tested by Wu and Bill[46] include chlorinated polyvinylchloride (CPVC), polyvinylidene fluoride (PVDF), gray polyvinylchloride (PVC gray), white polyvinylchloride (PVC white), polysulfone (PSU), polycarbonate (PC), polymethylmethacrylate (PMMA) and fire-retarded polypropylene (FRPP). They show for these materials that "the ranking by heat release rate in the propagation test with a vertical sample in air containing 40 % oxygen is identical to that found in a Parallel Panel test." The ranking order is shown in Table 3.2.

Table 3.2   Ranking of materials tested by Wu and Bill. [46]

Ranking of Materials by Heat Release Rate	Parallel Panel Propagation
CPVC	No
PVDF	No
PVC gray	No
PVC white	No
PSU	Yes
PC	Yes
PMMA	Yes
FRPP	Yes

They also found that "the propagation test with enhanced oxygen provided the best correlation with fire propagation behavior (propagating vs. non propagating) in the Parallel Panel test." Note that propagation is defined as self sustained flame spread while non propagation defines a flame that is not self sustained.

SUMMARY AND CONCLUSIONS

The Advanced Flammability Measurements Apparatus[1] (AFM) was used to conduct small scale experiments at ambient oxygen concentrations of 20.9 to 40 % oxygen for various materials. Black PMMA, propylene and Delrin were chosen and the total flame heat flux was experimentally measured with a heat flux gage as well as calculated from flame emissivity and temperature measurements.

For black PMMA, the measured total flame heat flux in the pyrolysis zone was 33 ± 3 kW/m^2 at 20.9 % oxygen. The radiative and convective heat flux is calculated as 28 ± 8 kW/m^2 and 5 ± 2 kW/m^2 respectively for the 20.9 % ambient oxygen concentration which is consistent with the experimentally measured value. For the 40 % ambient oxygen concentration, the radiative and convective heat flux is calculated as 69 ± 8 kW/m^2 and 6 ± 2 kW/m^2 respectively, which is "essentially" consistent with the measured value of 58 ± 3 kW/m^2. For propylene, the total flame heat flux measurements were 32 ± 3 kW/m^2 at 20.9 % oxygen and 55 ± 3 kW/m^2 at 40 % oxygen regardless of the fire size. Since the propylene flow rate is controlled and there is no increase in the mass loss flux, these results show, similar to the horizontal work, that oxygen is having an effect on the gas phase in the vertical orientation. For Delrin, the measured total flame heat flux results were 36 ± 3 kW/m^2 at 20.9 % oxygen and 49 ± 3 kW/m^2 at 40 % oxygen concentration.

These results show that enhanced ambient oxygen is indeed increasing the flame heat flux. The general mechanism, as determined from the data of the current study and Chapter 2, is described. The addition of oxygen displaces nitrogen in the gas phase which raises the temperature of the flames. This causes the combustion reactions of the fuel vapors to occur faster than at lower

concentrations due to the increased temperature and increased oxygen available such that more fuel per "height" is burned resulting in the concentration of soot in the flame being greater. The increased soot concentration results in an increased flame emissivity. This increased soot leads to more radiative energy loss than at lower oxygen concentrations. This loss of energy lowers the flame temperature. The competing processes of the added oxygen raising the temperature and the increased emissivity lowering the flame temperature reaches a balanced state of flame emissivity and temperature, the values of which depend on the fuel. This results in an increase in the total flame heat flux where the distribution between radiative and convective heat flux also depend on the fuel.

Using the simple flame spread model of Subilkin and Kim,[22] the "average" calculated flame spread for 20.9 % ambient oxygen concentration is 1.3 ± 0.8 mm/sec for black PMMA. For 40 % the calculated flame spread velocity is 4.1 ± 0.8 mm/sec. These are consistent with the measured "average" flame spread rates of 1.3 ± 0.2 mm/sec at 20.9 % oxygen and 3.0 ± 0.2 mm/sec for 40 % oxygen concentration. For Delrin, the measured flame spread velocity is 0.5 ± 0.2 mm/sec while the calculated is 1.5 ± 0.8 mm/sec at 20.9 % ambient oxygen concentration. For the 40 % oxygen concentration, the measured velocity is 2.8 ± 0.2 mm/sec while the calculated is 2.6 ± 0.8 mm/sec. From the consistent results between the measured velocity and those calculated using a "thermal" model for these two materials, it is reasonable to suggest that the increase in the flame spread velocity is due predominately to the increase in the flame heat flux (thermally driven) although the oxidative pyrolysis issue needs to be more thoroughly investigated.

From the literature data of Orloff, Modak and Alpert[27] and Orloff, de Ris and Markstein,[29] extrapolation of the flame heat flux for a height of 0.15 m and 0.25 m (which are the present

study heights) gives approximately 15 to 18 kW/m^2. These values are lower than the values measured directly in the current study or by other researchers. Additionally, these papers show a very distinct increase of the flame heat flux with height. When the data is viewed in aggregate, the variation of total heat flux with height is not as clearly defined. Hence, the extent of the flame heat flux variation with height is inconclusive, although it is understood that it should increase with height, and needs to be explored further in a future study.

Interestingly, the current study measurements show that the small scale flame heat flux for 20.9 % oxygen concentration is approximately the same as for the geometrically similar large scale up to 3.4 m for thermally thick behaving PMMA when the uncertainty is considered. This should be investigated further in a future study. The flame heat flux for 0.1 m high vertical PMMA, is 36 ± 3 kW/m^2 while for 3.4 m high it is 44 ± 7 kW/m^2. Note that the small scale tests conducted in the current study had a turbulent flame structure over its entire height.

The heat flux the sample is exposed to in the small scale test, being only that contributed by the flame itself, can be increased by enriching the ambient oxygen concentration of the sample environment as was shown in the current study. However, since the flame heat flux is already about the large scale level, the increase is greater than that obtained in the same single wall geometry. In fact, the flame heat flux for PMMA obtained for 40 % ambient oxygen concentration is 58 ± 3 kW/m^2 which is the level obtained, up to 0.6 m high, from parallel panel tests of PMMA.[45] For the parallel panel, the total heat flux is from the flame (25 kW/m^2) and the source fire (40 kW/m^2) which is 65 kW/m^2 at 0.6 m height. As such, the flame spread results of small scale, enhanced ambient oxygen concentration should correlate well with parallel panel results. This has been observed by Wu and Bill.[46]

Measurements and Calculation Results Summarized in Table Form

Table 3.3   Black PMMA vertical small scale (pyrolysis zone) flame heat flux results summary.

	Measured Flame Heat Flux kW/m^2		Calculated Flame Heat Flux kW/m^2	
	20.9 %	40 %	20.9 %	40 %
Radiative	-	-	28 ± 8	69 ± 8
Convective	-	-	5 ± 2	6 ± 2
Total	33 ± 3	58 ± 3	33 ± 10	75 ± 10

Table 3.4   Black PMMA vertical small scale (pyrolysis zone) results summary.

Oxygen %	$\dot{m}''$ g/m^{2}s	T_s* K	T_f K	ε* -	h_f cm	f_v* -
	± 1	± 50	± 100	± 0.08	± 0.64	± 0.6 x 10^{-6}
20.9	-	623	1121	0.06	-	11.3 x 10^{-6}
40	-	543	1208	0.16	-	27.3 x 10^{-6}

* Values from horizontal study presented in Chapter 2.

Table 3.5   Propylene vertical small scale flame heat flux results summary.

	Measured Flame Heat Flux kW/m²		Calculated Flame Heat Flux kW/m²	
	20.9 %	40 %	20.9 %	40 %
Radiative	-	-	28 ± 8	41 ± 8
Convective	-	-	6 ± 2	9 ± 2
Total	32 ± 3	55 ± 3	34 ± 10	50 ± 10

Table 3.6   Propylene vertical small scale results summary.

Oxygen %	$\dot{m}''$ g/m²s	T_s K	T_f K	ε^* -	h_f cm	f_v^* -
	± 1	± 50	± 100	± 0.05	± 0.64	± 0.6 x 10^{-6}
20.9	-	-	1013	0.08	-	12.3 x 10^{-6}
40	-	-	1083	0.12	-	22.6 x 10^{-6}

* Values from horizontal study presented in Chapter 2.

Table 3.7   Delrin vertical small scale (pyrolysis zone) flame heat flux results summary.

	Measured Flame Heat Flux kW/m^2		Calculated Flame Heat Flux kW/m^2	
	20.9 %	40 %	20.9 %	40 %
Radiative	-	-	0	0
Convective	-	-	30 ± 2	42 ± 2
Total	36 ± 3	49 ± 3	30 ± 2	42 ± 2

Table 3.8   Delrin vertical small scale (pyrolysis zone) results summary.

Oxygen %	$\dot{m}''$ g/m^{2}s	T_s* K	T_f K	ε* -	h_f cm	f_v* -
	± 1	± 50	± 100	± 0.08	± 0.64	± 0.6 x 10^{-6}
20.9	-	513	592	-	-	-
40	-	473	1363	-	-	-

* Values from horizontal study presented in Chapter 2.

Table 3.9   Flame spread summary

	Measured Flame Propagation Velocity mm/sec		Calculated Flame Propagation Velocity mm/sec	
	20.9 %	40 %	20.9 %	40 %
Black PMMA	1.3 ± 0.2	3.0 ± 0.2	1.3 ± 0.8	4.1 ± 0.8
Delrin	0.5 ± 0.2	2.8 ± 0.2	1.5 ± 0.8	2.6 ± 0.8

REFERENCES

1   Beaulieu, P., Dembsey, N., and Alpert, R., "A New Material Flammability Apparatus and Measurement Techniques," Composites 2003, Anaheim, CA, 2003.

2   Tewarson, A., "Flammability Parameters of Materials: Ignition, Combustion and Fire Propagation," Journal of Fire Sciences, 12, p. 329-356, 1994.

3   Factory Mutual Research Clean Room Materials Flammability Test Protocol 4910, FM Global Research, Norwood, MA, 1997.

4   NFPA 287, Standard Test Methods for Measurement of Flammability of Materials in Cleanrooms, National Fire Protection Association, Quincy, MA, 2001.

5   Wu, P., and Bill, R., "Laboratory Tests for Flammability Using Enhanced Oxygen," Fire Safety Journal, 38, p. 203 – 217, 2003.

6   Tewarson, A., Lee, J and Pion, R., "The Influence of Oxygen Concentration on Fuel Parameters for Fire Modeling," Eighteenth International Symposium on Combustion, The Combustion Institute, p. 563-570, 1981.

7   Handbook of Fire Protection Engineering, 2nd edition, "Chapter 3-4, Generation of Heat and Chemical Compounds in Fires," Society of Fire Protection Engineers, Boston, MA, 1995.

8   Standard Test Methods for Measurement of Synthetic Polymer Material Flammability Using a Fire Propagation Apparatus, ASTM E 2058, American Society of Testing Materials, Philadelphia, PA, 2001.

9   ASTM Standard Method for Heat and Visible Smoke Release Rates for Materials and Products Using an Oxygen Consumption Calorimeter, ASTM E 1354, American Society of Testing Materials, Philadelphia, PA, 1999.

10   Medtherm Corporation Catalog, Huntsville, AL, 2004.

11   Cotronics Corporation Catalog, Brooklyn, NY, 2000.

12   Thermal Radiation Heat Transfer, Sigel and Howell, Hemisphere Publishing Company, New York, NY, 1981.

13   Heat Transfer, Holman, J., McGraw Hill Book Company, New York, NY, p. 622-624, 1986.

14   Mowrer, F., "An Analysis of Effective Thermal Properties of Thermally Thick Materials," Fire Safety Journal, 40, 5, p. 395 – 410, July 2005.

15   Quintiere, J. and Harkleroad, M., "New Concepts for Measuring Flame Spread Properties," Fire Safety: Science and Engineering, ASTM STP 882, American Society for Testing and Materials, Philadelphia, p. 239 – 267, 1985.

16   Janssens, M., "Fundamental Thermophysical Characteristics of Wood and Their Role in Enclosure Fire Growth," PhD dissertation, University of Gent, Belgium, 1991.

17   Handbook of Fire Protection Engineering, 3rd edition, Chapter 1-4, Radiation Heat Transfer, Society of Fire Protection Engineers, Boston, MA, 2002.

18   An Introduction to Error Analysis, John Taylor, University Science Books, Sausalito, CA, 1982.

19   Brown, J., and Kashiwagi, T., "Gas Phase Oxygen Effect on Chain Scission and Monomer Content in Bulk PMMA Degraded by External Thermal Radiation," Polymer Degradation and Stability, V. 52, 1996.

20   Kashiwagi, T and Ohlemiller, T., "A Study of Oxygen Effects on Nonflaming Transient Gasification of PMMA and PE During Thermal Irradiation, 19th International Symposium on Combustion," The Combustion Institute, p. 815 – 823, 1982.

21   Cullis, C., "The Involvement of Oxygen in the Primary Decomposition Stage of Polymer Combustion," Fire Safety Science: Proceedings of the 1st International Symposium, p. 371 – 380.

22   Sibulkin, M. and Kim, J., Combustion Science and Technology, 17, p. 39-49, 1977.

23   Polymers: A Property Database (Online CD), CRC Press, 2000.

24   Putnam, S., Cahill, D., Ash, B and Schadler, L., "High Precision Thermal Conductivity Measurements as a Probe of Polymer/Nanoparticle Interfaces," 2003.

25   Handbook of Fire Protection Engineering, 2nd edition, "Chapter 3-4, Generation of Heat and Chemical Compounds in Fires," Society of Fire Protection Engineers, Boston, MA, 1995.

26   Ignition Handbook, Babrauskas, V., "Chapter 7: Common Solids," Fire Science Publishers, Issaquah, WA, 2003.

27   Orloff, L., Modak. A., and Alpert, R., "The Effect of Radiative Heat Transfer From Flames on Burning Rate of Large Scale Vertical Plastic Surfaces," FM Global Report FMRC 22361-1, 1975.

28   Orloff, L., Modak, A. and Alpert, R., "Burning of Large Scale Vertical Surfaces," 16th International Symposium on Combustion, Combustion Institute, p. 1354 – 1354, 1976.

29   Orloff, L., de Ris, J. and Markstein, G., "Upward Turbulent Fire Spread and Burning of Fuel Surface," 15th International Symposium on Combustion, Combustion Institute, p. 183 – 192, 1974.

30   Handbook of Fire Protection Engineering, 3rd edition, Chapter 1-3, Convection Heat Transfer, Society of Fire Protection Engineers, Boston, MA, 1995.

31   Hasemi, Y., "Thermal Modeling of Upward Wall Flame Spread," Fire Safety Science – Proceedings of the 1st International Symposium.

32   Ahmad, T. and Faeth, G., "Turbulent Wall Fires," Seventeenth International Symposium on Combustion, The Combustion Institute, Philadelphia, p. 1149 – 1160, 1979.

33   Quintiere, J., Harkleroad, M. and Hasemi, Y., "Wall Flames and Implications for Upward Flame Spread," Combustion Science and Technology, 48, p. 191 – 222, 1985.

34   Quintiere J., and Cleary, T, "Heat Flux From Flames to Vertical Surfaces," Fire Technology, 30, 2, p. 209 – 231, 1994.

35   Tewarson, A. and Ogden, S., "Fire Behavior of Polymethylmethacrylate," Combustion and Flame, 89, p. 237 – 259, 1992.

36   Brehob, E. and Kulkarni, A., "Experimental Measurements of Upward Flame Spread on a Vertical Wall with External Radiation," Fire Safety Journal, 31, p. 181 – 200, 1998.

37   Kim, C., 'Upward Flame Spread on Vertical Walls," Master's Thesis, Pennsylvania State University, 1991.

38   Ohlemiller, T. and Cleary, T., 'Upward Flame Spread on Composite Materials," Fire Safety Journal, 32, p. 159 – 172, 1999.

39   Wu. P., and Tewarson, A., "Pyrolysis Efficiency in Upward Flame Spread," Interflam 1996.

40   Conduction in Solids, 2nd edition, Carslaw, H.S., and Jaeger, J.C, Chapter 2-8 Semi-Infinite Solid, Oxford University Press, Oxford, 1959.

41   Delichatsios, M., "Flame Heat Fluxes and Correlations of Upward Flame Spread Along Vertical Cylinders in Various Oxygen Environment," Proceedings of the Combustion Institute, 28, p. 2899 – 2904, 2000.

42   Delichatsios, M., Mathews, M., Delichatsiois, M., "An Upward Fire Spread and Growth Simulation," Fire Safety Science – Proceedings of the 3rd International Symposium, p. 207-216.

43   Saito, K., Quintiere, J. and Williams, F., "Upward Turbulent Flame Spread," Fire Safety Science – Proceedings of the 1st International Symposium, p. 75 – 86.

44   Kulkarni, A., Brehob, E., Manohar, S. and Nair, R, "Turbulent Upward Flame Spread on a Vertical Wall under External Radiation," National Institute of Standards and Technology, Report # NIST-GCR-94-638, 1994.

45   Wu, P., "Parallel Wall Fire Tests with PMMA and FRPPMMA," FM Global Technical Memorandum, dated 9 December 1997.

46   Wu, P., and Bill, R., "Ranking of Polymers for Clean Room Applications," Fire Safety Journal, 38, p. 203 – 217, 2003.

CONCLUSIONS AND FUTURE WORK

CONCLUSIONS

This dissertation documents two interrelated studies that were conducted to more fundamentally understand the scalability of flame heat flux. The first study, documented in Chapter 1, used an applied heat flux in the bench scale horizontal orientation which simulates a large scale flame heat flux. The second study, documented in Chapters 2 and 3, used enhanced ambient oxygen to actually increase the bench scale flame heat flux itself.

In Chapter 1, ignition and steady state burning behavior in the horizontal orientation were investigated. The key aspect was the use of real scale applied heat flux up to 200 kW/m^2 which is well beyond that typically considered in contemporary testing. An unexpected non-linear trend is observed in the typical plotting methods currently used in fire protection engineering for ignition and mass loss flux data for several materials tested and this non-linearity is found to be a true material response. There also exist literature results showing the same non-linear trend as the current study.

To investigate the ignition data non-linearity, the temperature profile in the condensed phase was measured and compared to a predicted profile during heat up to ignition. The predicted profile is from the inert material, one dimensional conduction equation which is used extensively in the study of ignition. Using this approach shows that viewing ignition as an inert material process is inaccurate at predicting the temperature profiles, especially the surface temperature, at higher heat fluxes. This analysis of thermal effects suggests that decomposition kinetics at the surface and

possibly even in-depth may need to be included in an analysis of the temperature profile and the process of ignition. This is further evidenced by the results of investigating burning behavior using the temperature profile obtained during burning.

The temperature profile in the condensed phase was measured and compared it to a predicted profile during burning. The predicted profile in the solid comes from applying a constant temperature boundary condition at the surface. The measured profiles appear to be invariant with applied heat flux, and do not match those predicted.

This possible inaccuracy was investigated by obtaining the heat of gasification via the "typical technique" energy balance (using the mass loss flux data) and comparing it to the commonly considered "fundamental" value obtained from differential scanning calorimetry measurements. They are not the same. This comparison suggests that the "typical technique" energy balance is too simplified to represent the physics occurring for any range of applied heat flux and a new energy balance needs to be developed. Since the typical technique views burning strictly as a surface process where the decomposition kinetics is lumped into the heat of gasification, the experimentally observed bubbling phenomena provides a possible direction of study.

In Chapter 2, steady state burning behavior in the horizontal orientation at ambient oxygen concentrations of 20.9 to 40 % ambient oxygen concentration for several materials was investigated. The key aspect of this study was direct experimental measurements of flame heat flux back to the burning surface for 20.9 to 40 % ambient oxygen concentrations. Enhanced ambient oxygen increases the bench scale flame heat flux back to the burning surface, although it does not simulate large scale flame heat flux in the horizontal orientation.

In Chapter 3, steady state burning behavior in the vertical orientation at ambient oxygen concentrations of 20.9 to 40 % ambient oxygen concentration for several materials was investigated. The key aspect of this study was direct experimental measurements of flame heat flux back to the burning surface for 20.9 to 40 % ambient oxygen concentrations. The main conclusion is that the bench scale total flame heat flux in enhanced ambient oxygen simulates a more severe large scale geometry flame heat flux in the vertical orientation.

Results from the solid and gas fuel experiments conducted in Chapters 2 and 3, as well as similar literature results, lead to the following explanation of what enhanced ambient oxygen concentration is doing. The addition of oxygen displaces nitrogen in the gas phase which raises the temperature of the fuel gases. This causes the chemical reactions of the fuel vapors leaving the sample surface to occur faster than at lower concentrations due to the increased temperature and increased oxygen available such that more fuel per "height" is burned and the flame gets shorter resulting in the concentration of soot in the flame near the surface being greater. The increased soot concentration results in an increased flame emissivity. This increased soot leads to more radiative energy loss than at lower concentrations. This loss of energy lowers the flame temperature. The competing processes of the added oxygen raising the temperature and the increased emissivity lowering the temperature reach a balanced state of flame emissivity and temperature, the values of which depend on the fuel. From a practical viewpoint, the higher flame heat flux, which is mostly the radiative component for typical fuels, results in an increased mass loss flux and heat release rate. This explanation of the effect of oxygen does not preclude oxidative pyrolysis from happening but the major effect is in the gas phase for steady state burning in the horizontal orientation.

FUTURE WORK

The future work suggestions will lead to better scientific understanding of fundamental "fire" behavior of materials. Engineering techniques can then be developed to obtain true scalable properties to better model ignition, burning and flame spread behavior.

Include decomposition kinetics in an analysis of the process of ignition. This is needed since the inert material viewpoint currently used in the community is too simplified to properly describe the behavior of even simple materials, never mind more complex materials such as composites. This new analysis should be able to predict actual temperatures profiles as well as explain and resolve the non-linearity of ignition data.

Develop a new energy balance for the burning process which includes the in-depth decomposition occurring. This is needed since "surface decomposition only" viewpoint currently used in the field is too simplified as evidence by observed in-depth bubbling. This energy balance should be able to obtain a "proper" heat of gasification to be used in models as well as explain and resolve the non-linearity of mass loss flux data.

Determine why the apparent heat of gasification obtained in a nitrogen atmosphere is different than obtained from an air atmosphere in bench scale experiments. Also understand the relationship between differential scanning calorimetry results for heat of gasification and those obtained from bench scale apparatuses. This is needed since it will be extremely difficult, if not impossible, to capture the "in-homogeneity" of complex materials such as composites given the very small specimen size required by the differential scanning calorimeter.

APPENDIX A: EFFECT OF OXYGEN LITERATURE REVIEW

A literature review was completed to determine the effect of ambient oxygen concentration on flame soot, height, temperature and heat flux. Surface temperature, time to ignition, mass loss rate, flame spread and understanding of general mechanisms were also included.

FLAME SOOT, HEIGHT AND TEMPERATURE

Tewarson, Lee and Pion[1] Results for horizontal orientation fires with areas of about 0.007 and 0.07 m^2 of polyoxymethylene, PMMA, heptane, polypropylene, and polystyrene show that the generation of unburnt soot increases as ambient oxygen concentration is enriched above ambient. They state that this appears due to a decrease in flame height and an increase in flame temperature and soot concentration in the flame zone. Santo and Taminini [2,3] and Mikkola[4] also suggest a decrease in soot concentration, for PMMA, with a decrease, below ambient, in oxygen concentration, since the emissivity of the flame decreases as the ambient oxygen concentration decreases. However, Wu and Chaffee[5] found that the smoke yield of small scale experiments with increased ambient oxygen was lower for chlorinated polyvinylchloride (CPVC), polyvinylchloride (PVC) and gray polyvinylchloride (Gray PVC) than the tests run with air.

Wang et al[6] found that soot formation in a turbulent jet flame strongly depends on oxygen content. Soot increases up to 40 % oxygen but then decreases with further oxygen addition. They also found that adding oxygen to the environment shortens the flame length and increases in flame temperature occur.

Stepniczka[7] has found that the flame temperature increases a maximum of approximately 100 K with increasing oxygen concentration up to 100 % oxygen for various non flame retarded polymers including polystyrene, ABS and polyester.

FLAME HEAT FLUX

Wu and Chaffee[5] suggest their observed soot reduction with increased ambient oxygen concentration reduces blockage so more flame radiation gets to the sample. Tewarson, Lee and Pion[1] found that the flame radiation increases with oxygen concentration as evidenced by the mass loss rate increase rather than using the soot concentration information.

Tewarson and Ogden[8] claim that for well ventilated conditions, the chemical reactions are not affected by the ambient oxygen and the combustion is expected to be primarily governed by the flame heat flux. They show an increase in radiative, with a corresponding decrease in convective, flame heat flux with increasing ambient oxygen concentration. Tewarson[17] shows that the flame heat flux back to the burning surface of a horizontal sample increases with oxygen concentration. For methane fires, Atreya and Mekki found that flame radiation increases with increasing ambient oxygen concentration.[9]

Tewarson et al.[10] state that the flame radiation increases with an increase in ambient oxygen concentration. They believe this is due to the increase in flame temperature and soot concentration combined with the decreased flame height (producing a reduced residence time in the flame).

SURFACE TEMPERATURE

A summary by Cullis[11] shows the surface temperature of polyethylene increased with ambient oxygen concentration whereas it decreased for PMMA. A two dimensional axisymmetric configuration numerical study was done by Tsai et al.[12] for horizontal black PMMA to simulate the transient processes in the solid and gas phases, including radiative absorption by the gas. The surface temperature from simulation and experiment for pilot ignition was found to be constant and not a function of applied flux. However, Rhodes and Quintiere[13] and Hopkins and Quintiere[14] found that the surface temperature at ignition varied with applied heat flux.

For several gaseous fuels, Gibbs and Williams found that the ignition temperature decreased with increasing ambient oxygen concentration.[15] Kashiwagi and Ohlemiller[16] show that for polymers of thick samples, the surface temperature at ignition is significantly affected by oxygen concentration. Tewarson[17] shows that the surface temperature at ignition decreases for filter paper as the oxygen concentration is increased.

Dakka, Jackson and Torero[18] show that the temperature at which degradation initiates, which they claim is not necessarily the ignition temperature, for PMMA changes as function of ambient oxygen concentration.

IGNITION

Drysdale[19] claims that increased oxygen causes combustible materials to ignite more readily. A two dimensional axisymmetric numerical study of time dependent ignition for a horizontal solid

fuel was made by Nakamura et al.,[20] who showed that the ignition is accelerated by an increase in the ambient oxygen concentration. Khan and de Ris[21] experimentally show ignition occurring in a shorter time period for several materials at enriched ambient oxygen concentration. Luo et al[22] shows no difference in ignition time for polyurethane foams in oxygen depletion experiments at 15 % ambient oxygen concentration. Hshieh et al.[23,24] found for several materials that enriched oxygen concentration had little effect on time to ignition except for low applied heat flux conditions.

Fuels with fire retardant compounds or high halogen composition, which ignite and combust in real fire scenarios, may not ignite, or may burn erratically, in ambient air small scale tests, leading to incorrect conclusions about real scenarios. For example, Gandi studied highly fire resistant materials with the ASTM E1354 Cone Calorimeter and found that the samples had irregular burning behavior and did not exhibit steady flaming combustion.[25] For highly fire retarded materials, ignition phenomena are better behaved in enhanced oxygen atmospheres for small scale tests.[31]

MASS LOSS RATE AND FLAME SPREAD

Krishnamurthy and Williams[26] and Kashiwagi and Ohlemiller[16] have shown that ambient oxygen substantially influences the regression rate of PMMA. The fuel mass loss rate for Tewarson and Pion[27] approach the asymptotic value with an environment oxygen concentration of approximately 35 % and is in agreement for large scale fires of horizontal PMMA. From this, they assert that large scale combustion can be achieved by an increased oxygen environment in small scale experiments. Santo and Taminini[3] see a decrease in burn rate with a decrease in oxygen concentration below ambient.

Drysdale[19] claims that increased oxygen causes combustible materials to spread flame more rapidly and burn more vigorously. Chao and Fernandez-Pello[28] show experimentally for PMMA in a ceiling and floor configuration that the flame spread rate increases approximately linearly with oxygen mass fraction in a 0.19 to 0.23 range.

Tewarson and Odgen[8] show that for PMMA vertical slabs, the flame spread rate increases with an increase in environment oxygen. They hypothesize, by extrapolation of the experimental data, that the asymptotic values match the large scale results of Orloff, de Ris and Markstein.[29] This match does not unquestionably show that the flame heat flux is increasing with increasing oxygen, since other parameters contribute to the flame spread rate.

Tewarson and Khan[30] state from a comparison of vertical small and large scale electrical cable experiments that increased oxygen environment, small scale flame propagation experiments can be used to simulate large scale flame propagation results. This statement is based on a correlation of increased oxygen, small scale flame propagation vs. "corrected" large scale propagation velocity. The correction was required since the large scale used a two parallel sheet configuration, which was thought to enhance the heat flux by about 50 % as opposed to the single sheet used in small scale. The comparison of flame propagation from a small scale configuration to a "corrected" value obtained from a different configuration in large scale is not a strong basis to claim that increased ambient oxygen at small scale simulates large scale.

Hshieh[23] found that the peak mass loss rate is a linear function of ambient oxygen concentration and that the dependence decreases as the incident flux increases. Stepniczka states "with rising amounts of oxygen in the environment, polymers burn faster" indicating mass loss rate increase.

Tewarson[17] shows for increased oxygen, flame spread increases for vertical samples of PMMA cylinders. Delicahtsios

OTHER

Wu and Bill[31] and Wu and Chaffee[5] show for tests in the FPA, the heat release rate increased only slightly for horizontal tests with 40 % ambient oxygen concentration.

Tewarson and Ogden[8] believe that oxidative pyrolysis, where oxygen from the air chemically reacts on the surface, is occurring. Brown and Kashiwagi[32] show for PMMA that this effect of ambient oxygen on the solid surface is limited to the depth of the bursting bubbles, which is 1 mm or less. They also show that MMA monomer is the primary component of decomposition.

Wang et al[6] found that NO_x emissions are highly dependent on ambient oxygen concentration and that CO emission decreases with increasing ambient oxygen concentration due to the promotion of complete combustion.

REFERENCES

1   Tewarson, A., Lee, J.L., and Pion, R.F., "The Influence of Oxygen Concentration on Fuel Parameters for Fire Modeling," Eighteenth Symposium (International) on Combustion, p. 563-570, 1981.

2   Santo, G., "Influence of Oxygen Depletion on the Radiative Properties of PMMA Flames," FMRC Technical Report J.I. 0A0E6.BU-3, FM Global Research, Norwood, MA, August 1979.

3   Santo, G., and Tamanini, F., "Influence of Oxygen Depletion on the Radiative Properties of PMMA Flames," Eighteenth International Symposium on Combustion, 1981.

4   Mikkola, E., "Effects of Oxygen Concentration on Cone Calorimeter Results," Proceedings of Conference Interflam93, Interscience Communications Company, London, UK, p. 49-56, 1993.

5   Wu, P., and Chaffee, J., "Evaluation of Test Protocol 4910 With Large Scale Propagation Tests," FMRC Technical Report J.I. 000300780, FM Global Research, Norwood, MA, February 2000.

6   Wang, L, Endrud, N., Turns, S., D'sgostini, M and Slavejkov, A., "A Study of the Influence of Oxygen index on Soot, Radiation and Emission Characteristics of Turbulent Jet Flames," Combustion Science and Technology, 174 (8) p. 45 – 72, 2002.

7   Stepniczka, H., "The Influence of Oxygen-Enriched Atmospheres on the Combustion Behavior of Polymers," Journal of Fire and Flammability, 5, p.16, 1974.

8   Tewarson and Ogden, "Fire Behavior of Polymethylmethacrylate," Combustion and Flame, 89, p. 237-259, 1992.

9   Handbook of Fire Protection Engineering, 3rd edition, "Chapter 2-14, Heat Fluxes From Fires to Surfaces: Effects of Other Variables" Society of Fire Protection Engineers, Boston, MA, 2002.

10 Tewarson, A., Khan, M., Wu, P., and Bill, R., "Flammability Evaluation of Clean Room polymeric Materials for the Semiconductor Industry," Fire and Materials, 25, p. 31 – 42, 2001.

11 Cullis, C.F., "The Involvement of Oxygen in the Primary Decomposition Stage of Polymer Combustion," Fire Safety Science-Proceedings of the First International Symposium, p. 371-377.

12 Tsai, T., Li, M., Jih, R. and Wong, S., "Experimental and Numerical Study of Autoignition and Pilot Ignition of PMMA Plates in a Cone Calorimeter," Combustion and Flame, 124, p. 466-480, 2001.

13 Rhodes, B. T., and Quintiere, J. G., "Burning Rate and Flame Heat Flux for PMMA in a Cone Calorimeter," Fire Safety Journal, 26, p. 221-240, 1996.

14 Hopkins, D., and Quintiere, J. G., "Material Fire Properties and Predictions for Thermoplastics," Fire Safety Journal, 26, p. 241-268, 1996.

15 Oxygen Enhanced Combustion, edited by Baukal, C., Air Products and Chemicals, Allentown, Pennsylvania, 1998.

16 Kashiwagi, T., and Ohlemiller, T., Nineteenth Symposium on Combustion, The Combustion Institute, Pittsburgh, p. 815, 1982.

17 Tewarson, A., "Nonmetallic Material Flammability in Oxygen Enriched Atmospheres, Workshop on International Fire Safety Standards for Hyperbaric Medicine Facilities, Boston, Ma, 1999.

18 Dakka, S., Jackson, G. and Torero, J., "Mechanisms Controlling the Degradation of Polymethylmethacrylate Prior to Piloted Ignition," Proceedings of the Combustion Institute, 29, p. 281 – 287, 2002.

19 Fire Dynamics, Drysdale, D., 2nd edition, Wiley Publishing Company, New York, NY, p. 246, 1999.

20 Nakamura, Y., Hiroshi, Y., Takeno, T. and Kushida, G., "Effects of Gravity and Ambient Oxygen on Gas Phase Ignition Over a Heated Solid Fuel," Combustion and Flame, 120, p. 34-48, 2000.

21 Khan, M., and de Ris, J., "Material Flammability Measurements," FMRC Technical Report J.I. 0D0J7.MT, FM Global Research, Norwood, MA, August 2000.

22 Luo, M., He, Y., Dowling, V., Bowditch, P., and Leonard, J., "Combustion Behavior of Polyurethane Foams Under Depleted Oxygen Environment," Fire Science and Technology, Proceedings of the Third Asia-Oceania Symposium, 1998.

23 Hshieh, F., Motto, S., Hirsh, D and Beeson, H., "Flammability Testing Using a Controlled Atmosphere Cone Calorimeter," p. 299 – 325.

24 Hshieh, F. and Buch, R., "Controlled Atmosphere Cone Calorimeter Studies of Silicones," Fire and Materials, 21, p. 265 – 270, 1997.

25 Alpert, R., and Khan, M., "Rating Materials as Noncombustible," FMRC Technical Report J.I. 3003507, FM Global Research, Norwood, MA, October 1999.

26 Krishnamurthy, L., and Williams, F.A., "Laminar Combustion of Polymethylmethacrylate in O2/N2 Mixtures," Fire and Explosion, p. 1151-1164.

27 Tewarson, A. and Pion, R, "Flammability of plastics – I. Burning Intensity,: Combustion and Flame, 26, p. 85 – 103, 1976.

28 Chao, Y.H., and Fernandez-Pello, .C., "Flame Spread in a Vitiated Concurrent Flow," Heat Transfer in Fire and Combustion Systems, 199, p. 135-142, 1992.

29 Orloff. L., de Ris, J. and Markstein, G. H., "Upward Turbulent Fire Spread and Burning of Fuel Surface," Fifteenth Symposium (International) on Combustion, p. 183-192, 1974.

30 Tewarson, A., and M., Khan, "Flame Propagation for Polymers in Cylindrical Configuration and Vertical Orientation," Twenty Third Symposium (International) on Combustion, p. 1231-1240, 1988.

31 Wu, P., and Bill, R., "Laboratory Tests for Flammability Using Enhanced Oxygen," Fire Safety Journal, 38, p. 203 – 217, 2003.

32 Brown, J., and Kashiwagi, T., "Gas Phase Oxygen Effect on Chain Scission and Monomer Content in Bulk PMMA Degraded by External Thermal Radiation," Polymer Degradation and Stability, 52, p. 1, 1996.

APPENDIX B: APPARATUS SUMMARY

ABSTRACT

A key aspect of fire safety performance is to limit the potential for fire growth and spread through the use of appropriately specified material systems. Specification of material systems currently depends significantly on empirical evaluation of material flammability characteristics. As part of an on going apparatus improvement and development program, the Advanced Flammability Measurements (AFM) Apparatus was created. The AFM is of intermediate scale and is closely related to the bench scale Fire Propagation Apparatus (ASTM E 2058), and similar to the bench scale Cone Calorimeter (ASTM E 1354). It was developed to provide an apparatus with greater capability in terms of applied heat flux range, maximum sample size, and incorporation of additional measurement techniques needed to assess flame and material heat transfer directly. These characteristics of the AFM will improve measurement of key material fire characteristics needed for computer simulation of end use fire scenarios. Results from a recent study demonstrating the performance of the AFM compared to the Fire Propagation Apparatus and the Cone Calorimeter in terms of measurement of material fire characteristics will be discussed. Additionally, information on improved techniques for the measurement of flame and material heat transfer will be presented.

INTRODUCTION

Mechanical and chemical properties are usually used to choose a suitable material system for a given application. However, the fire performance of this system is also needed by designers and

engineers to help design active protection systems that would control the fire and minimize damage if the system ignites. Alternatively, if no active protection system is to be used, selection of another appropriate material system for the application would be prudent. This system would have fire performance that includes greater resistance to ignition and flame spread.

There are two basic approaches to determine the fire performance of materials in realistic scenarios. The first is to conduct an extremely expensive and time consuming full scale evaluation and obtain the results directly. The second is to conduct bench scale experiments to obtain material flammability parameters for ignition and combustion and use these in conjunction with mathematical models or calculation procedures to estimate full scale performance. Of the two basic approaches, the bench scale experiment is more desirable from a practical viewpoint, since it is more versatile and time and cost efficient[1]. However, for a flammability parameter obtained from bench scale experiments to be considered a true material "property" it must be independent of apparatus or scale.

The flammability parameters obtained from the typical bench scale apparatuses include time to ignition, heat release rate and smoke specific extinction area.[2,3] However, these parameters do not always correspond, or scale, to results for realistic large scale fire conditions.[4] As part of an ongoing apparatus improvement and development program to investigate this issue of scalability, the Advanced Flammability Measurements Apparatus (AFM) was created. It is of intermediate scale and is closely related to the bench scale Fire Propagation Apparatus[2] (ASTM E 2058), and is similar to the Cone Calorimeter[3] (ASTM E 1354). The AFM was developed to provide an apparatus with greater capability in terms of applied heat flux, maximum sample size and incorporation of additional measurement techniques needed to assess flame and material heat

transfer directly. These characteristics of the AFM will improve measurement of key material flammability parameters needed for computer simulation of end use fire scenarios. The AFM is currently used in "research mode," but has potential to become a commercial production apparatus.

THE APPARATUS

The AFM shown in Figure B.1 is an intermediate scale fire instrument consisting primarily of (i) radiant heaters to supply an applied heat flux to a sample, (ii) a spark igniter to ignite the pyrolysis products as the sample is heated, (iii) a load cell system to determine the mass loss rate of the sample as it is burning, (iv) gas analyzers to measure the level of CO, CO_2, O_2 and total gaseous hydrocarbons in the combustion products, (v) a smoke obscuration system to determine the soot yield and (vi) a data acquisition system to record all the measurements for analysis.
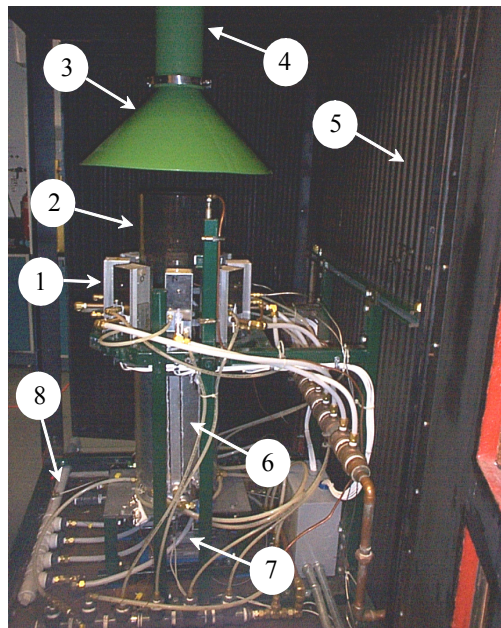
(a)
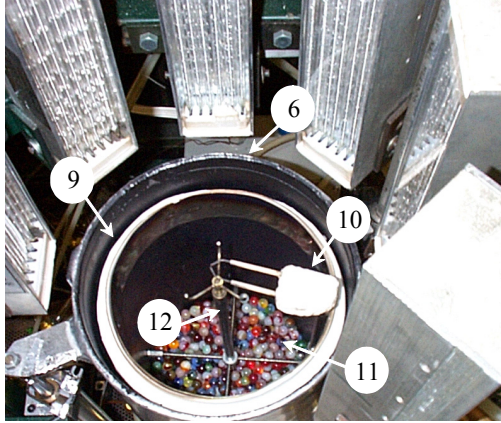
(b)

Figure B.1 Advanced Flammability Measurements Apparatus (a) front view and (b) top view.

1	radiant lamps	7	load cell
2	quartz tube	8	inlet air piping
3	exhaust duct	9	distribution box
4	instrument section	10	spark igniter
5	cooled walls	11	glass beads
6	shutter	12	sample rod/support

The apparatus is surrounded with a water cooled structure for safety during high applied heat flux. A quartz tube is used to keep the sample environment controlled by supplying air for combustion at a known rate and oxygen concentration. A shutter is used to protect the sample from the applied heat flux until the user is ready, allowing a precisely timed application.

The core of the instrument consists of eight, water and air cooled, vertical radiant lamp heaters having a 0.9 to 1.5 µm peak emission wavelength. Each of the heaters is located on a 32.5 cm diameter circle. The heat flux level is set and controlled via a manually set power controller. The maximum applied heat flux to a horizontal sample is 220 kW/m^2 with an uncertainty, including day to day variations, apparatus heat up, data acquisition system resolution and spatial variation

of ± 2 kW/m^2. Note that the Cone Calorimeter using a single electrical coil heater can reach a maximum of 100 kW/m^2 applied heat flux while the Fire Propagation Apparatus can reach a maximum of 65 kW/m^2 using 4 horizontal radiant heaters.

A continuous spark igniter, powered by a 10,000 V transformer and a 3 mm gap electrode, located 13 mm above a horizontal sample, provides a piloted ignition source. Note that the Cone Calorimeter uses an intermittent spark while the Fire Propagation Apparatus uses an ethylene-oxygen premixed flame ignition source.

The mass loss measurement system consists of a load cell excited by a power supply, and a digital weight indicator with an analog output module. The load cell has a 1 kg range with a 0.01% FS (100 mg) resolution and a manufacturers stated uncertainty of $\pm 0.02\%$ FS (± 200 mg). It has an analog 2 mV/V nominal output at rated range. The digital weight indicator allows for amplification, taring, filtering and data output of the load cell signal. Including all sources for error, the uncertainty of the mass loss measurement is ± 150 mg in the AFM.

The gas stream containing the products of combustion is captured at the exhaust duct test section by a system consisting of a high temperature fan, a hood and an orifice plate. Gas analyzers measure the concentration of O_2, CO, CO_2 and total gaseous hydrocarbon in this stream. Various filters to remove soot before they enter the analyzers are used. Water is also removed.

Light extinction measurements are made in the exhaust duct test section by a "smoke meter." The main components are a stabilized helium neon laser with silicon photodiodes as main and reference detectors and assorted optics and electronics.

The data acquisition system consists of an Agilent model 349740A data acquisition unit and three 16 channel multiplexer modules connected via a GPIB cable to a computer. A HPVEE software program is used to interface with the data acquisition unit and save test data actively to disk. Data reduction and analysis is conducted post test using a custom Excel spreadsheet.

TEST PROCEDURE AND MEASUREMENTS

<u>Horizontal Setup:</u> The horizontal orientation is shown in Figure B.2. The sample material is placed in a sample holder designed by de Ris and Khan[5] and sits on an insulated sample rod connected to the load cell. The lamps are set for the desired heat flux, the spark igniter is activated and the data acquisition system is started. A 60 second baseline reading is acquired and the shutter is then dropped allowing for a distinct external heat flux application. The material will pyrolyze and may ignite. If ignition occurs, time to ignition is measured visually. The mass loss, exhaust duct volume flow rate, extinction coefficient, CO, CO_2, O_2 and total hydrocarbon concentrations are recorded throughout the test.

<u>Vertical Setup:</u> The vertical orientation is shown in Figure B.3. The sample material is placed in a holder analogous to the horizontal orientation. The sample ignition can be accomplished in two ways depending on the desired test conditions. The first is to use an external applied heat flux with the spark igniter and the experiments are run similar to the horizontal orientation. The second ignition method is to use a small amount of alcohol in a dish at the base of the sample, which then ignites the sample and initiates a freely burning condition. In both ignition cases, the mass loss, exhaust duct volume flow rate, extinction coefficient, CO, CO_2, O_2 and total gaseous hydrocarbon concentrations are recorded identical to the horizontal orientation.
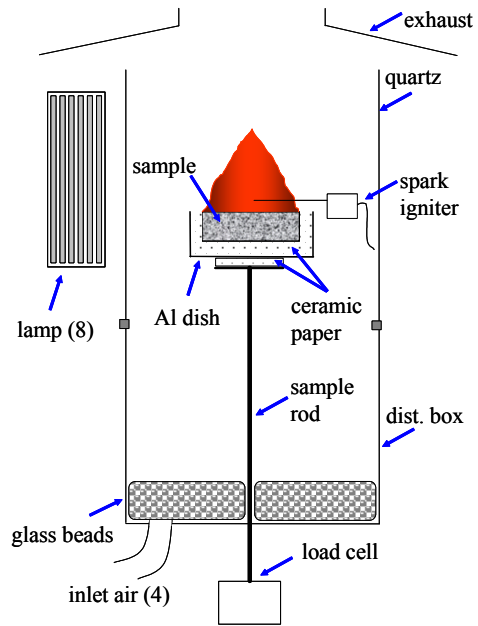
Figure B.2   Horizontal orientation experimental set-up (not to scale).
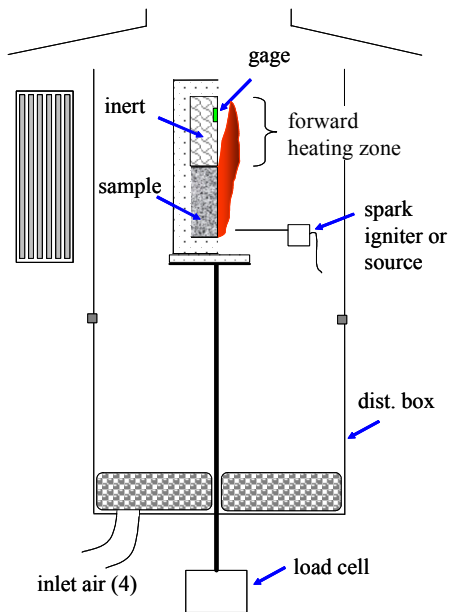

Figure B.3   Vertical orientation experimental set-up (not to scale).

Flame heat flux to the forward heating zone is also be measured by mounting heat flux gages at various positions on an inert panel above the burning sample. Note that the setup can also measure flame propagation if the inert material is replaced with an elongated sample.

Ignition: Time to ignition, defined as the time from external heat flux application to sustained flaming, is measured visually during testing. A flame is determined to be present when a visually observed "distinct change in color of the pyrolysis products or gases in the volume above the sample" (i.e., orange or bluish color) is seen.

Heat Release Rate: The heat release rate is calculated using both oxygen consumption and carbon dioxide generation techniques. Calculation of the heat release rate by oxygen consumption for an open system has been derived by Parker[6], and is given by

$$\dot{Q} =$$
$$E'X_{O_2}^{a0}\left(1-X_{H_2O}^0\right)\left[\phi - \frac{(1-\phi)}{2}\frac{X_{CO}^a}{X_{O_2}^a}\left(\frac{E''}{E'}-1\right)\right]CA\sqrt{\frac{2T_0}{\rho_0}\frac{\Delta P}{T_d}}\left(\frac{1}{1+(\alpha-1)\phi}\right)$$

$$\phi = \frac{X_{O_2}^{a0} - \frac{X_{O_2}^a\left(1-X_{CO_2}^{a0}-X_{CO}^{a0}\right)}{\left(1-X_{CO_2}^a-X_{CO}^a\right)}}{X_{O_2}^{a0}\left(1-\frac{X_{O2}^a}{\left(1-X_{CO_2}^a-X_{CO}^a\right)}\right)}$$

where ϕ is called the oxygen depletion factor. E' is the net heat of complete combustion per unit volume oxygen consumed, E'' is the heat released per unit volume O_2 consumed in the burning of CO to CO_2, T is temperature, ρ is density, α is the expansion factor for the combustion process, X is mole fraction, A is duct cross sectional area, ΔP is the differential pressure measured by a pitot

tube and C is the pitot tube coefficient. The superscript "a" stands for "dry sample" analyzer reading.

Calculation of the heat release rate by CO_2 generation is given in ASME E 2058[2] and is shown below. This is a commonly used technique although strictly speaking this equation is for a "wet sample" analyzer reading.

$$\dot{Q} = \left(\frac{\Delta H_T}{k_{CO_2}}\right)\left(\dot{G}_{CO_2} - G^0_{CO_2}\right) + \left[\frac{\left(\Delta H_T - \Delta H_{CO}k_{CO}\right)}{k_{CO}}\right]\left(\dot{G}_{CO} - G^0_{CO}\right)$$

$$\dot{G}_j = \dot{m}_d X_j MW_j$$

where G is the product generation. ΔH_T is the net heat of complete combustion per unit mass fuel consumed, ΔH_{CO} the heat released per unit volume oxygen consumed in the burning of CO to CO_2, MW is molecular weight and k is the stoichiometric product to fuel mass ratio.

Smoke Specific Extinction Area: ASTM E 1354 for the Cone Calorimeter[3] defines the specific extinction area as

$$\sigma_f = \frac{K\dot{V}_d}{\dot{m}_f}$$

which is a measure of the relative smokiness of a material. $\dot{V}_d$ is the duct volume flowrate and $\dot{m}_f$ is the fuel mass burn rate. Another measure is the smoke yield. Smoke yield,[7,8] defined as the mass of smoke particles produced per mass of material burned, is

$$\in = \frac{C_s K \dot{V}_d}{\sigma_s \dot{m}_f}$$

where σ_s is the mass specific extinction coefficient of smoke, K is the light extinction coefficient and C_s is the smoke profile factor which corrects for the slight radial decrease near the wall of the smoke concentration. Mullholland[7] has determined for "post flame smoke" of over ventilated fires, that σ_s has a nearly universal value of 8.7 ± 1.1 m^2/g assuming smoke is basically carbon soot particles with primary sphere sizes much smaller than the wavelength of the light used. This allows a light extinction measurement to be used to infer the mass concentration of smoke.

ADDITIONAL TECHNIQUES

To provide insight and improve the understanding of material flammability "properties," additional measurement techniques are used to assess flame and material heat transfer directly. Three techniques are used to assess flame heat flux back to the burning sample and to provide in-depth heat transfer information within the sample. The AFM is also suitable for the Flame Radiation Scaling Technique,[10] which can simulate realistic scale results for heat release rate and flame propagation through small scale tests in enriched ambient oxygen.

Flame Heat Flux - Infer From Mass Loss Technique: This is the commonly used engineering technique of inferring the flame heat flux from the mass loss rate.[9,11] It comes from a steady state ablation solution[12] using the surface energy balance shown in Figure B.6.

B-10
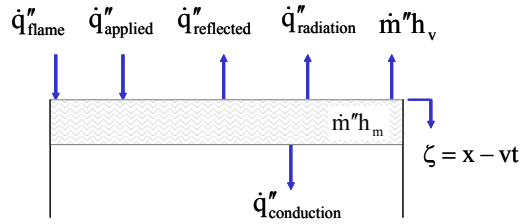
$$\dot{q}''_{flame} = \dot{q}''_{radiation} - a\dot{q}''_{applied} + \dot{m}''(h_m + h_v) + \dot{q}''_{conduction}$$

Figure B.6 Surface energy balance for Infer From Mass Loss Technique and Measure Conduction Technique.

The energy flux per unit area is $\dot{q}''$, a is absorbtivity, $\dot{m}''$ is mass burn rate, h_m is the heat of melting, h_v is the heat of vaporization, x is the initial surface location, v is regression velocity and t is time. Assuming the melt layer is very thin and noting that the experimental data is used to obtain h_g, the solution is

$$\dot{q}''_{flame} = \dot{q}''_{radiation} - a\dot{q}''_{applied} + \dot{m}''h_g$$

Flame Heat Flux - Measure Conduction Technique: This method to determine the flame heat flux also starts with the same surface energy balance but the conduction heat loss is measured directly either from the measured temperature profile in the solid or an embedded thin film heat flux gage. Note that h_m and h_v are measured independently and not determined from the experimental data.

Embedded Thermocouples: The temperature profile is obtained from thermocouples embedded in

the solid. Conduction into the sample at the surface is obtained from the derivative of the temperature profile from

$$\dot{q}''_{conduction} = k\frac{dT}{d\zeta}\bigg|_{\zeta=0}$$

assuming constant thermal conductivity for simplicity. The thermal conductivity as a function of temperature can also be incorporated into the analysis. Figure B.7 shows a typical profile. The surface thermocouple can also be used to obtain the surface temperature at ignition.
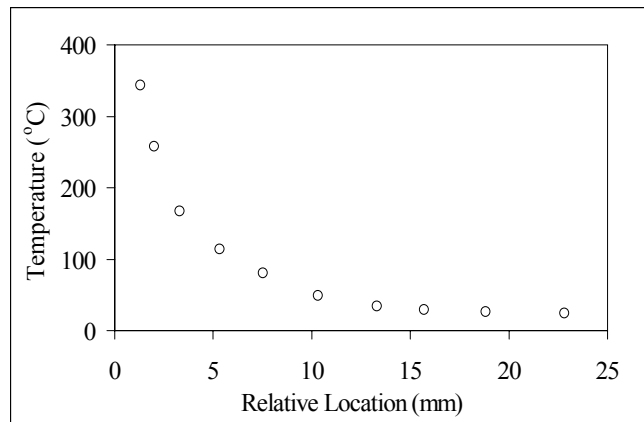

Figure B.7 Typical temperature profile from thermocouples embedded in a sample.

Embedded Thin Film Gages: Thin film heat flux gages are sometimes called Micro-foil heat flux sensors.[13] They function as a self-generating thermopile transducer with low thermal impedance that measures heat flux from the temperature difference between opposite sides of a certain material. The RdF thin film heat flux gages used in the AFM are polyimide film bonded using a Teflon lamination process and are 0.18 mm thick.

Gages embedded in the sample will measure the heat flowing through the gage and hence the heat flowing through the sample. An embedded gage will measure the in-depth conduction in the solid while a gage placed at the back surface will measure the heat lost at the boundary surface.
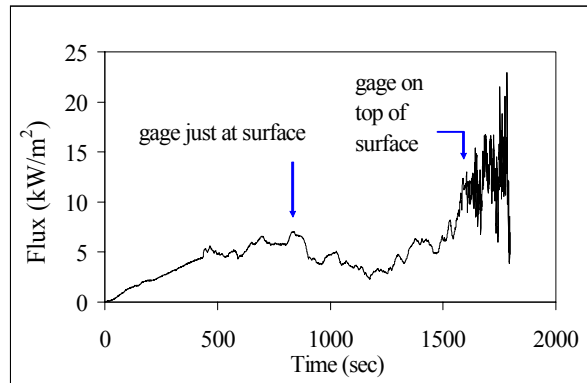

Figure B.8   Typical trace from a thin film heat flux gage embedded in a sample.

As the sample burns and regresses, an embedded gage "moves" closer to the sample surface until it is reading the conduction into the sample at the burning surface. Figure B.8 shows a typical trace from an embedded thin film heat flux gage.

Flame Heat Flux - Measure Flux Technique: This technique is an "extension" of the Measure Conduction Technique. After the thin film gage reaches the surface, the sample material covering it will soon burn off exposing the gage. Depending on the designed installation, the gage can either ride "on top" of the regressing surface or stay "above" it. This technique assumes that the gage is not in good thermal contact with the solid and the energy balance given in Figure B.9 is applicable.

$$\dot{q}''_{applied} \qquad \dot{q}''_{flame} \qquad \dot{q}''_{radiation}$$
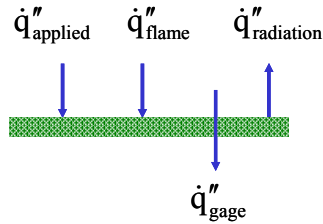
$$\dot{q}''_{gage}$$

$$\dot{q}''_{flame} = \dot{q}''_{gage} - \dot{q}''_{applied} + \dot{q}''_{radiation}$$

Figure B.9   Gage energy balance for Measure Flux Technique.

Flame Radiation Scaling Technique: The Flame Radiation Scaling Technique[10] is hypothesized to simulate ignition and combustion at large, realistic scale from small scale experiments at 50 kW/m^2 applied heat flux and greater than 35 % ambient oxygen concentration. It basically states that the flame heat flux, which is one of the most important parameters that control surface flame spread over a material, at large scale can be achieved in small scale tests with enriched oxygen. This technique has been used to simulate large scale results for heat release rate and flame propagation in the Fire Propagation Apparatus using 40 % ambient oxygen and 50 kW/m^2 applied heat flux, which is the concept underlying the FM 4910 Clean Room Materials Flammability Test Protocol.[14,15] Time to ignition, heat release rate and smoke specific extinction area are calculated the same way as for "typical ambient air" tests. The additional techniques described in the previous three sections can also be incorporated.

CONCLUSIONS

The Advanced Flammability Measurements Apparatus (AFM) is an intermediate scale fire

instrument with capability to provide an applied heat flux at the levels seen in realistic large scale fires. Additional techniques to assess flame and material heat transfer directly are incorporated in the design as well as typical calculations currently used in ASTM E 2058[2] and ASTM E 1354.[3] The AFM shows promise for an improved understanding of material flammability parameters and the issue of scalability. An understanding of key material flammability characteristics will improve computer simulations of end use fire scenarios. Preliminary results for a simple material show that black PMMA performs better than the first generation theory would indicate. This demonstrates the need for second generation theories to be developed.

REFERENCES

1 Handbook of Fire Protection Engineering, 2nd edition, "Chapter 3-4, Generation of Heat and Chemical Compounds in Fires," Society of Fire Protection Engineers, Boston, MA, 1995.

2 Standard Test Methods for Measurement of Synthetic Polymer Material Flammability Using a Fire Propagation Apparatus, ASTM E 2058, American Society of Testing Materials, Philadelphia, PA, 2001.

3 ASTM Standard Method for Heat and Visible Smoke Release Rates for Materials and Products Using an Oxygen Consumption Calorimeter, ASTM E 1354, American Society of Testing Materials, Philadelphia, PA, 1999.

4 Tewarson, A., and Ogden, S, "Fire Behavior of Polymethylmethacrylate," Combustion and Flame, 89, p. 237-259, 1992.

5 De Ris, J., and Khan, M., "A Sample Holder for Determining Material Properties," Fire and Materials, 24, p. 219-226, 2000.

6 Parker, W.J., "Calculations of the Heat Release Rate by Oxygen Consumption for Various

Application," NBSIR 81-2427, National Institute of Standards and Technology, Gaithersburg, MD, 1982.

7 Mulholland, G., Johnsson, E., Fernandez, M., and Shear, D., "Design and Testing of a New Smoke Concentration Meter," Fire and Materials, 24, p. 231-243, 2000.

8 Mulholland, G. and Croarkin, C., "Specific Extinction Coefficient of Flame Generated Smoke," Fire and Materials, 24, p. 227-230, 2000.

9 Hopkins, D., and Quintiere, J., "Material Fire Properties and Predictions for Thermoplastics," Fire Safety Journal, 26, p. 241-268, 1996.

10 Tewarson, A., "Flammability Parameters of Materials: Ignition, Combustion and Fire Propagation," Journal of Fire Sciences, 12, p. 329-356, 1994.

11 Tewarson, A., Lee, J.L., and Pion, R.F., "The Influence of Oxygen Concentration on Fuel Parameters for Fire Modeling," Eighteenth Symposium (International) on Combustion, p. 563-570, 1981.

12 Heat Transfer, Holman, J., McGraw Hill Book Company, New York, NY, p. 622-624, 1986.

13 RdF Corporation Temperature Measurement Catalog, 2000.

14 Factory Mutual Research Clean Room Materials Flammability Test Protocol 4910, FM Global Research, Norwood, MA, 1997.

15 Tewarson, A., Khan, M., Wu, P., and Bill, R., "Flammability Evaluation of Clean Room Polymeric Materials for the Semiconductor Industry," Fire and Materials, 25, p. 31-42, 2001.

APPENDIX C: PRELIMINARY CHECKS

Various checks were conducted to confirm proper operation of the Advanced Flammability Measurements apparatus (AFM). Checks were also conducted to confirm that the proper experimental procedure for ignition and combustion tests were being performed such that the data acquired was extremely well characterized.

EXPERIMENTAL CHECKS FOR APPARATUS

Due to the orientation of the quartz lamps, more than just the sample is exposed to the applied heat flux. This includes the quartz tube, lamp frame, air distribution box and shield. The air distribution box and shield are water cooled so they don't increase in temperature however the quartz tube and lamp frame will heat up, radiating to the sample. This effect was measured using a Schmidt Bolter gage and is shown in Figure C.1. The horizontal variation of applied heat flux across the sample surface was also measured and is shown in Figure C.2.
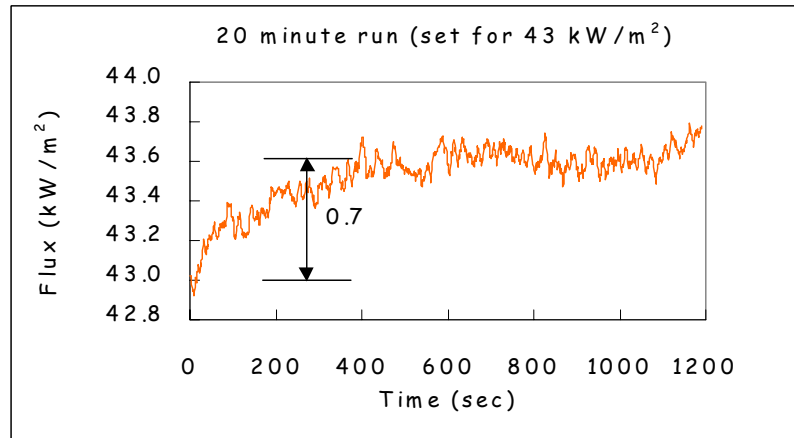

Figure C.1   Effect of apparatus heat up on applied heat flux.

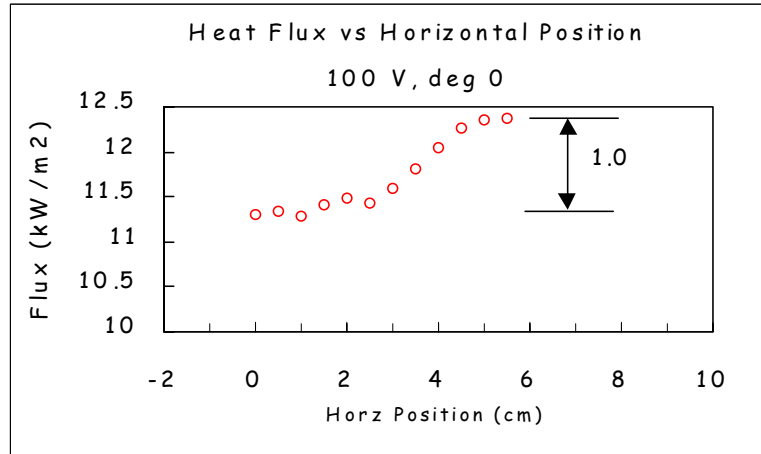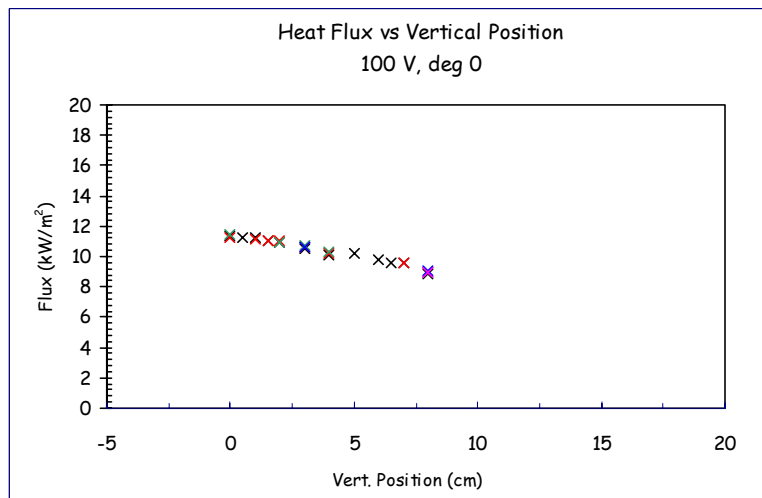Figure C.2   Horizontal spatial variation of applied heat flux.

Figure C.3   Vertical spatial variation of applied heat flux.

Note that it is only 1 kW/m^2 across a 12 cm diameter. This is an extremely uniform applied heat flux especially compared to the Cone which has a variation of 10 kW/m^2 across the same size sample. Figure C.3 shows the vertical variation of 1 kW/m^2 as the sample either regresses or

intumesces 2 cm. These are all simplied to give a total applied heat flux uncertainty, including apparatus heat up, spatial variation, day to day variations and DAS resolution as ± 2 kW/m^2.

The inlet air flowrate across the quartz tube was measured with a hot wire anemometer in 1 cm increments and found to be uniform to ± 20 lpm across quartz diameter for an inlet air flowrate up to 1000 lpm. Smoke visualization in the quartz tube was also done to insure a laminar flow past the sample. The flow in the exhaust duct was found to be uniform to ± 20 lpm for a flowrate of 2000 lpm through the exhaust duct.

The possibility that the applied heat flux was blocked by the pyrolysis products from reaching the surface was investigated. The applied heat flux was measured using a Schmidt-Boelter gage embedded in the sample surface for black PMMA and Gray PVC but the result should be applicable to other materials.
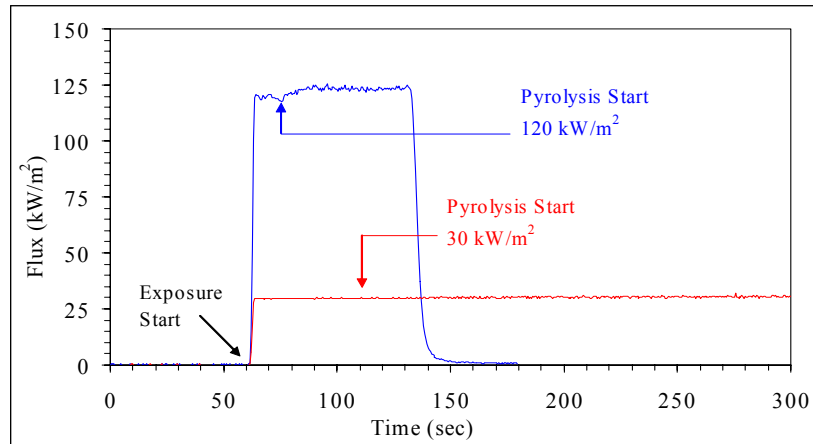

Figure C.4 Applied heat flux measured at sample surface during pyrolysis of black PMMA.

See from Figure C.4 that there is a minor fluctuation of the applied heat flux once pyrolysis

C-3

begins but there is no reduction in the mean heat flux. This minor variation is within the uncertainty of the applied heat flux and as such is considered insignificant. Hence, all of the applied heat flux is reaching the sample surface.

The possibility that the applied heat flux was blocked by the flame from reaching the surface was also investigated. A burning sample could not be used since the separation of flame heat flux and applied heat flux can not be made with certainty. Propylene gas was used (so it would have soot comparable to the test materials) with a 4" diameter burner in which a Schmidt-Bolter gage was embedded. The gas flow was controlled to a constant flow rate via a mass flow meter and needle valve such that any blockage of the applied heat flux by the flame could be measured. Figure C.6 shows gage measurements from the propylene flame without and with added heat flux.
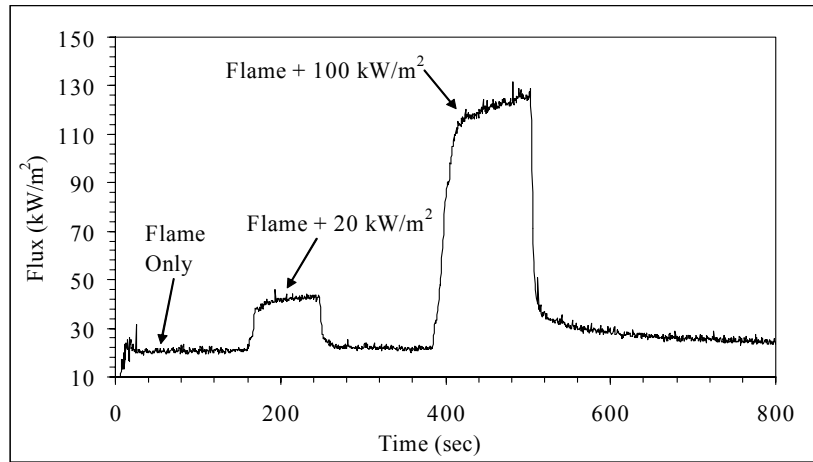

Figure C.6   Gage measurements from propylene gas flame without and with applied heat flux.

Note the slight rise of the "flame plus flux" signal with time for the 100 kW/m^2 case. The rise is about 6 kW/m^2 which is slightly greater than the uncertainty of the applied heat flux of ± 2 kW/m^2. It is believed that this is due to the heating up of the glass beads of the burner which

increases the convective heat transfer to the gage. This can be ignored since the initial application of the heat flux is the important item of interest and it shows no blockage of the applied heat flux by the flame. Rhodes and Quinterie[1] suggest flame to be transparent to the radiant coil source of the Cone Calorimeter. The possibility of a changing absorption for the different peak emission wavelengths present at various applied heat fluxes was considered during burning. The surface of a burning sample is experimentally observed to be covered with soot and as such, the absorptivity should be unity. As was seen for ignition, the applied heat flux should be absorbed for all ranges identically during combustion.

EXPERIMENTAL CHECKS FOR IGNITION

Various checks were conducted to confirm that the proper experimental procedure for ignition tests was being performed such that the data acquired was extremely well characterized. These checks relate to the definition of ignition, the assumption of 1D conduction behavior in the sample, the assumption of thermally thick behavior, sample shape effects, inlet air velocity effects and wavelength effects of the radiation source used.

Definition of Ignition: The first check relates to using a visual technique for the determination of ignition. The brightness of the quartz lamps used in the AFM makes visual observation of the sample difficult especially at higher applied heat fluxes. A video camera and monitor was set-up that allowed for a clearer view of the sample, however, the visual time could still be very subjective depending on the test operator. To address this issue, the present study also determines time to ignition by several other techniques. Carbon dioxide, oxygen and sample surface temperature readings are monitored to determine when they each make a significant jump from their test baseline level. It is shown experimentally for several materials that if no flaming

combustion occurred, then no significant change from the test baseline occurred for these readings. Hence these times, accounting for travel of the decomposition/combustion gas from the sample to the instrument, can also be used to define ignition.

Table C.1   Comparison of ignition times for the different techniques used in this study.

Material	Applied Flux kW/m^2	Time to Ignition ± 2 sec			
		CO_2*	O_2*	E-1354	T_{surf}
black PMMA	40	58.5	58.0	57.7	na
	70	na	na	24.4	25.0
	120	17.1	17.5	14.0	15.0
	200	10.0	9.5	9.0	7.2
gray PVC	40	50.0	50.0	na	49.0
	80	16.0	14.0	52	12.0
	120	6.0	6.5	34	na
	180	3.0	3.0	15	na
Plywood	40	92	91	93	na
	80	27	29	30	na
	120	11.5	13.5	17.0	na
	180	6.5	6.5	7.0	na

* 20 sec travel   ^ 5 sec travel   na not available

Decomposition products would clog up on igniter putting out spark before flame attached to surface.

Table C.1 shows a comparison of ignition times for a variety of tests. Note that limitations of the data acquisition system limit the time resolution to 0.5 sec. The uncertainty for ignition is a maximum of ± 2 sec taken as the full variation obtained for a statistical run of a mid-range heat flux.

The table shows that the visual definition of ignition matches the other techniques except for gray PVC. This halogenated material was experimentally observed to have a sustained flame at the sparker location well before the flame attached to the surface as required by ASTM E-1354 definition of ignition. It is interesting to note that the time of the appearance of this "non-attached flame" is the same as the time to ignition determined by the non-visual techniques.

The derivative of the mass loss flux can also be used, in theory, to determine ignition however practical issues in the AFM make this unfeasible. The design of the apparatus allowed for too much vibration to get into the load cell during "the dropping of the shield" rendering the signal quite noisy for up to 30 sec after exposure of the applied heat flux.

1D Conduction: The second check relates to the assumption of the sample having 1D material conduction. This was confirmed experimentally by measuring the temperature across the sample surface. Thermocouples were placed at three layers plus the surface as shown in the left side of Figure C.5. Each layer had thermocouples placed at various locations around the diameter as shown. The sample was exposed to several heat fluxes. The sample showed uniform temperature, as seen in Figure C.6, within the uncertainty of the thermocouple measurements except for approximately 5 mm from the holder edge.
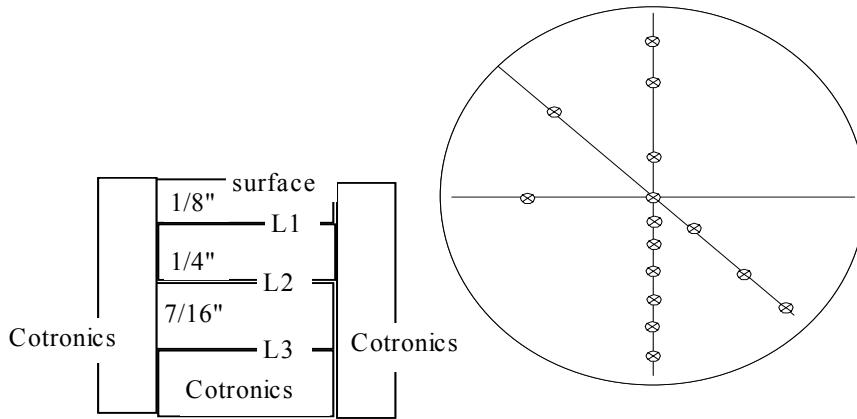
Figure C.5   1D conduction checks.
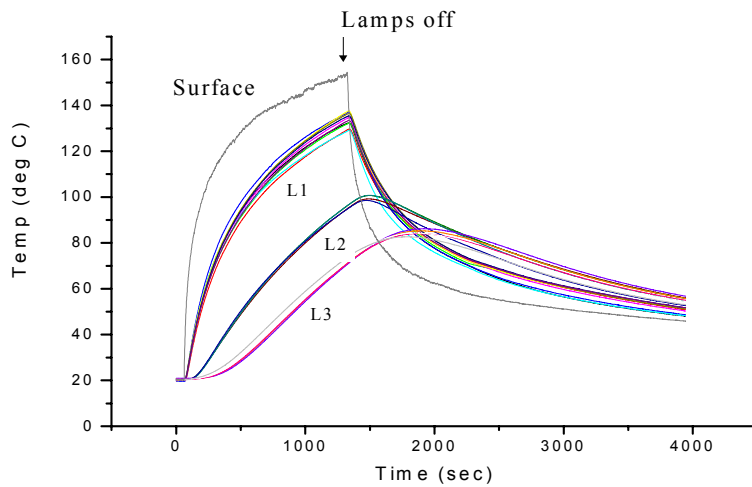
Figure C.6   Temperature traces for 1D check for a black PMMA sample.

Thermally Thick Behavior: The assumption of thermally thick behavior of the sample was confirmed by measurements from thermocouples either embedded within the sample or placed at the back surface. The experimental criteria for thermally thick behavior was a temperature rise at the back face of less than 4 °C. This value was chosen for convenience since it is the temperature

uncertainty. The experimental value of 4 °C happens to be about 1 % of the measured surface temperature rise of 330 °C expected for the black PMMA material. As such, the experimental value is consistent with the typical engineering theory that the sample thickness should be greater than the characteristic thermal conduction length, $L > 3.6\sqrt{\alpha t}$, in order to consider it to be behaving as thermally thick. The numerical value in the equation comes from considering a significant temperature rise at the back face to be 1 % of the temperature rise at the surface.[2] It is understood that the experimental definition is not an exact match to the engineering theory, which shows non-thermally thick behavior for 10 kW/m^2. It is also understood that different materials having lower surface temperatures at ignition would require a smaller experimental value and as such a measuring instrument with smaller resolution.

Sample Shape: The fourth experimental check for ignition relates to sample shape. No significant difference in time to ignition by any of the techniques was found for round and square samples of PMMA. The square samples were in a holder analogous to the sample holder designed by de Ris and Khan used for the round samples.

Table C.2   Comparison of ignition times for round and square samples.

Applied Flux kW/m^2	Visual Time to ignition ± 2 sec	
	round	square
28.4	104.7	100.3
50	43.0	42.1
120	14.0	11.6

C-9

Inlet Air: The fifth check relates to the inlet air used in the AFM. There was no effect of the inlet flow rate from 100 to 1000 lpm on the time to ignition. However, these inlet flow tests give a slight difference in absolute time to ignition from 0 lpm natural convection tests. This may explain why the Cone, which uses natural convection, and other apparatus, which use inlet flow, gets different absolute values.

Table C.3   Comparison of ignition times for different inlet flowrates. Applied heat flux = 38.4 kW/m^2.

Flowrate lpm	Visual Time to ignition ± 2 sec
0	71.4
100	58.7
500	58.5
1000	56.9

Radiation Source: The sixth check relates to the radiation source since quartz lamps, which are used in the AFM apparatus, have a different emission wavelength spectrum than the Cone Calorimeter, which is the most commonly used apparatus. In-depth radiation absorption of the quartz lamp source was an issue of concern. Table C.4 shows a difference in the time to ignition between the two apparatuses for black PMMA.

The quartz lamp source gives a longer time to ignition for this material, theorized to be due to some of the applied energy being lost deeper in the sample and not absorbed at the surface. This

in-depth radiation absorption was measured experimentally by taking temperature readings under the sample surface before ignition for both radiation sources for black PMMA.

Table C.4   Comparison of ignition times for AFM and Cone experiments for thermally thick behaving black PMMA.

Applied Flux kW/m^2	Time to Ignition ± 2 sec	
	AFM	Cone
15	na	521.0
30	105.1	56.6
40	57.7	39.9
50	43.0	24.0
70	24.4	13.0
90	21.4	9.1

In-depth radiative absorption was defined by a temperature increase within the sample immediately at application of applied heat flux. The quartz lamp radiation source shows in-depth absorption to 3 mm but the radiant coil source shows no in-depth absorption at all.

Coating of a sample surface with a fine layer of graphite powder, known as carbon black coating, can be done to address the in-depth radiation absorption problem for ignition tests in the AFM where necessary. Carbon black coating is thought to cause all absorption of the applied heat flux to occur at the sample surface.[3] The in-depth radiation absorption was again measured

experimentally by taking temperature readings under the sample surface before ignition for both radiation sources for black PMMA with carbon black coating. The carbon black coating had no effect on the sample exposed to the radiant coil source. The quartz lamp source showed no in-depth absorption, i.e., the carbon black coating caused all absorption to occur at the surface. This effect was also seen by Tewarson[4] for black PMMA.

Table C.5 Comparison of ignition times for AFM experiments with and without carbon black coating for thermally thick behaving black PMMA.

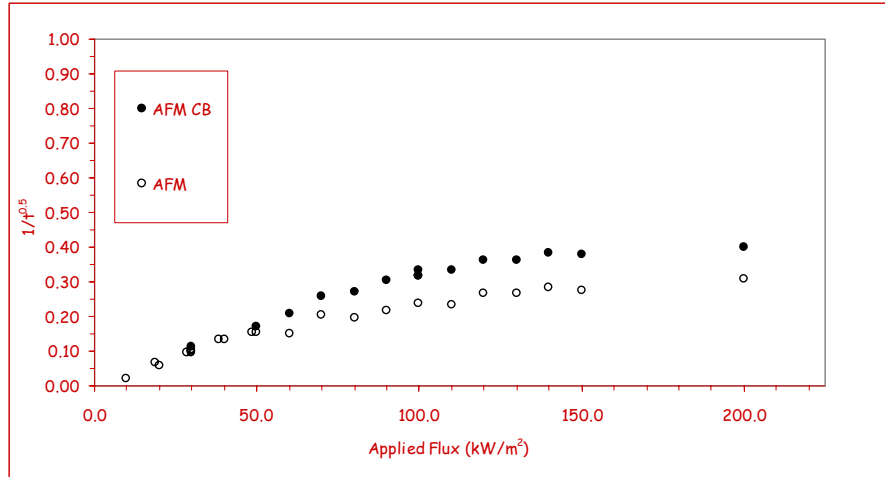| Applied Flux kW/m^2	Time to Ignition ± 2 sec	
	Carbon black	Virgin
10	1462.0	2243.4
18.7	192.2	227.5
38.7	42.2	58.0
70	15.2	24.4
100	9.1	18.0
120	7.6	14.0
200	6.2	10.4

Figure C.7   Inverse of the square root of time to ignition vs. applied heat flux for thermally thick behaving black PMMA with and without carbon black coating conducted in the AFM.

EXPERIMENTAL CHECKS FOR MASS LOSS

The in-depth absorption of the quartz lamp radiation source that caused differences in time to ignition is not an issue during burning, since, at ignition, the surface becomes coated with soot, causing all absorption to occur at the surface. This is seen in Figure C.8. Urbas, Parker and Luebbers found that the spectral emissivity could be considered unity in the burning phase for several materials. No differences in steady state mass loss flux between the AFM and Cone Calorimeter occurred for a consistent sample holder (i.e., thermally thick behavior) as can be seen in Table C.6.
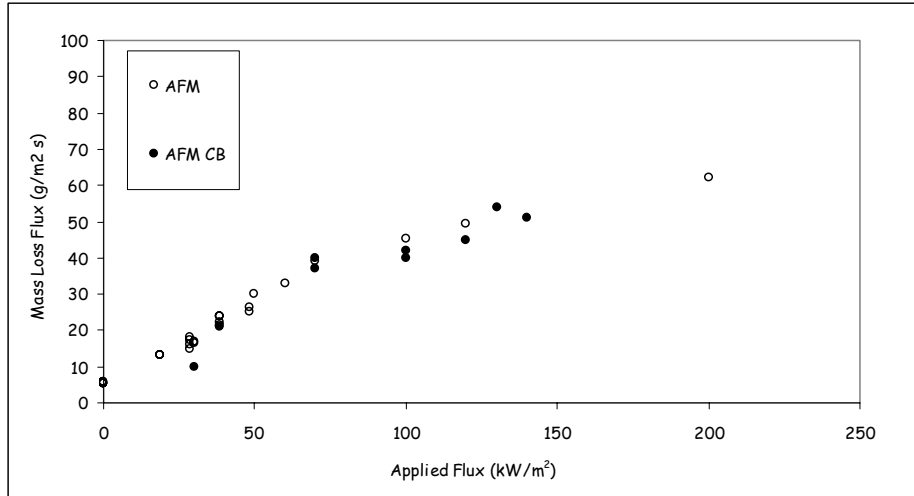
Figure C.8 Mass loss flux vs. applied heat flux for thermally thick behaving black PMMA with and without carbon black coating conducted in the AFM.

Table C.6 Comparison of steady state mass loss flux for AFM and Cone experiments for thermally thick behaving black PMMA.

Applied Flux kW/m^2	Mass Loss Flux $\pm$ 3 g/m^2 sec	
	AFM	Cone
0	5.5	5.8
30	16.5	15.0
50	30.0	24.8
70	39.0	34.2

Steady State Definition: Mass loss data is collected during testing and a standard five point differentiation technique[5] is used to obtain mass loss flux. The mass loss flux is determined to be steady when the mass loss flux trace, as well as the CO_2 and O_2 traces, is "flat" as shown in the Figure C.9. To confirm thermally thick behavior, the back surface temperature is also monitored.
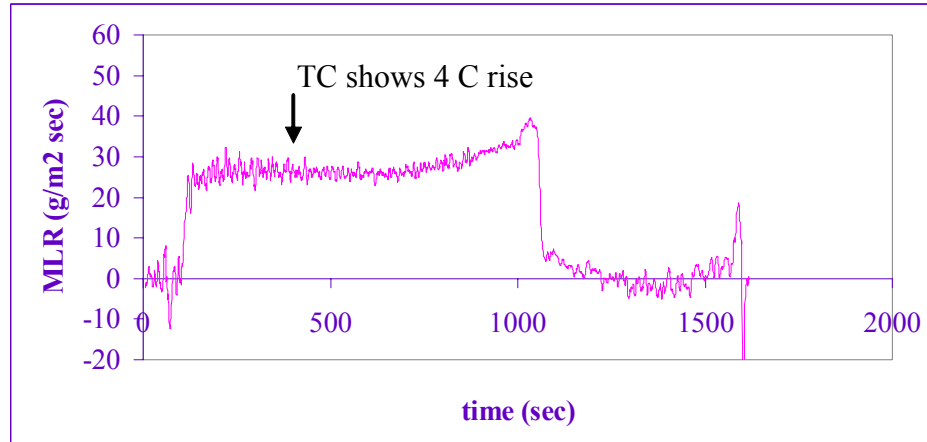

Figure C.9   Mass loss flux for PMMA to full sample burnout for applied heat flux = 48.4 kW/m^2. Curve typical for all applied heat fluxes.

Note from the figure that even when the sample is no longer thermally thick as indicated from the thermocouple at the back face, the mass loss flux and gas traces are still flat. The rise at the end occurs when the temperature at the back face reaches about ½ the ignition temperature. This shows that the typical assumption is incorrect about the rise at end of curve being the thermal wave just reaching the back face. The thermal wave actually reaches the back face rather quickly but doesn't affect the mass loss flux significantly until the back face temperature is about ½ of the ignition temperature.

REFERENCES

1   Rhodes, B., and Quintiere, J., "Burning Rate and Flame Heat Flux for PMMA in a Cone Calorimeter," Fire Safety Journal, 26, p. 221 – 240, 1996.

2   An Introduction to Fire Dynamics, 2nd edition, Drysdale, D., "Chapter 2-2 Conduction," John Wiley and Sons, West Sussex, England, 1999.

3   Handbook of Fire Protection Engineering, 2nd edition, "Chapter 3-4, Generation of Heat and Chemical Compounds in Fires," Society of Fire Protection Engineers, Boston, MA, 1995.

4   Tewarson, A., and Ogden, S, "Fire Behavior of Polymethylmethacrylate," Combustion and Flame, 89, p. 237-259, 1992.

5   Standard Test Method for Heat and Visible Smoke Release Rates for Materials and Products Using an Oxygen Consumption Calorimeter, ASTM E 1354, American Society of Testing Materials, Philadelphia, PA, 1994.

APPENDIX D: SECONDARY CHECKS

As part of characterizing the AFM, the effect of sample shape, sample thickness, sample surface preparation, inlet airflow velocity, heater type, igniter type, heater orientation and a limited variation of material brand on time to ignition and mass loss rate was investigated for black PMMA. These results were also compared to several "in-house" apparatus and literature results. Test results obtained in the AFM are repeatable and consistent with in-house and literature results. Hence, the AFM apparatus and test procedure provide results that are considered valid.

SAMPLE SHAPE AND THICKNESS

The effect of sample shape on time to ignition was investigated in the AFM for round and square pieces of Crystalite brand material with matte surface preparation. The effect of thickness (3/8" and 1" round) was also checked although the 3/8" samples were Plexiglas G brand material. There was no effect on time to ignition as can be seen in the following figure. It was observed that the variation of the 1" thick sample was ± 1 second while the 3/8" sample was ± 2 second. Tests done in the WPI cone also showed no effect of shape.
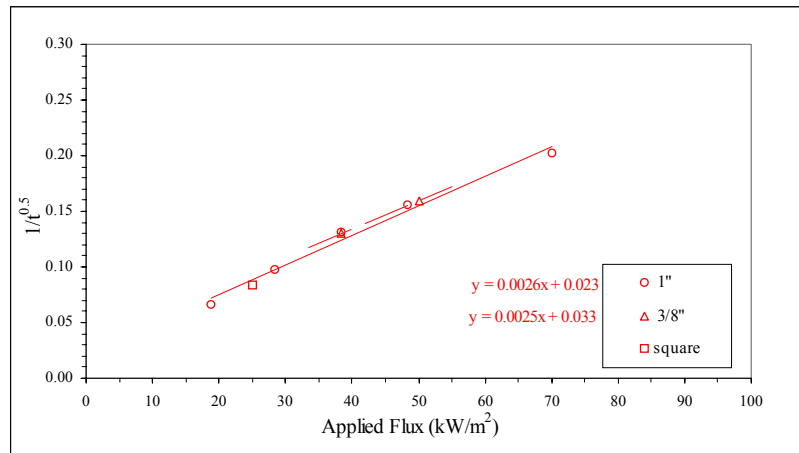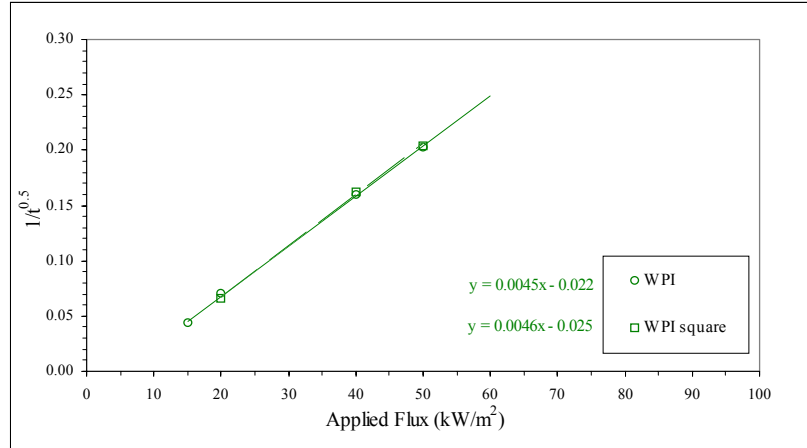
Figure D.1 Effect of (top) sample shape and thickness on time to ignition for tests conducted in the AFM and (bottom) sample shape in WPI cone with 1" samples.

INLET VELOCITY

The inlet velocity was varied from 100 to 1000 lpm for a round, 1" thick, matte finish Crystalite brand sample in the AFM and determined that there was no effect on the time to ignition, considering the time uncertainty of ± 1 second, since it varied from 56.9 to 58.7 seconds.

The inlet airflow effect on ignition behavior was also investigated by conducting tests in the AFM with natural convection burning, although the quartz tube must still be in place for safety reasons. A longer ignition time is seen although the magnitude varies with applied heat flux as seen in the Table D.1.

These natural convection burning experiments showed agreement, within the time uncertainty, of the visually observed ignition time and the time indicated via the 2nd derivative of the mass data.

Table D.1   Time to ignition for different inlet flowrates.

Applied Heat Flux	Time to Ignition (sec)	
(kW/m²)	200 lpm Inlet Airflow	0 lpm Inlet Airflow
18.7	227.5	251.5
28.4	104.7	120.3
38.4	58.0	71.4
48.4	41.3	46.4

Agreement was <u>not</u> seen for experiments conducted with inlet airflow. Although they do not agree, they have a significant negative peak at approximately the same time as the visual ignition. This combined with the change in ignition time, show that the inlet airflow is affecting the ignition process and should be evaluated. The temperature profile in the solid will be compared in the near future for both cases in an attempt to determine if the difference is in the solid phase or gas phase.

CONE DATA

Data was acquired in the WPI cone, which uses a radiant heat source, using the same round, 1" thick Crystalite brand material sample, with matte surface preparation, and holder as used in the AFM. Note that the cone has a pulsed sparker as opposed to the continuous spark of the AFM. As can be seen in Figure D.2 below, significantly different results were seen. Further tests done in the AFM with carbon black coating showed shorter ignition times than without coating such that the results came into line with the cone. It has been found in the past that the carbon black coating has made no difference in the ignition times of various materials tested in the cone.
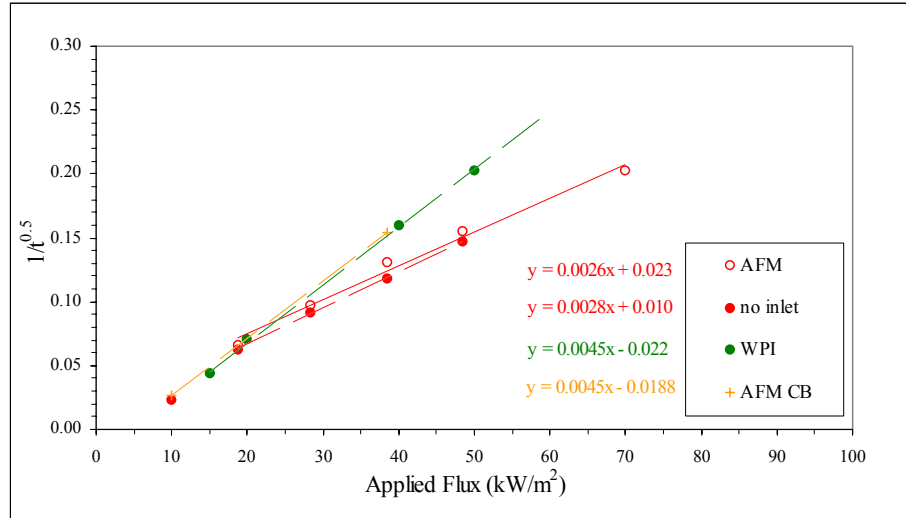
Figure D.2 AFM and WPI Cone data comparison for the same test sample. Also shown are
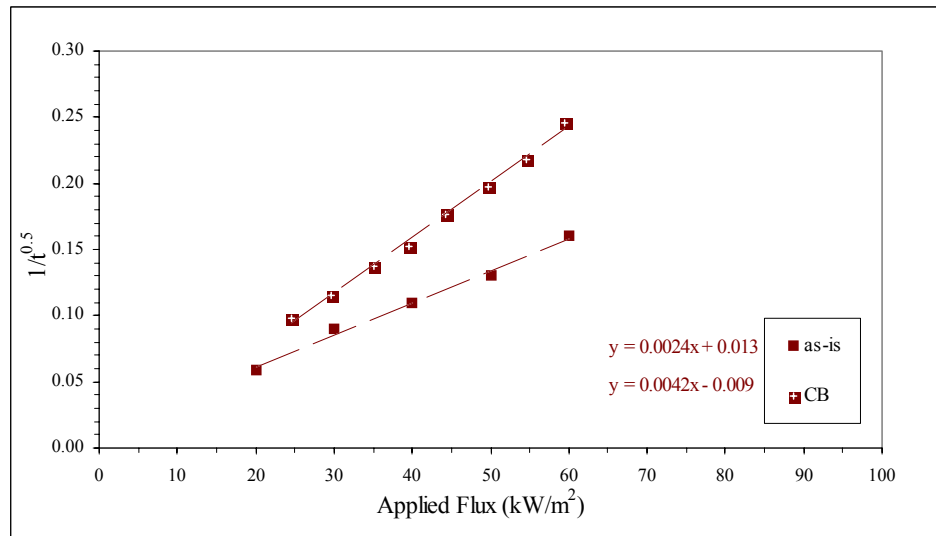results for the AFM sample with carbon black coating.

Figure D.3 Effect of carbon black coating on results obtained by Tewarson.[1]

Tewarson[1] data performed in the FPA on black pmma with no coating also shows a significant difference in ignition times from those obtained with coating as seen in Figure D.3. Hence, the carbon black seems to affect the ignition times only with a quartz heat source as opposed to a non quartz radiant heater. This possible wavelength difference is an issue that should be investigated in the future.

CONE STANDARD HOLDER

Since some of the literature data that is compared to in the next section use the standard cone sample holder, the results using this holder in the cone was checked. The frame is relatively massive and might affect the 1D conduction assumptions. As can be seen in Figure D.4, there is a significant effect. It is most likely that the top plate is conducting heat into the side of the sample thus causing non 1D conduction behavior as was observed by Choi.[2] It was shown that the sample has 1D behavior in the AFM. This issue most likely contributes to different results obtained in different apparatuses and should be investigated further.
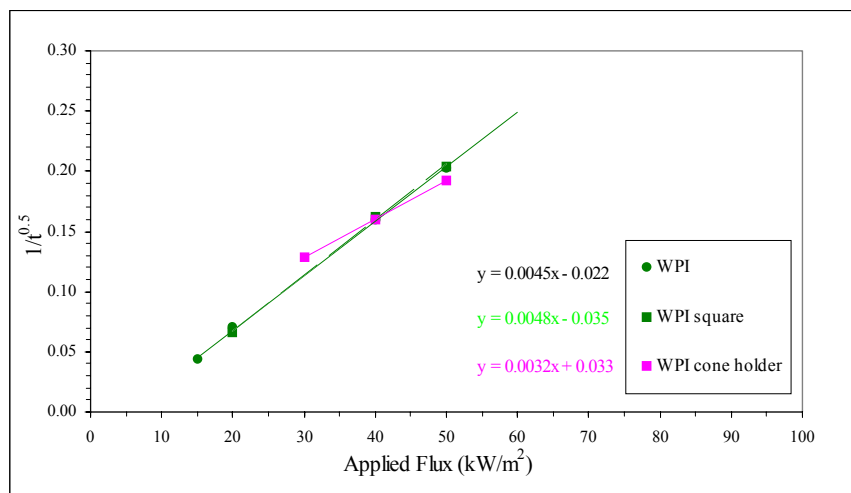
FigureD.4   Comparison of cone standard holder.

COMPARISON TO OTHERS

The AFM data was compared to "in-house" data from the Research FPA, FTT, Ineris, and Approvals apparatuses.[3] These are shown in the Figure 5, where all samples were 3/8" thick, coated with carbon black and tested with natural convection conditions. Note that the sample holder was different for each of these cases and most likely contributes to the variation in time to ignition for samples having non-thermally thick behavior.

The AFM data was also compared to literature data from Hopkins and Quintiere[4], NIST[4], and Tsai,[5] who used a cone with a radiant heater source, although Hopkins and Quintiere used a gas ignition source instead of a spark igniter. As seen from Figure D.6, in tests conducted with the WPI cone, only the carbon black coated AFM samples matched this literature data. In Figures D.5 and D.6, as elsewhere in the memo, the circles define round samples while the squares define square samples.

Figure D.5 Comparison to "in-house" data.
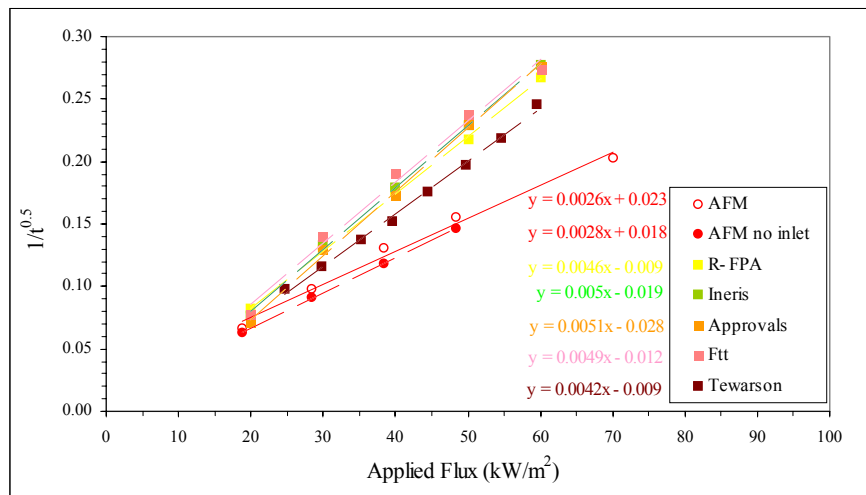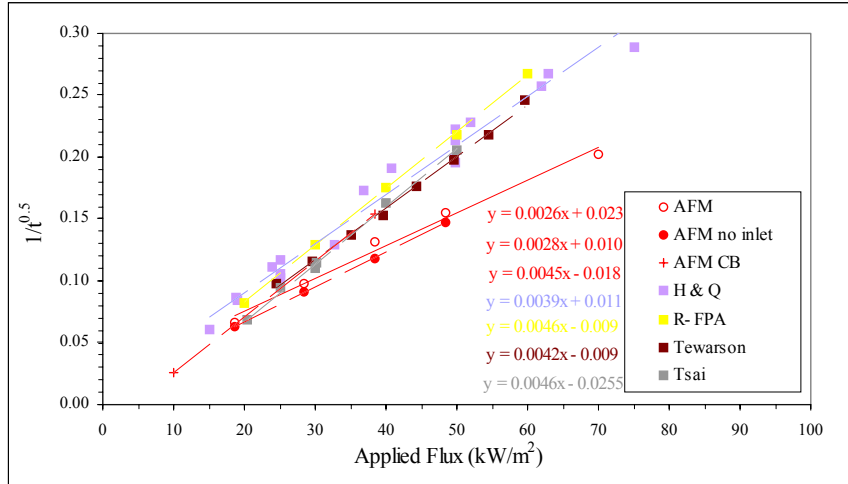
Figure D.6 Comparison to literature data.

MASS LOSS FLUX

Mass loss flux data was found to be reasonably consistent between the various apparatuses. The variation in results that is seen between the AFM and literature result of Hopkins and Quintiere is most likely due to the different resolution and data reduction technique used in each apparatus.
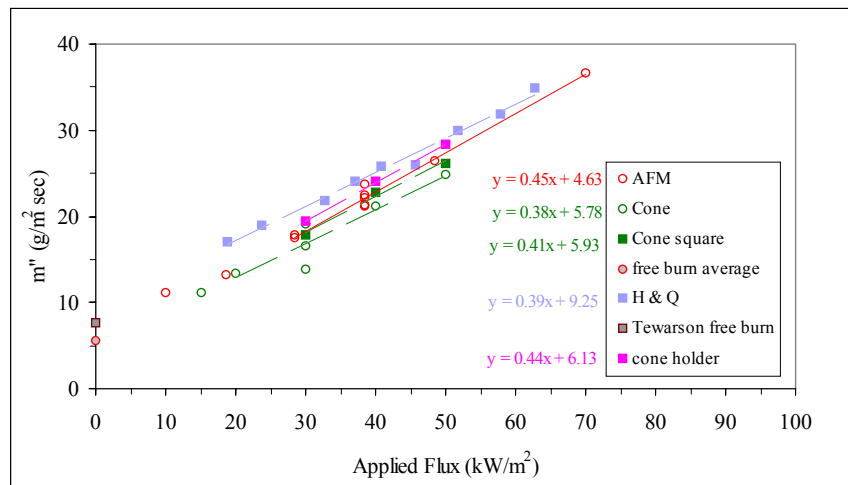

Figure D.7 Mass loss flux data.

CONCLUSIONS

It was found by conducting tests in the AFM and cone, plus using in-house and literature test results, that the time to ignition for a consistent sample holder (i.e., thermally thick behavior) was not affected by certain test parameters. These included sample shape, sample thickness, igniter type, heater orientation and a limited variation of material brand, which included Crystalite, Acrylite, Polycast and Plexiglas G.

There was an effect of the heater type since the ignition time obtained when using a quartz lamp is only the same as that using a radiant heater when the lamp sample has a carbon black coating. This may be due to the different wavelengths of each source and their interaction with the material.

It was shown that natural convection ignition is not the same as with inlet airflow. However, for the inlet airflow case, the magnitude of the airflow from 100 up to 1000 lpm had no effect on the ignition time.

The mass loss rate was found to be reasonably consistent between the various apparatuses. The variation in results that is seen between the AFM and literature results is most likely due to the different resolution and data reduction technique used in each apparatus.

Test results for time to ignition and mass loss rate obtained in the AFM are repeatable and consistent with in-house and literature results. Hence, the AFM apparatus and test procedure provide results that are considered valid and reasonable.

TEST PARAMETER SUMMARY

	Heater Type	Igniter Type	Sample Thickness	Surface Prep
AFM	v. quartz lamps	c. spark	3/8", 1"	as is, matte, CB
FPA	h. quartz lamps	gas flame	3/8"	CB
FTT	h. quartz lamps	gas flame	3/8"	CB
Ineris	h. quartz lamps	gas flame	3/8"	CB
Approvals	h. quartz lamps	gas flame	3/8"	CB
WPI Cone	radiant coil	p. spark	1"	matte
H&Q	radiant coil	gas flame	1"	as is
NIST	radiant coil	p. spark	1"	as-is
Tsai	radiant coil	p. spark	1"	as-is
Tewarson	h. quartz lamps	gas flame	1"	as is, CB

Note: V. = vertical, h. = horizontal, c. = continuous, p. = pulsed, CB = carbon black

REFERENCES

1   Tewarson, A., and Ogden, S, "Fire Behavior of Polymethylmethacrylate," Combustion and Flame, 89, p. 237-259, 1992.

2   Personal communication with Keum-Ran Choi, WPI.

3   "Data Correlations Between the ASTM E 2058 Apparatuses at FMRC and at Ineris," FMRC Report J.I. 0003006752.

4   Data extracted from Hopkins, D., and Quintiere, J., "Material Fire Properties and Predictions for Thermoplastics," Fire Safety Journal, 26, p. 241-268, 1996.

5   Tsai, T., Li, M., Shih, I., Jih, R., and Wong, S., "Experimental and Numerical Study of Autoignition and Pilot Ignition of Pmma Plates in a Cone Calorimeter," Combustion and Flame, 124, p. 466-480, 2001.

APPENDIX E: FLAME HEAT FLUX MEASUREMENT TECHNIQUES

Five techniques to obtain the flame heat flux of black PMMA were investigated. Included is the commonly used engineering technique of inferring the flame heat flux from the mass loss rate intercept as well as from the individual mass loss rate at each applied heat flux. Also included are using embedded thin film gages and embedded Medtherm Gardon gages to measure (early) the conduction in the solid as well as (later) the flame heat flux directly. Embedded thermocouples are also used to obtain the solid conduction.

INFER FROM MASS LOSS INTERCEPT

This commonly used engineering technique was the first method attempted. It comes from a steady state ablation solution[1] using the following control volume
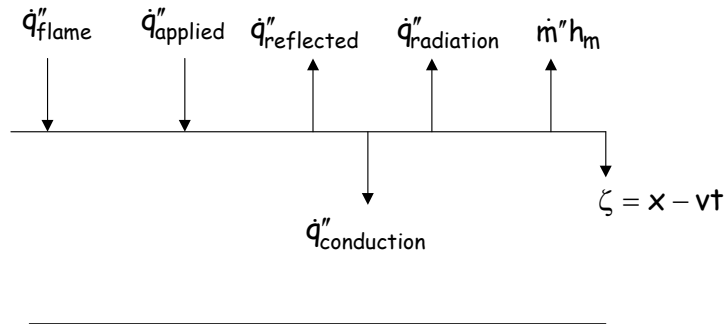
where h_m is the heat of melting. The surface energy balance is

$$\dot{q}''_{flame} = \dot{q}''_{radiation} - a\dot{q}''_{applied} + \dot{m}''h_m + \dot{q}''_{conduction} \qquad (1)$$

In solid, the governing equation for 1D conduction is

$$\frac{\partial^2 T}{\partial x^2} = \frac{1}{\alpha}\frac{\partial T}{\partial t}$$

with a moving coordinate system for a burning sample regressing surface of

$$\zeta = x - vt$$

so the governing equation becomes

$$\frac{d^2 T}{d\zeta^2} = \frac{v}{\alpha}\frac{dT}{d\zeta}$$

which has the general solution form

$$T = C_1 + C_2 \exp\left(\frac{-v\zeta}{\alpha}\right)$$

with boundary conditions of

$$T = T_m \ @ \ \zeta = 0$$

$$T = T_0 \ @ \ \zeta = \infty$$

which leaves a final solution of

E-2

$$T = (T_m - T_0)\exp\left(\frac{-v\zeta}{\alpha}\right) + T_0 \tag{2}.$$

The conduction term

$$\dot{q}''_{conduction} = -k\frac{dT}{d\zeta}\bigg)_{\zeta=0} = v\rho c_s(T_m - T_0)$$

such that the energy balance becomes

$$\dot{q}''_{flame} = \varepsilon\sigma T_{surface}^4 - a\dot{q}''_{applied} + \dot{m}''(h_m + c_s[T_m - T_0]) \tag{3}.$$

Adding in burning, the equation becomes

$$\dot{q}''_{flame} = \varepsilon\sigma T_{surface}^4 - a\dot{q}''_{applied} + \dot{m}''(h_m + c_s[T_m - T_0]) + \dot{m}''(h_v + c_l[T_v - T_m])$$

and assuming $c_s = c_l$ then the final typically used equation in this technique becomes

$$\dot{q}''_{flame} = \varepsilon\sigma T_{surface}^4 - a\dot{q}''_{applied} + \dot{m}''h_g \tag{4}.$$

This equation can be put into a "y=mx+b" form of

$$\dot{m}'' = \frac{a\dot{q}''_{applied}}{h_g} + \frac{\dot{q}''_{flame} - \varepsilon\sigma T^4_{surface}}{h_g} \qquad (5)$$

where the intercept is the second term on the right. Note that this solution is only valid if the temperature profile in the solid is indeed the one that drops out of the constant temperature boundary condition as given by equation 2. This is the same technique used by H&Q,[2] Tewarson[3] and the SFPE Handbook.[4]
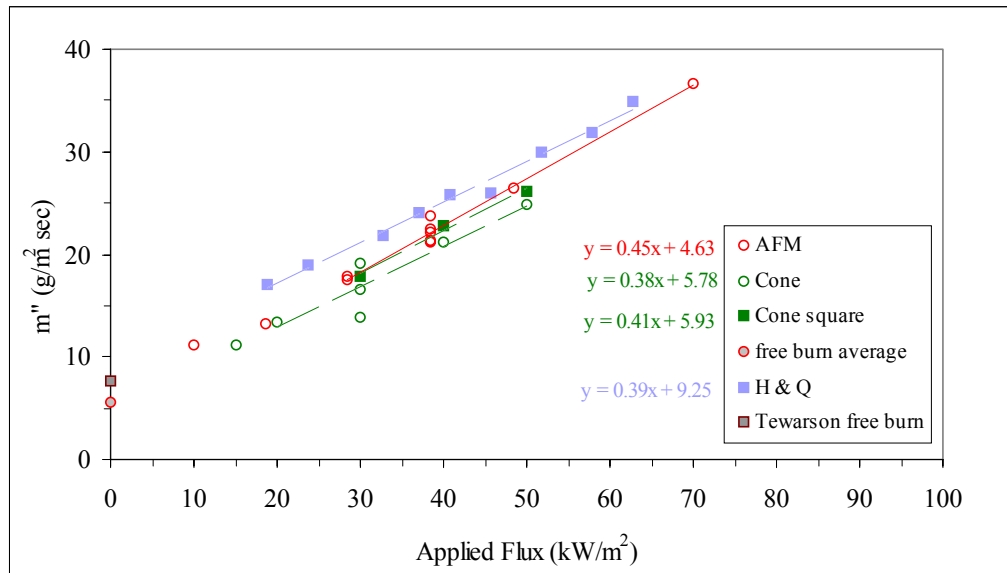

Figure E.1 Mass loss rate vs. applied heat flux.

From the intercepts shown in Figure E.1 for the AFM, Cone and Hopkins and Quintiere, the flame heat flux is 16.9, 22.3 and 30.7 kW/m^2 respectively, using h_g from each data set. Note that Hopkins and Quintiere data was used directly since the data fits given in their paper were, in my opinion, debatable.

The flame heat flux obtained directly from the free burn mass loss rate data obtained in the AFM and from Tewarson is 22.3 and 19.6 kW/m^2 respectively, again using h$_g$ from each data set.

INFER FROM INDIVIDUAL MASS LOSS

Following the derivation given above, but using equation 4 instead of the intercept form of equation 5, one can calculate the flame heat flux from the individual mass loss rate at each applied heat flux. The AFM varied randomly from 18 to 22 kW/m^2, while the cone varied from 22 to 29 kW/m^2 and Hopkins and Quintiere was 28 to 34 kW/m^2.

EMBEDDED THIN FILM GAGES

Thin film heat flux gages are sometimes called Micro-foil heat flux sensors.[5] They function as a self-generating thermopile transducer with low thermal impedance that measures heat flux by differentiating temperature between opposite sides of a certain material. The RdF gages used in the AFM are polyimide film bonded using a Teflon lamination process and are 0.18 mm thick.

The gages are placed between thin layers of black PMMA. These layers are built up to approximately 1" thickness and are held together using a liquid PMMA mix, to effectively embed the gages in the sample. The output wires are slightly thicker than the gage itself and are placed outside the sample edge such that the sensing surface was still in the uniform 1D area of the sample.
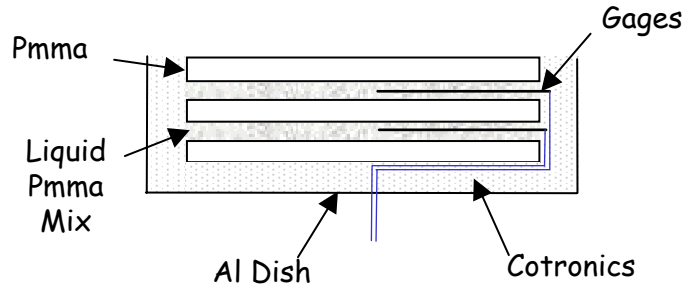
Figure E.2   Sample with thin film gages. Drawing is exaggerated to show construction.

These embedded thin film heat flux gages measure conduction into the solid until the regressing surface reaches the level of each gage. The gage then gets exposed and becomes very quickly coated with soot. The gage appears to move with the regressing surface, giving possibly a "hot gage" flame heat flux reading. Below is a typical trace. Gages placed on the surface get burned up during the ignition process but gages placed on the back surface show essentially no heat loss out the back face for the entire test time.

Figure E.3   Typical trace from thin film heat flux gage placed near surface

As seen in the above trace from 1000 sec to 2000 sec, where the gage is sitting on top of the bubbling surface, free burn tests measure an average "hot" he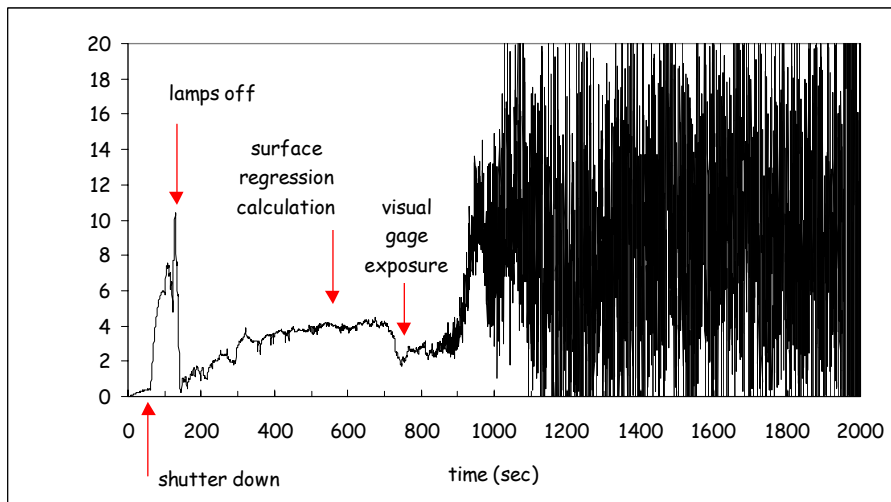at flux reading of 10 kW/m^2 which gives a flame heat flux of 16 kW/m^2 for a surface temperature of 598 K. At approximately 700 sec, when the burning surface has regressed visually to the gage location such that the gage can be considered "effectively at the surface, " a conduction heat flux of $\approx$ 4 kW/m^2 calculates to a flame heat flux of 19.4 kW/m^2. Note that the lamps were shut off immediately after ignition.

Note the in-depth absorption of the applied heat flux at shutter down. Also note the slight increase before shutter down indicating "pre-exposure" or that the wires are heating up. This increase was not seen with the thermocouple measurements.

The drop that is seen when the gage becomes exposed is thought to be the low absorptivity of the polyimide material. The gage slowly becomes covered with soot as the surface starts to regress. New gages have been fabricated with a black surface in an effort to reduce this drop.

The flame heat flux values obtained in this technique are comparable to values obtained in other techniques. The gages are not as intrusive as other methods, although one needs to be aware of the local pyrolysis blockage of the gage. Also, one needs to be aware of the possibility of "thin" behavior if the layers are not secured together properly. This can happen if the liquid pmma mix is not cured correctly.

EMBEDDED MEDTHERM GARDON GAGE

A Gardon gage of approximately 5 mm diameter was embedded in a black PMMA sample. A hole, almost level bottomed, was drilled in the sample from the back surface and filled with a

small amount of liquid PMMA. The gage was then positioned and the hole was filled completely

and allowed to cure. The gage was cooled with 65 °F water during the test, which affected the

local conduction in the material, as observed visually and shown in the following figure. This

technique will be tried again while cooling the gage with hot water to see if the local cooling
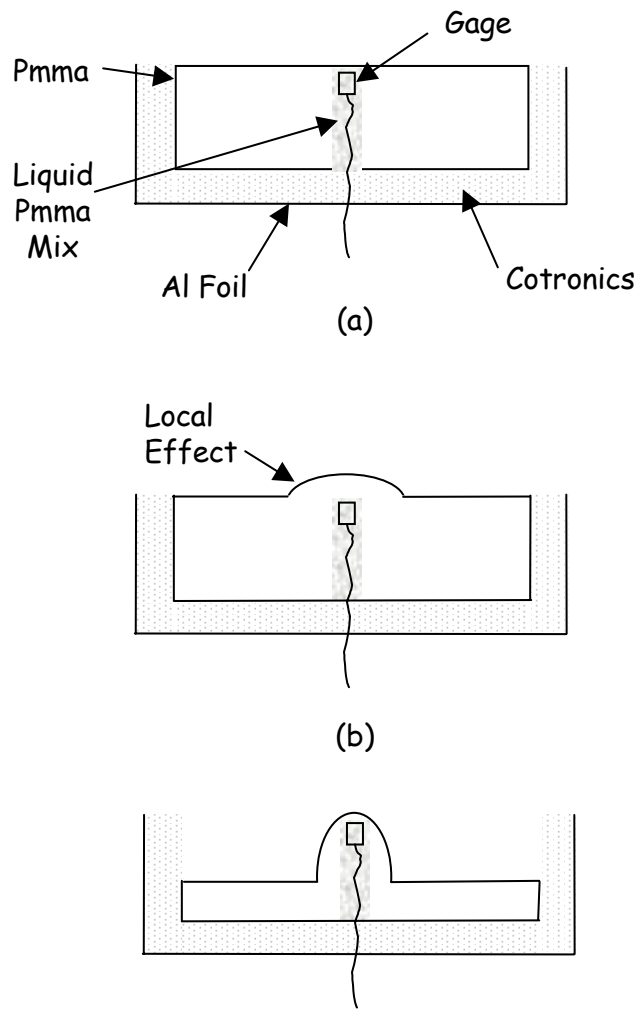
effect can be reduced.

Figure E.4   Embedded Medtherm gage (a) as constructed, (b) soon after ignition and (c) during

steady state burning.

E-8

From the free burn trace below, the heat flux value where the calculated surface is level with the gage is approximately 20 kW/m^2. This value may be skewed by the local cooling effect, but it shows that the technique seems reasonable.
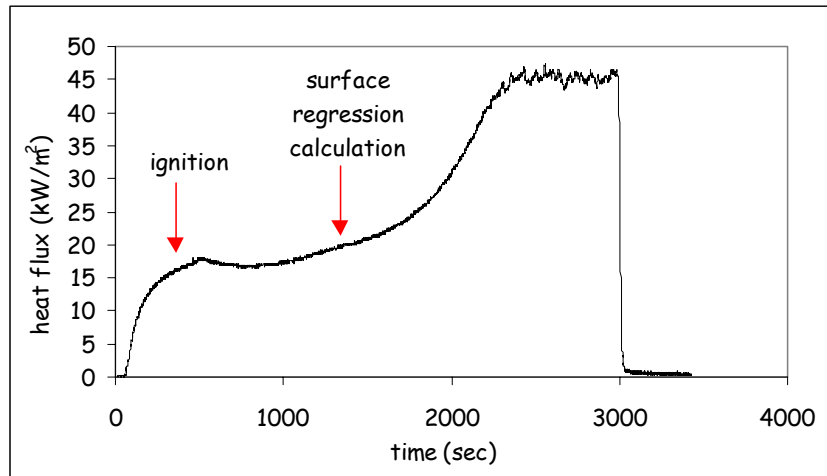
Figure E.5   Trace from embedded Medtherm Gardon gage.

EMBEDDED THERMOCOUPLES

Similar to the thin film gages, thermocouples were placed between thin layers of PMMA. Additionally though, the thermocouples were "melted" into the material surface using a soldering iron. Also (another technique) a hole was drilled, the thermocouple placed in it and filled, from the bottom up, with liquid PMMA using a syringe. This was originally constructed with clear PMMA to show that no air bubbles were present in the filled thermocouple hole.

The thermocouples were used to obtain the temperature profile in the solid, which was then used to get the energy balance conduction term. The profile measured does not match the assumed profile used in the common engineering technique of inferring the flame heat flux from the mass

loss. It was found that the temperature profile in the solid, normalized to the regressing surface location, is constant during steady burning and does not change with the mass loss rate. The flame heat flux is found to be changing with applied heat flux. This technique <u>may</u> not have enough resolution to obtain the proper gradient at the surface or something may be missing from the energy balance, such as a blockage term. Since this issue also raises questions about the mass loss inference technique (which gives a constant flame heat flux) it is still under investigation.

Early attempts to embed thermocouples by melting some black PMMA and casting it into a mold were unsuccessful. Staying below the pyrolysis temperature of 300 °F did not melt the material but only softened it. For safety reasons, higher temperatures were not used and the method was discontinued.
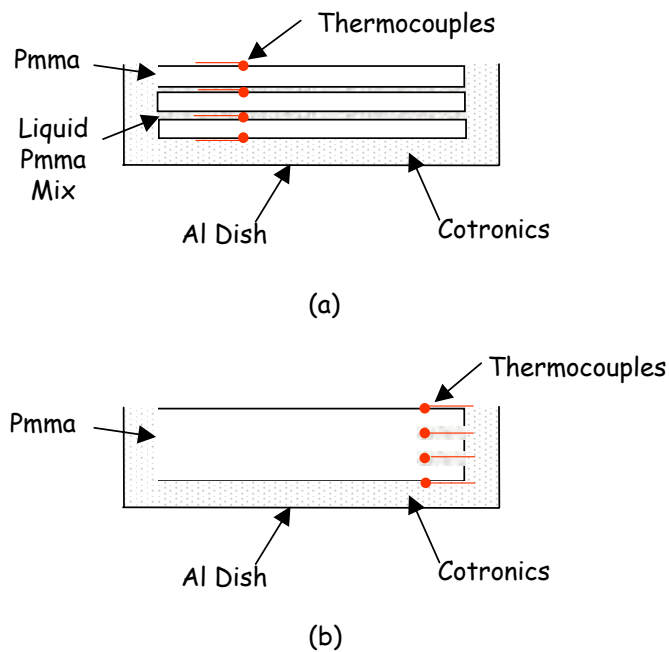
Figure E.6   Embedded thermocouples by (a) layers and (b) hole drilling.
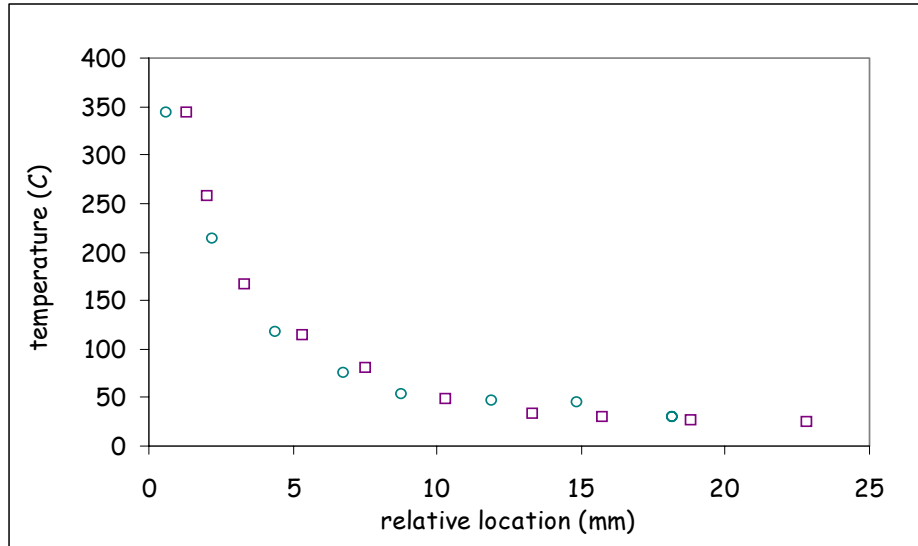
Figure E.7   Steady state temperature profiles of (circles) 0 kW/m^2 and (square) 60 kW/m^2 applied heat flux.

CONCLUSIONS

The common engineering technique of inferring flame heat flux from mass loss rate data gives a constant flame heat flux that doesn't vary with mass loss rate. The embedded thermocouple technique gives a flame heat flux that decreases with increasing mass loss rate. This technique also sees a constant temperature profile in the solid as opposed to one that is a function of mass loss rate. The surface energy balance may need to be modified to include a soot blockage term as a function of mass loss rate or other effect.

Embedded Medtherm Gardon gages are very invasive and have a local cooling effect. This may be reduced if hot cooling water is used. Embedded thin film gages are the least invasive and are very promising.

Table E.1   Flame heat flux results from different techniques.

Technique	kW/m^2
infer from mass loss rate intercept	16.9
infer from mass loss rate at each applied heat flux (average)	20.0
infer from mass loss rate at 0 applied heat flux	22.3
thin film gage, conduction term (free burn)	19.4
thin film gage, "hot gage" measurement (free burn)	16.0
embedded Medtherm gardon gage (free burn)	20.0
conduction term from temperature profile (free burn)	38.3

REFERENCES

1   Holman, J.P., Heat Transfer, p. 622-624, 1986.

2   Hopkins, D., and Quintiere, J., "Material Fire Properties and Predictions for Thermoplastics,"

    Fire Safety Journal, 26, p. 241-268, 1996.

3   Tewarson, A., and Ogden, S, "Fire Behavior of Polymethylmethacrylate," Combustion and

    Flame, 89, p. 237-259, 1992.

4   SFPE Handbook, Section 3, 2nd edition, NFPA, 1995.

5   RdF Corporation Temperature Measurement Catalog, 2000.

APPENDIX F: HEAT RELEASE RATE

ABSTRACT

Reducing uncertainty and minimizing error allows the calculation of a more accurate heat release rate. This is important from material development and engineering perspectives for various reasons. In order to reduce the uncertainty and minimize errors, experimental measurements need to be improved and refined since they dominate the problem. This study is the first step of a continuing process determining what improvements to make.

Carbon dioxide based calorimetry is commonly used to calculate the heat release rate of materials in bench scale fires and fuel packages in large scale fires. However, the equation given in the Fire Propagation Apparatus ASTM E-2058 Standard and the SFPE Handbook is unnecessarily simplified for modern data analysis. These simplifications were justified by the experimental methods of the era it was developed and the form worked well for many common materials. However, more sophisticated equipment continues to be developed as well as more complicated materials. Hence, a more "detailed" equation should be used as a platform to aid identification of needed measurement improvements and refinements that would lead to more accurate heat release rate calculations. The present study develops equations for carbon dioxide based calorimetry in a way analogous to that developed by Parker for oxygen consumption calorimetry. As an added feature, carbon dioxide generation and oxygen consumption calorimetry can now be more readily compared.

Oxygen consumption calorimetry is also used to calculate the heat release rate of materials. The

most commonly used equations are those developed by Parker which are given in simplified form in the Cone Calorimeter ASTM E-1354 Standard, however, the simplifications are not the same as those used by carbon dioxide generation calorimetry. The present study shows improvements and refinements to obtain more accurate equations of heat release rate using oxygen consumption calorimetry.

INTRODUCTION

A short background is given, followed by the derivation of the current study carbon dioxide generation calorimetry equations. Experimental heat release rate results are then presented. Experimental improvements and refinements to the equations are shown including modifications for various oxygen concentration atmospheres. These are also applied to the heat release rate equations for oxygen consumption calorimetry.

BACKGROUND

Reducing uncertainty and minimizing error which allows the calculation of a more accurate heat release rate is important from a material development perspective since small changes in formulation can have large economic effects. Reducing the uncertainty will more easily show if small changes in heat release rate values from one material formulation to the next are significant. Reducing uncertainty and minimizing error are also important from an engineering perspective since materials currently in use may have combustion product species such as soot, hydrochloric acid and hydrofluoric acid[1] that are not accounted for in the commonly used calorimetry equations. This study is the first step of a process to obtain a more accurate heat release rate

equation that includes these combustion product species as well as improved and refined experimental measurements.

HEAT RELEASE RATE BY CARBON DIOXIDE GENERATION CALORIMETRY

The carbon dioxide generation calorimetry equation given in the Fire Propagation Apparatus ASTM E-2058 Standard[2] and the SFPE Handbook[1] is unnecessarily simplified for modern data analysis. The equation is based on the premise that knowing the molar flow rate of carbon dioxide and carbon monoxide produced allows the heat release rate to be calculated. To do this, it has an equation which contains the difference between the volume fraction carbon dioxide in the exhaust duct gas and the volume fraction carbon dioxide in the ambient gas. This is an attempt to correct for the ambient carbon dioxide. Note however, that a subtraction of the volume fractions does not truly represent a subtraction of the molar flow rates when each volume fraction is defined by a different mixture. The difference in the mixtures of exhaust duct gas and ambient gas is due to the combustion process expansion. A simplification of the carbon dioxide generation calorimetry equation given in E-2058 is that it does not include this expansion. Another simplification is that in normal testing procedures water is removed from the gas sample before it reaches the gas analyzers but the equations assume a "wet" gas sample.

Although these simplifications were justified by the experimental methods of the era it was developed and the form worked well for many common materials, more sophisticated equipment continues to be developed as well as materials of more complex composition. Hence, a more "detailed" equation should be used as a platform to move forward with identifying where to make measurement improvements and refinements that leads to more accurate heat release rate

calculations. The present study develops equations for carbon dioxide generation calorimetry in a way analogous to that developed by Parker[3] for oxygen consumption calorimetry.

It is assumed in this analysis that all of the products of combustion are captured by the exhaust duct and that the burning is not ventilation controlled. Issues concerning ventilation will be addressed in a future study. The components[4] of the "incoming" gas are assumed to be nitrogen (N_2), oxygen (O_2), carbon dioxide (CO_2) and water vapor (H_2O) where the minor components are included in the nitrogen term. The heat release rate $\dot{Q}$ due to the generation of CO_2 is

$$\dot{Q}_{co_2} = \Delta h_{co_2} \dot{m}_{co_2} \tag{1}$$

where Δh_{co_2} is the heat of combustion of the fuel per unit mass CO_2 generated. The mass generation rate of carbon dioxide is given as $\dot{m}_{co_2} = MW_{co_2} \dot{n}_{co_2}$ such that the heat release rate is $\dot{Q}_{co_2} = \Delta h_{co_2} MW_{co_2} \dot{n}_{co_2}$ where $\dot{n}_{co_2}$ is the mole rate of CO_2 generated. This is the difference between the moles in the "outgoing" gas and the "incoming" gas and is given by $\dot{n}_{co_2} = \dot{n}^s_{co_2} - \dot{n}^0_{co_2}$ where, following Parker's[3] convention, the superscript "0" stands for "into the control volume" and the superscript "s" stands for "out of the control volume." Similar to Parker's oxygen depletion factor, the carbon dioxide generation factor is defined as

$$\theta = \frac{\dot{n}^s_{co_2} - \dot{n}^0_{co_2}}{\dot{n}^0_{co_2}}$$

which leaves the heat release rate as $\dot{Q}_{co_2} = \Delta h_{co_2} MW_{co_2} \theta \dot{n}^0_{co_2}$ where MW_{co_2} is the molecular weight of CO_2. The mole rate of CO_2 "incoming" can be written as

$$\dot{n}^0_{co_2} = X^0_{co_2} \dot{n}^0_a \qquad (2)$$

where X is the volume fraction and the total moles of "incoming" gas is given by

$$\dot{n}^0_a = \frac{\dot{V}^0_a \rho^0_a}{MW^0_a}$$

where ρ^0_a is the density, MW^0_a is the molecular weight and $\dot{V}^0_a$ is the volume flow rate of the "incoming" gas. The subscript "a" stands for "gas." This leaves the heat release rate equation as

$$\dot{Q}_{co_2} = \Delta h_{co_2} \frac{MW_{co_2}}{MW^0_a} \rho^0_a \theta \dot{V}^0_a X^0_{co_2} \qquad (3)$$

which assumes complete combustion. Of course, real world materials do not undergo complete combustion but produce carbon monoxide (CO), soot and sometimes other products of combustion such as unburnt fuel, gaseous hydrocarbons, hydrochloric acid and hydrofluoric acid.[1] The current study addresses the CO production only but in the future soot, gaseous hydrocarbons and other products will need to be incorporated. The "actual" heat release rate corrected for incompleteness defined by having only CO production can be obtained per the technique of Parker[3] and Tewarson.[1] The energy that would have occurred if the process was complete is calculated and the energy of converting the CO to CO_2 that did not occur is

subtracted out $\dot{Q}_{actual} = \dot{Q}_{complete} - \dot{Q}_{co \to co_2}$. This is done since the heat of combustion of the fuel per unit mass CO generated is not easily measured. For incomplete combustion, there is a fraction "f" of CO that did not burn to CO_2 so the energy that did not occur converting CO to CO_2 is

$$\dot{Q}_{co \to co_2} = fF'' \theta \dot{V}_a^0 X_{co_2}^0$$

where "f" is defined as $f = \dot{n}_{co}^s / \left(\dot{n}_{co_2}^s - \dot{n}_{co_2}^0 \right)$ but can be rewritten as

$$f = \frac{\dot{n}_{co}^s}{\dot{n}_{co_2}^s} \frac{(1 + \theta)}{\theta}$$

and the heat released per unit volume CO_2 generated in the burning of CO to CO_2 is defined as

$$F'' = \Delta h_{co_2}^{co \to co_2} \frac{MW_{co_2}}{MW_a^0} \rho_a^0 \tag{4}$$

where $\Delta h_{co_2}^{co \to co_2}$ is the heat of combustion per unit mass CO_2 generated in the burning of CO to CO_2. For complete combustion, the energy that would have occurred if all CO had gone to CO_2 is given as

$$\dot{Q}_{complete} = (1 + f) \Delta h_{co_2} \frac{MW_{co_2}}{MW_a^0} \rho_a^0 \theta \dot{V}_a^0 X_{co_2}^0$$

which can be rewritten as

$$\dot{Q}_{complete} = (1 + f)F'\theta\dot{V}_a^0 X_{co_2}^0$$

where F' is the heat of combustion of the fuel per unit volume CO_2 generated and is defined as

$$F' = \Delta h_{co_2} \frac{MW_{co_2}}{MW_a^0} \rho_a^0 \tag{5}.$$

Using these equations, the actual heat release rate is

$$\dot{Q}_{actual} = \theta\dot{V}_a^0 X_{co_2}^0 \left[(1 + f)F' - fF''\right]$$

when using the definition of the carbon dioxide generation factor θ. Incorporating the form for "f" and using Equation 2 to get the mole fraction leaves the actual heat release rate as

$$\dot{Q}_{actual} = F'\theta\dot{V}_a^0 X_{co_2}^0 \left[1 - \frac{(1 + \theta)}{\theta} \frac{X_{co}^s}{X_{co_2}^s}\left(\frac{F''}{F'} - 1\right)\right] \tag{6}.$$

The carbon dioxide generation factor, the volume flow rate of the "incoming" gas and the volume fraction of CO_2 in the "incoming" gas need to be related to concentrations in the exhaust duct where experimental measurements are normally taken. Each of these items will now be addressed.

CARBON DIOXIDE GENERATION FACTOR

In order to relate the carbon dioxide generation factor θ to the concentrations in the exhaust duct, recall that the volume fraction of CO_2 is

$$X_{co_2}^s = \frac{\dot{n}_{co_2}^s}{\dot{n}_a^s}$$

and assuming that N_2, CO, CO_2, O_2 and H_2O are the only products of combustion when the production of soot and other products are ignored

$$\dot{n}_a^s = \dot{n}_{n_2}^s + \dot{n}_{co}^s + \dot{n}_{co_2}^s + \dot{n}_{o_2}^s + \dot{n}_{h_2o}^s$$

which after rearranging becomes

$$\dot{n}_{co_2}^s = \frac{X_{co_2}^s \left(\dot{n}_{n_2}^s + \dot{n}_{co}^s + \dot{n}_{o_2}^s + \dot{n}_{h_2o}^s \right)}{1 - X_{co_2}^s} \tag{7.}$$

Adding together the moles of CO, O_2 and H_2O gives

$$\dot{n}_{co}^s + \dot{n}_{o_2}^s + \dot{n}_{h_2o}^s = \left(X_{co}^s + X_{o_2}^s + X_{h_2o}^s \right)\left(\dot{n}_{n_2}^s + \dot{n}_{co}^s + \dot{n}_{co_2}^s + \dot{n}_{o_2}^s + \dot{n}_{h_2o}^s \right)$$

but recall from above that

$$\left(\dot{n}^s_{n_2} + \dot{n}^s_{co} + \dot{n}^s_{co_2} + \dot{n}^s_{o_2} + \dot{n}^s_{h_2o}\right) = \frac{\dot{n}^s_{co_2}}{X^s_{co_2}}$$

so that

$$\dot{n}^s_{co} + \dot{n}^s_{o_2} + \dot{n}^s_{h_2o} = \left(X^s_{co} + X^s_{o_2} + X^s_{h_2o}\right)\left(\frac{\dot{n}^s_{co_2}}{X^s_{co_2}}\right)$$ (8).

Plugging this into Equation 7 and rearranging to solve for $\dot{n}^s_{co_2}$

$$\dot{n}^s_{co_2} = \frac{X^s_{co_2}\,\dot{n}^s_{n_2}}{1 - X^s_{co_2} - X^s_{o_2} - X^s_{co} - X^s_{h_2o}}$$ (9a)

and similarly for the "incoming" gas

$$\dot{n}^0_{co_2} = \frac{X^0_{co_2}\,\dot{n}^0_{n_2}}{1 - X^0_{co_2} - X^0_{o_2} - X^0_{h_2o}}$$ (9b).

The carbon dioxide generation factor can be rewritten as $\theta = \dot{n}^s_{co_2}\big/\dot{n}^0_{co_2} - 1$ which after inserting

Equation 9 gives the carbon dioxide generation factor as

$$\theta = \frac{\left(\dfrac{X^s_{co_2}\,\dot{n}^s_{n_2}}{1 - X^s_{co_2} - X^s_{o_2} - X^s_{co} - X^s_{h_2o}}\right)}{\left(\dfrac{X^0_{co_2}\,\dot{n}^0_{n_2}}{1 - X^0_{co_2} - X^0_{o_2} - X^0_{h_2o}}\right)} - 1$$ (10).

Typically, gas analyzers require a "dry" gas sample. As such, the water is removed before the gas sample reaches the analyzers. Hence, the "dry" gas sample readings of the analyzers need to be related to the actual "wet" gas concentrations in the duct. It is assumed that the molar flow rates of all the other components are in the same ratio to each other in the analyzers as they are in the exhaust duct.[3,5,6] This assumption leads to the following general relationship between the wet and dry sample

$$X_{yy}^s = X_{yy}^a \left(1 - X_{h_2o}^s\right) \tag{11}$$

where the superscript "a" stands for "at the analyzer" as per Parker's convention and the subscript "yy" stands for each species. The equation is now

$$\theta = \frac{\left(\dfrac{X_{co_2}^a \left(1 - X_{h_2o}^s\right) \dot{n}_{n_2}^s}{1 - X_{co_2}^a \left(1 - X_{h_2o}^s\right) - X_{o_2}^a \left(1 - X_{h_2o}^s\right) - X_{co}^a \left(1 - X_{h_2o}^s\right) - X_{h_2o}^s}\right)}{\left(\dfrac{X_{co_2}^0 n_{n_2}^0}{1 - X_{co_2}^0 - X_{o_2}^0 - X_{h_2o}^0}\right)} - 1$$

which is simplified to

$$\theta = \frac{X_{co_2}^a \left(1 - X_{o_2}^0 - X_{h_2o}^0\right) - X_{co_2}^0 \left(1 - X_{o_2}^a - X_{co}^a\right)}{X_{co_2}^0 \left(1 - X_{co_2}^a - X_{o_2}^a - X_{co}^a\right)} \tag{12}$$

assuming that the molar flow rate of nitrogen is the same for the "incoming" and "outgoing" gas. Multiplying Equation 12 by

$$\left[1/\left(1 - X_{o_2}^a - X_{co}^a\right)\right] / \left[1/\left(1 - X_{o_2}^a - X_{co}^a\right)\right]$$

allows the carbon generation factor θ be written as

$$\theta = \frac{\dfrac{X_{co_2}^a \left(1 - X_{o_2}^0 - X_{h_2o}^0\right)}{\left(1 - X_{o_2}^a - X_{co}^a\right)} - X_{o_2}^0}{X_{co_2}^0 \left(1 - \dfrac{X_{co_2}^a}{1 - X_{o_2}^a - X_{co}^a}\right)}$$

where the initial concentrations $X_{o_2}^0$ and $X_{co_2}^0$ refer to the "incoming" gas. These can be obtained from the analyzer readings prior to sample ignition assuming the "incoming" conditions do not change during the test. However, the water has been removed from the gas sample in the analyzers so the initial readings need to be related to the "wet" gas concentrations of the "incoming" gas via

$$X_{yy}^0 = X_{yy}^{a^0}\left(1 - X_{h_2o}^0\right) \tag{13}$$

which leaves the carbon dioxide generation factor as

$$\theta = \frac{\dfrac{X_{co_2}^a \left(1 - X_{o_2}^{a^0}\right)}{\left(1 - X_{o_2}^a - X_{co}^a\right)} - X_{co_2}^{a^0}}{X_{co_2}^{a^0} \left(1 - \dfrac{X_{co_2}^a}{1 - X_{o_2}^a - X_{co}^a}\right)} \tag{14}.$$

This is comparable to the equation of Parker[3] for the oxygen depletion factor.

INCOMING GAS VOLUME FLOW RATE

In order to relate the "incoming" gas flow rate used in Equation 6 to the measurements taken in the exhaust duct, note that the volume flow rate in the duct is given by[3]

$$\dot{V}_a^s = \alpha\Phi\dot{V}_a^0 + (1-\Phi)\dot{V}_a^0$$

where Φ is the oxygen depletion factor and α is the expansion factor for the gas used for combustion. The first term of the equation represents the "combusted" gas and the second term represents the "non-combusted" gas including that entrained by the flame and the exhaust duct. This can be rearranged to

$$\dot{V}_a^0 = \frac{\dot{V}_a^s}{1+(\alpha-1)\Phi}$$

where the volume flow rate in the duct is typically measured with a pitot static tube, a bi-direction probe or an averaging pitot tube. Strictly speaking, the composition of the "outgoing" gas needs to be known to calculate its density and obtain the volume flow rate from the measured differential pressure. For the control volume approach taken in this study, the amount of entrained gas is much greater than the products of combustion. Hence, from a practical viewpoint for volume flow rate calculations, the density of the gas "leaving the control volume" (i.e., in the exhaust duct) can be considered the same as that "incoming" except for temperature effects. However, an ideal gas assumption allows the density to be related to the temperature. This simplification allows the "incoming" gas flow rate to be written as

$$\dot{V}_a^0 = kCA\sqrt{\frac{2T_a^0}{\rho_a^0}}\sqrt{\frac{\Delta P}{T_a^s}}\left(\frac{1}{1+(\alpha-1)\Phi}\right) \qquad (15)$$

where ΔP is the differential pressure, T is the temperature, A is the exhaust duct cross sectional area, C is the flow coefficient and k is a correction for relating the average velocity to the centerline velocity. For a pitot static tube and bi-directional probe where the measurement is taken at a single location (usually the centerline of the duct) the k value is determined from the predetermined velocity profile in the duct. For an averaging pitot tube which takes readings across the duct diameter, k=1. The expansion factor can be determined from the equation[3]

$$\alpha = 1 - X_{o_2}^0 - \beta X_{o_2}^0 \qquad (16)$$

$$\beta = \frac{1-\Phi}{\Phi}\frac{1}{X_{o_2}^a}\left(\frac{X_{h_2o}^s}{1-X_{h_2o}^s} + X_{co_2}^a + X_{co}^a\right)$$

where β is the ratio of the moles of the combustion products formed to the moles of oxygen consumed and the O_2, CO_2 and CO values are taken from the "dry" gas sample while the H_2O value is obtained from the gas sample before the water has been removed. Alternatively, β can be estimated[3] from the material composition.

INCOMING GAS VOLUME FRACTION

The initial concentration $X_{co_2}^0$ used in Equation 6 refers to the "incoming" gas. As stated previously, this can be obtained from the analyzer readings prior to heat flux exposure using Equation 13 assuming the ambient conditions do not change during the test.

$$X_{co_2}^0 = X_{co_2}^{a^0} \left(1 - X_{h_2o}^0\right)$$ (17).

EXPERIMENTAL DATA

Figure 1 shows the heat release rate for methane, PMMA and propylene calculated by the equations derived in this study for carbon dioxide generation calorimetry (PAB-CO_2) as well by ASTM E-2058 for well ventilated conditions. The fuel specific heat of combustion is used for both cases rather than the generic "average" value. The results from PAB-CO_2 and E-2058 are quite close to each other. This shows that the simplifications made by ASTM E-2058 including ignoring the combustion process expansion and water removal do not have a dramatic effect, from a practical viewpoint, for the materials tested. The results virtually overlap for methane and propylene but the PMMA results show a slight difference between PAB-CO_2 and ASTM E-2058. This is consistent for all PMMA tests conducted in this study but presently the reason for this difference is not understood.
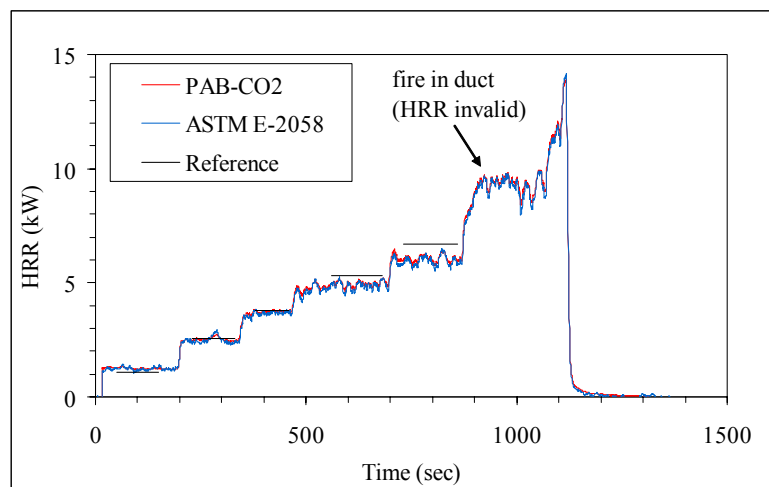
(a)
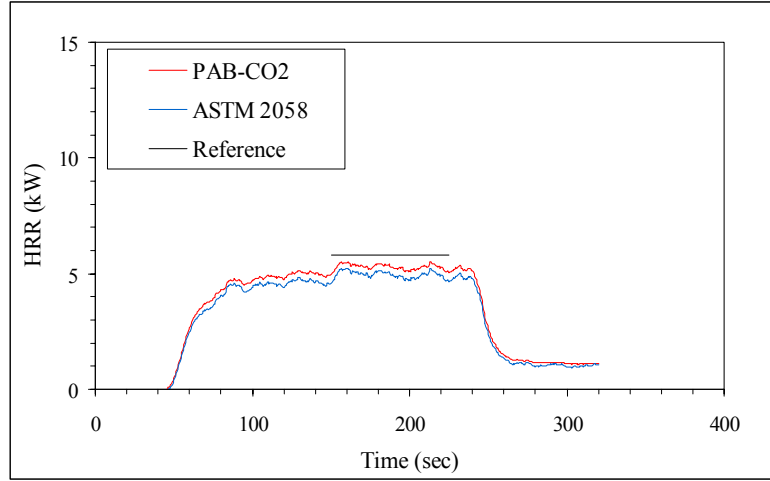
(b)
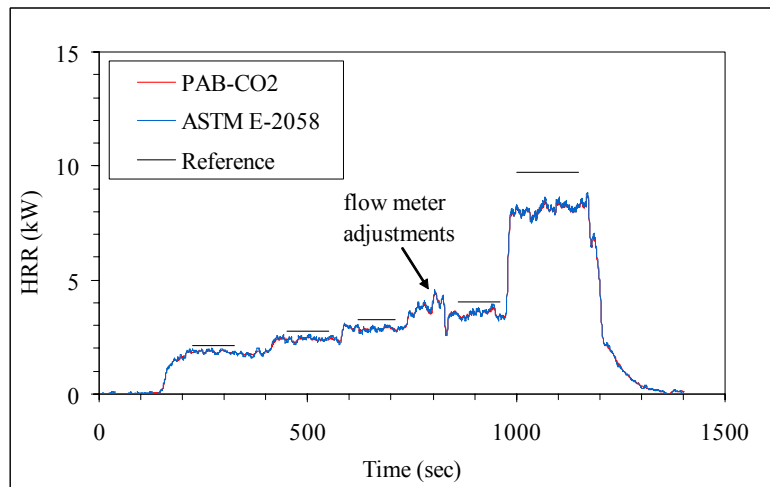
(c)

Figure F.1. Heat release rate calculated by PAB-CO$_2$ and ASTM E-2058 for (a) various size methane fires, (b) PMMA with 60 kW/m^2 applied heat flux and (c) various size propylene fires.

A more interesting observation is the relationship between the calculated heat release rate and the

reference values presented in the figures. The reference value is determined from $\dot{Q}_{reference} = \dot{m}_f \Delta h_{ch}$ where Δh_{ch} is the "chemical" heat of combustion and $\dot{m}_f$ is the mass flow rate of the fuel. The "chemical" heat of combustion is defined as the heat of reaction determined from the chemical equation using experimental measurements for fuel, CO_2, CO, soot and water. Defined this way, the chemical heat of combustion accounts for the production of CO as well as other products of incomplete combustion including soot. Recall that both the PAB-CO_2 and ASTM E-2058 carbon dioxide generation calorimetry equation accounts for incomplete combustion by including CO production only. As such, the calculated heat release rate value should be lower than the reference value when soot is produced. This difference should become more pronounced as the fuel produces more soot. Although a full uncertainty analysis remains to be completed, this trend can be seen in Figure 3. This shows that the heat release rate equations need to account for incomplete combustion more correctly by including the formation of soot. This is also suggested by others.[7,8] Note also that the first three fire sizes on the methane plot were blue flames that produced no CO or soot. The larger fire sizes were observed to become luminous and produce CO and soot. This, by design, change in fire size and efficiency was done to show the effect of increasing soot production for the same fuel. This shows the same trend of the calculated heat release rate value being lower than the reference value when soot is produced.

EXPERIMENTAL IMPROVEMENTS

Experimental measurements need to be improved and refined in order to reduce uncertainty and minimize errors. This will lead to more accurate heat release rate calculations. There are several variables in either the PAB-CO_2 and ASTM E-2058 carbon dioxide generation calorimetry equations for which generic constants are typically used. The errors produced by these generic

values are repeated here from other sources as a reminder to consider these often overlooked sources. Additionally, two generic values that have not been given much thought elsewhere are also discussed.

Use of the generic value of 1.105 for the expansion factor[3] produces approximately 3% error while ignoring the water content[3] of the incoming gas can be 1% error for normal laboratory conditions of 50% relative humidity. Use of the generic[1] "average" heat of combustion value of 13.3 kJ/gCO$_2$ instead of the fuel specific heat of combustion can lead to large error depending on the fuel. For materials such as acetone (13.1), octyl-acetate (13.1) and nylon (13.3) with values close to the "average" the error would be small. For materials such as propane (15.3), polyvinyl chloride (11.7) and some rigid polyurethane foams (10.7) with fuel specific heat of combustion values that are significantly different from the generic "average" value, the error would be quite large. The range stated by Tewarson in the SFPE Handbook is ± 11% for the heat of combustion which would translate into the same error for the heat release rate. Note however, that several fuels are not included in the statistics such as methane (18.2), Douglas Fir (9.5) and Teflon (5.3) which have heat of combustion values drastically different than the "average."

Others have also presented reminders that use of the generic "average" heat of combustion adds to the error and uncertainty of the heat release rate calculations. Brohez[7,8] states that the fuel specific value of the heat of combustion is required to obtain accurate heat release rate calculations. The ASTM E-2058[2] Standard also implies that use of the generic heat of combustion increases the heat release rate error by stating that "accuracy is improved if the composition of the test specimen is known".

New materials under development can also have significantly different values for the heat of combustion. Use of the generic "average" heat of combustion value for these materials would result in even greater error in the heat release rate. It is imperative that the fuel specific heat of combustion be obtained for these materials using an oxygen bomb or other appropriate instrument. Use of an oxygen bomb for new materials which are typically non-homogenous such as composites presents its own difficulties, issues and problems but that is a topic for another study.

It is quite clear that use of the generic "average" heat of combustion when the material is known is a major contribution to the total error while the expansion factor and incoming water content is a minor contribution. When the material is unknown, use of the generic expansion factor and "average" heat of combustion can be used but the uncertainty needs to be clearly stated for the heat release rate calculation. This is rarely done in the fire engineering field.

MODIFICATION FOR ENHANCED OR REDUCED OXYGEN ATMOSPHERES

Two typically used generic constants that are not given much thought are the density and molecular weight of the "incoming" air. These are used to convert the heat of combustion per unit mass CO_2 generated to the heat of combustion per unit volume CO_2. The generic values used are for "standard" ambient air of 20.95% oxygen concentration. However, the density and molecular weight of the incoming air would be different for atmospheres of other oxygen concentrations. The expanding use of reduced and elevated oxygen atmospheres in bench scale testing shows the need for the heat release rate equation to incorporate this situation.
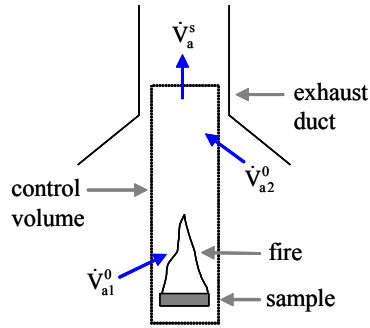
Figure F.2. Fire in an open system showing control volume for analysis of various oxygen atmospheres.

For an enhanced or reduced oxygen atmosphere, the "incoming" gas is made up of two flows with different oxygen concentrations as shown in Figure 2. The "incoming" gas flow rate is simply the sum of these two flows $\dot{V}_a^0 = \dot{V}_{a1}^0 + \dot{V}_{a2}^0$ where in general terms

$$\dot{V}_a = \frac{MW_a}{\rho_a} \frac{\dot{n}_{co_2}}{X_{co_2}}$$

such that

$$\dot{V}_a^0 = \left(\frac{MW_{a1}^0}{\rho_a^0} \frac{\dot{n}_{co_2}^0}{X_{co_2}^0} \right)_{a1} + \left(\frac{MW_{a2}^0}{\rho_a^0} \frac{\dot{n}_{co_2}^0}{X_{co_2}^0} \right)_{a2} = \left(\frac{MW_a^0}{\rho_a^0} \frac{\dot{n}_{co_2}^0}{X_{co_2}^0} \right)_{amix} \tag{20}.$$

For the control volume approach taken in this study, the ratio of the two flows does not change during the test. Assuming that the "incoming" conditions do not change during the test, the mixture molecular weight and density is determined from baseline analyzer readings prior to

sample ignition. (If it is desired that the "incoming" conditions change in "stages" during the test, then the mixture molecular weight and density must be calculated for each stage.) The molecular weight is calculated

$$
\begin{aligned}
MW^0_{amix} = \left(MW_{o_2}\right)X^0_{o_2} + \left(MW_{co_2}\right)X^0_{co_2} \\
+ \left(MW_{h_2o}\right)X^0_{h_2o} + \left(MW_{n_2}\right)\left(X^0_{n_2}\right)
\end{aligned}
\tag{21}
$$

where $X^0_{n_2} = 1 - X^0_{o_2} - X^0_{co_2} - X^0_{h_2o}$ is used to obtain the nitrogen fraction. The density is from

$$
\rho^0_{amix} = \frac{MW^0_{amix}}{\mathfrak{R}T^0_{amix}}
\tag{22}
$$

where $\mathfrak{R}$ is the universal gas constant. The heat of combustion of the fuel per unit CO_2 generated becomes

$$
F' = \Delta h_{co_2} \frac{MW_{co_2}}{MW^0_{amix}} \rho^0_{amix}
\tag{23}
$$

and the heat released per unit volume CO_2 generated in the burning of CO to CO_2 becomes

$$
F'' = \Delta h^{co \rightarrow co_2}_{co_2} \frac{MW_{co_2}}{MW^0_{amix}} \rho^0_{amix}
\tag{24}
$$

where $\Delta h^{co \rightarrow co_2}_{co_2}$ is the heat of combustion per unit mass CO_2 generated in the burning of CO to

F-20

CO_2. The enhanced heat release rate equation is

$$\dot{Q}_{actual} = F'\theta CA \sqrt{\frac{2T^0_{amix}}{\rho^0_{amix}}} \sqrt{\frac{\Delta P}{T^s_{amix}}} \left(\frac{1}{1+(\alpha-1)\Phi}\right)$$
$$X^{a^0}_{co_2}\left(1-X^0_{h_2o}\right)\left[\theta-(1+\theta)\frac{X^a_{co}}{X^a_{co_2}}\left(\frac{F''}{F'}-1\right)\right]$$

(25)

where equations 22, 23 and 24 are used for ρ^0_{amix}, F' and F''. The equations for θ, Φ and α are the same as for "standard" atmospheres given by equations 14, 19 and 16 respectively. The additional uncertainty that occurs if the proper gas mixture is not accounted for is approximately 3%.

HEAT RELEASE RATE BY OXYGEN CONSUMPTION CALORIMETRY

Oxygen consumption calorimetry is also used to calculate the heat release rate. The two commonly used equations are those developed by Parker[3] and the "simplified version of Parker" given in the Cone Calorimeter ASTM E-1354[9] Standard. These equations are only valid for a "standard" 20.95% O_2 atmosphere. These equations can be applied to other oxygen concentration atmospheres if they are modified in a way similar to the change discussed above for carbon dioxide generation calorimetry. The improvements are more readily shown using the "full" Parker form of the equations rather than the "simplified" form given by the Cone Standard. Starting with Parker Equation 17 for the actual heat release rate by oxygen consumption calorimetry

$$\dot{Q}_{actual} = E'X^0_{o_2} \dot{V}^0_a \left[\Phi - \frac{(1-\Phi)}{2} \frac{X^a_{co}}{X^a_{o_2}} \left(\frac{E''-E'}{E'} \right) \right]$$

inserting Parker Equation 24 for $X^0_{o_2}$, Parker Equation 33 for $\dot{V}^0_a$ Parker Equation 42 for $\dot{V}^s_a$

gives

$$\dot{Q}_{actual} = E'\Phi CA \sqrt{\frac{2T^0_a}{\rho^0_a}} \sqrt{\frac{\Delta P}{T^s_a}} \left(\frac{1}{1+(\alpha-1)\Phi} \right) X^{a^0}_{o_2}$$
$$\left(1 - X^0_{h_2o} \right) \left[\Phi - \frac{(1-\Phi)}{2} \frac{X^a_{co}}{X^a_{o_2}} \left(\frac{E''}{E'} - 1 \right) \right]$$

(26).

The heat of combustion of the fuel per unit volume O_2 consumed is defined as

$$E' = \Delta h_{o_2} \frac{MW_{o_2}}{MW^0_a} \rho^0_a$$

where Δh_{o_2} is the heat of combustion of the fuel per unit mass O_2 consumed. The heat released

per unit volume O_2 consumed in the burning of CO to CO_2 is

$$E'' = \Delta h^{co \to co_2}_{o_2} \frac{MW_{o_2}}{MW^0_a} \rho^0_a$$

where Δh_{o_2} is the heat of combustion per unit mass O_2 consumed in the burning of CO to CO_2.

Analogous to what was done for carbon dioxide generation calorimetry, these equations can also

be modified to account for other oxygen concentration atmospheres.

$$\dot{Q}_{actual} = E'\theta CA \sqrt{\frac{2T_{amix}^0}{\rho_{amix}^0}} \sqrt{\frac{\Delta P}{T_{amix}^s}} \left(\frac{1}{1 + (\alpha - 1)\Phi}\right) X_{o_2}^{a^0}$$

$$\left(1 - X_{h_2o}^0\right) \left[\Phi - \frac{(1-\Phi)}{2} \frac{X_{co}^a}{X_{o_2}^a}\left(\frac{E''}{E'} - 1\right)\right]$$

where

$$E' = \Delta h_{o_2} \frac{MW_{o_2}}{MW_{amix}^0} \rho_{amix}^0$$

$$E'' = \Delta h_{o_2}^{co \to co_2} \frac{MW_{o_2}}{MW_{amix}^0} \rho_{amix}^0 \qquad (27).$$

The error that occurs if the proper gas mixture is not accounted for is approximately 3%. Use of the generic constants for incoming water content[3] (1%) and expansion factor[3] (3%) also contribute. Similar to carbon dioxide generation calorimetry, use of the generic "average" heat of combustion value of 12.8 kJ/gO$_2$ instead of the fuel specific heat of combustion can lead to large error depending on the fuel. The range stated by Tewarson in the SFPE Handbook[1] is ± 7% for the heat of combustion which would translate into the same error for the heat release rate.

It is an important point to note that the "simplified version of Parker" equation given in the Cone Calorimeter Standard assumes complete combustion. For materials that undergo complete combustion, the "simplified" result will match the "full" Parker result. For materials that are incomplete and produce CO, the simplified form given in the Cone Calorimeter Standard will have an error compared to the more accurate result produced by the "full" Parker equation. Hence, the "full" Parker oxygen consumption calorimetry equations should be used, however, the

modifications shown here can also be applied to the Cone Calorimeter Standard equation.

SUMMARY

Reducing uncertainty and minimizing error allows the calculation of a more accurate heat release rate. This is important from both material development and engineering perspectives. In order to reduce the uncertainty and minimize errors, experimental measurements need to be improved and refined. This study is the first step of a continuing process determining what improvements to make.

The carbon dioxide generation calorimetry form given in the Fire Propagation Apparatus ASTM E-2058[2] Standard and the SFPE Handbook[1] is unnecessarily simplified for modern data analysis. It does not account for the combustion process expansion or the removal of water from the gas sample that reaches the analyzers. Hence a more "detailed" equation is developed for carbon dioxide generation calorimetry in a way analogous to that developed by Parker for oxygen consumption calorimetry. The equations developed in this study will be used as a platform to move forward with identifying where to make measurement improvements and refinements that lead to more accurate heat release rate calculations. Additionally, carbon dioxide generation and oxygen consumption calorimetry can be more readily compared.

REFERENCES

1. <u>Handbook of Fire Protection Engineering</u>, 2nd edition, "Chapter 3-4, Generation of Heat and Chemical Compounds in Fires," p. 371, Society of Fire Protection Engineers, Boston, MA,

1995.

2. Standard Test Methods for Measurement of Synthetic Polymer Material Flammability Using a Fire Propagation Apparatus, ASTM E-2058, American Society of Testing Materials, Philadelphia, PA, 2001.

3. Parker, W. J., "Calculations of the Heat Release Rate by Oxygen Consumption for Various Applications," National Bureau of Standards Report # NBSIR 81-2427, 1982.

4. Handbook of Chemistry and Physics, 84th edition, "Chapter 14, Geophysics, Astronomy and Acoustics," CRC Press, Boca Raton, FL, 2003.

5. Huggett, Clayton, "Estimation of Rate of Heat Release by Means of Oxygen Consumption Measurements," Fire and Materials, Volume 4, 2, p. 61-65, 1980.

6. Janssens, Marc. L., "Measuring Rate of Heat Release by Oxygen Consumption," Fire Technology, August, p. 234-249, 1991.

7. Brohez, S., Delvolsalle, C., Marlair, G. and Tewarson, A., "Soot Generation in Fires: An Important Parameter for Accurate Calculation of Heat Release," Fire Safety Science – Proceedings of the Sixth International Symposium, p. 265-276.

8. Brohez, S., Delvolsalle, C., Marlair, G. and Tewarson, A., "The Measurement of Heat Release From Oxygen Consumption in Sooty Fires," Journal of Fire Sciences, V. 18, p. 327-353, 2000.

9. Standard Test Method for Heat and Visible Smoke Release Rates for Materials and Products Using an Oxygen Consumption Calorimeter, ASTM E-1354, American Society of Testing Materials, Philadelphia, PA, 1999.

APPENDIX G: SOOT YIELD

The soot yield $\in$ can be obtained using the method presented by Mulholland[1] et al. using a light extinction measurement of the post flame smoke via

$$\in = \frac{\dfrac{K}{\sigma_s}\dot{V}C_s}{\dot{m}_f}$$

where K is the extinction coefficient, σ_s is the mass specific extinction coefficient, V is the volume flow rate in the duct, C_s is a duct profile correction and m_f is the mass loss rate of the fuel. The mass specific extinction coefficient was found by Mulholland et al. to be nearly universal for post flame smoke produced from well ventilated fires with an average value of 8.7 ± 1.1 m^2/g for a wavelength of 0.623 nm. They state that this is due to the fact that soot from all flames is basically spherical shaped particles of carbon with a diameter much smaller than the wavelength of the light.

PROPYLENE

The soot yield for propylene free burn tests at 20.9 % oxygen concentration is 0.050 ± 0.005 and for 40 % oxygen is 0.023 ± 0.008. Recall that the mass flow rate of propylene is held constant. The decrease in the soot yield with the addition of oxygen is showing that the oxygen is having an effect on the gas phase.

When applied heat flux is added to the free burn propylene flame, an interesting observation is

made. The smoke yield changes regardless of the oxygen concentration. For 20.9 %, the yield

increases from 0.050 at free burn conditions to 0.109 with applied flux. For 40 % oxygen

concentration, the yield changes from 0.023 to 0.037 with applied flux. This indicates that *the*

applied heat flux is having an effect on the soot production in the flame. This can be seen quite

clearly qualitatively by looking at the laser measurements in the duct shown in the figure below.

The trace labeled "main" is the transmitted light while the trace labeled "comp" is the incident

light. Note that when applied heat flux is added, less light gets transmitted, or in other words,

more soot is present. The slight trend of increasing soot with time is thought to be some buildup

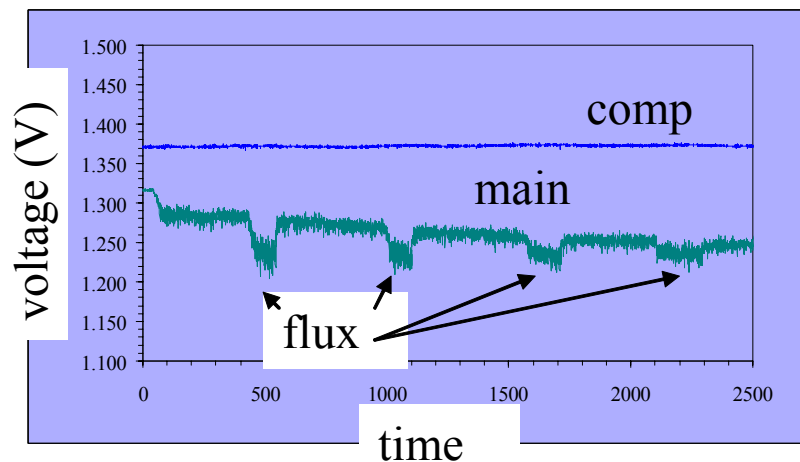of soot on the duct walls but this has not been confirmed.

Figure G.1 Raw extinction data in exhaust duct.

BLACK PMMA

The smoke yield for PMMA free burn tests at 20.9 % oxygen concentration is 0.024 ± 0.022 and

for 40 % oxygen concentration is 0.008 ± 0.001. (For tests with applied heat flux, the average is

the same.) Considering for the uncertainty range, defined as the maximum variation, there is no significant difference between 20.9 % and 40 % atmospheres, however, the trend shows a decrease in the soot yield indicating that the flame has increased in efficiency. Stepniczka has published work that shows smoke generation decreases with increasing oxygen concentration atmosphere for Polystyrene, ABS and polyester.

OTHER MATERIALS

The amount of soot produced by Delrin was below the resolution of the smoke meter so no soot yield measurements are available. The soot yield for Gray PVC at 20.9 % oxygen is 0.108 ± 0.001 and for 40 % oxygen is 0.136 ± 0.026. These were run with applied heat flux since the material would not free burn. Considering for the uncertainty range, defined as the maximum variation, there is no significant difference between 20.9 % and 40 % atmospheres, however, the trend shows an *increase* in the smoke yield. Interestingly, this result is opposite to the result for PMMA but the reason for this is unknown.

REFERENCES

[1]   Mulholland, G. and Croarkin, C., "Specific Extinction Coefficient of Flame Generated Smoke," Fire and Materials, 24, p. 227-230, 2000.

APPENDIX H: IGNITION ANALYSIS

REVIEW OF OTHERS "TYPICAL" METHODS

Current techniques commonly utilized for the analysis of ignition do not include decomposition kinetics. These "first generation techniques" assume that ignition is a "surface" event, which means that decomposition and ignition occur simultaneously when the surface reaches the ignition temperature. The reason for this is that heating the solid from ambient to pyrolysis temperature is the longest characteristic time in the development of the ignition phenomena and many studies have considered the heating process as the primary mechanism controlling material flammability.

LAWSON AND SIMMS

Lawson and Simms[1] were the first to consider the 1D inert material conduction equation as a starting point. Their solution is based on the assumptions of thermally thick behavior and all incident heat flux being absorbed at the material surface. They include convective and radiative heat losses at the surface. They also assume constant thermal properties. Since an exact solution to this is difficult, they lumped the radiative loss into the convective loss by use of a fictional value for the effective heat transfer coefficient, called H. This leads them to the classical solution[2] for x=0 given as

$$T_{surface} = T_0 + \frac{\dot{q}''_{applied}}{H}\left[1 - \exp\left(\frac{\alpha H^2 t}{k^2}\right)\text{erfc}\left(\sqrt{\frac{\alpha H^2 t}{k^2}}\right)\right] \qquad (3)$$

which is a fully correct mathematical solution. For ease of use, they do not use the full equation as given but make mathematical simplifications for the exponential and complementary error function terms by using a series expansion approximation to represent each. Assuming $t_{ignition} \rightarrow 0$, they then only use 2 terms of the series expansion for the exponential term and only 1 term from the series expansion of the complementary error function term leaving

$$\exp\left(\frac{\alpha H^2 t}{k^2}\right) \approx 1 + \left(\frac{\alpha H^2 t}{k^2}\right) \tag{4}$$

for the exponential term and

$$\text{erfc}\left(\sqrt{\frac{\alpha H^2 t}{k^2}}\right) \approx 1 - \left[\frac{2}{\sqrt{\pi}}\left(\sqrt{\frac{\alpha H^2 t}{k^2}}\right)\right] \tag{5}$$

for the complementary error term. Then only two terms of their product is used leaving

$$\exp\left(\frac{\alpha H^2 t}{k^2}\right)\text{erfc}\left(\sqrt{\frac{\alpha H^2 t}{k^2}}\right) \approx 1 - \frac{2}{\sqrt{\pi}}\sqrt{\frac{\alpha H^2 t}{k^2}} \tag{6}$$

which causes the surface loss information, H, to be dropped from the approximated solution for x=0 as

$$T_{surface} = T_0 + \frac{2\dot{q}''_{applied}}{\sqrt{\pi}}\sqrt{\frac{t\alpha}{k^2}} \tag{7}$$

H-2

to be an inaccurate approximation for the fully correct analytical solution for $t_{ignition} > 10$ sec as can be seen in Figure H.1.

TEWARSON

Tewarson[3] also starts with an inert material solution for x=0 from Carslaw and Jaeger[2] although this solution does not include convective or radiative losses from the surface. Constant thermal properties are again assumed. He found that a slight modification to include the surface loss information led to the equation as

$$T_{surface} = T_0 + \frac{2(\dot{q}''_{applied} - \dot{q}''_{critical})}{\sqrt{\pi}} \sqrt{\frac{t\alpha}{k^2}} \tag{8}$$

which produced a better correlation with experimental data. The assumption of absorbitvity =1 is unambiguous by the required use of carbon black coating for all tests using his equation. He states that phase changes as well as surface and condensed phase processes should not be neglected, however, this is not included in his solution. The $\dot{q}''_{critical}$ value is taken from the current experimental data as 4 kW/m^2 for the plot shown.

MIKKOLA AND WICHMAN

Mikkola and Wichman[4] also start with the 1D inert material conduction equation. Their solution is based on a constant applied heat flux, semi-infinite behavior, constant thermal properties and constant, linearized heat loss from the sample surface. They also assume all incident heat flux is

absorbed by the material at the surface. In order to solve this governing equation and boundary conditions, they assume that the heat losses from the surface are small which allows them to make a mathematical approximation of including the loss term in the heat flux term. This is a different route than Lawson and Simms[1] took but Mikkola and Wichman arrive at a very similar solution given as

$$T_{surface} = T_0 + \frac{2\left(\dot{q}''_{applied} - \dot{q}''_{loss}\right)}{\sqrt{\pi}}\sqrt{\frac{t\alpha}{k^2}} \tag{9}$$

where $\dot{q}''_{applied} - \dot{q}''_{loss} = \dot{q}''_{net}$ is the overall flux that includes the surface heat losses. Observe that this is very similar to Tewarsons[3] solution where $\dot{q}''_{critical}$ represents the surface loss information.

JANSSENS

Janssens[5] also starts with the classical solution from Carslaw and Jaeger,[2] for the same governing equation and boundary conditions but does not assume absorptivity = 1 giving the equation as

$$T_{surface} = T_0 + \frac{a\dot{q}''_{applied}}{H}\left[1 - \exp\left(\frac{\alpha H^2 t}{k^2}\right)\text{erfc}\left(\sqrt{\frac{\alpha H^2 t}{k^2}}\right)\right] \tag{10}$$

where a = absorptivity. He does assume that the absorption occurs at the surface. He uses a constant, linearized heat loss from the sample surface, that is, he lumps the radiation loss term into the effective heat transfer coefficient H. Janssens takes a slightly different approach than Lawson and Simms,[1] Tewarson[3] or Mikkola and Wichman[4] to evaluate the surface temperature

H-4

equation. Rather than use a mathematical simplification or experimental correlation, he uses a statistical approach using numerical solutions to approximate the exponential and complementary error function term as

$$\left[1 - \exp\left(\frac{\alpha H^2 t}{k^2}\right) \text{erfc}\left(\sqrt{\frac{\alpha H^2 t}{k^2}}\right)\right] \approx \frac{1}{1 + 0.73\left(\frac{\alpha H^2 t}{k^2}\right)^{-0.55}} \tag{11}$$

which leaves the equation for surface temperature as

$$T_{surface} = T_0 + \frac{a\dot{q}''_{applied}}{H}\left[\frac{1}{1 + 0.73\left(\frac{\alpha H^2 t}{k^2}\right)^{-0.55}}\right] \tag{12}$$

$$H = \frac{a\dot{q}''_{critical}}{\left(T_{ignition} - T_0\right)}$$

Since Janssen only gives a definition of H for $t = t_{ignition}$, the H value presents a problem for obtaining the temperature vs. time during heat up. He specifically did not want to use a linearized H. For purposes of comparison, this study uses the H value as he defines it, recognizing that this will over-predict the surface losses during heat up.

DELICHATSIOS, PANAGIOTOU AND KILEY

Delichatsios, Panagiotou and Kiley[6] represent the surface temperature of a material, for the same

physical case except ignoring convective heat losses, as a Volterra-type integral equation given as

$$T_s - T_0 = \frac{1}{\sqrt{\pi k \rho c}} \int \frac{a\dot{q}'' - \varepsilon\sigma\left(T_{surface}^4 - T_0^4\right)}{\sqrt{t - \tau}} d\tau$$ (13)

Where a is absorptivity, ε is the emissivity and σ is the Stefan-Boltzmann constant. This equation is transformed to a single free parameter. This changes equation 13 to a single parameter integral equation

$$\psi = \int_0^\tau \frac{1 - \left[\beta + (1 - \beta)\psi\right]^4}{\sqrt{\tau - \tilde{\tau}}} d\tilde{\tau}$$ (14)

where β is a parameter that characterizes that magnitude of radiation losses to the applied heat flux. They solve this equation numerically using the continuation method. Since this result is not very useful to the experimentalist, they develop approximate solutions to the equation based on asymptotic analysis. After several mathematical approximations and manipulations, they end up with the equation for surface temperature, converted back to primitive variables, as

$$T_{surface} = T_0 + \frac{2\left[\dot{q}''_{applied} - 0.64\sigma\left(T_{surface}^4 - T_o^4\right)\right]}{\sqrt{\pi}} \sqrt{\frac{t\alpha}{k^2}}$$ (15)

which ignores convective heat loss and considers all surface losses as radiative and can be rewritten as

$$T_{surface} = T_0 + \frac{2\left[\dot{q}''_{applied} - 0.64\dot{q}''_{radiative\,loss}\right]}{\sqrt{\pi}} \sqrt{\frac{t\alpha}{k^2}}$$ (16)

which interestingly is quite similar to the form given by Tewarson and Mikkola and Wichman although a very different approach was taken. Figure H.1 shows a comparison of all the methods being reviewed.
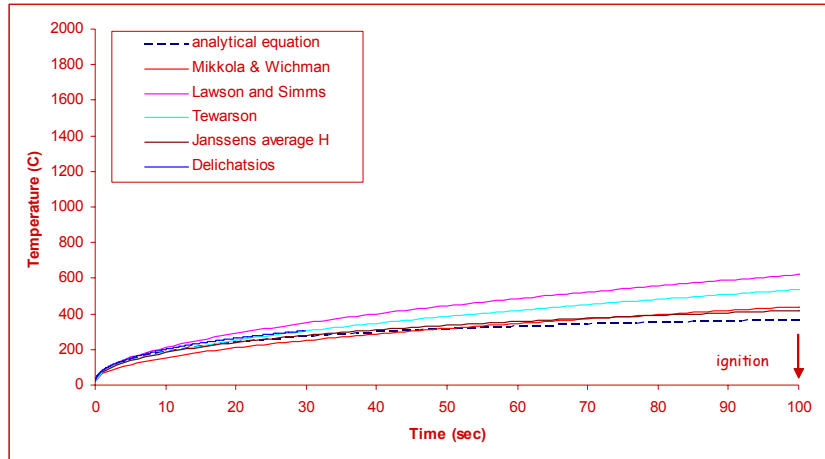

Figure H.1 Surface temperature vs. time for the typical techniques and the inert analytical solution. Applied heat flux = 28.4 kW/m^2.
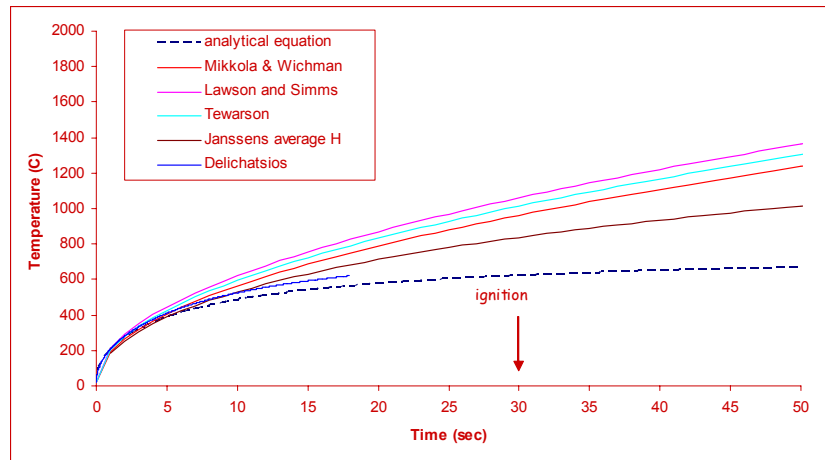

Figure H.2 Surface temperature vs. time for the typical techniques and the inert analytical solution. Applied heat flux = 60 kW/m^2.
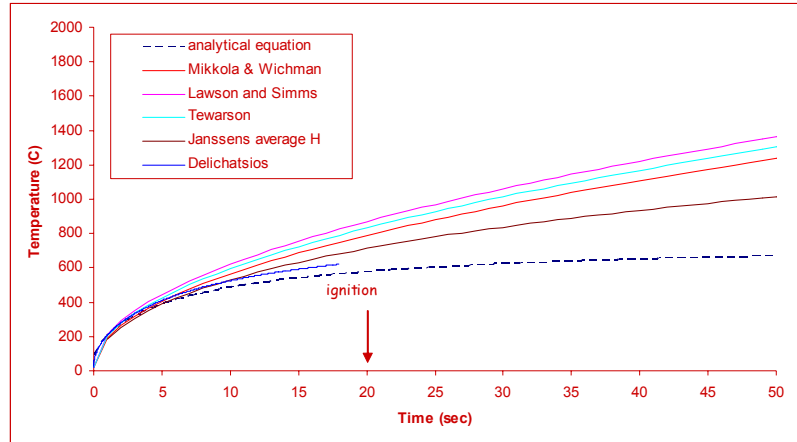
Figure H.3 Surface temperature vs. time for the typical techniques and the inert analytical solution. Applied heat flux = 90 kW/m^2.

These figures show that these "first generation" approximate solutions of the inert material conduction equation are too mathematically simplified to reproduce the surface temperature that comes from the full inert material conduction equation. The full equation has been shown experimentally to predict the measured temperature profile up to when decomposition starts. Hence, the "first generation" techniques are not expected to predict scalable thermal properties from ignition data even for a truly inert material. Additionally, the current study shows that inert material conduction is not sufficient to predict ignition behavior as decomposition physics needs to be included. Irregardless, let us look at how these "first generation" techniques are used by the engineering community to see if more information can provide insight.

ENGINEERING USE OF OTHERS "TYPICAL" METHODS

All of the current techniques above use small scale ignition information to obtain the thermal

inertia, kρc for use in simulations of large scale scenarios, especially flame spread. These "first generation techniques" assume that ignition is a "surface" event, which means that decomposition and ignition occur simultaneously when the surface reaches the ignition temperature and as such, decomposition is not included. Since the temperature profile work done in the current study shows that decomposition needs to be included in a fully correct analysis of ignition and thermal properties, let us see how the current methods do for some experimental ignition data. Typically, an "easy to use" graphical representation of the equations developed in each method is used to obtain kρc but let us first delve into the equations themselves. All the techniques define at ignition, $t = t_{ignition}$ and $T_{surface} = T_{ignition}$ such that with some algebraic effort they obtain the following forms

Simms
$$k\rho c = t_{ignition} \frac{4}{\pi} \frac{\dot{q}''^2_{applied}}{\left(T_{ignition} - T_0\right)^2} \tag{17}$$

Tewarson
$$k\rho c = t_{ignition} \frac{4}{\pi} \frac{\left(\dot{q}''_{applied} - \dot{q}''_{critical}\right)^2}{\left(T_{ignition} - T_0\right)^2} \tag{18}$$

where $q_{critical}$ comes from the x intercept of the data plotted as the inverse of the 0.5 root of time to ignition vs. applied heat flux.

Mikkola and Wichman
$$k\rho c = t_{ignition} \frac{4}{\pi} \frac{\left(\dot{q}''_{applied} - \dot{q}''_{loss}\right)^2}{\left(T_{ignition} - T_0\right)^2} \tag{19}$$

where q_{loss} comes from
$$\dot{q}''_{loss} = h_c\left(T_{ignition} - T_0\right) + \varepsilon\sigma T^4_{ignition}$$

Janssen
$$kpc = t_{ignition}\left[\frac{1}{0.564}\left(\frac{\dot{q}''_{applied}}{\dot{q}''_{critical}} - 1\right)^{1.82}\right]H^2 \text{ which can be re-written as}$$

$$k\rho c = \left(1.77a^2\dot{q}''^{0.2}_{critical}\right)t_{ignition}\frac{4}{\pi}\frac{\left(\dot{q}''_{applied} - \dot{q}''_{critical}\right)^{1.8}}{\left(T_{ignition} - T_0\right)^2} \qquad (20)$$

where $q_{critical}$ comes from the x intercept of the data plotted as the inverse of the 0.55 root of time to ignition vs. applied heat flux.

Delichatsios
$$k\rho c = t_{ignition}\frac{4}{\pi}\frac{\left(a\dot{q}''_{applied} - 0.64\dot{q}''_{critical}\right)^2}{\left(T_{ignition} - T_0\right)^2} \qquad (21)$$

where $q_{critical}$ comes from $\dot{q}''_{critical} = \varepsilon\sigma\left(T^4_{ignition} - T^4_0\right)$

The absorbtivity is 0.95 and $T_{ignition}$ is measured experimentally as an average of 350 °C. Table H.5 shows the thermal inertia values calculated by each technique for black PMMA. The data shown is for carbon black coating so the in-depth absorption would not be an issue. However, the data for the virgin material shows the same results.

Recall that the material has been experimentally proven to be behaving as thermally thick for all applied heat flux *including the low end of the range* so that the whole range is able to use the techniques to calculate kρc. Other experimental conditions have also been proven such as constant applied heat flux and 1D conduction. Remember that these "first generation" techniques assume constant thermal properties, k, ρ and c, such that kρc should also be constant.

Table H.1   kρc values calculated from each technique using the full equation. Experimental data

   is for black PMMA with carbon black coating. Independently measured kρc value =

   0.287×10^5 $W^2 \sec/m^4 K^2$ at 20 C and 0.614×10^5 $W^2 \sec/m^4 K^2$ at 200 C.

Applied Heat Flux (kW/m^2)	t_{ig} (sec)	kρc ($W^2 \sec/m^4 K^2$)				
		Simms[1]	Tewarson $q_{critical}=4.0$	Mikkola[4] $q_{loss}=9.0$	Janssen[5] $q_{critical}=4.8$	Del.[6] $q_{critical}=9.8$
10	1462.0	1.71	0.72	0.00	0.57	0.85
18.7	192.2	0.79	0.52	0.17	0.45	0.53
38.4	42.2	0.73	0.60	0.37	0.49	0.57
70	15.2	0.87	0.79	0.59	0.59	0.73
100	9.1	1.06	1.09	0.86	0.77	1.00
120	7.6	1.28	0.99	0.79	0.70	0.91
130	7.6	1.50	1.21	0.98	0.83	1.11
140	6.8	1.56	1.42	1.16	0.97	1.30
150	7.0	1.84	1.48	1.22	1.00	1.36
200	6.2	2.90	1.76	1.46	1.17	1.61

Observe from Table H.1 that the kρc value obtained for a particular technique is not constant with

applied heat flux. This shows immediately that here is a concern with the current techniques

which assume it to be constant. Earlier, the variation of k, ρ and c with temperature for the range

of 300 to 475 K, which is the range that the material experiences from room temperature to the

beginning of pyrolysis, was shown from independent measurements. The independently measured

values for kρc are 0.287 to 0.614 for this temperature range. The values above change with applied heat flux, especially at the higher heat flux end, which suggests that the first generation techniques of inert material conduction are too simplified to describe the physics occurring. The physics that could be missing, ignoring the "no decomposition" assumption already made, include a dependence of the surface temperature at ignition (i.e., a constant ignition temperature) with applied heat flux and a rate of heating effect on the thermal properties.

A two dimensional axi-symmetric configuration numerical study was done by Tsai et al.[7] for horizontal black PMMA to simulate the transient processes in the solid and gas phases, including radiative absorption by the gas. The surface temperature from simulation and experiment for pilot ignition was found to be constant and not a function of applied flux. However, Rhodes and Quintiere[8] and Hopkins and Quintiere found that the surface temperature at ignition varied with applied heat flux. Hence, these conflicting results show that more investigation is needed into the dependence of surface temperature at ignition on applied heat flux.

The possibility is raised that the thermal properties, k, ρ and c are indeed truly different for the ignition tests conducted in the AFM, Cone or FPA since it is different heating rate than obtained by a TGA or other instrument used to determine these properties independently. The good match of the measured experimental temperature profile of a "fast" heating rate AFM test to the predicted profile of that same test using independent properties obtained from a "slow" heating rate procedure indicate that the heating rate most likely does not have a major effect on the thermal properties in the range tested for black PMMA. This should be investigated further for other materials.

ENGINEERING USE OF OTHERS "TYPICAL" METHODS GRAPHICALLY

Even though it seems from looking at the results from the first generation techniques that they are too simplified, one must look at the typical graphing procedure "for completeness sake to finish the analysis" before concluding this. Starting with Lawson and Simms,[1] equation 17, and re-arranging to a straight line "y=mx" form gives the equation as

$$\frac{1}{\sqrt{t_{ignition}}} = \frac{1}{\sqrt{\frac{\pi}{4} k\rho c \left(T_{ignition} - T_0\right)}} \dot{q}''_{applied} \tag{22}$$

where the slope "m" contains the thermal inertia. The data is graphed as the inverse of the square root of time to ignition vs. applied heat flux, a straight line drawn through the data points and the slope "m" used to calculate the thermal inertia as

$$k\rho c = \frac{1}{m^2} \frac{4}{\pi \left(T_{ignition} - T_0\right)^2} \tag{23}$$

Ignoring the non-linear results at the high heat flux end for a moment, the experimental data is shown as a straight line. However, it does not go through the origin as the "y=mx" line described by the equation above. They are trying to fit "y=mx+b" data to a "y=mx" form given in equation 23. This "graphical" equation is a valid replication of the original equation, hence, Simms approximate equation is not a valid representation of the ignition results, even in the linear portion. The probable cause for this is the exclusion of surface loss information. Figure H.4 shows an example for black PMMA.
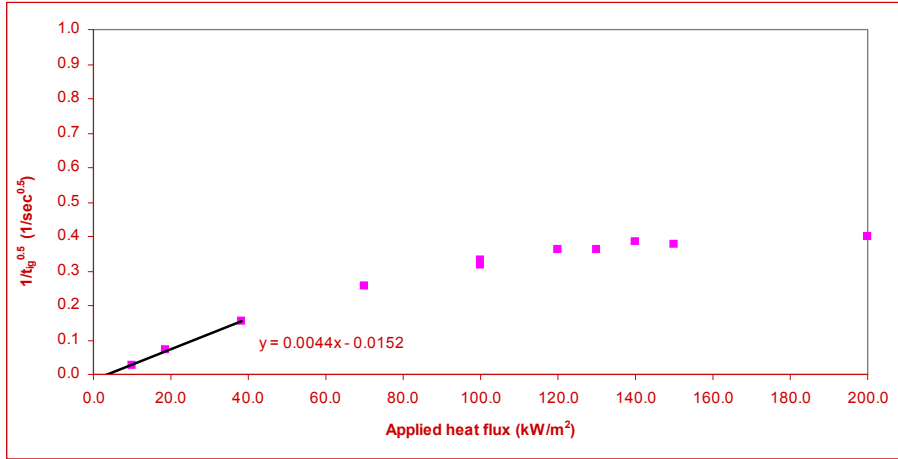
Figure H.4 Ignition plot for Simms black PMMA showing y=mx +b

Tewarson,[3] starting with equation 18, and re-arranging to a straight line "y=mx" form gives the equation

$$\frac{1}{\sqrt{t_{\text{ignition}}}} = \frac{1}{\sqrt{\frac{\pi}{4}k\rho c\left(T_{\text{ignition}} - T_0\right)}}\left(\dot{q}''_{\text{applied}} - \dot{q}''_{\text{critical}}\right) \tag{24}$$

where the slope "m" contains the thermal inertia. The data is graphed as the inverse of the square root of time to ignition vs. applied heat flux, a straight line drawn through the data points. Tewarson then takes the x-intercept as the critical heat flux and replots the data as the inverse of the square root of time to ignition vs. (applied heat flux minus critical heat flux) to force the data through the intercept such that this equation would be a valid representation of the data. The slope "m" is used to calculate the thermal inertia

H-14

$$k\rho c = \frac{1}{m^2} \frac{4}{\pi \left(T_{ignition} - T_0\right)^2} \tag{25}$$

from this new graph. Ignoring the non-linear results at the high heat flux end for a moment, the experimental data is shown as a straight line as shown in Figure 5. As expected, the slope is no different than Simms value since the critical heat flux or x intercept information is not contained in the slope. This surface loss information has been in effect, lost, by the adjustment of the data. It is expected that this will then give the same result as Simms who doesn't have any surface loss information to begin with. This "graphical representation" equation is not a valid replication of the original equation which contains surface loss information. This is confirmed by looking at Tewarson slightly differently. Staring with his original full equation, it can be split up to a "y=mx+b" form as

$$\frac{1}{\sqrt{t_{ignition}}} = \frac{1}{\sqrt{\frac{\pi}{4} k\rho c}\left(T_{ignition} - T_0\right)} \dot{q}''_{applied} - \frac{1}{\sqrt{\frac{\pi}{4} k\rho c}\left(T_{ignition} - T_0\right)} \dot{q}''_{critical} \tag{26}$$

which shows clearly that both the slope and intercept are required to solve for $k\rho c$ graphically to match that obtained from his full equation.
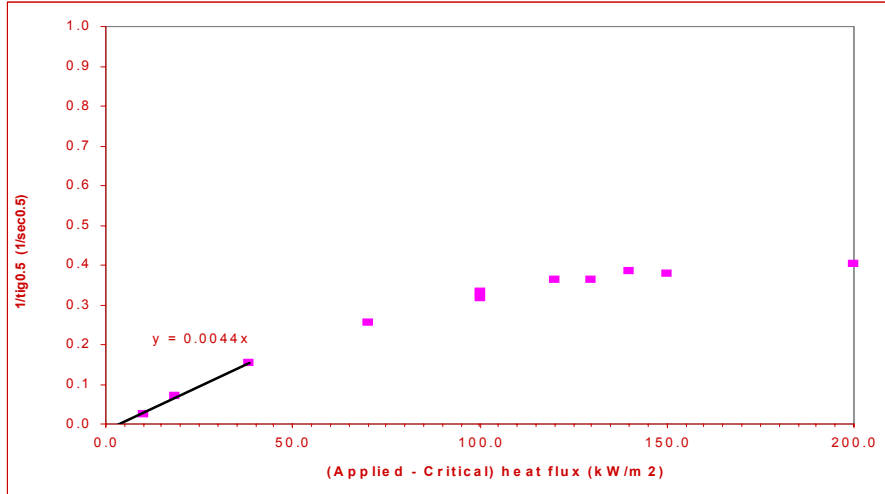
Figure H.5 Ignition plot for black PMMA Tewarson

Mikkola and Wichman,[4] starting with equation 19 and re-arranging to a straight line "y=mx+b" get

$$\frac{1}{\sqrt{t_{ignition}}} = \frac{1}{\sqrt{\frac{\pi}{4}k\rho c}\left(T_{ignition} - T_0\right)}\dot{q}''_{applied} - \frac{1}{\sqrt{\frac{\pi}{4}k\rho c}\left(T_{ignition} - T_0\right)}\dot{q}''_{loss} \qquad (27)$$

The data is graphed as the inverse of the square root of time to ignition vs. applied heat flux, a straight line drawn through the data points and the slope "m" used to calculate the thermal inertia as

$$k\rho c = \frac{1}{m^2}\frac{4}{\pi\left(T_{ignition} - T_0\right)^2} \qquad (28)$$

H-16

which is missing the surface loss information, defined by $\dot{q}''_{loss}$, contained in the "b" term. It is expected that this will then give the same result as Simms who doesn't have any surface loss information.
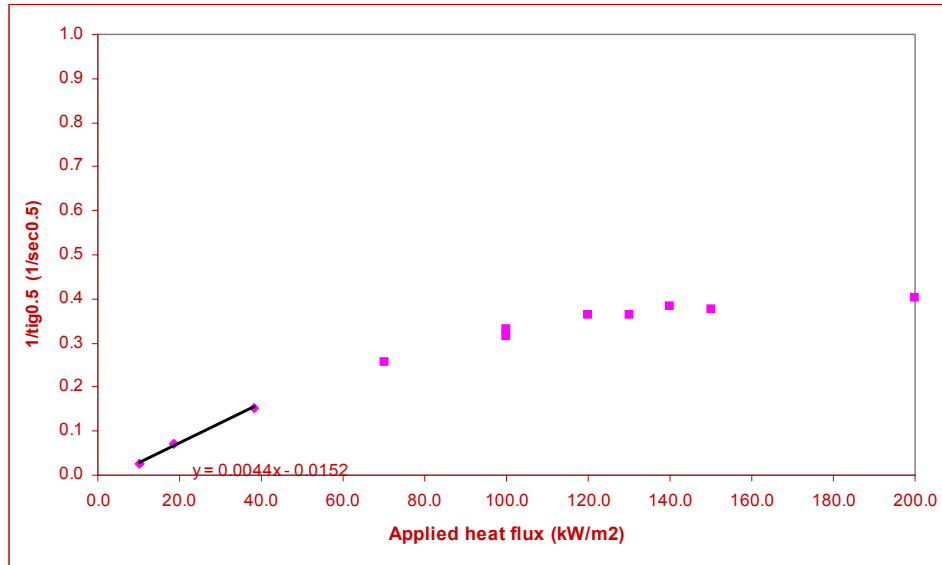

Figure H.6 Ignition plot for black PMMA showing y=mx+b for Mikkola and Wichman

Delichatsios et al.,[6] starting with equation 21, and re-arranging to a straight line "y=mx+b" get

$$\frac{1}{\sqrt{t_{ignition}}} = \frac{a}{\sqrt{\frac{\pi}{4} k\rho c}\left(T_{ignition} - T_0\right)} \dot{q}''_{applied} - \frac{.64}{\sqrt{\frac{\pi}{4} k\rho c}\left(T_{ignition} - T_0\right)} \dot{q}''_{critical} \qquad (29)$$

The data is graphed as the inverse of the square root of time to ignition vs. applied heat flux, a straight line drawn through the data points and the slope "m" used to calculate the thermal inertia as

$$kρc = \frac{1}{m^2} \frac{4a}{π\left(T_{ignition} - T_0\right)^2}$$

(30)

which is again missing the surface loss information, defined by $0.64\dot{q}''_{critical}$, contained in the "b" term. This "graphical representation" equation is again not a valid replication of the approximate equation which contains surface loss information.
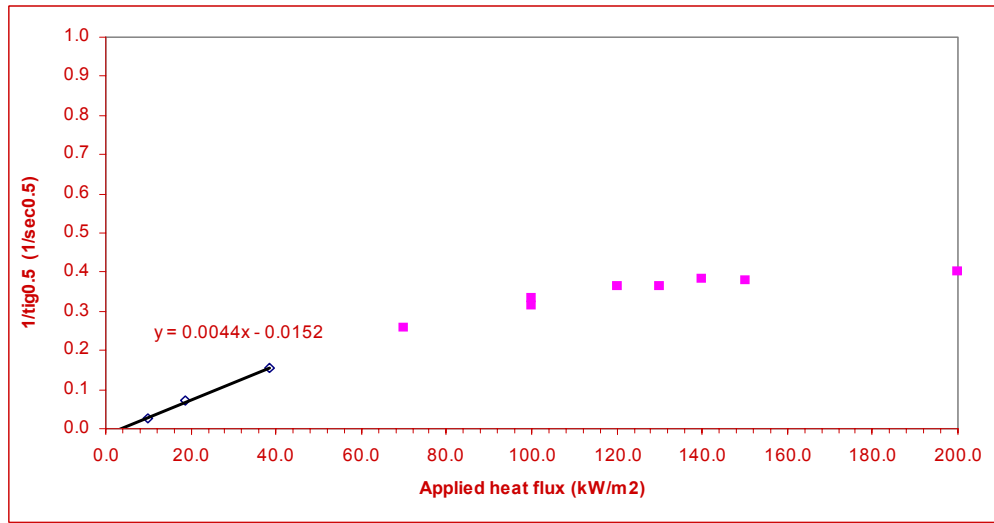

Figure H.7 Ignition plot for black PMMA showing Delichatsios

Janssen,[5] starting with equation 20, and re-arranging to a straight line form "y=mx+b" gets

$$\frac{1}{\left(t_{ignition}\right)^{0.55}} = \frac{1}{0.73}\left(\frac{H^2}{kρc}\right)^{0.55} \frac{\dot{q}''_{applied}}{\dot{q}''_{critical}} - \frac{1}{0.73}\left(\frac{H^2}{kρc}\right)^{0.55} \dot{q}''_{critical}$$

(31)

$$m = \frac{1}{0.73}\left(\frac{H^2}{k\rho c}\right)^{0.55}\frac{1}{\dot{q}''_{critical}}$$

where $\dot{q}''_{critical}$ is the x intercept. The data is graphed as the inverse of the 0.55 root of time to ignition vs. applied heat flux, a straight line drawn through the data points and the slope "m" is used to calculate the thermal inertia as

$$k\rho c = \frac{a^2\dot{q}''^{0.2}_{critical}}{0.56m^{1.8}(T_{ignition} - T_0)^2} \tag{32}$$

which is missing information contained in the "b" term. Hence, once again, the "graphical representation" equation is not a valid replication of the full equation.
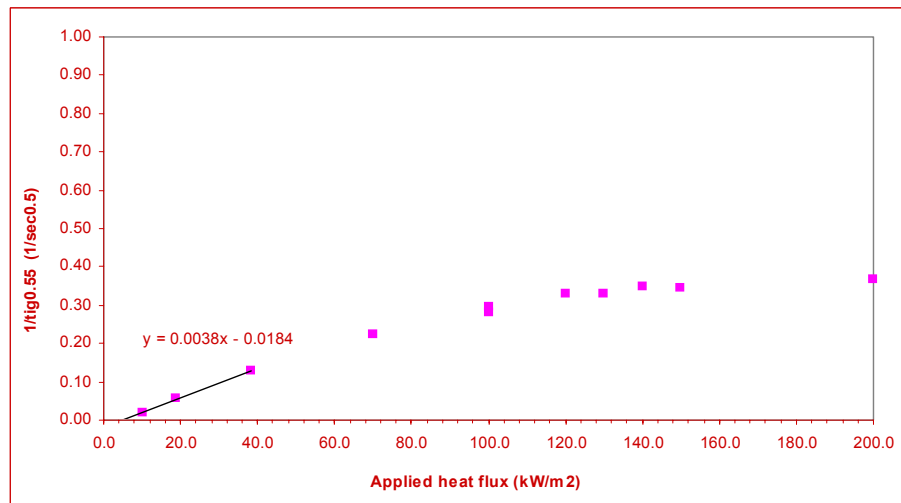

Figure H.8 Ignition plot for black PMMA showing Janssen

Investigation of the typical graphing procedure used by the first generation techniques, except for

Simms, shows that the "graphical representation" does not fully represent the approximate

equation of that technique. This is shown in Table 2 which shows calculations for kρc from the

graphing procedure and average kρc from the full approximate solutions.

Table H.2   kρc values calculated from each technique using the graphical procedure.
             Experimental data is for black PMMA.

kρc technique	Simms	Tewarson	Mikkola	Janssen	Delichat
graphing procedure	0.604	0.604	0.604	0.444	0.574
full equation average from all flux (18.7-200)	1.355	1.169	0.919	0.971	0.922
full equation average from mid flux (30-50)	1.12	0.93	0.68	.82	.71

The inaccurate graphical representation is true for any heat flux, even the lower end where the ignition data is plotted linearly. Hence, the graphical procedure to obtain kρc provides no additional information about each technique and, in fact, makes further inaccurate simplifications. The "first generation" techniques of inert material conduction are too simplified from making mathematical simplifications and ignoring decomposition to describe the actual physics occurring. So stated once again, the "first generation" techniques are not expected to predict scalable thermal properties from ignition data.

HOW THERMAL INERTIA IS USED

Now that we see from information obtained in the current study that the first generation techniques really can't get scalable thermal properties for the full range of heat flux expected in the real world, what does this mean since kρc is used in flame spread models with some success? It is noted that the thermal inertia obtained via a specific technique is a "model parameter" that can not be disconnected from the experiments that were used to obtain it, i.e., it is not a true scalable material property. Regardless, let us look at these "model parameter" results. The thermal inertia by itself is not useful for modeling, so this requires the "split up" of the thermal inertia to obtain k, ρ and c separately for use in various models. This is a problem addressed in different ways by modelers attempting to use k, ρ and c in their models.

The "split-up" of the thermal inertia value obtained from the first generation techniques to obtain the same diffusivity as obtained from independent measurements should lead to a match of the predicted and measured temperature profiles, with only a small effect of the actual value of thermal inertia. In the current study, this was found to be true, *up to when decomposition starts*,

for black PMMA. The thermal inertia value differed by a range of 0.278 to 1.4 as seen in Table 6 for black PMMA, however, the predicted temperature profiles are about the same using the proper "split-up" to obtain the same diffusivity as independently measured. Splitting up the thermal inertia to obtain $k/\rho c$ differently causes the profile to be either too shallow if $k/\rho c > \alpha$ or too deep if $k/\rho c < \alpha$. That is, the thermal inertia value used didn't matter as long as the independent properties were in the correct ratio. This was shown earlier. This reason is most likely why the current technique results, which are quite off from independent measured values, seem to work in models. The actual value they get for $k\rho c$ is not important, it is all in how they "split" their results to get k, ρ and c properly and this is where, probably, all the accumulated errors of the approximated solutions and their inaccurate graphical representations, as well as the missing decomposition kinetics, gets "adjusted out."

TEMPERATURE PROFILE

A detail of solid material behavior observed while doing the above analysis was that the thermal diffusivity had the most significant effect on the predicted temperature profile. That is, the actual values of k, ρ and c didn't matter and even using values double or quadruple the actual values had no effect as long as the diffusivity was the same. On further thought, this observation seems plausible, since the thermal diffusivity, under the approximation of constant thermal properties, is the controlling parameter for the temperature profile according to classic conduction theory. Lautenberger et al.[9] show from their Arrhenius reaction model for solid phase fuel pyrolysis that the thermal diffusivity appears explicitly. Since the thermal diffusivity determines the temperature profile in the solid, and the temperature profile could contribute to the process of ignition, then diffusivity should be an important property to the study of ignition. The numerical

results of Launtenberger et al. for a hypothetical material show that the thermal diffusivity is a more relevant measure of ignition susceptibility. Dietenberger[10] uses a criterion that requires thermal diffusivity to separate thermally thin and thick behavior for ignition tests. He also says that $k\rho c$ is not the parameter of interest for ignition but α/k...i.e., need k, ρ and c separately. Di Blasis and Wichman[11] have pointed out that flame spread, which can be viewed as a series of ignitions, correlates with thermal diffusivity. Cordova and Fernadez-Pello[12] conclude that the thermal diffusivity is the material property to determine the rate of thermal penetration depth, or in other words, the temperature profile within the solid, when exposed to an external heat flux.

The details found using the temperature profile are consistent with each other. Thermal diffusivity is an important property to determine the temperature profile in an inert material solid while it heats up to decomposition temperature. Once it starts to decompose, then decomposition kinetics at the surface and possibly in-depth needs to be included in the analysis of ignition and flame spread.

WHY IS PLOT LINEAR

The linear relationship between the inverse of the square root of time to ignition and the applied heat flux is the nature of the inert solution mathematics as shown in Figure H.9. Observe that the relationship between inverse square root of time and applied heat flux is linear.
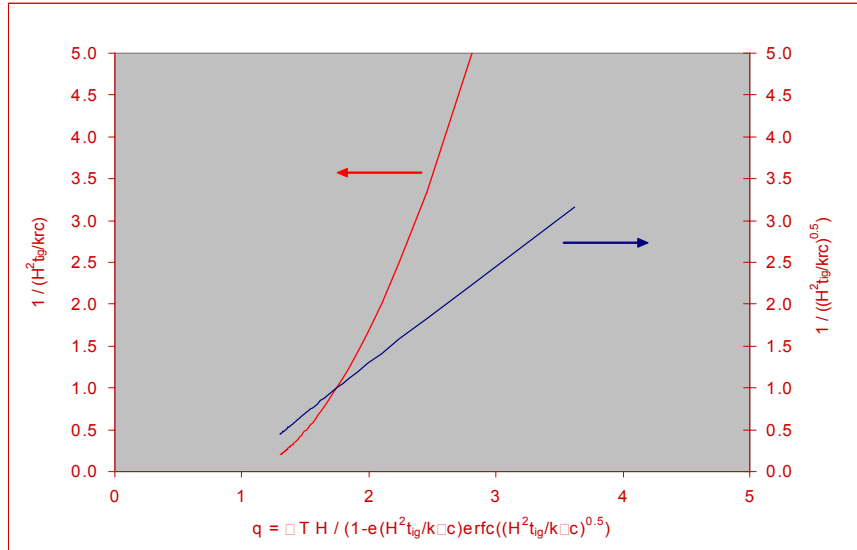
H-23

Figure H.9 Inverse of the representative time to ignition vs. applied heat flux. Also shown is the inverse of the square root of the representative time to ignition vs. applied heat flux.

REFERENCES

1   Lawson, D. and Simms, D., "The Ignition of Wood by Radiation," British Journal of Applied Physics, 3, p. 288-292, 1952.

2   Conduction in Solids, 2nd edition, Carslaw, H.S., and Jaeger, J.C, "Chapter 2-9 Semi-Infinite Solid," Oxford University Press, Oxford, 1959.

3   Tewarson, A., Factory Mutual Research Technical Report # JI 1A6R1.RC, FM Global Research, Norwood, MA, 1979.

4   Mikkola, E., and Wichman, I., "On the Thermal Ignition of Combustible Materials," Fire and Materials, 14, p. 87-96, 1989.

5   Janssens, M., "Improved Method of Analysis for The Lift Apparatus, Part 1:Ignition," Proceedings of the 2nd Fire and Materials Conference, p. 37-46, 1993.

6   Delicahtsios, M., Panagiotou, T., and Kiley, F., "The Use of Time to Ignition Data for Characterizing the Thermal Inertia and the Minimum (Critical) Heat Flux for Ignition or Pyrolysis," Combustion and Flame, 84, p. 323-332, 1991.

7   Tsai, T., Li, M., Jih, R. and Wong, S., "Experimental and Numerical Study of Autoignition and Pilot Ignition of PMMA Plates in a Cone Calorimeter," Combustion and Flame, 124, p. 466-480, 2001.

8   Rhodes, B. T., and Quintiere, J. G., "Burning Rate and Flame Heat Flux for PMMA in a Cone Calorimeter," Fire Safety Journal, 26, p. 221-240, 1996.

9   Lautenberger, C., Stevanovic, A., Rich, D., Torero, J, and Fernandez-Pello, A., "Effect of material Composition on Ignition Delay of Composites," Composites 2003, Composites Fabricators Association, October 1-3, 2003.

10 Dietenberger, M., "Ignitability Analysis of Siding Materials Using Modified Protocol for Lift Apparatus," Fire and Materials, 20, p. 115-121, 1996.

11 Di Blasi, C., and Wichman, I., "Effects of Solid Phase Properties on Flames Spreading Over Composite Materials," Combustion and Flame, 102, p. 229 – 240, 1995.

12 Cordova, J. Fernandez-Pello, A., "Convection Effects on the Endothermic Gasification and Piloted Ignition of a Radiatively Heated Combustible Solid," Combustion Science and Technology, 156, p. 271-289, 2000.